LENTIVIRAL GENE THERAPY

FOR

ARGININOSUCCINIC ACIDURIA

Loukia Touramanidou

A thesis submitted for the degree of Doctor of Philosophy

University College London

2023

DECLARATION

I, Loukia Touramanidou, hereby confirm that the thesis entitled "Lentiviral Gene Therapy for Argininosuccinic Aciduria" represents my original work, and all sources used or referred to in this thesis are properly cited and acknowledged.

Any contributions made by others in this work have been clearly identified and acknowledged below:

- The embedding with paraffine and cutting of liver samples derived from mice were performed by the Histopathology Department, Institute of Neurology, University College London, UK (**Section 2.3.5**).

- Liver samples derived from animals were processed for Electron microscopy by Dr Glenn Anderson at Great Ormond Street Hospital, University College London, UK (**Section 2.4**).

- Hydrophilic interaction liquid chromatography-tandem mass spectrometry (HILIC-MS/MS) of dried urine and blood spots were analysed by Dr Sonam Gurung at Great Ormond Street Institute of Child Health, University College London, UK (**Section 2.3.4**).

- [18F]FSPG studies were performed by Dr Oskar Timmermand and Mr Dany Perocheau at the School of Biomedical Engineering and Imaging Sciences, King's College London, UK (**Section 2.3.8**)

ACKNOWLEDGEMENTS

ABSTRACT

The urea cycle facilitates the disposal of nitrogen waste and the elimination of harmful ammonia. Argininosuccinic aciduria (ASA), a urea cycle defect caused by a deficiency in argininosuccinate lyase (ASL), is the second most frequent urea cycle defect. Individuals with this condition may experience hyperammonaemia, leading to coma and death if not treated, along with an increased likelihood of severe cognitive impairment and epilepsy. Liver transplantation can be a curative option, but this requires perpetual immunosuppression. Lentiviral vector gene therapy has shown effective results in *ex vivo* gene replacement treatment in various inherited metabolic disorders. Furthermore, *in vivo* studies have shown remarkable safety in self-inactivating lentiviral vectors gene therapy. This study aimed to develop a safe *in vivo* liver-directed gene therapy strategy for ASA using a lentiviral vector carrying the wild-type *hASL* transgene. This neonatal *in vivo* lentiviral gene therapy with codon-optimisation of the transgene was tested in an ASL-deficient $Asl^{Neo/Neo}$ mouse model. A single intravenous administration of gene therapy showed a normalisation of the growth, fur coat pattern, and urea cycle biomarkers, a significant increase of liver ASL activity and expression comparable to physiological levels at 3 months. Safety study was conducted to assess the presence of genotoxic events driven by the lentiviral vector *in vivo*. The results showed no significant difference in survival, liver/body ratio, and pathology analysis revealed no signs of tumours. Prior to administering lentiviral and AAV injections in wild-type animals, we evaluated liver transduction subsequent to systemic administration of clodronate, a macrophage inhibitor. Results showed a significant liver transduction increase following clodronate liposomes with lentiviral but not with AAV vector. This research showed the feasibility of lentiviral gene therapy for ASA *in vivo*, and a substantial enhancement in hepatocyte transduction using macrophage inhibitors.

IMPACT STATEMENT

Lentiviral vector gene therapy has emerged as a promising approach for treating genetic disorders. One such condition is ASA, a rare metabolic disorder caused by the deficiency of the enzyme ASL. As a PhD student, my research focused on using lentiviral vectors to correct the neonatal mouse model of ASA.

My research findings will help develop a new and effective treatment for individuals with ASA, who currently have limited treatment options. ASA is a rare but serious genetic disorder that affects the urea cycle, leading to hyperammonaemia and potentially fatal consequences such as coma and seizures. Liver transplantation can be a curative option but requires life-long immunosuppression. This work demonstrates the feasibility of lentiviral gene therapy for ASA, which could provide a more effective and less invasive treatment option for affected individuals. A single neonatal administration is sufficient for the correction of this disease's phenotype suggested by the ASA mouse model.

This research could have broader implications for the development of gene therapy strategies for other inherited metabolic disorders. Lentiviral vector gene therapy has shown effective results in *ex vivo* gene replacement treatment for various inherited metabolic disorders. My study provides valuable insights into the optimization of the lentiviral vector transgene and the use of macrophage inhibitors to enhance liver transduction efficiency. These findings can be leveraged in the expanding development of lentiviral gene therapy for other liver inherited metabolic disorders, while a significant reduction of the vector dose will improve safety with a similar liver transduction and subsequently disease correction.

TABLE OF CONTENTS

LIST OF TABLES

LIST OF FIGURES

ABBREVIATIONS

[^{18}F]FSPG (S)-4-(3-18F-fluoropropyl)-L-glutamate

AAP   Assembly-activating protein

AAV   Adeno-associated virus

ABCD1   ATP-binding cassette sub-family D member 1

ALD   Adrenoleukodystrophy

ALT   Alanine aminotransferase

ARG1   Arginine

ARG1D   Arginase 1 deficiency

ASA   Argininosuccinic aciduria

ASL   Argininosuccinate lyase

ASLD   Argininosuccinic acid lyase deficiency

ASS   Argininosuccinate synthase

ASSD   Argininosuccinic acid synthetase deficiency

ATP   Adenosine triphosphate

BCA   Bicinchoninic acid

BH$_4$ Tetrahydrobiopterin

bp   Base pairs

CALD   Cerebral adrenoleukodystrophy

Cap   Capsid gene

CAT-1   Cationic amino acid transporter

cDNA   Complementary DNA

CFTR   Cystic fibrosis transmembrane conductance regulator

cGMP   Nitric oxide-cyclic guanosine monophosphate

CMV   Cytomegalovirus

CNS   Central nervous system

Co   Carbon monoxide

co   Codon optimised

CO$_2$ Carbon dioxide

CpG   Cytosine–guanine dinucleotide

cPPT   Central polypurine tract

CPS l	Carbamoyl phosphate synthetase I
CPS1D	Carbamoylphosphate synthetase 1 deficiency
Ct	Cycle threshold
CT	Computerized tomography
CTL	Cytotoxic T lymphocyte
CTS	Central termination sequence
DAB	Diaminobenzidine
DNA	Deoxyribonucleic acid
DMEM	Dulbecco's Modified Eagle's Medium
EDTA	Ethylenediaminetetraacetic acid
EF1α	Elongation factor-1α
ELISA	Enzyme-linked immunosorbent assay
eNOS	Endothelial nitric oxide synthase
ET	Hepatocyte-specific enhanced transthyretin
F5	Generation 5
FCS	Fetal calf serum
FRT	Flippase recombination target
FVIII	Factor VIII
FIX	Factor IX
GFP	Green fluorescent protein
GSA	Guanidinosuccinate
H_2O_2	Hydrogen peroxide
hAAT	Human α1-antitrypsin
hASL	Human argininosuccinate lyase gene
HCI	Hydrochloric acid
HCR	Hepatic control region
HEK	Human embryonic kidney
Het	Heterozygote
HILIC	Hydrophilic interaction liquid chromatography
HIV-1	Human immunodeficiency virus type 1
hMUTh	Human methylmalonyl-CoA mutase
HS90	Heat shock protein
Huh7	Human hepatoma cells
ID/g	Injected dose per gram of tissue

IgG	Immunoglobulin
iNOS	Inducible nitric oxide synthase
IP	Intraperitoneal
K-ATPase	Sodium–potassium adenosine triphosphatase
Kb	Kilobase
kDa	Kilodaltons
LDL	Low-density lipoprotein
LEDGF	Lens epithelium-derived growth factor
LMO2	LIM Domain Only 2
LNP	Lipid nanoparticles
LoxP	Locus of x-over P1
LP1	Liver-specific promoter 1
LPI	Lysinuric protein intolerance
LTR	Long terminal repeat
Luc	Luciferase
LV	Lentiviral vector
MAAP	Membrane-associated accessory protein
MBq	Megabecquerel
MM	Master mix
MMA	Methylmalonic acidemia
MOI	Multiplicity of infection
mRNA	Messenger ribonucleic acid
MS/MS	Tandem mass spectrometry
NA	Sodium
NAD	Nicotinamide adenine dinucleotide
NADPH	Nicotinamide adenine dinucleotide phosphate
NADH	Nicotinamide adenine dinucleotide reduced form
NAG	N-acetyl-glutamate
NAGS	N-acetylglutamate synthase
NAGSD	N-acetylglutamate synthase deficiency
Neo	Neomycin
NFκB	Nuclear factor kappa B
NH4$^+$	Ionised molecule of ammonia
NMDA	N-methyl-D-aspartate

NO	Nitric oxide
NO_3^-	Nitrate
NOS	Nitric oxide synthase
ns	Not significant
O_2^-	Oxygen
OAT	Ornithine aminotransferase
ONO_2^-	Peroxynitrite
$ONOO^-$	Oxidant peroxynitrite
ORF	Open reading frame
ORNT1	Ornithine citrulline transporter
OTC	Ornithine transcarbamylase
OTCD	Ornithine transcarbamylase deficiency
p	Penicillin
PAMP	Pathogen-associated molecular patterns
PBS	Phosphate-buffered saline
PBS	Primer-binding site
PEI	Polyethylenimine
PES	Polyethersulfone
PET	Positron emission tomography
PGK	Phosphoglycerate kinase
pH	Potential hydrogen
PIL	Personal animal license
PRR	Pattern recognition receptors
PPL	Project animal license
PPT	Polypurine tract
qPCR	Quantitative polymerase chain reaction
R	Repeat region
Rep	Replication gene
RNA	Ribonucleic acid
ROI	Region of interest
RRE	*Rev* response element
RSNO	Nitrosothiols
RT	Reverse transcriptase
s	Second

s	Streptomycin
SA	*Tat/rev* splice acceptor
SCID-X	X-linked severe combined immunodeficiency
SD	Splice donor
SD	Standard deviation
SIN	Self-inactivating
SLC7A7	Solute carrier family 7 member 7
SMA	Spinal muscular atrophy
SOC	Optimal broth with catabolite repression
ssRNA	Single stranded ribonucleic acid
SV40	Simian virus 40
T3	Bacteriophage T3 RNA polymerase
TLR	Toll-like receptors
tRNA	Transfer ribonucleic acid
U3	Unique 3' region
UbiC	Ubiquitin C
UGT1A	Uridine diphosphate glucuronosyltransferase 1A1
UK	United Kingdom
USA	United States of America
VCN	Vector copy number
VP1	Viral protein 1
VP2	Viral protein 2
VP3	Viral protein 3
Vpr	Viral protein R
VSV-G	Vesicular stomatitis virus G envelope glycoprotein
Wk	Weeks
WPRE	Woodchuck hepatitis virus post-transcriptional regulatory element
WT	Wild-type
X-ALD	X-linked adrenoleukodystrophy
XSCID	X-linked severe combined immunodeficiency
Δ *gag*	Group specific antigen Δ
Δ U3	Truncated HIV-1 3' long terminal repeat
Ψ	Psi sequence

1. INTRODUCTION

1.1 The urea cycle and related inherited human defects

1.1.1 The urea cycle

Ammonia is a naturally occurring by-product in the human body and an intermediate metabolite generated by the catabolism of amino acids [1]. However, ammonia is neurotoxic and is rapidly metabolised into urea in the liver by the urea cycle and excreted in urine [2, 3]. The liver enables wasting excretion of excess nitrogen by converting neurotoxic ammonia into urea (**Figure 1**) [4]. This energy-dependent process takes place mainly in the matrix of mitochondria and cytoplasm [5]. When this pathway is impaired, ammonia accumulates and can cause acute, chronic, or intermittent clinical symptoms, which can be observed at any age [6-8].

The urea cycle entails 6 biochemical reactions catalysed by 3 mitochondrial enzymes first, then 3 cytoplasmic ones (**Figure 1**). The first rate-limiting step involves the transformation of carbon monoxide (CO) and ammonia to carbamoyl phosphate, which is catalysed by carbamoyl phosphate synthetase I (CPS I) enzyme. Ammonia is the origin of the first amine group of urea. This enzymatic reaction is activated by N-acetyl-glutamate (NAG), synthesized from glutamate and acetyl-CoA via the enzyme NAG synthase [9].

Carbamoyl phosphate and ornithine react to produce citrulline, that is then catalysed by ornithine transcarbamylase (OTC) [10]. Subsequently citrulline is transferred from the mitochondria to the cytoplasm of the hepatocyte by an ornithine citrulline transporter (ORNT1) or ornithine translocase [11].

Citrulline then reacts with aspartate to generate argininosuccinate. This reaction is catalysed by argininosuccinate synthetase (ASS1) enzyme, at the expense of adenosine triphosphate (ATP). Aspartate transaminase facilitates the transamination of oxaloacetate and glutamate, resulting in the production of aspartate. Aspartate then serves as the source of the second amine group in urea synthesis. Such reaction also requires a vitamin B6 metabolite, pyridoxal phosphate which takes part as a coenzyme [10].

Argininosuccinate is transformed into arginine via argininosuccinate lyase (ASL). This reaction further produces fumarate, that is highly implicated in the mitochondrial generation of nicotinamide adenine dinucleotide (NAD) reduced form (NADH) in the citric acid cycle as well as tyrosine catabolism.

In order to generate urea and ornithine, arginine (ARG1) undergoes hydrolysis [10].
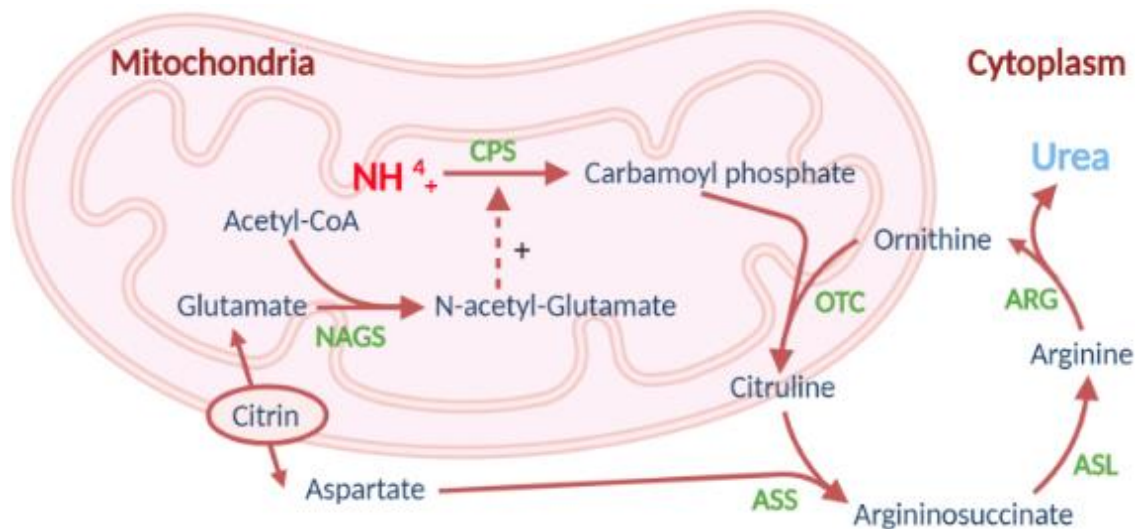
Figure 1. The urea cycle. ARG: Arginase; ASL: Argininosuccinic acid lyase; ASS: Argininosuccinic synthetase; CPS1: Carbamoylphosphate synthetase type 1; NAGS: N-acetylglutamate synthetase; NH4$^+$: Ionised molecule of ammonia; OTC: Ornithine transcarbamylase.

1.1.2 Urea cycle disorders

Urea cycle disorders refer to a group of congenital metabolic disorders that arise from deficiencies in any of the 6 enzymes or 2 transporters that participate in the elimination of ammonia from the bloodstream by converting it into urea, followed by its elimination by the kidneys. These are rare monogenic disorders with a global incidence estimated between 1 in 8,200 [12] to 1 in 35,000 live births [13].

Overall, there are 10 clinically relevant disorders. Because all 10 of these disorders can lead to the development of increased ammonia and decreased urea in plasma, most of them have a similar clinical phenotype (**Table 1**) [14, 15]. Hyperammonaemia is a key pathophysiological mechanism in urea cycle diseases and plays a crucial role in central nervous system (CNS) toxicity. This causes encephalopathy, with symptoms including cerebral oedema, vomiting, blurred vision, asterixis, and seizures [16]. The toxic effects of ammonia on the CNS are more severe in the developing brain compared to the adult brain [17].

Disease	Clinical feature	Specific change of amino acids		Urinary orotic acid	Inheritance	Gene symbol	Gene locus
		Plasma	Urine				
CPSID	Hyperammonemia	Citrulline ▼		-	AR	*CPS1*	2q25
OTCD	Hyperammonemia	Citrulline ▼		++	X-linked	*OTC*	Xp21.1
ASSD	Hyperammonemia	Citrulline ▲	Citrulline ▲	++	AR	*ASS*	9q34
ASLD	Hyperammonemia	Argininosuccinic acid ▲	Argininosuccinic acid▲	+	AR	*ASL*	7q11.21
	Hepatomegaly	Citrulline ▲					
	Hair abnormality						
ARG1D	Hyperammonemia	Arginine ▲▲	Arginine ▲	++	AR	*ARG*	6q23
	Retardation		Lysine ▲				
	Spastic paraplegia		Cystine ▲				
NAGSD	Hyperammonemia			-	AR	*NAGS*	17q21.31
Ornithine aminostransferase deficiency	Gyrate atrophy of the choroid and retina with	Ornithine ▲		+~±	AR	*OAT*	10q26
HHH syndrome (ornithine transporter)	Hyperammonemia	Ornithine ▲	Homocitrulline ▲	+	AR	*ORNT1*	13q14
Lysinuric protein intolerance (basolateral membrane)	Hyperammonemia		Lysine ▲▲	+~±	AR	*SLC7A7(LP1)*	14q11-13
	Hepatomegaly		Ornithine ▲				
	Osteoporosis		Arginine ▲				

Table 1. Urea cycle disorders. AR: autosomal recessive; *ARG*: arginase; ARG1D: Arginase 1 deficiency; *ASL*: argininosuccinic acid lyase; ASLD: Argininosuccinic acid lyase deficiency; *ASS*: argininosuccinic acid synthetase; ASSD: Argininosuccinic acid synthetase deficiency; *CPS1*: carbamoylphosphate synthetase 1; CPS1D: Carbamoylphosphate synthetase 1 deficiency; LPI: Lysinuric protein intolerance; *NAGS*: N-acetylglutamate synthase; NAGSD: N-acetylglutamate synthase deficiency; *OAT*: ornithine aminotransferase; *ORNT1*: ornithine transporter; *OTC*: ornithine transcarbamylase; OTCD: Ornithine transcarbamylase deficiency; *SLC7A7*: solute carrier family 7 member 7 [15].

1.2 Argininosuccinic aciduria

1.2.1 Argininosuccinate Lyase

ASL is the only enzyme in humans responsible for the final step of endogenous L-arginine synthesis. This amino acid can be obtained from dietary sources, protein breakdown, or endogenous production and is a precursor for several vital metabolites, such as urea, nitric oxide (NO), glutamate, proline, creatine, and agmatine, participating in various physiological processes. [18]. ASL is prominently expressed in the liver, however it is also found in numerous different organs, including the brain, small intestine, red blood cells, muscle, heart, kidney, and fibroblast. [18, 19].

ASL takes part in the urea cycle (**Figure 1**) by breaking down argininosuccinate into arginine and fumarate. The liver expresses all the enzymes required for the urea cycle. A multiprotein complex incorporating argininosuccinate synthase (ASS), a heat shock protein (HS90) as well as a cationic amino acid transporter (CAT-1) also contains ASL as one of its components (**Figure 2**). In addition to its catalytic role breaking down argininosuccinate, ASL has a crucial structural role in maintaining a multiprotein complex, that involves both CAT-1 and nitric oxide synthase (NOS). CAT-1 channels arginine from the extracellular space to the cytoplasm and delivers it to NOS in order to enable NO production [20]. ASL deficiency causes reduced arginine channelling to NOS and decreased arginine synthesis, subsequently causing NO deficiency [21].
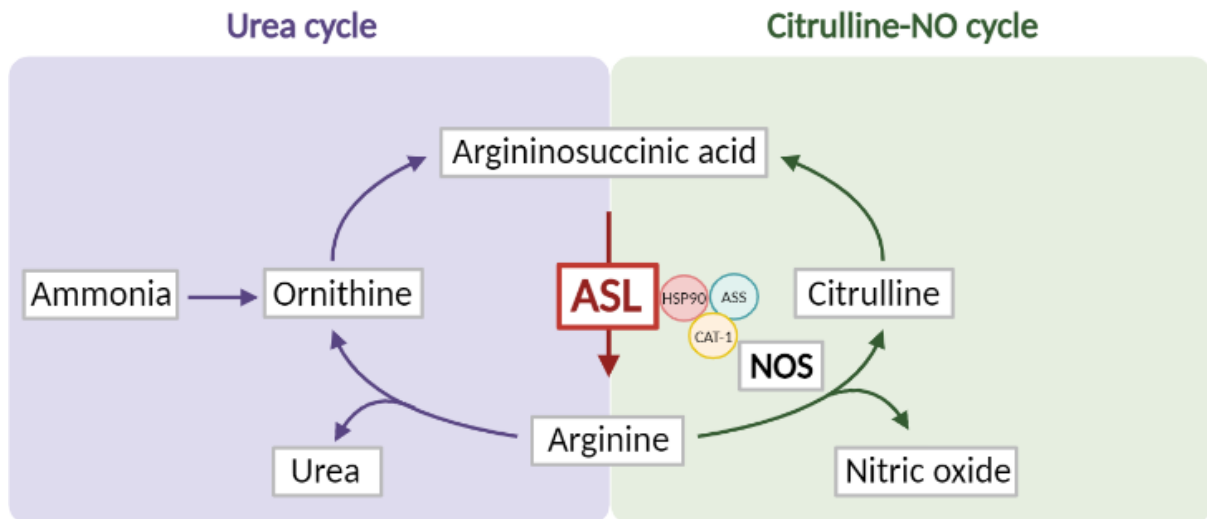
Figure 2. Metabolic pathways of argininosuccinate lyase. ASL: argininosuccinate lyase; ASS: argininosuccinate synthase; CAT-1: cationic amino acid transporter; HSP90: heat shock protein 90; NO: nitric oxide; NOS: nitric oxide synthase.

ASL is a homotetramer constructed by 4 different active enzymatic sites [22] with a total molecular weight of 187 kDa [23]. The enzymatically active ASL tetramer is predominantly composed of α helices and consists of 3 domains that differ in structure. Domains 1 and 3 share a comparable topology and feature 2 helix-turn-helix motifs, while domain 2 contains 9 helices, and 5 of them are responsible for the formation of the fundamental unit structure in an up-down-up-down-up sequence. [24]. The tetramer is formed when 2 pairs of dimers combine in an antiparallel orientation. The central core of the homotetramer comprises a bundle of 4 helices, and each individual subunit contributes one helix to the overall structure. Hydrophobic interactions between the 4 central helices, in conjunction with ionic interactions among arginine and glutamic acid residues on the 2 separate dimeric structures, play a crucial role in holding the tetramer together [24].

The human argininosuccinate lyase gene (*hASL*) that encodes ASL is located on the 7th chromosome (7q11.21) and includes 17,554 bp, split into 16 exons [23, 25]. *ASL* is a well conserved gene that is found in numerous mammalian species as well as birds, plants, yeast, and bacteria [24, 26, 27].

In humans, the endogenous arginine supply is enabled by ASL-dependent endogenous synthesis, that is predominantly involved in the kidney, or provided by exogenous nutritional intake [18]. Arginine is categorised as semi-essential amino acid since, under typical

physiological circumstances, its endogenous production is adequate to fulfil physiological requirements. However, individuals affected by ASA experience a reduction in arginine synthesis, resulting in arginine becoming an essential amino acid. This insufficiency further persists following liver transplantation, as the renal production of arginine is not adequately maintained in these patients. [28].

The "arginine paradox" illustrated the phenomenon when supplementation of exogenous arginine causes high levels of NOS-dependent production of NO, regardless of the fact that NOS is theoretically saturated with intracellular arginine levels [29]. The transport of arginine substrate to the NOS active site involves an intracellular compartmentalization or channelling effect. However, this feature is not present in ASA, as the deficiency of NO persists even after the administration of exogenous arginine. The importance of ASL in sustaining a multiprotein complex that includes the cationic amino acid transporter CAT-1, ASS1, ASL, and NOS was discovered, emphasizing its critical role. [20, 30]. Therefore, ASL is pivotal together as a catalyst for arginine production and as a structural component that upholds the multiprotein complex responsible for channelling arginine to NOS via NO [20].

1.2.2 Pathophysiology

Argininosuccinic aciduria (ASA) is a rare metabolic disease, and it is a result of ASL deficiency. ASA has an autosomal recessive pattern of inheritance and represents the second most frequent urea cycle defect, constituting 16% of all urea cycle disorders. ASA has a prevalence of ~ 1:100,000 live births, i.e., 11 and 73 new patients per year in the UK and the European Union, respectively [31].

Although the pathophysiology of ASA remains partially unknown, specific mechanisms can explain the disease phenotype (**Figure 3**).

27
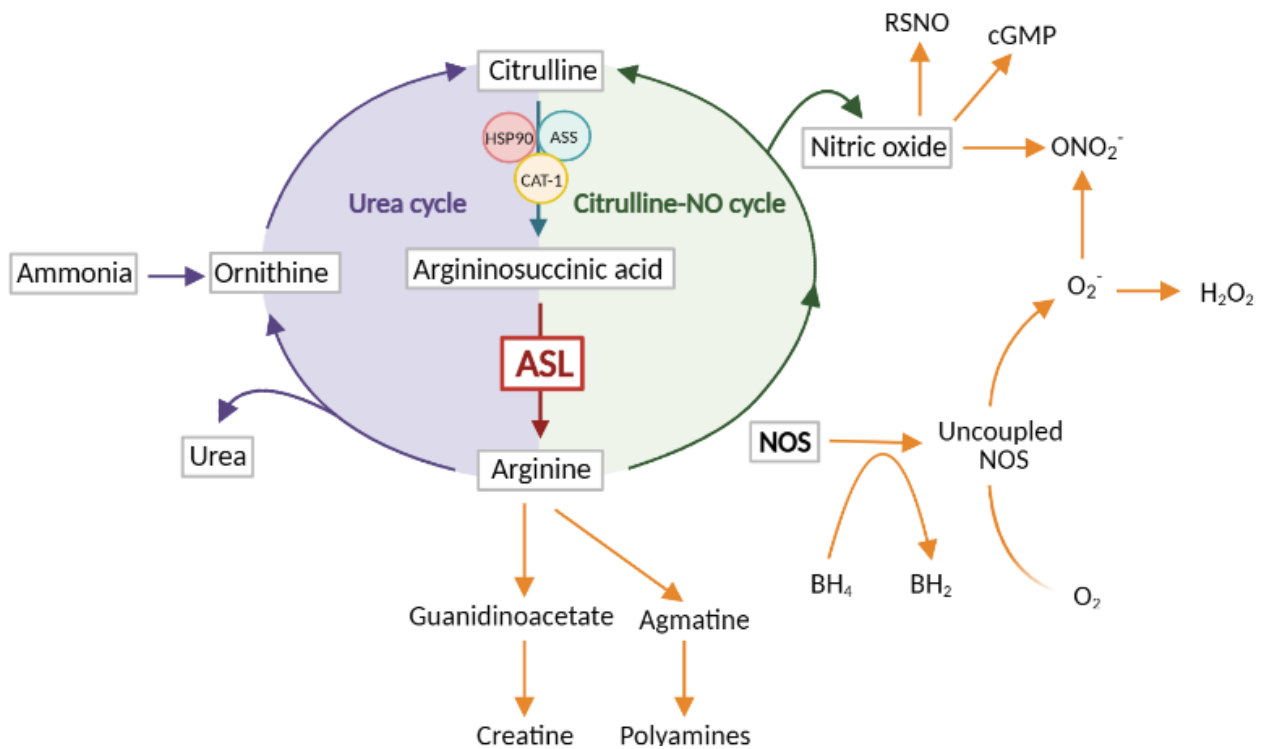
Figure 3. Pathophysiology of ASL deficiency. ASL: argininosuccinate lyase; ASS: argininosuccinate synthase; BH$_4$: tetrahydrobiopterin; cGMP: NO-cyclic guanosine monophosphate; H$_2$O$_2$: hydrogen peroxide; NO: nitric oxide; NOS: nitric oxide synthase; O$_2^-$: superoxide ion; ONO$_2^-$: peroxynitrite; RSNO: nitrosothiols.

a) Hyperammonaemia

Ammonia is a highly neurotoxic compound [32]. In case of hyperammonaemia, there is a large increase in cerebral glutamine content, but only minor shifts in glutamate and α-ketoglutarate levels. Increased levels of glutamate and glutamine will present various detrimental effects. High levels of intracellular glutamate, the major excitatory neurotransmitter, activate the N-methyl-D-aspartate (NMDA) receptors and trigger apoptosis [33]. Elevated levels of glutamine can lead to an osmotic effect, leading to the swelling of astrocytes and cerebral cytotoxic oedema. Such swelling is linked to astrocytic dysfunction, which impairs osmoregulation and leads to cerebral oedema, heightened intracranial pressure, and, in severe cases, brain herniation. [34-36].

b) Arginine deficiency

Arginine is regarded as conditionally essential in ASA, as its deficiency can impact various physiological pathways as a result of its function as a substrate for protein synthesis and a precursor for vital compounds including NO, polyamines, proline, glutamate, creatine, as well as agmatine. Therefore, a deficiency of arginine can disrupt the synthesis of its downstream metabolites, leading to altered physiological functions. [37, 38]. Hypoargininaemia also disturbs the synthesis of arginine-enriched collagen structures, such as hair [18].

c) NO deficiency

ASA is the only inherited disease known for generating systemic NO deficiency [20]. NO signalling is mediated by the pathway of NO-cyclic guanosine monophosphate (cGMP). It also generates nitrosothiols (RSNO) by protein nitrosylation. NOS enables NO synthesis from arginine. NOS is a dimer that can uncouple into 2 distinct monomers in particular conditions including arginine or tetrahydrobiopterin (BH_4) deficiency (**Figure 4**) [39]. Arginine deficiency in ASA leads to NOS uncoupling, resulting in the generation of superoxide. This alteration in NOS-dependent NO production requires cells to rely on NOS-independent NO production via the nitrite-NO pathway. The uncoupling of NOS, generating superoxide and reactive oxygen species, leads to elevated levels of nitrosative stress (**Figure 4**) [21].
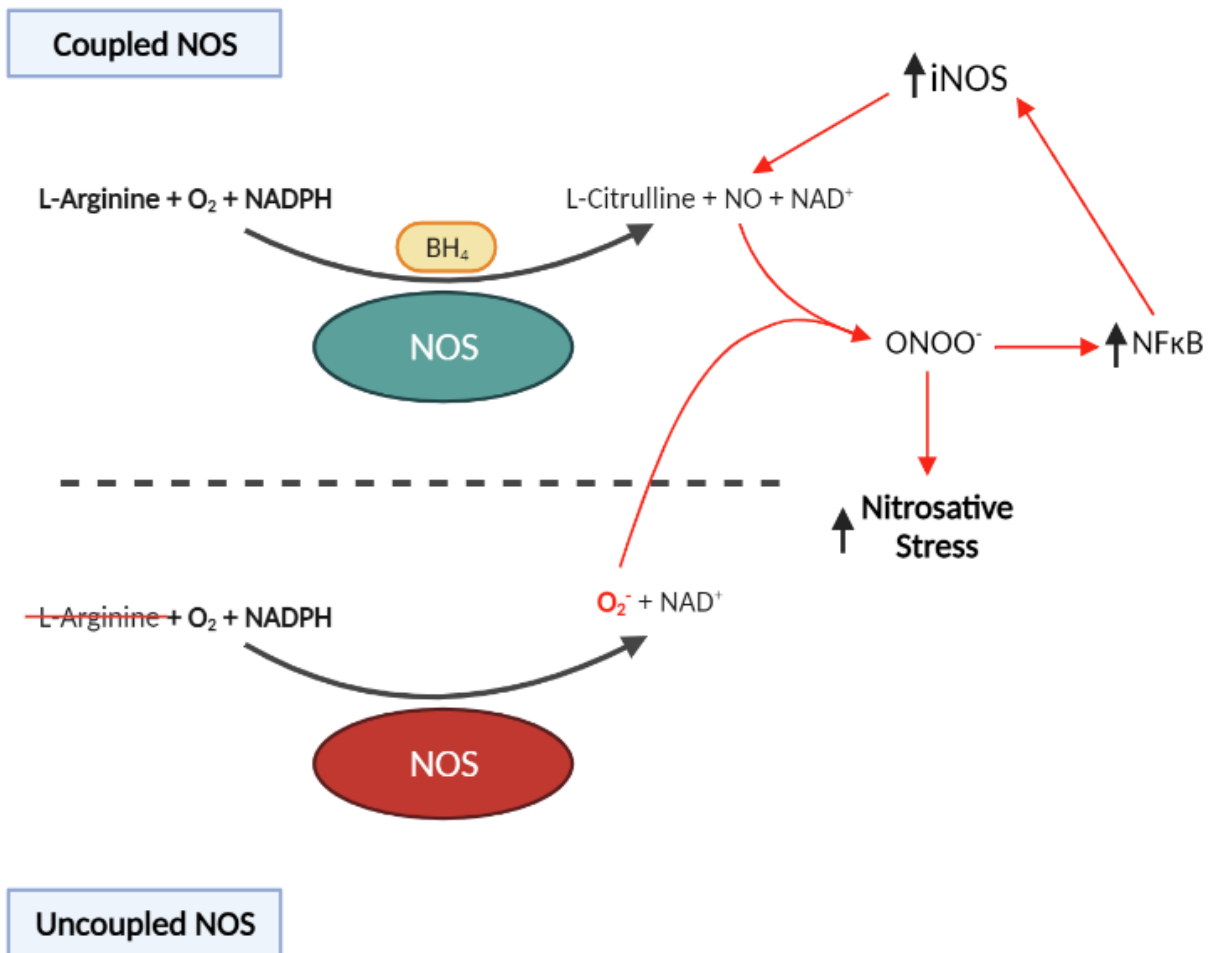
Figure 4. Uncoupling of NOS and generation of nitrosative stress. BH_4: tetrahydrobiopterin; iNOS: inducible nitric oxide synthase; NADPH: nicotinamide adenine dinucleotide phosphate; NFκB: nuclear factor kappa B; NO: nitric oxide; NOS: nitric oxide synthase; O_2^-: superoxide; $ONOO^-$: peroxynitrite;.

d) Creatine deficiency and increased guanidinoacetate levels

Creatine is a naturally occurring nitrogenous organic acid. Brain synthesises creatine, although most of the total body synthesis occurs in kidney, pancreas, liver, and muscle. Arginine is a precursor of creatine. A secondary creatine deficiency subsequent to reduced arginine levels can cause cerebral energy deficiency. This is most likely to take place in neurons [40] and changes the production of both respiratory chain and ATP [41]. This can lead to inhibition of sodium (Na), K-ATPase activities and cell apoptosis [42]. Higher concentrations of guanidinoacetate and creatine in plasma and urine can be observed after arginine supplementation in ASA patients [32, 43, 44].

e) Direct ASA toxicity

Argininosuccinate and guanidinosuccinate (GSA) are proposed to have a toxic role in pathophysiology of ASA. High doses of arginine supplementation in ASA patients is associated with increased levels of argininosuccinate and transaminases compared to low doses [45]. This suggests the direct liver toxicity of ASA. Similarly, early-onset patients who present significantly higher argininosuccinate levels show a more severe chronic liver disease suggesting that ASA might contribute to hepatic toxicity [21, 46].

f) Oxidative/nitrosative stress

Brain analysis of ASL-deficient $Asl^{Neo/Neo}$ mice shows elevated downstream NO metabolites, nitrite and nitrate, oxidative stress markers, and the neuronal accumulation of nitrotyrosine, a biomarker of nitrosative stress. The generation of reactive oxygen species, including superoxide from uncoupled NOS enables the generation of peroxynitrite [20, 47-49]. Peroxynitrite reacts with tyrosine motifs and produces nitrotyrosine, which is responsible for structural alteration and inactivation of proteins [50]. Neurons are highly vulnerable to oxidative and nitrosative stress, as they depend on reduced glutathione supply from astrocytes (**Figure 4**) [51]. Increased oxidative stress biomarkers can also be observed in other organs such as the liver and in biofluids such as plasma and urine [20, 47].

1.2.3 Clinical phenotype

Patients with ASL deficiency can be divided into two categories: early-onset (symptoms observed by day 28 of life) and late-onset (symptoms observed from 28 days following birth) patients [52]. Patients may exhibit two main presentations of ASA that include, neonatal hyperammonaemic coma, which can be fatal, or a wide phenotypic spectrum that ranges from hyperammonaemic crisis to chronic phenotype. The chronic phenotype may include symptoms such as neurocognitive, gastrointestinal, and liver manifestations, with or without hyperammonaemia [18]. As detailed below, various organs can be affected in ASA.

a) Liver

Half of the patients with ASA show liver associated symptoms predominantly affecting early-onset cases [21]. Chronic hepatomegaly and increased transaminases are the most frequent liver related symptoms [21, 53, 54] and can be the first sign leading to diagnosis [55]. Hepatomegaly can worsen during hyperammonaemia episodes and can be observed from the first days of life. Therapies controlling ammonaemia have not shown an effect on hepatomegaly [56]. Mild liver failure *i.e.* impairment of liver synthetic function can also be detected [57]. Both fibrosis and cirrhosis have been recorded and can be life-threatening [55, 57, 58]. Hepatocellular carcinoma can rarely be a complication of ASA liver phenotype [21]. Findings from liver biopsies often show either no abnormality, or a specific change similar to other urea cycle diseases. These features include enlarged hepatocytes [33, 55, 59], cholestasis, inflammation [33, 59], glycogen deposits [54, 55], cirrhosis [57], or fibrosis [55, 60]. It has been proposed that the supplementation with essential amino acid mixtures enriched with leucine as well as diet with high carbohydrate content could as well partially contribute [61]. Findings from electron microscopy revealed enlarged mitochondria with dense matrix and tubular cristae indicating mitochondria dysfunction [54].

b) Central nervous system

Over 90% of patients present a neurological disease, which can be identified in both early- and late-onset patients [21]. A broad spectrum of intensity characterizes neurocognitive dysfunction, ranging from borderline IQ to profound intellectual disability [21, 53, 62, 63]. Several subsets of neurodevelopment can be impacted, including gross and fine motor skills, speech, learning, memory, and attention span [21, 53]. The recognition of neurocognitive difficulties takes place usually early within the second year of life [53, 64, 65]. Epilepsy is a major ASA manifestation detected in 40% of ASA patients, and is described with tonic-clonic, clonic or myoclonic seizures [21, 65]. Neonatal seizures can also occur in early-onset patients and are often the consequence of hyperammonaemia. These neonatal seizures can as well present with subclinical manifestations with electroencephalographic seizures only. Neonatal seizures are not a prognostic indicator for the development of epilepsy later in life [66]. Ataxia, hypotonia, and tremor represent regular characteristics in late-onset ASA patients, including cerebellar dysphonia and dysarthria [63]. Behavioural and psychiatric complications

can occur in ASA patients covering a broad spectrum, including hyperactivity, auto-aggression with self-mutilation, autism, paranoia, psychosis or even schizophrenia [63, 67].

c) Systemic hypertension

Hypertension can occur in both early- and late-onset ASA patients. There is no link between age-onset presentation or hypertension severity [68]. Arterial hypertension in ASA is expected to have a low prevalence [68]. NO deficiency affecting endothelial cells causes hypertension. Indeed, systemic NO deficiency leads to reduce of the physiological NO-mediated vascular vasodilatation following acetylcholine-induced relaxation [20]. Earlier research has connected arterial hypertension with reduced endothelial NOS (eNOS)-dependent NO production in endothelial cells, which can lead to abnormal relaxation of major blood vessels, including the aorta, as seen in the ASA mouse model [47].

d) Hair and skin

Late-onset untreated ASA patients present brittle hair, that includes trichorrhexis nodosa which causes the hair to break off easily, monilethrix that affects hair growth, and pili torti where the hair shaft is compressed at irregular intervals and coiled around its axis. These hair abnormalities can be an isolated phenomenon or associated with genetic diseases such as ASA [69-71]. Facial and genital dermatitis can also occur in patients [53, 72]. Defective immunity with loss of NO antimicrobicidal activity has been suspected to account for disease manifestation [73]. Arginine is an essential amino acid in ASA, and its impaired function is a result of ASL deficiency in patients. Hair consists of 10.5% of arginine. Subsequently chronic hypoargininaemia is likely to have a role in hair and skin abnormalities in ASA patients [18].

e) Asymptomatic

Some ASA patients present with no clinical disease and a phenotype limited to the excretion of argininosuccinate, which enables the diagnosis of ASA. A recent study showed that 36% of ASA patients have been diagnosed through a dedicated newborn screening programme with this clinically asymptomatic presentation [73].

1.2.4 ASA Diagnosis

Hyperammonaemia is a key biomarker in urea cycle disorders. Ammonia levels in severe hyperammonaemia can reach 4,500μM in neonatal-onset disease for a normal level < 100μM in neonates [65]. However late-onset patients can present with normal ammonia levels [21]. It is possible that the relatively lower incidence of chronic hyperammonaemia and acute hyperammonaemic decompensations in ASA in comparison to other proximal urea cycle defects such as CPS1 deficiency, OTC deficiency or ASS deficiency, is due to the ability of argininosuccinate, which contains 2 nitrogen moieties, to facilitate partial nitrogen detoxification. As a result, there may be less frequent use of ammonia scavenger drugs in ASA [73-75], in contrast to other urea cycle defects.

In urea cycle disorders, the plasma concentrations of the urea cycle related amino acids can help identifying the enzymatic block in the pathway. ASA causes an increase of argininosuccinic acid in all biofluids [64]. ASA patients may exhibit argininosuccinic acid levels that are twice as high in cerebrospinal fluid as compared to plasma [62]. Plasma amino acids show increased levels of citrulline and argininosuccinic acid as well as significantly reduced levels of arginine [64]. Increased levels of glutamine and glutamate in the plasma are indirect biomarkers of hyperammonaemia [76].

Prenatal diagnosis is available by amniocentesis or fetal blood sampling by DNA sequencing or argininosuccinate lyase enzymatic analysis [77].

1.2.5 Therapeutics

a) Protein restricted diet

A protein-restricted diet is critical in the management of ASA patients. This enables to decrease ammonia production from protein catabolism [78]. To avoid any nutritional deficiencies, supplements with high content of vitamins, energy and trace elements are prescribed following standard age-related specifications in addition to continuous examining

of the patients. Because chronic protein restriction can result in severe amino acid imbalance, trigger catabolism and subsequently hyperammonaemia, supplementation with essential amino acids is recommended during excessively low protein consumption to maintain healthy growth and metabolic control [17]. High doses of sodium phenylbutyrate, an ammonia scavenger, can lead to a decrease of branched chain amino acids [79]. With this protein-restricted diet, patients have a better control of ammonia levels, however it does not cure the disease [80].

b) Ammonia scavengers

These drugs, sodium benzoate, sodium phenylbutyrate and glycerol phenylbutyrate, are prescribed on a daily basis for controlling ammonia levels and are the only approved drugs for urea cycle disorders [81].

c) Arginine supplementation

Arginine supplementation aims to compensate hypoargininaemia and is prescribed in multiple doses daily. The suggested course of action is to determine the minimum effective dose required to normalize arginine levels [82], as high doses (500mg/kg/day) can cause hepatitis and increase both argininosuccinate and transaminases levels [45].

d) Creatine

Creatine is a downstream metabolite of arginine. Arginine deficiency can cause secondary creatine deficiency in urea cycle diseases. Monitoring of plasma creatine concentration is necessary in ASA [43]. Creatine supplementation is a potential therapeutic option [31].

e) NO donors

Several studies in ASL-deficient murine models and induced pluripotent stem cells, have shown that dysregulation of NO signalling contributes to the ASA phenotype [20, 47, 83, 84]. A supplementation strategy, using the NOS-independent NO pathway, promotes weight-gain and survival, and improves the hypertension and the endothelial dysfunction in ASL-deficient mice [20, 84].

NO supplementation is oxidized in nitrate and nitrite, which can in turn be reduced in NO in blood and tissues [85, 86]. The pathway of nitrate-nitrite-NO is an alternative to generate NO by bypassing NOS (**Figure 5**). Nitrate releasing drugs are therapies developed for cardiovascular diseases, such as peripheral vascular disease, myocardial infarction and both systemic and pulmonary hypertension [86-89]. An ASA patient with refractory arterial hypertension despite multiple antihypertensive medication treatments, was successfully controlled with isosorbide dinitrate supplementation and subsequently with a customized inorganic nitrite formulation, which enabled to control his hypertension whilst stopping his other anti-hypertensive therapies [47]. Furthermore, NO supplementation showed an improvement in some neuropsychological parameters. Building upon these outcomes, NO supplementation is currently in phase I/II clinical trials in ASA patients [90].
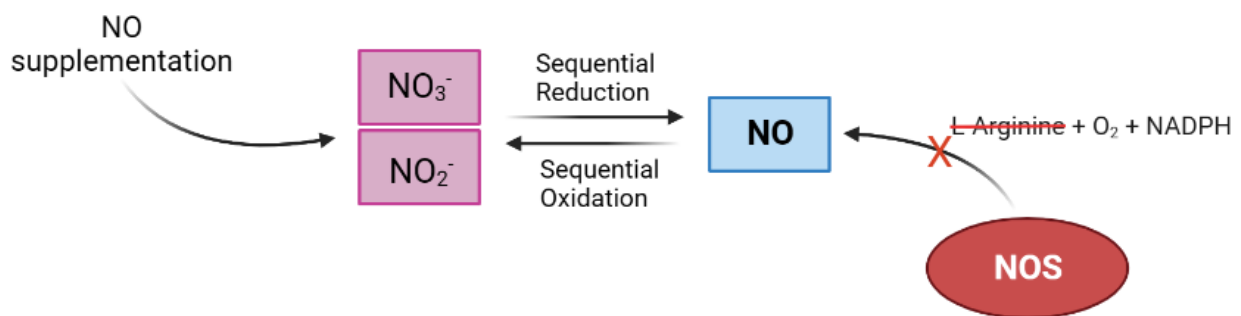
Figure 5. Pathway of nitrate-nitrite for NO generation in ASA. NADPH: nicotinamide adenine dinucleotide phosphate; NO: nitric oxide; NO_2^-: nitrite; NO_3^-: nitrate; NOS: nitric oxide synthase; O_2^-: superoxide.

f) Gene Therapy

Gene therapy has emerged as an appealing substitute for transplantation in the management of hereditary liver disorders [91]. Serotype 8 adeno-associated viral (AAV) and adenoviral vectors carrying murine or human *ASL* transgene have demonstrated effectiveness regarding the normalisation of ureagenesis in ASL-deficient mice [47, 83, 92]. Improvement of survival along with normalisation of ammonia levels have been maintained for up to 1 year following a single systemic administration in adult mice [83]. Specific liver-directed gene therapy could normalize ureagenesis and cure the urea cycle disorders, especially for patients who are at an elevated risk of developing hyperammonaemic decompensation.

Also, a liver-targeting gene therapy approach could improve partially the neurological disease as shown in ASL-deficient mice and in liver-transplanted ASA patients [57, 83, 93]. However, a full correction of the primary neurological disease in ASA requires a normalization of hepatic ureagenesis to prevent hyperammonaemia and a restoration of the ASL activity in cerebral neurons [31]. Similar findings have been shown in ASA mice, where ureagenesis normalisation in the mice did not show full correction of the neurological disease [83, 94].

1.2.6 Liver Transplantation

The urea cycle defect in ASA patients can be treated by liver transplantation, making it a feasible treatment option that has been considered. By acting as an enzyme replacement therapy, liver transplantation facilitates the normalization of ammonaemia, which in turn leads to the reinstatement of a functional urea cycle. As a result, liver transplanted patients can normalise their diet and stop their ammonia scavengers without risking an acute decompensation. An improvement of the neurological development can be observed with a greater metabolic control of ammonia; however neurologic issues remain [93], even in cases where the liver transplantation is completed at an early-stage of the disease in infancy [57]. Although a liver transplant can prevent long-term neurological complications related to high ammonia levels, it cannot correct the elevated levels of argininosuccinic acid and citrulline in the bloodstream. Arginine, which is essential for the body, still depends on the kidney to synthesize it as the deficiency of argininosuccinate lyase remains in tissues outside of the liver [57]. Limited evidence is available about the long-term benefits on the neurological outcome following liver transplantation. Up to date, over 30 ASA patients have received liver transplantation [57, 93, 95-101]. However, publications are essentially reporting procedure-related issues and the dramatic effect on restoring ureagenesis, but the information available is severely limited on long-term neurological assessments.

1.3 The *Asl^Neo/Neo* animal model

The fist *Asl* hypomorphic mouse model was generated by Reid-Sutton *et al.*, in 2003 [102]. This ASA mouse model however, presented with a very severe phenotype with early hyperammonaemia leading to early death (~48 hours after birth). In addition, mutants only had 2 to 5% of wild-type residual ASL activity in the liver. Despite that, animals presented with normal levels of nitrite or creatine metabolites possibly due to early death [102].

Another mouse model was subsequently generated with a conditional hypomorphic allele by the addition of a Neomycin (*Neo*) selection cassette into the intron 9 of the mouse *Asl* gene [20]. The *Neo* resistance gene cassette served as an identifier for cells in which the target gene disruption was successful via homologous recombination. The homologous recombination process inserted locus of X-over P1 (loxP) sites at specific locations within introns 6 and 9 of the targeting construct. Additionally, upstream of the 3' loxP site within intron 9, the *Neo* selection cassette, encompassed by flippase recombination target (FRT) sites, was introduced. Insertion of an expression cassette into the intron induced a hypomorphic allele through transcriptional interference [103, 104]. Mice that are homozygotes for the hypomorphic *Asl* mutations are born at the expected Mendelian pattern, however they typically exhibit a short lifespan from multi-organ failure within the first 3-4 weeks post-birth. The *Asl^Neo/Neo* mouse model effectively mimics the human phenotype, as evidenced by hyperammonaemia, pronounced multi-organ dysfunction, and systemic NO deficiency, coupled with a reduction in markers indicative of NO production and abnormal flow-mediated vascular relaxation. Notably, 75% of the *Asl^Neo/Neo* mice do not survive beyond the third week of life. *Asl^Neo/Neo* homozygotes, exhibit substantial decreases in both gene and protein expression. The residual RNA and protein is 25%, while the residual ASL enzymatic activity is 16% of the original level in the liver [31] and brain [83].

1.4 Gene therapy in monogenic disorders

Different treatment technologies have been developed over time including gene editing strategies, and gene addition therapies **(Table 2)**. For gene editing strategy, nucleases such as Cas9 are used to create DNA cuts or base editing at precise locations, which result in gene silencing, gene addition or *in situ* correction of mutations [105]. However, off-target effects create a risk of carcinogenesis and the maturation towards *in vivo* application remains limited [105]. Gene addition treatments allow the correction of the phenotype for monogenic diseases including ASA. Correction with gene addition strategy is performed by inserting a safe copy of the transgene into the cells of interest to address a clinical need of the disease by using viral and non-viral vectors [106].

1.4.1 Strategies for gene transfer

Gene transfer for therapeutic benefit has been in development for almost 50 years [107]. The fundamental concept of gene therapy involves identifying a faulty or absent gene responsible for a necessary protein in a patient with a genetic disease. This gene is then incorporated into a modified virus's genetic material, creating a viral vector that can introduce the new genetic material into the patient's cells.

Various gene delivery strategies have been established over time with non-viral and viral vectors, with different features summarised in **Table 2** [108].

a) Vector construct

Gene therapy vectors are essential tools for delivering therapeutic genes into target cells, and their efficacy depends on multiple factors, including (i) the transgene cassette which design is critical for genetic expression [109], (ii) the viral capsid and/or envelope which enhances the potency of gene transfer by determining the cell-specific expression of the vector [110] and iii) the 'regulatory cassette' referring to the collection of genetic elements such as

enhancers, promoters, and auxiliary components controlling the manner that the introduced gene functions in the host's cells. This function can be short-term or long-term, with the gene being separate from the host's chromosomes or integrated into them [111].

The delivery of the transgene cassette into the host cell does not require presence of an envelope. [112]. Hence, various strategies for transferring genes to target cells have been generated, involving the use of non-enveloped DNA, viral or non-viral vectors.

Naked DNA refers to plasmid DNA not packaged in a protective envelope or coat, which is administered without a delivery vehicle. The main advantages of this gene delivery system include ease of production, ability to transfer large transgene cassettes showing sustained transgene expression in non-dividing cells [113, 114], absence of immune response to viral proteins and having safety profile with no risk of viral replication [113]. However, naked DNA also has several limitations, including low efficiency of transduction and susceptibility to degradation by nucleases, limiting its potential to achieve phenotypic correction in monogenic disorders.

Chemically engineered nanoparticles such as liposomes or polymers can be utilized in non-viral vectors to create bioparticles that encapsulate the transgene, as opposed to viral vectors, which use modified viruses for gene delivery. [115]. Their main advantages include safety, low immunogenicity, no transgene size restriction, and easy production making this approach appealing [116]. However, major limitation of non-viral vectors is the absence of long-lasting transgene expression [117].

The use of viral vectors for therapeutic transgene delivery is a popular approach, as viruses have evolved to efficiently transport their genetic material into host cells. Adenoviral, AAV, as well as lentiviral vectors include some of the most common viral vectors used in clinical trials. Many types of viral vectors have been established and are currently being assessed for clinical translation (**Table 2**) [118].

The design of an expression cassette in a gene therapy vector varies significantly based on the type of vector and the therapeutic application, though common elements can be found across different systems. For instance, promoters such as the cytomegalovirus (CMV) promoter, are ubiquitous components found in a range of vectors such as lentiviral, adenoviral, plasmid, and

AAV vectors due to their broad activity and stable, long-term expression [119, 120]. The immediate early promoter, CMV, is extensively utilized for the expression of transgenes both *in vivo* and *in vitro*. It has also been adapted for use in clinical trials targeting the CNS [121, 122]. These elements facilitate the initiation of transcription for the gene of interest, the critical therapeutic protein.

Incorporation of polyadenylation signals, include the Simian Virus 40 (SV40) polyA, a feature found across various vector platforms. SV40 polyA signal is recognized and employed by the host's RNA polymerase II complex. This facilitates the processing of precursor mRNA leading to increased stability of the mature mRNA as well as enhanced efficiency of mRNA translation in eukaryotic cells [123, 124]. Transcription rates are modulated by enhancers and silencers, such as the Woodchuck Hepatitis Virus Posttranscriptional Regulatory Element (WPRE) in a variety of vectors including lentiviral vectors [125-127]. WPRE has been shown to improve expression by modification of RNA polyadenylation, export and translation [125, 128, 129]. Kozak sequences are another universal feature encouraging the initiation of protein synthesis by positioning the start codon (AUG) in the mRNA in the right location for the ribosome to start translation [130, 131]. The presence of a Kozak sequence enhances the efficiency of translation initiation, leading to a greater expression of the protein encoded by the mRNA [132].

Multiple cloning sites, short segment of DNA which contains several restriction sites, simplify insertion of the therapeutic gene [133] and a selection marker, such as a neomycin resistance gene, identifies successfully transduced cells.

Insulator sequences, such as the cHS4 insulators, shield the therapeutic gene from the influence of neighbouring genomic sequences, enhancing reliable expression. Insulators can block the spread of heterochromatin, maintain active chromatin, and prevent enhancers or silencers from acting on the gene of interest [134-136].
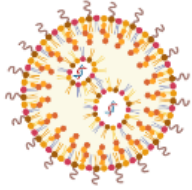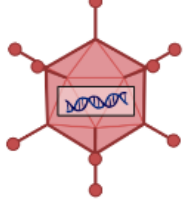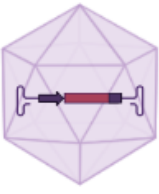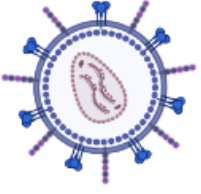
	Non-viral	Adenovirus	AAV	Lentivirus
Cargo	DNA/RNA/Protein	dsDNA	ssDNA	ssRNA
Transgene size	No limit	37kb	4.7kb	14kb
Chromosomal Integration	No	No	Rare	Yes
Expression longevity	Transient	Transient	Long-Lasting*	Long-Lasting
Safety concerns	No	Inflammatory Response/ Toxicity	Inflammatory Response/ Toxicity	Risk of Insertional Mutagenesis
Cons	Re-administration	Inflammation	Loss of transgene in dividing cells	Possible insertional mutagenesis limited with SIN-lentivirus

Table 2. Overview of non-viral, adenoviral, AAV and lentivirus gene therapy strategies [137].

*Transient in rapidly dividing cell population.

b) Vector delivery

A successful gene therapy depends on the delivery of therapeutic genes to the target tissues or cells offering high specificity and efficiency, while minimizing the risk of toxicity and immune response.

The minimal effective dose of a gene therapy vector is the smallest amount needed to accomplish a treatment. Lower doses of the gene therapy vector are desirable, as they can reduce the potential for toxicity and immune response [138, 139]. However, low dose might not achieve the high transgene expression which is vital for the correction of the severe phenotype in monogenic disorders [140].

Delivery route is another important factor that can influence the efficacy and safety of gene therapy, the distribution and persistence of the vector, as well as the risk of immune response. Local injection of the gene therapy vector is able to reach the target cells easier restricting the loss of the vector by distribution in other organs and immune response [141]. When targeting the liver for gene therapy, administering the therapy via intravenous injection yields liver transduction levels similar to those obtained with intraportal or intrahepatic routes [142-144]. The direct administration of gene therapy vector in the animal or patient is called *in vivo* gene therapy.

Ex vivo gene therapy involves the extraction of specific cells derived from the patient, that are then transduced with the gene therapy vector in a laboratory setting, followed by the reintroduction of the genetically modified cells back into the patient or animal. This approach has proven to be effective, particularly using vectors that are able to integrate into the host cell such as retroviral and lentiviral vectors for treating X-linked severe combined immunodeficiency (SCID-X1) [145], X-linked adrenoleukodystrophy [146] and metachromatic leukodystrophy [147], respectively.

c) Host immune response

The immune reaction of the host to gene therapy vectors can be classified into the innate and adaptive immune responses. The innate immune system serves as the initial defence mechanism against foreign invaders, and it can be activated by the vector itself or by cellular

damage caused by the vector. Adaptive immune response is a more precise response that is directed against specific components of the vector or the transgene [148].

The innate immune response can be triggered by the vector by different ways. One mechanism is the activation of toll-like receptors (TLRs), which recognize conserved motifs present in the vector or the transgene [149]. For example, adenoviral vectors can activate TLR-9 through their cytosine–guanine dinucleotide (CpG) motifs, resulting in the generation of cytokines with inflammatory properties and the attraction of immune cells can result in severe adverse events, similar to those seen in clinical trials for OTC deficiency [138] or hemophilia A [150]. Another mechanism is the activation of the complement system, which is triggered by the vector surface proteins or by the transgene. This has been shown with lentiviral vectors through the activation of the complement membrane attack complex, which forms pores on the vector surface and causes its destruction [151-153]. Another way in which the complement system can affect lentiviral vectors is through the recruitment of immune cells [154, 155]. It has been previously shown that complement activation can lead to the recruitment of macrophages at the site of vector administration, which can phagocytose and eliminate lentiviral vector leading to reduced transduction efficiency [156].

The adaptive immune response against gene therapy vectors can be directed to the vector or the transgene. The vector-specific immune response is directed against the vector surface proteins or the viral genome, and it can lead to vector neutralization or the generation of anti-vector antibodies [157]. The immune response directed against the therapeutic gene product, can lead to the generation of anti-transgene antibodies or T cell responses [158]. It was previously suggested that the adaptive immune response is initiated by the recognition of AAV vectors as foreign antigens by antigen-presenting cells, such as dendritic cells [158]. These cells then present the AAV antigens to T cells, which can become activated, proliferate, and initiate an immune response against the vector. For example, findings from previous studies have described that AAV vectors can trigger both CD4+ and CD8+ T cell responses, which can lead to the generation of pro-inflammatory cytokines and the activation of cytotoxic T cells that can eliminate transduced cells [159-161].

1.4.2 Clinical applications of gene therapy vectors

a) Non-viral vectors

Non-viral vectors are synthetic 'vehicles' with the ability to encapsulate other therapeutic complexes including nucleic acids and deliver them to the site of interest [117]. These nanoparticles have several advantages such as low immunogenicity, potential to deliver larger genetic payloads and simple production [162, 163]. The proof of concept of mRNA therapy carried by non-viral vectors to treat liver inherited metabolic diseases has been rapidly increasing [94, 164-167]. In 2017, intravenous administration of mRNA encoding the human methylmalonyl-CoA mutase (*hMUT)* gene encapsulated in lipid nanoparticles (LNP) showed 75%-85% reduction in plasma methylmalonic acid in 2 different mouse models of methylmalonic acidemia (MMA) [164]. Subsequently, a 12-week study with repeated intravenous dosing of *hMUT* mRNA LNP in 2 murine models of MMA showed substantially improved survival and growth of treated animals with no adverse effects [166]. Recently, it has been reported that hASL mRNA LNPs were able to rescue and correct the neonatal and adult ASL-deficient mouse phenotypes, respectively. This was achieved by enhancing ureagenesis and the metabolism of glutathione, as well as by correcting the chronic liver disease [94]. While mRNA LNPs are showing great promise regarding efficacy in gene therapy, a vital limitation includes their temporary gene expression, requiring repeated administration to maintain the efficacy [117].

b) Adenoviruses

Adenovirus is a DNA virus with a double-stranded genome that has been extensively investigated for its therapeutic potential due to its well-established biology, genetic stability, high efficiency in transducing cells, and ability to be produced on a large scale [168-170]. Adenoviruses are viruses that do not contain envelope, carrying linear double-stranded DNA genome. These viruses can enable transduction of several different cell types, including dividing and non-dividing cells, while having a 36kb long transgene cassette. Adenoviruses can trigger a sustained innate and cytotoxic-mediated immunity, that may lead to the rapid elimination of transduced cells [171, 172].

The first gene therapy treatment of adenoviral vectors in humans was successfully reported in 1992 in AAT-deficient patients [173]. Intraportal infusion of AAT maintained elevated serum levels of human AAT for 4 weeks [173]. Then adenoviral vectors were used for delivering deficient or dysfunctional genes, as a gene therapy treatment. Cystic fibrosis is an example where a mutated cystic fibrosis transmembrane conductance regulator (*CFTR*) gene was inserted by an adenoviral vector to generate long-term expression of the human CFTR in the airway epithelia of immunocompetent mice [174]. In a different study, *OTC* gene was delivered via adenoviral vectors, however, these studies had challenges such as triggering of humoral and cellular immune responses against adenoviral capsid peptides, cellular cytotoxicity, and oncogenesis, raising concerns regarding the virus safety [175, 176]. As a result, immune reaction to the virus led to the tragic death of Jesse Gelsinger following adenoviral treatment for OTC clinical trial [177].

c) AAV vectors

AAV is a non-enveloped vector whose virion consists of a 25nm diameter icosahedron encompassing a 4.7kb single-stranded DNA genome, that incorporate the replication (*rep*) and capsid (*cap*) genes flanked by 2 inverted terminal repeats [178, 179]. The *rep* gene encodes, from a single open reading frame (ORF), Rep78, Rep68, Rep52 and Rep40, that enable the replication of the AAV genome, and the virion assembly. The *cap* gene generates the 3 capsid proteins viral protein 1 (VP1), VP2 and VP3 and assembly-activating protein (AAP) and membrane-associated accessory protein (MAAP).

During the early 2000s, a new family of naturally occurring primate AAV serotypes and variants was discovered, which significantly expanded the number of wild-type AAV capsids available. As a result, the AAV toolkit was expanded to include specific organ tropism for each serotype. [180, 181]. This is due to the virus ability to invade cells through initial interactions with capsid-specific glycoproteins found on the surface of target cells acting as receptors and co-receptors [178, 182]. Slight differences in sugar-binding preferences, can determine different cell-type transduction of the different AAV variants [178, 183]. Up to date, 13 different wild-type AAV capsids have been identified and classified [184, 185].

The number of gene therapy studies using AAV vector *in vivo* in human and animal models focusing on liver monogenic disorders, such as urea cycle defects, phenylketonuria, homozygous familial hypercholesterolemia, primary hyperoxaluria type I, long chain fatty acid oxidation disorders and progressive familial intrahepatic cholestasis is rapidly increasing [186, 187].

Various clinical trials have occurred during the last 15 years, many of them including multiple hemophilia gene therapy strategies [188, 189]. A study conducted in 2004, administered AAV vector serotype 2, and showed an increase of plasma factor IX (FIX) that varied from <1% to 11% for 4 weeks post administration; however, that was followed by a slow decline due to cellular immune response against hepatocytes [190]. Few years later, a single intravenous infusion of serotype 2/8 AAV vector enabled long-term expression for up to 10 years and increase of plasma FIX up to 8% [191]. Following years of drug development, the FDA has granted priority review to the Biologics License Application for etranacogene dezaparvovec, which could be a potential treatment for managing hemophilia B [192, 193]. In addition, in June 2022, the European Medicines Agency recommended conditional marketing authorization for valoctocogene roxaparvovec, representing the initial gene therapy for addressing severe hemophilia A [194, 195]. Gene augmentation using AAV has demonstrated therapeutic efficacy in preclinical studies of various genetic metabolic liver diseases, such as familial hypercholesterolemia [196], Crigler-Najjar syndrome [197], OTC deficiency [198], phenylketonuria [199], Wilson disease [200], acute intermittent porphyria [201], progressive familial intrahepatic cholestasis [202], glycogen storage disease type Ia (GSD1a) [203], and MMA [204]. Many of these clinical trials have shown promising clinical outcomes. For example, AAV-OTC treatment showed positive responses in 6 out of 9 patients with OTC deficiency, with 3 being complete responders [193]. Furthermore, administration of AAV-based gene therapy containing the PAH gene has been discovered to cause substantial reduction in the levels of phenylalanine and increase in tyrosine levels in phenylketonuria patients [193]. Clinical trials focusing on AAV-mediated delivery of uridine diphosphate glucuronosyltransferase 1A1 (UGT1A1) enzyme in Crigler-Najjar syndrome patients have shown promising outcomes, with the highest doses leading to lower bilirubin levels and enabling 2 out of 3 patients to discontinue phototherapy. [193]. However, due to the fact that AAV vectors do not integrate into the host cell's genome and are subject to anti-AAV immune

responses that restrict vector re-administration [91], utilizing this form of gene therapy for paediatric patients may pose challenges.

Over the past few years, there has been growing concern regarding the safety of AAV vector gene therapy. A recent study, which followed hemophilia A dogs treated with AAV gene therapy for 10 years, revealed 1,741 distinct AAV integration events in their genomic DNA. Out of the 9 dogs treated, 5 exhibited expanded cell clones, with 44% of the integrations found in close proximity to genes that play a role in cell growth, as indicated by the analysis of integration sites. These findings suggest that some of the treated animals experienced clonal expansion of cells containing integrated vectors [205].

d) Retroviruses

Retroviruses is a family of single-stranded RNA spherical viruses of around 80 to 120nm diameter [206].

Gamma retroviruses are a type of RNA virus that carry the *gag*, *pol*, and *env* genes between long terminal repeats. These repeats contain enhancer and promoter elements required for the integration of the viral vector. These viruses are incapable of infecting non-dividing cells as the retroviral vectors cannot penetrate the nuclear membrane. [207]. This type of viral vector was initially used for liver monogenic disorders with *ex vivo* approach in homozygous familial hypercholesterolemia patients, showing moderate improvement in the profile of lipids patients with a 17% lower rate of stable engraftment following 4 months of gene therapy [208, 209]. Nevertheless, the design of the gene therapy procedure limited its wider use, as it required the need of 2 invasive procedures, a partial hepatectomy first, then re-intraportal infusion through a catheter in the portal vein with many potential adverse events including venous thrombosis, catheter misplacement and haemorrhage [210]. Although this first trial showed limited hepatocyte transduction, this has been optimized succeeding up to 90% efficacy of *in vitro* transduction [211]. Although there have been improvements in the protocol, hepatocyte transplantation has still remained a challenging process with many limitations. These limitations include the scarcity of liver tissues, the need for rigorous quality control evaluation of hepatocytes prior to the transplantation, the requirement for hypothermic cell storage, the necessity of preconditioning treatments to improve engraftment, the need for continuous monitoring of cells post-transplantation, and the

development of optimal immunosuppression protocols for patients that receive the transplant.[212].

Gene therapy using retroviral vectors has been well tolerated *in vivo*, via intravenous injections in patients with hemophilia A, however, did not show any clinical benefit [213].

In the first officially approved retrovirus-mediated gene therapy clinical trial, the gene for neomycin phosphotransferase was introduced into the tumor-infiltrating lymphocytes and was administered to patients with advanced cancer. Consequently, clinical trials where the gene for tumor necrosis factor was inserted by retroviral vector into the tumor-infiltrating lymphocytes were performed to maximize their therapeutic efficacy [214-216]. During the late 1990s, a clinical trial took place in Paris and London targeting 20 X-linked severe combined immunodeficiency patients, using retrovirus-mediated gene therapy. Patients were treated by *ex vivo*–transduced autologous CD34$^+$ hematopoietic progenitor cells and showed excellent efficacy; however, 5 of the patients presented with secondary T-cell leukaemia between 23 and 68 months after the gene therapy administration, 1 of them dying from this complication caused by insertional mutagenesis [217]. These 5 cases presented with uncontrolled clonal proliferation of T cells. This resulted of deregulated expression of proto-oncogenes following the integration of the vector provirus. The enhancer activity of the viral long terminal repeat (LTR) was shown to transactivate and induce the transcription of the oncogenes [218].

e) Lentiviral vectors

Lentiviral vectors are derived from the human immunodeficiency virus type 1 (HIV-1), that is a single stranded RNA (ssRNA) enveloped virus, with the ability to integrate into the host cell genome [219]. Such vectors are members of the retrovirus family; however, they can transduce both dividing and non-dividing cells and provide low cytotoxicity [220, 221]. The genetic structure of lentiviral vectors comprises two LTR sequences that are present at their ends. These LTR and surrounding sequences act in *cis* during the processes of viral packaging, retro-transcription, transgene expression, and genome integration. The *gag*, *pol*, and *env* genes that encode structural proteins, nucleic-acid polymerases/integrases, and surface glycoproteins, respectively, are surrounded by the LTR sequences. Additionally to a variable

set of accessory genes, lentiviral vectors encode vital regulatory genes such as *tat* and *rev*, for the expression of the viral genome [221].

The envelope is made of viral proteins, which enhance the binding and uptake of the vector into the target cell [110]. Lentiviral vector envelope types include the vesicular stomatitis virus (VSV-G) envelope [222, 223], rabies G envelope [224], and MLV envelope [225, 226]. Several studies have investigated the efficacy of the VSV-G envelope in gene therapy vectors showing 10-fold increase in transduction efficiency of the retroviral vectors in human primary T cells compared to controls [227]. The efficacy of the VSV-G envelope has also been investigated in gene therapy studies for numerus diseases, including X-linked severe combined immunodeficiency (XSCID) in dogs, where results showed that the lentiviral vector with the VSV-G envelope corrected the immune deficiency in the treated dogs, with sustained gene expression for up to 3 years [228]. More recently, lentiviral vector with the VSV-G envelope used for the treatment of spinal muscular atrophy (SMA) in a mouse model showed that VSV-G lentivirus was able to significantly increase survival and improve motor function in the treated mice, with sustained gene expression for up to 9 months [229].

Lentiviral vector safety was improved by partial removal of the wild-type nucleic acid sequence in the transgene cassette. To avoid any mutagenesis risk and further induce safety of lentiviral vectors, self-inactivating (SIN) vectors were introduced by reduction of the wild-type sequences of the lentivirus such as the LTR enhancer/promoter elements in the U3 region (**Figure 6**) [230, 231].

Additional modifications to the transgene cassette include the integration of a synthetic chromatin insulator within lentiviral vectors, aiming to decrease the level of interaction between the introduced transgene and neighbouring genes [232-234].

1. Wild-type lentiviral vector genome
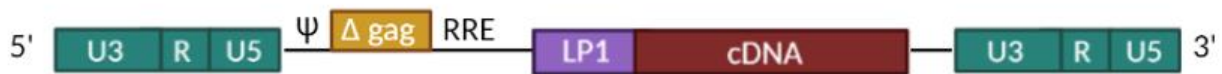
2. SIN lentiviral vector genome

Figure 6. Lentiviral vector genomes. (1) Genome of a wild-type lentiviral vector. (2) Genome of a SIN lentiviral vector that includes the modified 5'LTR in which the U3 region has been replaced by the constitutive CMV promoter. This vector also contains a cPPT and WPRE to improve the potency of the vector and the transgene expression. cDNA: complementary DNA; CMV; cytomegalovirus; Δ *gag*: group specific antigen Δ; ΔU3: truncated HIV-1 3' long terminal repeat; LP1: liver specific promoter; R: repeat region; RRE: *Rev* response element; SIN: self-inactivating; U3: untranslated 3' segment; U5: untranslated 5' segment; WPRE: Woodchuck hepatitis virus post-transcriptional regulatory element; Ψ: psi sequence.

The first diseases considered for gene transfer were monogenic blood diseases, including sickle cell disease or β-thalassemia, because gene transfer can be performed *ex vivo* by modifying a cell and reintroducing it into the patient. [235].

The initial clinical success of lentiviral gene therapy targeted X-linked adrenoleukodystrophy (X-ALD), a rare peroxisomal disease induced by ATP-binding cassette sub-family D member 1 (ABCD1) protein deficiency, which causes rapid neurodegeneration in children with demyelination of the brain. Two years following *ex vivo* gene therapy, a polyclonal reconstitution from autologous transduced hematopoietic stem cells was observed, with granulocytes, monocytes and T and B lymphocytes expressing the ABCD1 protein. One year following injection, demyelination had halted in the 2 patients treated. Efficacy outcomes were comparable to allogeneic hematopoietic stem cell transplantation, which remains the

standard of care for this disease [146]. Since then, these results have been confirmed in phase 2/3 trials [236]. E*x vivo* liver-directed gene therapy using lentiviral vectors had successful outcome in a pig model of tyrosinemia 1 as a result of the selective advantage of appropriately altered hepatocytes, which can then nearly completely repopulate the native liver [237].

Lentiviral vectors designed for liver-directed gene therapy are carefully targeted to express transgenes only in hepatocytes, using both transcriptional and microRNA-mediated regulation [238]. Studies in mice, dogs, and non-human primates have shown that systemic administration of these vectors can lead to stable and long-term expression of the transgene, including FIX, which can provide a continuous production of coagulation FIX in animals with hemophilia B [144, 239-241]. However, lentiviral vector systemic administration to dogs reported mild acute toxicity and low efficacy at certain doses [240]. Recent research has focused on engineering the lentiviral vector's surface to incorporate the human phagocytosis inhibitor CD47, can prevent uptake by phagocytes and subsequent recognition by the innate immune system [144]. When administered intravenously to non-human primates, these phagocytosis-shielded lentiviral vectors presented reduced targeting of liver and spleen, resulting in the increased transduction of hepatocytes, without any signs of insertional mutagenesis [144]. In a more recent study, engineered versions of the factor VIII (FVIII) transgene were delivered using lentiviral vectors in hemophilia A mice and non-human primates, resulting in long-term FVIII activity and restoration of hemostasis [241]. These findings suggest the potential of lentiviral vectors as a liver-directed gene therapy tool for the treatment of genetic disorders including hemophilia *in vivo*.

1.4.3 Lentiviral vector life cycle

The 3 essential genes required for lentiviral replication and function are the *gag, pol*, and *env* genes [242].

The life cycle of all retroviruses is highly comparable (**Figure 7**). It starts with the virus entering the host cell, which can occur either following direct membrane fusion or by receptor-mediated endocytosis. On the envelope of the virus, glycoproteins are able to bind to their corresponding receptors that are placed on the surface of the target cell to facilitate this

process [243]. When a virus attaches to a cell receptor like binding of the surface of the viral envelope to a CD4 on a T lymphocyte, structural changes happen to the glycoproteins of the envelope. This allows binding of the glycoprotein gp120 with other co-receptors such as CCR5 (or CXCR4) chemokine receptor. This represents the fusion step of the vector life cycle [244, 245].
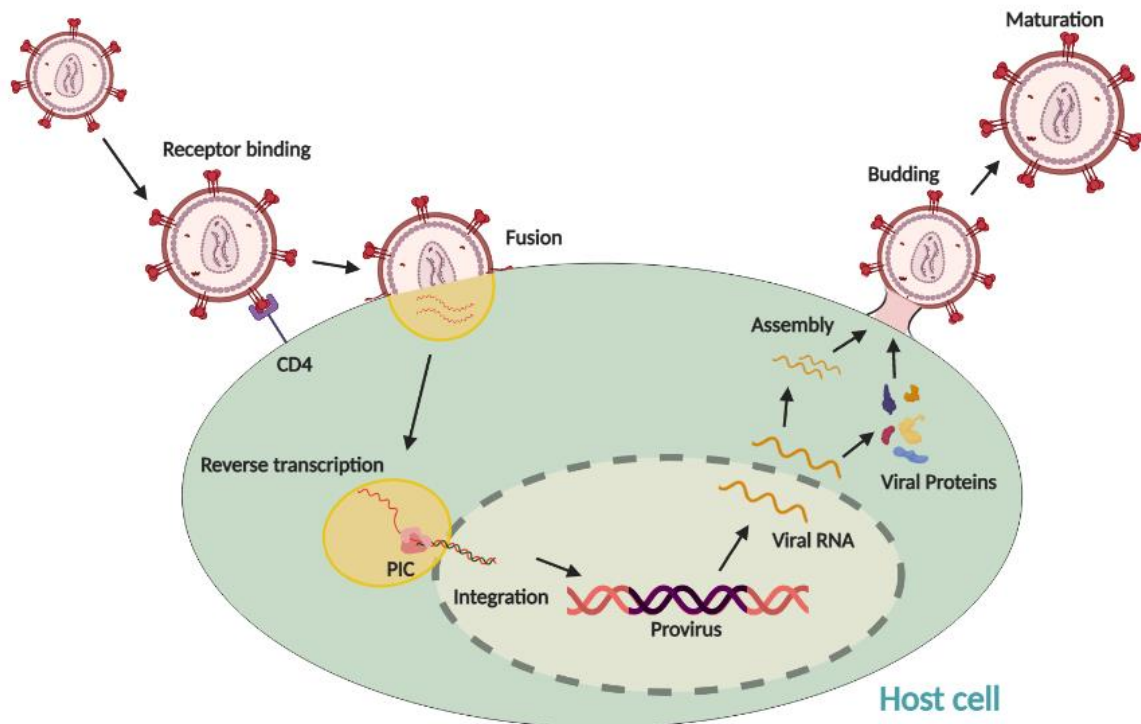
Figure 7. Lentiviral vector life cycle. CD4: receptors found primarily on the surface of CD4 T lymphocytes, necessary for HIV fusion; PIC: pre-integration complex.

Then, the viral capsid is transferred via intracellular trafficking through a microtubule network. As the capsid enters the host cell, capsid disassembling occurs and a reverse transcription of viral RNA takes place in the cytoplasm via a multistep pathway (**Figure 8**) before integration of the viral double-stranded DNA in the host genome [243, 246]. Viral reverse transcriptase, which consists of DNA-dependent DNA polymerase, RNA-dependent DNA polymerase and RNase H, catalyses reverse transcription [247].
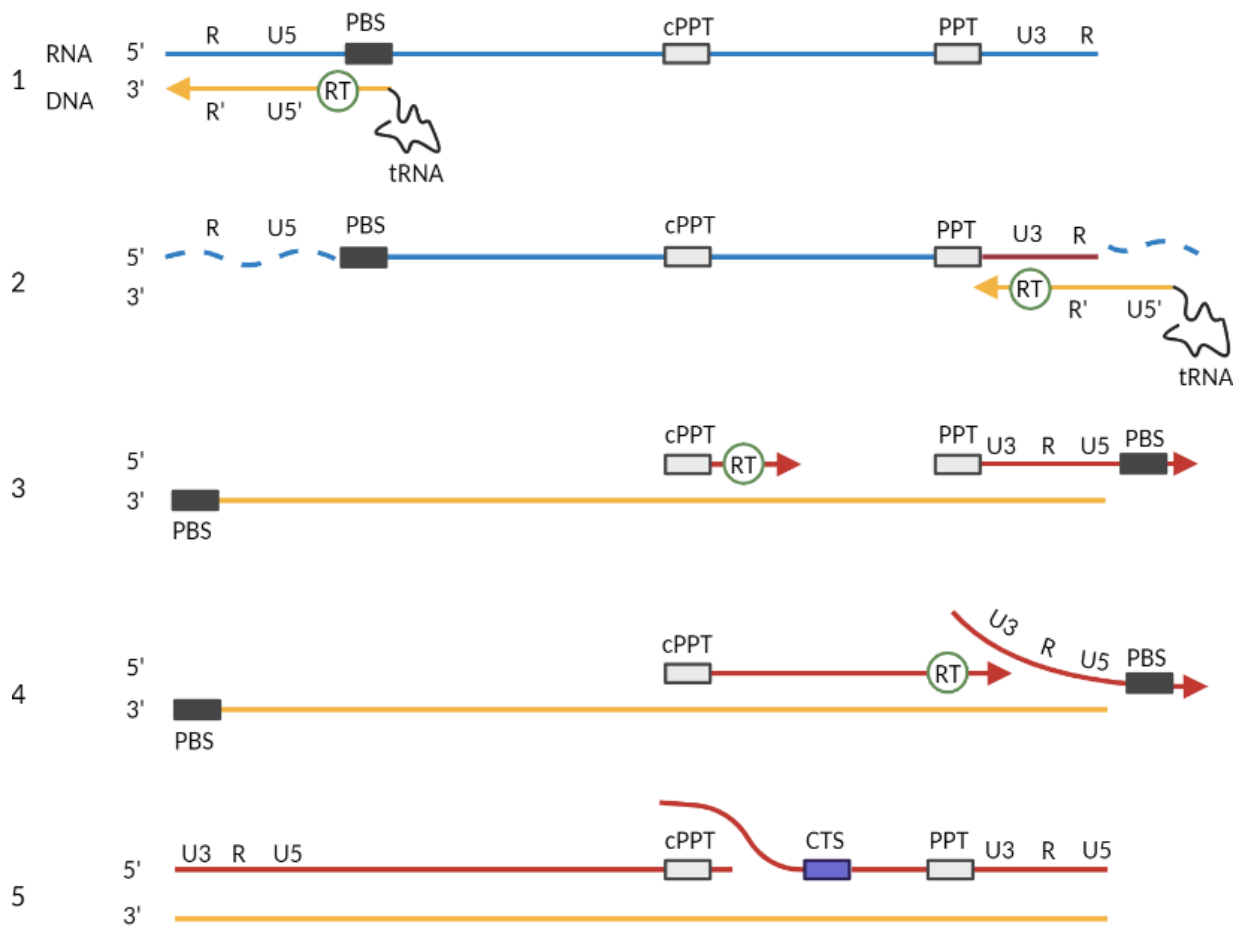
Figure 8. Reverse transcription in lentiviral vectors [248]. RNA is presented in blue, and DNA as yellow/red. (1) Reverse transcription commences with the introduction of a tRNA primer at the PBS site, close to the 5' end of the genome. (2) DNA synthesis starts when the R'U5' is translocated to the 3' end of the sequence. (3) cPPT and PPT function as primers to initiate plus strand DNA synthesis. (4) Following DNA synthesis, the reverse transcriptase (RT) progresses until it reaches the stop DNA site (U3-R-U5). (5) Finally, upstream DNA synthesis concludes at the CTS site, located near the centre of the genome, resulting in a complete plus-strand DNA with a discontinuity. cPPT: central polypurine tract; CTS: central termination sequence; PBS: primer-binding site; PPT: polypurine tract; R: repeat region; RT: reverse transcriptase; tRNA: transfer RNA; U3: untranslated 3' segment; U5: untranslated 5' segment.

Subsequently, the pre-integration complex which consists of provirus DNA, accessory gene *Vpr*, integrase and matrix p17 is formed [247, 249]. The entrance of the pre-integration complex into the nucleus is promoted by the interaction of specific sequences on the integrase and the matrix p17 with importin α and β [250, 251].

Integration of the provirus into the host cell genome is facilitated by the pre-integration complex. Some endogenous transcription factors that belong to host cells, including lens epithelium-derived growth factor (LEDGF), are also associated with the integration process [252, 253]. After integration, RNA polymerase II, which is recruited by a *trans* activator of *tat*, binds the U3 element located at the 5' end, which acts as the promoter for the transcription [254]. Transcription and translation of capsid proteins enable the assembly of the capsid in the cytoplasm, which is initiated by the binding of *gag* to the genomic RNA. As a result, viral progeny uses a budding system for release into the extracellular space [243, 255].

1.4.4 Lentiviral vector production

Production of lentiviral vectors requires a manufacturing cell line, human embryonic kidney (HEK) 293T cells, to generate the viral vector particles [256-258].

The packaging cells are expanded in tissue culture over several days before transient transfection with plasmids encoding the crucial proteins to produce lentiviral vector. To produce functional vector particles, a triple-transfection approach is used that includes essential packaging plasmids such as the VSV-G plasmid, an HIV-1 plasmid with *gag*, *pol* genes, and accessory proteins like *rev*, along with the lentiviral vector genome that contains the gene of interest. This approach is carried out in HEK 293T cells, which produce lentiviral vector particles over 48 hours. The lentiviral vector particles are then collected from the culture medium and undergo several filtration steps to remove cellular debris and sterilize the solution. [259-261].

The vector titre can vary between 1×10^8–1×10^9 viral particles/mL. Titration of the vector can be done by measuring p24 levels in a viral preparation via enzyme-linked immunosorbent assay (ELISA) and quantitative PCR (qPCR) for viral RNA [262].

1.5 Main challenges of lentiviral-mediated gene therapy for metabolic disorders

a) Genotoxicity

One of the major concerns associated with gamma retroviral and lentiviral vectors represents the risk of insertional mutagenesis [263-265]. In a previous study, 5 patients with SCID-X1, that were treated with gamma retroviral vector-mediated gene therapy developed secondary leukaemia due to the insertion of the transgene cassette near the LIM Domain Only 2 (*LMO2*) gene [218]. This raised fears regarding the safety profile of lentiviral vectors and the potential risk of oncogene activation. SIN lentiviral vectors vary from gamma retroviral vectors in significant manner, as SIN lentiviral vector designs have been developed to eradicate the viral enhancers and promoters present in the LTR. This, when combined with internal promoters that have minimal or no enhancer activity, has been demonstrated to effectively decrease the insertional mutagenesis [266-268]. Lentiviral vectors are regularly used in gene therapy clinical trials showing very low to negligible genotoxicity risk with sustained transgene expression [226, 230, 269-271]. Despite that, in a recent study investigated by the FDA in 2022, *ex vivo* transduction with the Lenti-D, used to manufacture eli-cel via transduction of CD34+ hematopoietic stem cells from patients with cerebral adrenoleukodystrophy (CALD), was performed. In this study 3 patients that received lentiviral treatment also presented with expansion of a clone that has lentiviral vector integration into a proto-oncogene within the first 2 years of the treatment [272].

b) Lentiviral vector immunity

Immune response against lentiviral vectors can limit the efficacy of this therapy, as the vectors are recognized by both the innate and adaptive immune systems [157]. The innate immune system recognizes lentiviral vectors through pattern recognition receptors (PRRs) on the macrophages, which recognize conserved pathogen-associated molecular patterns (PAMPs) located on the surface of the vectors. For instance, TLR-7 and TLR-8 recognize single-stranded RNA in the lentiviral vector genome, and TLR-9 recognises CpG motifs in the vector DNA [273].

Upon activation of TLRs, downstream signalling pathways induce the generation of proinflammatory cytokines and chemokines, which can recruit immune cells to the site of infection. In addition to PRRs, macrophages express scavenger receptors, can also recognize lentiviral vectors by binding to negatively charged and hydrophobic molecules, which are present on the surface of lentiviral vectors, leading to their internalization and degradation by macrophages. [274].

The complement system is a cascade of proteins that can recognize and eliminate foreign particles, including lentiviral vectors [275]. The activation of this system involves three pathways: the classical pathway, the alternative pathway, and the lectin pathway. In the classical pathway, lentiviral vectors' surface binding with antibodies triggers the activation, while the complement proteins' direct binding to the vectors activates the alternative and lectin pathways [276]. Once the complement system is activated, it results in the creation of the membrane attack complex. This complex can infiltrate the lipid bilayer of lentiviral vectors and induce their lysis [277]. The complement system can also opsonize lentiviral vectors, making them more easily recognized and phagocytosed by macrophages. B and T lymphocytes are responsible for initiating adaptive immune responses against lentiviral vectors, as they recognize the viral proteins that are expressed by the transduced cells. Lentiviral vectors can initiate both humoral and cellular immune reactions, resulting in the generation of neutralizing antibodies and the activation of cytotoxic T lymphocyte (CTL) responses, respectively. [278-280]. By binding to the viral envelope proteins, neutralizing antibodies can inhibit the transduction of target cells, while CTLs can directly kill transduced cells by recognizing the viral peptides presented on major histocompatibility complex molecules [281, 282].

c) Manufacturing challenges

Scalable manufacturing of lentiviral vectors presents several challenges that need to be overcome for their widespread application in clinical settings. While small-scale production of lentiviral vectors is relatively straightforward, the process becomes more challenging when scaling up to meet the requirements for clinical use. The use of large-scale culture systems, such as bioreactors, is necessary to generate the quantities of lentiviral vectors required for clinical applications [283]. Quality control is a critical aspect of the manufacturing of lentiviral

vectors, as it ensures the safety and efficacy of the final construct [284]. The cost of manufacturing lentiviral vectors is another challenge that requires attention for their widespread application [283]. The use of large-scale culture systems, such as bioreactors, and the need for specialized equipment and facilities, contribute to the high cost of lentiviral vector production. However, advances in manufacturing technology and process optimization are expected to reduce the cost of lentiviral vector production over time.

d) Metabolic zonation

The liver lobule is the crucial functional segment of the liver, composed of a central vein surrounded by several concentric layers of hepatocytes [285]. The different metabolic zones of the liver are defined based on their location relative to the central vein, and they have different functions and characteristics. Periportal hepatocytes, located at the outermost layer of the lobule, have a high capacity for oxidative metabolism, gluconeogenesis, and ureagenesis. Perivenous hepatocytes, located at the innermost layer of the lobule, have a high capacity for lipogenesis and glycogen synthesis [286].

The timing of vector administration can also play a role in achieving targeted delivery to specific liver zones. Administering lentiviral vectors during neonatal period results in more efficient and selective transduction of pericentral hepatocytes while delivery at later stages resulted in more diffuse hepatocyte transduction [287]. More recently, lentiviral vector encoding the *FIX* gene showed a higher percentage of transduced hepatocytes in periportal area after intravenous vector administration in adult mice compared to neonatally- and young adult-injected animals [288].

1.6 Hypothesis and aims of the project

Hypothesis 1:

A congenic mouse strain carrying the *Asl^Neo* allele on a CD1 background can be created, offering potential advantages for research due to its easy breeding and visible vein structure for simpler injections.

Aim 1:

i) To develop a congenic mouse strain carrying the *Asl^Neo* allele on a CD1 background.

ii) To evaluate if this CD1 congenic strain recapitulates the human ASA disease phenotype.

Hypothesis 2:

The use of an optimised lentiviral vector system represents a safe and effective therapeutic strategy for treating the neonatal *Asl^Neo/Neo* mouse model, potentially leading to disease correction and a normalised ASA phenotype.

Aim 2:

i) To develop an optimised lentiviral vector gene therapy to maximise disease correction in the *Asl^Neo/Neo* mouse model.

ii) To evaluate the disease correction efficacy of the lentiviral vector system by assessing survival, phenotypic characteristics, urea cycle biomarkers, and liver ASL activity.

iii) To evaluate the safety profile of the lentiviral vector construct in wild-type mice, observing for adverse events and characterising the biodistribution of the vector after nine months post-neonatal administration.

Hypothesis 3:

Transient macrophage depletion by clodronate administration before lentiviral or AAV injections can enhance liver transduction, allowing a higher amount of vector to transduce hepatocytes.

Aim 3:

i) To evaluate the effect of systemic clodronate administration on liver transduction following subsequent lentiviral and AAV injections in neonatal and young-adult wild-type mice.

2. MATERIALS AND METHODS

2.1 Phenotyping of *Asl^Neo/Neo* mice

2.1.1 Study approval

The study adhered to the regulations set by the UK Home Office and the ethical review committee of University College London. The experiments were conducted under the supervision of Dr Simon Waddington and Dr Julien Baruteau, who held Project Licenses (PPL licenses 14300 and 16381, respectively), and Miss Loukia Touramanidou, who held a Personal License (PIL I37345354).

2.1.2 Animals

The mice used in the study were *Asl^Neo/Neo* (B6.129S7-Asltm1Brle/J) obtained from Jackson Laboratory (Bar Harbor, ME). The animals were maintained with standard rodent chow (Harlan 2018, Teklab Diets, Madison, WI; protein content 18%) and free access to water. Mice were monitored daily to ensure their well-being and behaviour.

2.2 Genotyping

2.2.1 DNA extraction

The tissue for the DNA extraction was collected from ear (adult mice) or tail (neonatal mice) clip and placed in an appropriately labelled empty Eppendorf tube. For the extraction process, Phire Tissue Direct PCR Master Mix' Kit containing the Dilution buffer (F-132) and the DNA release additive (F170S, Thermo Fisher Scientific, UK) was used. Initially, 20 μL of dilution buffer and 0.5 μL of DNA release additive were added to the sample. The sample solution was incubated at room temperature for 2 minutes until it was heat-shocked at 95°C for 2 more minutes.

2.2.2 PCR amplification

A PCR reaction mix was prepared. The final volume for each one of the DNA samples genotyped was 24μL (**Table 3**).

Reagent	Volume (μL)
DNA sample	4
Q5 MM (2x)	12
Forward primer (25μM)	0.5
Reverse 1 primer (25μM)	0.5
Reverse 2 primer (25μM)	0.5
Nuclease-free water	6.5

Table 3. Reaction mix for genotyping. The table displays the name and volume of each reagent used for performing PCR reaction for genotyping. MM: master Mix.

The set of primers used for the reaction included: a forward primer: 5'-GGTTCTTGGTGCTCATGGAT-3'; a reverse primer for the wild-type allele: 5'-GCCAGAGGCCACTTGTGTAG-3' both binding within the 9th intron of the mouse *Asl* gene and a reverse primer which binds to the Neomycin cassette inserted in the 9th intron of the mouse *Asl* gene to detect the *Asl*^{Neo/Neo} allele: 5'-CATGACAGCTCCCATGAAGA-3'. The reaction cycle included: denaturation at 94°C for 15 seconds, 30 seconds at 63°C, 1 minute at 72°C. This cycle was repeated 40 times [83].

2.2.3 Sample electrophoresis on agarose gel

A cast appropriate for PCR was used for making the gel. Paper tape was carefully attached to seal the edges of the cast so that the gel would not leak out until it solidifies. The electrophoresis agarose gel 2% was made after mixing 2g of Agarose powder (16500500, Thermo Fisher, UK) with 100mL of 1 x TAE buffer solution (15558042, Thermo Fisher, UK). The buffer with the Agarose was then microwaved for 1.5 minutes. After that, 10µL of Safeview nucleic acid stain (NBS-SV1, NBS biologicals, UK) was added to the gel solution. The mixture was then poured into the pre-sealed cast and a 20-well comb was added. The gel was finally left to cool down and eventually solidify after approximately 20 minutes. Subsequently, the gel was positioned into the PCR tank filled with 1 x TAE buffer. From each one of the DNA samples, the amount of 24µL was mixed with 4µL of PCR loading buffer (7732-18-5, Melford, UK). 10µL of each sample were then loaded into a well in the gel. 1Kb plus DNA ladder (5µL) was also used to load the first well of the gel. For the electrophoresis, the samples were run for 1 hour at 90 Volts. For gel imaging, a benchtop ultraviolet transilluminator BioDoct-It Imaging system (UVP, Upland, CA, USA) was employed, along with UVO TS software (UVP, Upland, CA, USA). Following the optimized protocol, results were obtained for all genotypes, *Asl*^{+/+} (wild-type), *Asl*^{+/Neo} (heterozygote) and *Asl*^{Neo/Neo} mice were visualized (**Figure 9**).
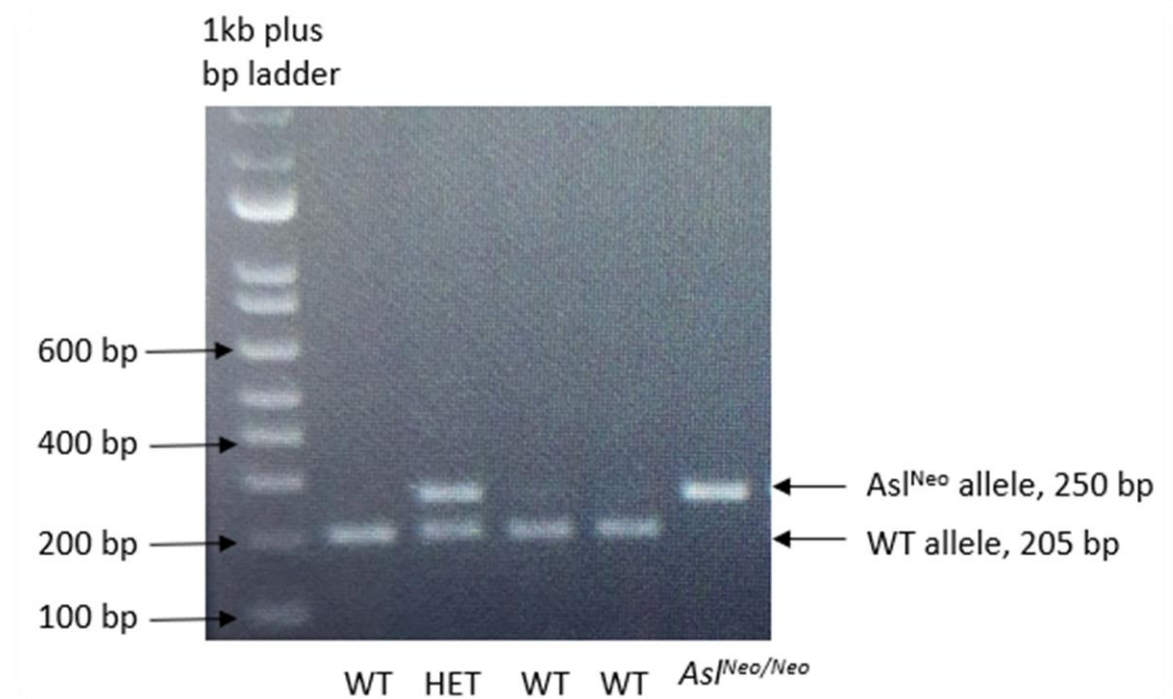
Figure 9. Imaging of gel of PCR for genotyping. This image displays the bands with 250bp and 205bp size for *ASL^Neo* and wild-type allele, respectively. Both bands are present in animals with both alleles that are heterozygous. HET: heterozygote; WT: wild-type bp: base pairs; kb: kilobase.

2.2.4 Weight and survival analysis

In the biodistribution and the gene therapy experiments, all animals were monitored daily until culling. Weights were recorded and mice that were losing more than 10% and up to 15% of their weights, were sacrificed.

2.3 Biomarkers

2.3.1 Blood sample collection and analysis

Whole blood was collected immediately after the animal was sacrificed, in a 0.5mL microcentrifuge tube containing Ethylenediaminetetraacetic acid (EDTA) (41.1504.005, SARSTEDT, Germany). Whole blood in the volume of 10µL was manually collected from the tube and were added onto whole blood ammonia specific cartridge (FDC NH3-WIIS 24, Fujifilm, UK). Cartridge containing the whole blood samples were inserted into the ammonia analyser for whole blood tests (DRI-CHEM NX10N, Fujifilm, UK).

For serum collection, blood was collected immediately after the animal was sacrificed, in a 0.5mL microcentrifuge and it was centrifuged at 13,000rpm for 5 minutes at room temperature. After the plasma was separated from red blood cells, it was isolated in a 1.5mL Eppendorf tube and was kept at -80°C for future analysis. Ammonia levels, alanine aminotransferase (ALT) activity and triglycerides concentration were measured from plasma using a Fujifilm NX500 analyzer (DRI-CHEM NX500, Fujifilm, UK). 10µL of diluted or undiluted plasma were added onto ammonia (FDC NH3-PIIS 24, Fujifilm, UK), ALT (FDC GPTPIIIS 24, Fujifilm, UK) and triglycerides (FDC TGPIIIS 24, Fujifilm, UK) specific cartridges and placed into the analyzer for measurement.

After culling, whole blood was collected using a 200µL pipette and deposited onto a Guthrie card obtained from the Newborn Screening Department at Great Ormond Street Hospital in London. Blood spots were air-dried for 24 hours at room temperature before being stored in a foil bag with desiccant and at -20°C. Urea cycle amino acids in blood (argininosuccinic acid, arginine, citrulline, and glutamate and glutamine) were analysed using Hydrophilic interaction liquid chromatography-tandem mass spectrometry (HILIC-MS/MS) by Dr Sonam Gurung at Great Ormond Street Institute of Child Health, London.

2.3.2 Urine sample collection and analysis

At the end of the experiments, urine was obtained from the mice by gently stimulating urination while holding them by the scruff of the neck. Urine was then pipetted and placed onto a Whatman filter paper (SKU – 1131058, Camlab Ltd, UK). Urine samples were left to dry for 24 hours at room temperature after collection and then were placed in in a foil bag with desiccant and stored at -20°C until analysis. Urine orotate levels were measured using HILIC-MS/MS by Dr Sonam Gurung at Great Ormond Street Institute of Child Health, London.

2.3.3 Perfusion of mice, organ collection and storage

Animals were put in an anesthetic chamber and anaesthetized by isoflurane. After 10 minutes, the anaesthetized mice were positioned on the procedure area with adaption of an anesthetic face mask. Absence of reaction after toe pinching confirmed the deep anesthesia of the animal before procedure. Using scissors, the skin, abdominal wall, diaphragm, and rib cage were meticulously cut to reveal the heart. A minor incision was then created in the right atrium, and a needle attached to a 10mL syringe filled with phosphate buffered saline (PBS) (14190169, Life Invitrogen, UK) was inserted into the left ventricle. PBS was then administered consistently for up to 2 minutes. During this process, blood was observed to exit from the right atrium, and the liver changed to a lighter brown color. Organs were then dissected in the desirable number of pieces and were collected in a labeled 1.5mL microcentrifuge tube and were stored at -80°C. To produce paraffin-embedded slides, the livers were first preserved in 10% formalin for 48 hours at 4°C, followed by storage in 70% ethanol at 4°C until additional processing was required. To prepare for electron microscopy, a liver sample approximately $1mm^3$ in size was obtained and immersed in a 3% glutaraldehyde solution, 0.1 M sodium cacodylate buffer pH 7.4, and 5 mM (111-30-8, Sigma-Aldrich, UK) at 4°C until further processing.

Brain was removed by separating the head from the body, then peeling the skin from the skull, and making precise incisions to remove the brain. The samples were collected in 1.5mL microcentrifuge tubes and preserved at -80°C.

For bone marrow isolation, the back leg was carefully cut above the hip joint to access the femur and tibia, while the knee and ankle joints stayed in place. Then using a surgical blade, the remaining muscle and tissue was debrided from the bone. Next, the bone edges were removed as close to the joints as feasible using scissors. A syringe filled with PBS was then used to flush out the bone marrow from one end of the bone and collect it in a 1.5mL microcentrifuge tube from the other end. The bone marrow solution was centrifuged at 1500rpm for 5 minutes, after which the supernatant was removed. The bone marrow palette was then preserved at -80°C until further analysis.

2.3.4 Hydrophilic interaction liquid chromatography-tandem mass spectrometry

Collection of whole blood dried spots and dried urine samples was performed as explained in **Section 2.3.2**.

For sample preparation a 3.2mm punch from centre of the dried blood spot (equivalent to blood volume of 3.2µL) was put into a 2mL glass vial without insert (60180-VT303, Thermo Fisher Scientific, UK). The volume of 100µl of extraction solution (90µL methanol + 10µL mixture of internal standards (IS)) was also added to the vial. IS refer to the stable isotopes were used for quantification. The 10µL of the IS mixture consists of 2nM L-Arginine-13C6, L-Citrulline-2,3,3,4,4,5,5-d7, L-Glutamic-2,3,3,4,4-d5 Acid and 0.6nM of L-Glutamine-1,2-13C2 and L-Ornithine-2,3,3,4,4,5,5-d7. The sample was sonicated in a sonication bath (USC200T, VWR International) for 15 minutes at room temperature. The supernatant of the sample was then moved to a 1.5mL microcentrifuge tube. The sample was then dried using microcentrifuge speedvac vacuum concentrator (SPD210-115, Thermo Fisher Scientific, UK) at room temperature and with V-AQ and brakes 'on'. Following that, the dried samples were reconstituted in 40µL of water and vortexed to mix before they were centrifuged at 13,000rpm for 2 minutes. After sample centrifugation, the supernatant was moved to a 300µL

insert glass vial (11565894, Thermo Fisher Scientific, UK). 40µL of 0.1M hydrochloric acid (HCl) was then added to the sample and was mixed by vortexing. The sample was later topped up with 280µL of a solution consisting of 10mM ammonium formiate (540-69-2, Merk, UK) 85% Acetonitrile (CAN) (271004, Merk, UK), 15% water, and 0.15% formic acid. Samples were then mixed by vortexing and were injected into the LC-MS/MS system.

Preparation of calibrators, chromatography separation, and analysis of amino acids from dried blood spot was kindly performed by Dr Sonam Gurung measuring L-Arginine, L-Citrulline, L-Glutamic Acid, L-Glutamine and L-Ornithine, following the protocol instructions by Baruteau *et al.*, 2018.

2.3.5 Paraffin-embedded immunohistochemical staining of liver sections

Livers were collected and fixed as described in **Section 2.3.4**. Subsequently, the samples were sectioned and embedded in paraffin by the Pathology laboratory located at the University College London Institute of Neurology in London. The resulting slides were then kept at room temperature until they were ready to be stained.

As a first step of the staining, paraffin-embedded slides were kept in Histoclear (HS-200, National Diagnostics, UK) solution for 10 minutes to remove the excess of wax from the sections and remove impurities and deposits. To prepare the slides for staining, they underwent a series of dehydration steps. Specifically, they were first immersed in 100% ethanol for 10 minutes, followed by 95% ethanol for 5 minutes, and then in 75% ethanol for an additional 5 minutes. Finally, the slides were briefly placed in distilled water for 30 seconds. To remove any remaining blood, slides were placed in 1% H_2O_2 diluted in Methanol and covered with cling film for 30 minutes. Then, slides were put under running tap water for 5 minutes to wash off the excess solution. Subsequently, sections were placed in citrate buffer (0.01M, pH 6) (C2488-500ML, Sigma-Aldrich, UK), which was placed in a plastic microwavable box and covered with cling film. The box containing the slides was placed in a heating microwave for 20 minutes to ensure dewaxing with boiling citrate buffer, allowing antigen retrieval. Once boiled, slides were allowed to reach room temperature gradually in citrate buffer at room temperature. Slides were blocked for non-specific binding by adding 15% goat

serum (ab7481-10ml, Abcam, UK) diluted in TBS-T (100μL per slide), followed by incubation in a moist chamber for 30 minutes. After blocking, the slides were washed in TBS three times (5 minutes each time). Primary human anti-ASL (1:1000; Ab97370, Abcam, UK) and primary rabbit polyclonal anti-GFP (1:1000; Ab290, Abcam, UK), diluted in 10% goat serum in TBS-T, were then added to the sections (100μL per slide) and incubated overnight at 4°C in a moist chamber. The following day, the primary antibody solution was removed, and the slides were washed three times in TBS for 5 minutes each. A rabbit antibody enhancer (D13-18, GBI Labs, USA) was then added on the sections (692 drops per slide or 40μL) and sections were incubated in the moist chamber for 10 minutes. After removing the rabbit antibody enhancer, the sections were washed three times in TBS (5 minutes per wash) before adding the secondary goat anti-rabbit biotinylated immunoglobulin G (IgG) antiserum. The antiserum was diluted in 10% goat serum in TBS-T and added to the sections (100μL per slide), which were then incubated for up to 45 minutes at room temperature. After incubation, the slides were washed three times with TBS (5 minutes per wash). The detection solution with 3,3'-Diaminobenzidine (DAB) was prepared by mixing a single drop of DAB chromogen, with 1mL of DAB substrate. DAB solution was then added to the sections (100μL per slide) and incubated in the moist chamber for 3 – 5 minutes. Color tint became noticeable under the microscope after the addition of the DAB solution. The slides were then washed three times in ice cold TBS (5 minutes per wash) to stop the DAB activation. Sections were then dehydrated again following the same steps as prior but in reverse order and allowed to dry. Following the dehydration process, slides were cover-slipped with DPX-new (MIC3114, SLS, UK) after wash in Histoclear.

2.3.6 Microscopy and Images

Images of liver samples with DAB staining were obtained using a microscope camera (DFC420, Leica Microsystems, Milton Keynes, UK), and the software (Image Analysis; Leica Microsystems) was utilized to capture representative images.

2.3.7 Quantification of staining

For each one of the slides, 10 random pictures were taken with a microscopic camera from the same sample **(Figure 10A)**. For the quantitative analysis of the sections, threshold analysis was performed using the Image J software (Bethesda, Maryland, USA). The threshold was adjusted for each experiment based of the intensity of the staining and applied to all samples, to achieve quantification restricted to antigen expressing cells **(Figure 10B)**.
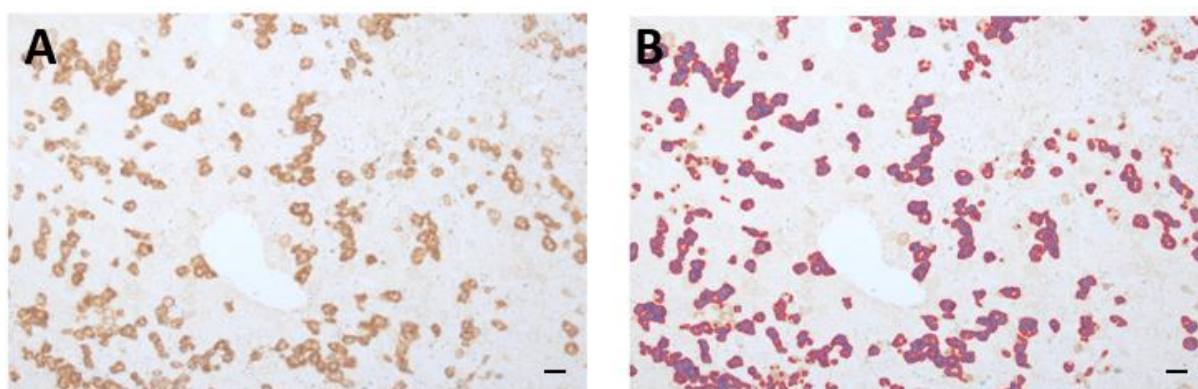
Figure 10. Quantification of DAB-stained tissue section. (A) Image of DAB-stained liver section expressing GFP-positive hepatocytes. **(B)** Same image showing automated Image J thresholding tool for quantification. Scale bars are 100µm for x10 magnification.

2.3.8 [^{18}F]FSPG PET imaging

[^{18}F]FSPG, which is (S)-4-(3-^{18}F-fluoropropyl)-L-glutamate, was synthesized using a GE FASTlab automated synthesis module by Dr Oskar Timmermand at the School of Biomedical Engineering and Imaging Sciences, King's College London, UK. The synthesis was carried out as previously reported, and the quality control was performed accordingly [289]. Young adult- (2-3-weeks-old) lentiviral vector treated *Asl^{Neo/Neo}* and untreated *Asl^{Neo/Neo}* mice, as well as wild-type littermates were anaesthetized by isoflurane. Mr Dany Perocheau along with Dr Oskar Timmermand kindly imaged and analyzed the computerized tomography (CT) images of all mice after tail vain intravenous injection of 1-3 MBq of radiotracer. All animals

underwent dynamic positron emission tomography (PET) scans on a Mediso NanoScan PET/CT system between 40 to 90 minutes after injection with [^{18}F]FSPG. After PET imaging, mice were euthanized by cervical dislocation, and various tissues such as the liver, skin, and others were collected, snap frozen, and stored at -80°C for further evaluation.

2.4 Electron Microscopy

The liver samples were promptly fixed in a 3% glutaraldehyde solution and 0.1 M cacodylate buffer solution at pH 7.4, 5 mM, and maintained at 4°C until further evaluation. The liver samples were then processed by Dr Glenn Anderson at Great Ormond Street Hospital, London. Images were obtained using a Philips CM10 Transmission electron microscope (Philips Electron Optics, Eindhoven, The Netherlands), equipped with the Megaview Olympus digital imaging system (EMSIS, Manchester, UK).

2.5 Quantitative PCR

Post liver perfusion, specimens were rapidly frozen using dry ice and stored at -80°C until genomic DNA extraction. The QIAgen DNeasy Blood & Tissue Kit (69504, QIAgen) was employed for genomic DNA extraction, adhering to the manufacturer's guidelines.

The plasmid standard curve was prepared by the serial dilutions ranging from 10^7 copies/5µL to 10^3 copies/5µL of a plasmid, containing for β-actin, titin, WPRE, and 5'LTR sequences.

To quantify the lentiviral vector genome copies, the targeting of the 5'LTR sequence was performed using the following set of primers: 5'- AGCTTGCCTTGAGTGCTT -3' (forward), 5'-GCGCCACTGCTAGAGATTT -3' (reverse), 5'- 56FAM/AAGTAGTGTGTGCCCGTCTGTTGT/3BHQ_1 -3' (probe). For quantification of AAV vector genome copies, the targeting of the WPRE sequence was performed using the following set of primers 5'- TGGATTCTGCGCGGGA -3'

(forward), 5'-   GAAGGAAGGTCCGCTGGATT   -3'   (reverse),   5'-   FAM-
CTTCTGCTACGTCCCTTCGGCCCT-TAMRA -3' (probe). The housekeeping genes *β-actin* and titin
for quantification of human and mouse cell copies respectively, were used to normalize the
results   and   was   targeted   by   the   following   set   of   primers;   for   titin: 5'-
AAAACGAGCAGTGACGTGAGC -3' (forward), 5'- TTCAGTCATGCTGCTAGCGC -3' (reverse), 5'-
56-FAM/   TGCACGGAAGCGTCTCGTCTCAGTC/3BHQ_1 -3' (probe); and for *β-actin*: 5'-
GTAGCACAGCTTCTCCTTAAT -3' (forward), 5'- GGACCTGACTGACTACCT -3' (reverse), 5'- 56-
FAM/CGCGCTCGGTGAGGATCTTCAT/3BHQ_1 -3' (probe). TaqMan Universal PCR Master Mix
(4304437, Thermo Fisher) was used to amplify the region of interest. The quantitative PCR
reactions were carried out in duplicates and prepared in 0.2 mL MicroAmp reaction tubes
(4346906, Thermo Fisher). The tubes were then placed in a StepOne™ Real-Time PCR System
(4376357, Thermo Fisher). The standard cycling conditions were used, starting with an initial
step at 50°C for 2 minutes, followed by a 10-minute activation step at 95°C, and then 40 cycles
of denaturation at 95°C for 15 seconds, annealing primers at 72°C for 1 minute, and extension
at 60°C for 1 minute.

To set up qPCR reactions, a reaction mix was prepared, with a final volume of 20μL per sample
(**Table 4**).

Reagent	Volume (µL)
DNA sample	5
TaqMan MM (2x)	10
Forward primer (25µM)	0.18
Reverse 1 primer (25µM)	0.18
Probe (25 µM)	0.05
Nuclease-free water	4.59

Table 4. Reaction mix for qPCR. The table displays the name and volume of each reagent used for performing quantitative PCR reaction for measuring the lentiviral vector titer. MM: master Mix.

Regression analysis was performed to extrapolate sample copy numbers from cycle threshold (Ct) values. To determine the vector genome copy number per cell, the vector copy number (VCN) was divided by the β-actin/titin copy number, and the result was multiplied by 2.

2.6 Cloning of the *co-hASL* plasmid

2.6.1 Bacterial transformation

On ice, 50µL of One Shot Skbl3 chemically competent E. coli strain (C404052, Thermo Scientific) was mixed with 5µL of the plasmid pCCL-LP1-ASL, resulting in Neomycin resistant colonies. After gently mixing, the solution was incubated on ice for 30 minutes. Heat shock was applied to the solution at 42°C for 45 seconds, followed by incubation on ice for 2 minutes. Then, 250µL of pre-warmed Super Optimal broth with catabolite repression (SOC) outgrowth medium was added to each solution. The solutions were then inserted in a moving incubator (M1282-0010, Eppendorf) at 37°C and 200rpm for 1 hour. Then, an amount of 25-

100μL from the transformation was spread on a pre-warmed selective plate and incubated, placed upside down overnight at 37°C. Three different volumes (1/1,000; 1/10,000; 1/100,000) per transformation were prepared and plated on Lysogeny broth (LB)/Agarose plates to ensure that at least one plate will have well-placed colonies. Transformation solution was diluted 1:1,000 and 1:10,000 into the SOC outgrowth medium. The following day, the preferred plate was the one coated by the least number of single colonies to avoid overlap between multiple clones. A single colony was carefully picked using a 20μL pipette tip and added to 10mL of LB that was then placed into a moving incubator at 37°C and 200rpm for up to 16 hours.

For the preparation of LB/Agarose plates for transformation of the plasmids, 4% LB/Agarose (L2897-1KG, Sigma, UK) solution was mixed and autoclaved. Once the solution had been autoclaved, it was allowed to cool to room temperature. At this point, 100 μg/mL of Neomycin (21810031, Thermo Fisher, UK) was added to the solution while it was still in a liquid state. Antibiotic was mixed with the LB/Agarose solution and 25mL of it was added to each culture dish.

2.6.2 Amplification of *hASL* plasmid

The transformed E. coli was grown in 10mL LB (L3022-1KG, Sigma) medium. From that solution, 1mL was added to autoclaved 500mL LB medium with antibiotic Neomycin 100mg/mL. That solution was then placed in the moving incubator (37°C – 200rpm), for up to 16 hours.

The following day, the hASL plasmid was amplified using a Maxiprep kit (K210006, Thermo Fisher, UK), following the manufacturer's instructions.

2.6.3 Restriction enzyme digestion

SalI-HF® and AgeI-HF® (New England Biolabs, UK) were the restriction enzymes used for the digestion of pCCL.LP1.*hASL* that was kindly provided by Dr Julien Baruteau. Lentiviral transfer backbones such as CCL, contain ∼ 10% of the wild-type HIV-1 genome and are pseudotyped with the liver specific (LP1) promoter that consists of the Apolipoprotein hepatic control region (HCR) and the promoter of the liver-specific α1-antitrypsin gene (*hAAT*). Digestion using these restriction enzymes enables the separation of the CCL backbone (6,981 bp) and the *hASL* (1,395 bp) sequences. For this, the SnapGene software was used (GSL Biotech LLC, Chicago, IL, USA) (**Figure 11**). The reaction was carried out in a total volume of 40μL, containing 1μg of DNA template, 1 unit of each restriction enzyme, 4μL of 10x NEB's restriction enzyme buffer, and nuclease-free water (B1500S, New England Biolabs, UK). After digestion of the *hASL* plasmid with the restriction enzymes at 37°C for 15 minutes, agarose gel electrophoresis was performed as described in **Section 2.2.3**.

2.6.4 Agarose gel electrophoresis

The amplified *hASL* plasmid was run in 1% agarose gel at 80 volts for 40 minutes. After confirmation of desired size of bands for both CCL backbone and *hASL* sequences on the gel, the CCL plasmid was extracted from the gel using a surgical blade while viewed under benchtop ultraviolet transilluminator BioDoct-It Imaging system (UVP, USA).

2.6.5 DNA gel extraction

The fragment of the gel that contained the CCL backbone sequence was isolated using the QIAquick Gel Extraction Kit (28706, QIAgen, UK) as per the instructions provided by the manufacturer.

2.6.6 Ligation

Ligation of the recipient CCL backbone and the *co-hASL* sequence was performed with the In-Fusion® HD Cloning Kit (639650, Takara Bio, USA) according to manufacturer's instructions. The *co-hASL* sequence was designed and ordered by GeneArt Sorfware (Thermo Fisher, UK) (**Figure ….**).
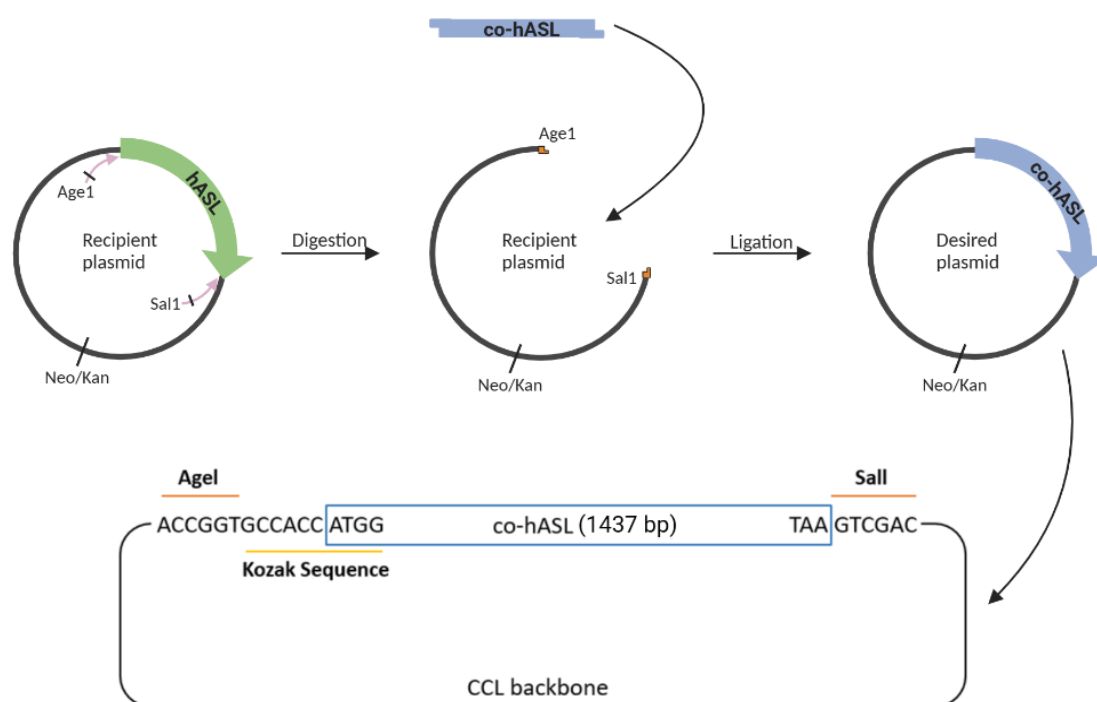
Figure 11. Digestion and cutting sites of the co-hASL. The *co-hASL* gene flanked by AgeI and SalI restriction cutting sites was designed with GeneArt software. For CCL.hASL plasmid digestion, AgeI and SalI restriction enzymes were used for the isolation of the backbone. Ligation of CCL vector and co-hASL sequence was then performed. *Co-hASL*: codon-optimised human argininosuccinate lyase; h*ASL*: human argininosuccinate lyase.

2.6.7 Bacterial transformation and expansion of colonies

The procedure for transforming the co-hASL plasmid and subsequent colony isolation was carried out according to the protocol detailed in **Section 2.6.1**. Individual colonies were selected using a 20µL pipette tip and transferred into 10mL of LB medium supplemented with Neomycin antibiotic. The culture was then incubated at 37°C with shaking at 200rpm for up to 16 hours.

2.6.8 DNA extraction and digestion

For each clone, DNA was extracted from 2mL of the solution as per manufacturer's instructions of the QIAgen Spin Miniprep Kit (27104, QIAgen, UK).

Digestion described in **Section 2.6.3** was performed using the same restriction enzymes (AgeI and SalI) to ensure the absence of homologous recombination. Reaction solution was then run in 1% agarose gel. It was shown that all cloned presented appropriate sizes for the targeted bands that are 1,437 bp for the co-hASL, and 6,981 for the CCL recipient sequence (**Figure 12**). The digestion of all plasmids presented the desirable band size, which confirmed the absence of homologous recombination.
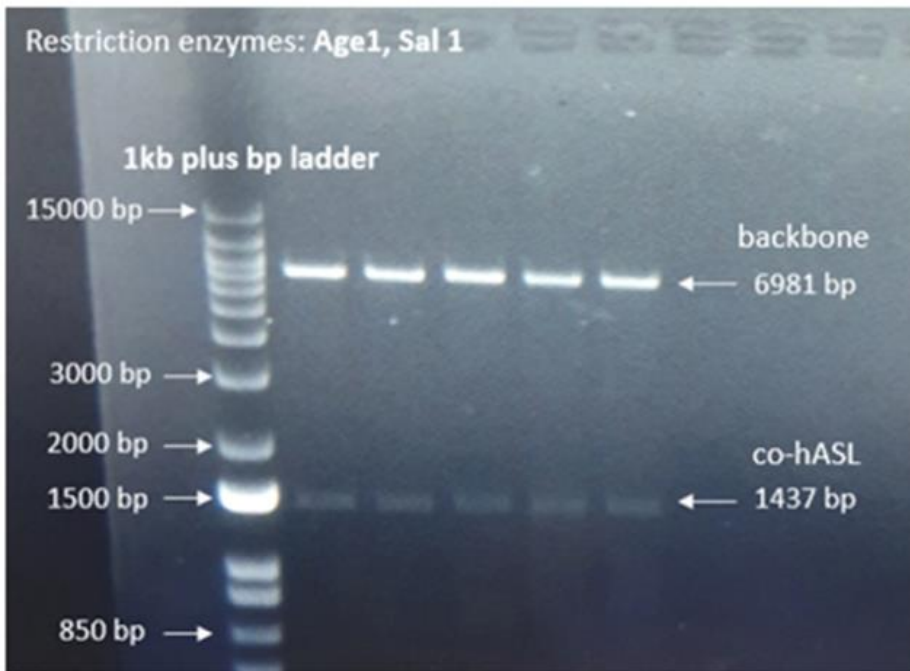
Figure 12. AgeI and SalI digestion of pCCL.LP1.*co-hASL* backbone. This image displays findings of the digestion of CCL.LP1.*co-hASL* plasmid following the cloning of *co-hASL* sequence into the CCL backbone in 5 different clones. Digestion was perform using Age1 and Sal1 restriction enzymes. 6981bp and 1437bp are the band sizes of CCL backbone and *co-hASL* sequences, respectively. Kb: kilobases; bp: base pairs.

2.6.9 DNA sequencing

Primers were designed for the sequencing of the pCCL.LP1.*co-hASL* backbone with 8,418 bp length. For designing high quality primers, the following parameters were considered: primer length to be between 18 and 22 bases, and primer's GC content to be around 45-55%. Further requirements involve the melting temperature being greater than 50°C but less than 65°C as well as the absence of secondary structures of primers or the potential to self-hybridize. Plasmid DNA was sent for sequencing using the primers listed in **Table 5**, to certify adequate cloning and absence of recombination or mutation (**Figure 13**). Primers were designed to be complementary to a specific region of the target CCL.LP1.*co-hASL* sequence. The length of the primers were 20-21 nucleotides, and the coverage of the target region was based on the number of fluorescently labelled dideoxynucleosides used in the sequencing reaction. The use of multiple overlapping primers was used to increase the coverage and accuracy of the

sequence obtained. The entire length of co-hASL DNA inserts and the purified plasmid were submitted to Source Bioscience for sequencing (Cambridge, UK).

Sequence (5' to 3')	Intended use	Number of bp	GC content	Annealing temperature
GAAAATCTCTAGCAGTGGCG	Sequencing	20	50%	55°C
AGACAATCAGCCCTCTGTTC	Sequencing	20	50%	56°C
AACCATGGTGGATAGAGCCG	Sequencing	20	55%	59°C
TAGGGAACCCACTGCTTAAG	Sequencing	20	50%	56°C
TGAGGAGGCTTTTTTGGAGG	Sequencing	20	50%	57°C
GCATTAAAGCAGCGTATCCACA	Sequencing	22	45%	58°C
GGAATTGTGAGCGGATAACA	Sequencing	20	45%	55°C
CCAGTCACGACGTTGTAAAAC	Sequencing	21	48%	56°C
TTTCCTGGCTACACCCATCT	Sequencing	20	50%	58°C
ATTGGCGTTACTATGGGAAC	Sequencing	20	45%	55°C
GGCACCTGTGGGAAGTTGAT	Sequencing	20	55%	59°C
TGAAGAATCGCAAAACCAGC	Sequencing	20	45%	56°C

Table 5. Primers designed for sequencing of pCCL.LP1.*co-hASL* backbone. This table displays the sequence, intended use, number of base pairs, GC content and the annealing temperature of each primer. Bp; base pairs.
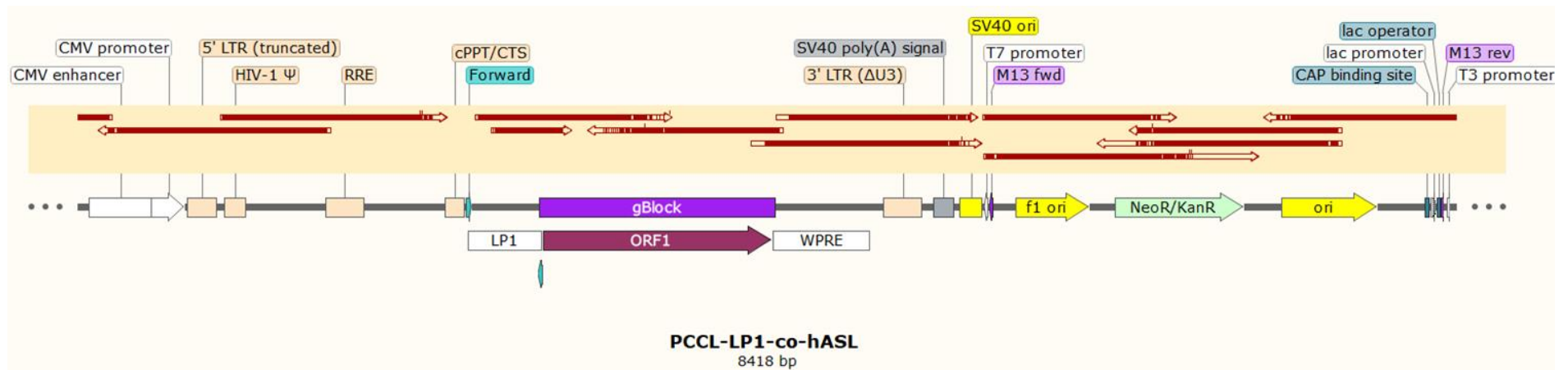
Figure 13. SnapGene image of co.hASL plasmid including sequences complementary to a CCL.LP1.*co-hASL* transgene. Red arrows indicate the sequences checked and then aligned to the CCL.LP1.*co-hASL* transgene to ensure integrity of the plasmid**.** CMV: human hepatomegaly promoter/enhancer; LTR: long terminal repeats; RRE: *rev* response element; cPPT/CTS: central polypurine tract/central termination sequence; gBlock: gene fragments; ORF1: gene that enhances readthrough of intergenic junctions during viral transcription; WPRE: woodchuck hepatitis virus post-transcriptional regulatory element; NeoR/KanR: aminoglycoside phosphotransferase confers resistance to kanamycin in bacteria, or neomycin and G418 (GeneticinI) in eukaryotes; SV40 ori: origin of replication from Simian Virus 40; CAP binding site: positive regulatory site that is bound by catabolite activator protein; T3 promoter: promoter for bacteriophage T3 RNA polymerase.

2.7 Lentiviral vector production

The second- and third-generation lentiviral vector systems are dependent on transfection with three and four separate plasmids in HEK 293T cells respectively, to create functional lentiviral particles (**Figure 14**). The second-generation lentiviral vector production requires a packaging and an envelope plasmids (Plasmid Factory, Bielefeld, Germany) coding for (i) the *gag-pol*, *rev* and *tat* plasmids, encoding the structural proteins, nucleic-acid polymerases/integrases and (ii) the *env* encoding for surface glycoprotein and the plasmid that carries the transgene sequence, respectively. In the third-generation system, the packaging system is split into two plasmids: one encoding *rev* and one encoding *gag* and *pol* while *tat* is eliminated from the third-generation system. The *env* one constitutes the fourth plasmid. After polyethylenimine (PEI)-mediated transfection, lentiviral vectors are harvested and filtered. Then the filtered media is ultracentrifuged at 23,000rpm for 2 hours and the pellet is resuspended in small volumes of PBS, aliquoted and stored in -80°C. After the virus collection, a titration step takes place by transfection of HEK293T cells with vector at different dilutions. Seven days after transfection, the transduced cells are collected, and qPCR is performed for the quantification of the vector genomes per mL.
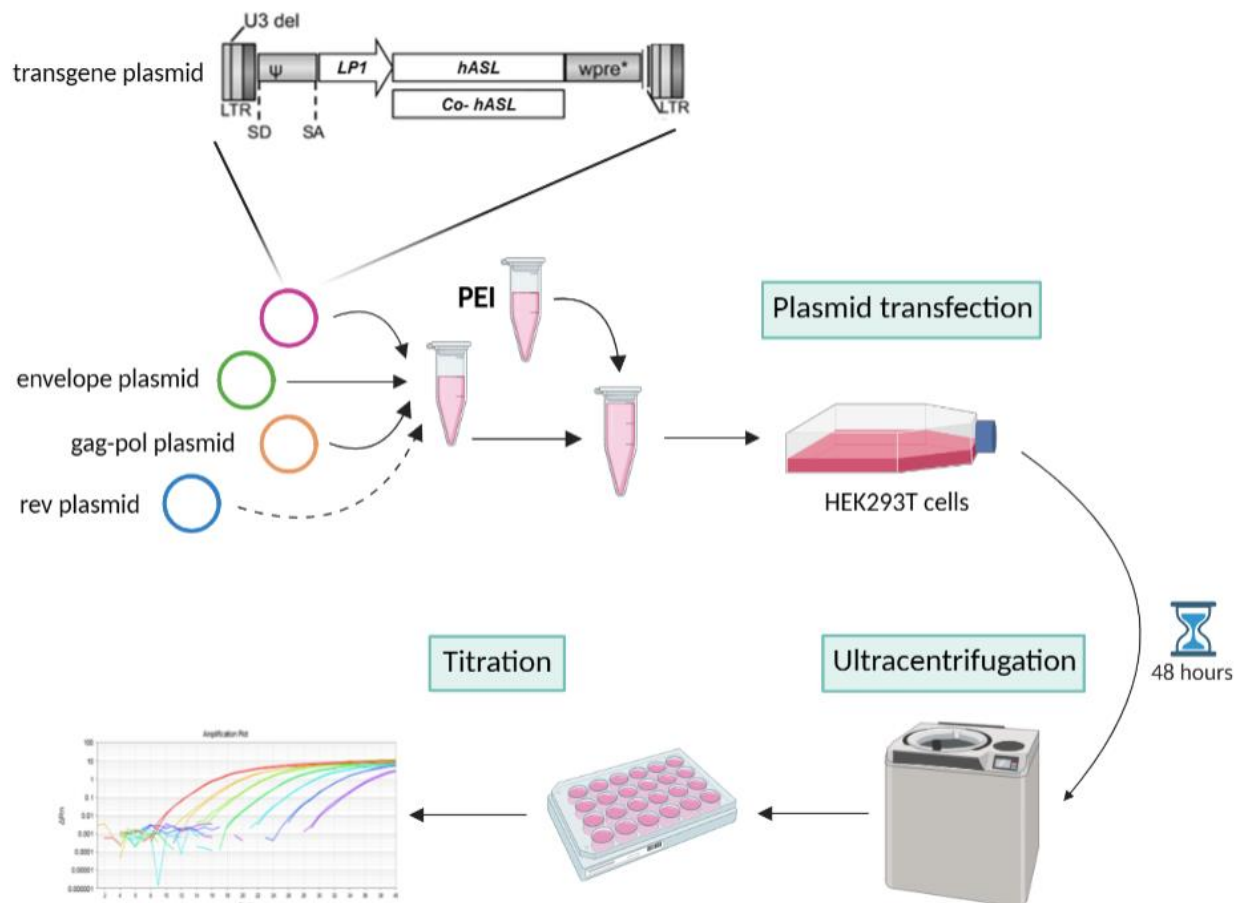
Figure 14. Schematic of production of lentiviral vector. The main steps for lentiviral vector production start with the plasmid transfection of 3 or 4 plasmids for second- or third-generation lentiviral vector system, respectively. Following the incubation of the manufacturing HEK293T cells with the lentiviral packaging plasmids, cells must incubate in cell culture media at the appropriate conditions for 48 hours, allowing the maximum vector production and its release from the cells to the supernatant. Following incubation, media is collected and then ultracentrifuged for the isolation of the pellet, which contains the viral particles. The last step involves manufacturing cells transduction with the lentiviral vector to determine the viral titer using qPCR. The dashed line represents the *rev* plasmid, encoding for a post-transcriptional regulator required as a separate plasmid for transfection of the cells for the third-generation lentiviral vector system. *Co-hASL*: codon-optimised human argininosuccinate lyase; *hASL*: human argininosuccinate lyase; WPRE: woodchuck hepatitis virus post-transcriptional regulatory element; LP1: liver specific 1 promoter; LTR: long terminal repeats; SD: splice donor; SA: *tat*/*rev* splice acceptor; U3: unique 3' region.

2.7.1 Plasmid production

The procedure for transformation of the hASL and co-hASL plasmids was performed in compliance with the guidelines specified in **Section 2.6.1**. Following transformation, LB medium containing Neomycin antibiotic was used to culture the bacteria in a moving incubator at 37°C and 200rpm for up to 16 hours. Plasmid DNA extraction was then performed using the method outlined in **Section 2.6.2**. Concentration of the DNA was assessed by evaluating the 260:280 nm ratio with a FLUOstar Omega spectrophotometer (BMG Labtech, Ortenberg, Germany).

2.7.2 Plasmid transfection for lentiviral vector production

Packaging HEK293T cells, kindly provided by Dr John Counsell, were used as producer cells for lentiviral vectors. The following steps describe the lentiviral vector production process.

HEK293T cells were cultured in 1 x T175 flasks at 37°C, 5% CO_2 in Dulbecco's Modified Eagle's Medium (DMEM; 61965059, Thermo Fisher, UK) + 10% fetal calf serum (FCS; F7524-500ML, Sigma, UK) and 1% penicillin and streptomycin (p/s; 15140-122, Invitrogen, UK). Cells were passaged once they were up to 70% confluent, using trypsin EDTA (25300054, Invitrogen). For the transfection of one T175 flask, 1.7×10^7 cells were seeded on day 0. On day 1, second-generation system transfection of transgene plasmids was performed by producing a DNA mixture, adding the 3 plasmids namely, transgene plasmid: *gag-pol* plasmid: *env* plasmid at a ratio of 40µg: 30µg: 10µg to 5mL Opti-Mem Medium (31985054, Invitrogen, UK) and filter through Polyethersulfone (PES) 0.22µm filter (83.3941.001, Sarstedt Ltd, UK). A similar process was followed for the third-generation system transfection of transgene plasmids by adding 4 plasmids namely, transgene plasmid: *gag-pol* plasmid: *env* plasmid: *rev* plasmid at a ratio of 40µg: 20µg: 20µg: 10µg to 5mL Opti-Mem Medium. To produce PEI solution, 1µL PEI was mixed 5mL Opti-Mem Medium and filter through polyethersulfone (PES) membrane 0.22µm filter. To obtain the final transfection solution, 5mL of filtered DNA mixture was combined with 5mL of PEI mixture and following a 20-minute incubation at room

temperature, DNA and PEI solution was added to the HEK293T cells. Cells were incubated in transfection solution for 4 hours at 37°C and 5% CO_2 before it was replaced with 20mL DMEM 10% FCS, 1% p/s and incubated for up to 48 hours at 37°C and 5% CO_2. At day 3, media was harvested from the cells and was centrifuged for 5 minutes at room temperature at 500xg and supernatant containing the vector was filtered through a 0.22µm filter. Supernatant was then ultracentrifuged for 2 hours, at 4°C and 23,000rpm. Then, the pellet was resuspended in 50µL cold PBS and was kept on ice for 1 hour. Virus was aliquoted in 25µL aliquots and kept in -80°C.

2.7.3 Lentiviral vector titration

50,000 HEK293T cells/well were seeded in 24-well plate, and the vector was added to the freshly seeded cells in different volumes i.e., 1µL, 2µL, 10µL. Transduced cells were incubated at 37°C and 5% CO_2 for 4 days and were passaged to a 6-well plate and incubated for an extra 3 days. Cells were collected and stored at -20°C until the extraction of the genomic DNA and qPCR process was followed as described in **Section 2.5**. Results were normalized using the housekeeping gene β-actin. To compute the viral vector titre, the VCN was divided by the titin copy number, multiplied by 2, and subsequently converted to yield a titre expressed in viral genomes per mL (vg/mL) using the following calculation:

- **VCN * 50,000 / vector volume added to cells (mL)**.

2.8 Analysis of ASL activity in liver tissue

All of the samples were analyzed in duplicates. Each liver sample stored in -80ºC (25–30mg) was added to 200μL of cold homogenizing buffer containing 50mM phosphate buffer (P3619-1GA, Sigma Aldrich, UK), and proteinase inhibitors (EDTA-free proteinase inhibitor; Switzerland). Samples were homogenized on ice and were centrifuged at 10,000g at 4°C for 20 minutes. Supernatant from the sample was then stored at -80°C. For each sample, 2μL of lysate was added to 48μL of 50mM phosphate buffer (pH 7.3) and 3.6mM argininosuccinic acid mixture (A5707-50MG, Merk, UK). The reaction was incubated at 37°C for 1 hour and stopped by heating for 20 minutes at 80 °C. The Fumarate Assay Kit was used to measure ASL activity levels (ab102516, Abcam, UK) as per manufacturer's instructions, using 5μL of reaction sample solution (**Figure 15**).
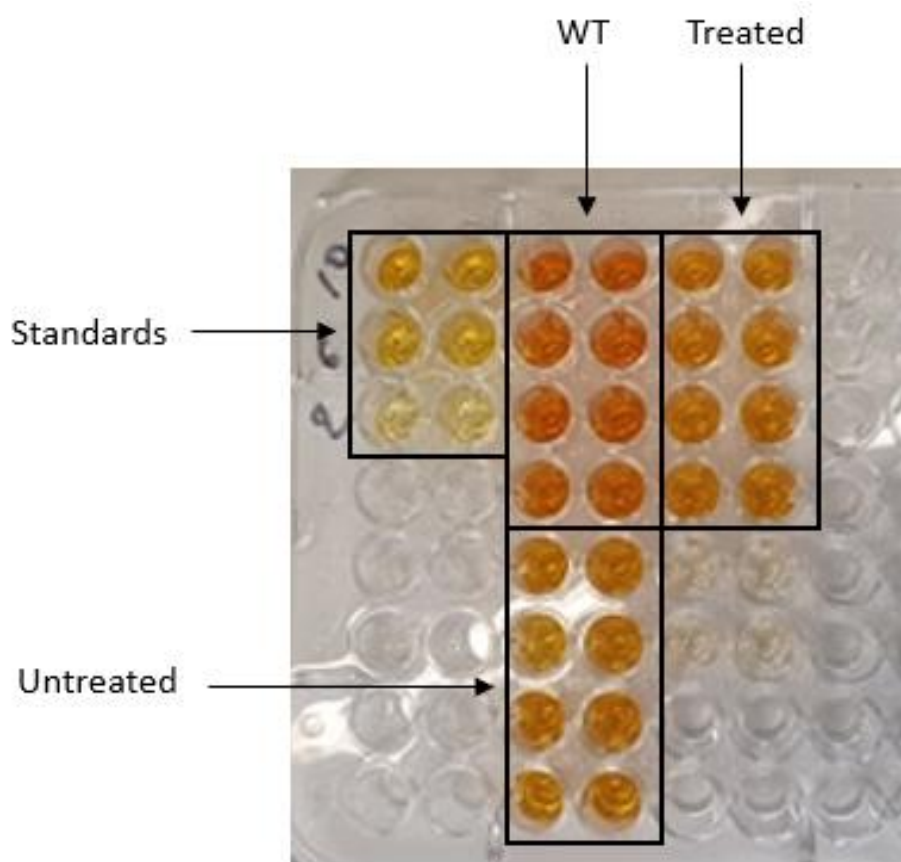
Figure 15. Read-out of ASL activity assay. Darker color indicates high ASL activity levels and high ASL activity; light color indicates low ASL activity levels and reduced ASL function. WT: wild-type.

2.9 Protein quantification

All samples were analyzed in duplicates.

Each liver sample stored in -80°C was added to 500µL of lysis buffer (E3971, Promega, UK). Samples were homogenized manually at room temperature by vortexing and were centrifuged at 10,000g for 15 minutes. Supernatants were collected and kept at -80°C. Protein was measured with micro bicinchoninic acid (BCA) Protein Assay Kit (23235, Thermo Fisher, UK) as per manufacturer's specifications, using 10µL of the lysed sample.

2.10 In-cell Western blot

Human hepatoma (Huh7) cells were seeded in a 96-well plate at a density of $1x10^4$ cells/well with a total volume of 50µL per well in DMEM 10% FCS, 1% p/s, and returned to the incubator at 37°C, 5% CO_2. At 24 hours after plating the cells, vials with vector were thawed. Vectors were diluted accordingly and added to each well making sure not to disrupt the cells. Wells for positive controls were removed from the media and 3% lipofectamine (18324010, Thermo Fisher, UK) diluted in Opti-MEM was mixed with 100 mg/well of control plasmid/ Opti-MEM solution. Lipofectamine/plasmid solution was incubated for 15 minutes at room temperature and was added to wells. Four hours later, lipofectamine/plasmid solution was carefully removed from the cells and media was added. At 72 hours after the transfection of the cells with vector, media was carefully removed, and the plate was washed with 300µL/well of PBS. Plate was then fixed using with 100µL/well of ice-cold methanol (stored at -20°C) for 10-15 minutes at room temperature. After methanol removal, the plate was washed with 300µL/well of PBS. Subsequently, 300µL/well of PBS Blocking Buffer (produced by LI-COR Biosciences, Cambridge, UK) was added to the plate and incubated for 1.5 hours at room temperature on the Belly Dancer (from Ibi Scientific, UK). Once the blocking buffer was taken out, the Anti-ASL antibody was diluted in the blocking buffer (1:1,000), and 100µL/well of the

antibody mixture was added to the plate, incubating for 2 hours at room temperature on the Belly Dancer. Following this, the antibody mixture was removed, and the plate was washed with 300µL/well of PBS containing 0.1% Tween (obtained from CAYM400035-1, VWR International, UK) for 5 minutes on the Belly Dancer, repeating this process 4 times. CellTag700 (LI-COR Biosciences, UK; product number 926-42091) and IRDye 800CW Goat anti-Rabbit IgG (LI-COR Biosciences, UK; product number 926-32211) were diluted in PBS Blocking Buffer (1:1,000), and 100µL/well of the diluted solution was applied to the plate (**Figure 16**). The plate was then covered with aluminium foil and incubated for 1 hour at room temperature on the Belly Dancer. Once the secondary antibody/dye solution was removed, the plate was washed with 300µL/well of PBS consisting of 0.1% Tween for 5 minutes on the Belly Dancer, a total of 3 times. Lastly, the plate was rinsed with 300µL/well of PBS for 5 minutes on the Belly Dancer. The plate was analyzed by reading with the Licor Odyssey CLx (9140-09, LI-COR Biosciences, UK).
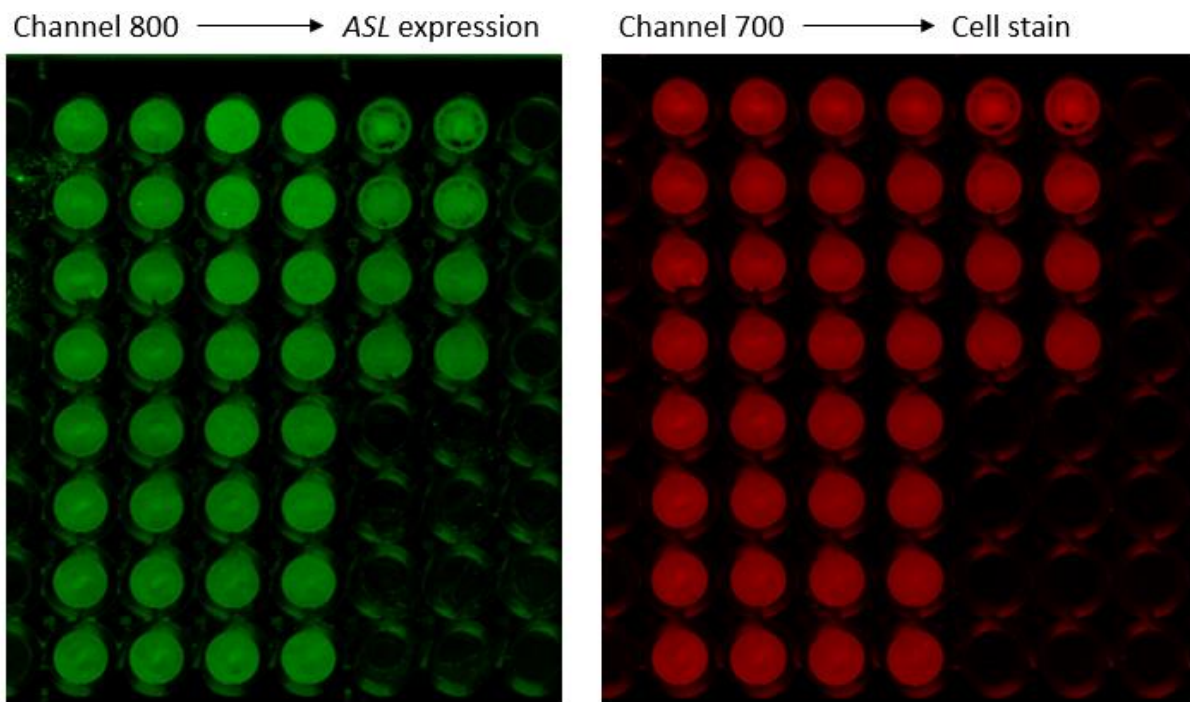
Figure 16. In-cell Western blot. Quantification of two signals at 700nm (red) and 800nm (green), for respectively the loading control and *hASL*, using spectrally distinct infrared dye conjugates.

3. NATURAL HISTORY STUDY FOR CD1 *Asl^Neo/Neo* MICE

3.1 Introduction

Asl^Neo/Neo mouse, which carries the Neomycin selection cassette in the intron 9 of the murine *Asl* gene, has a C57BL/6J background. In theory, the fundamental characteristic of an inbred strain is that every individual possesses the same homozygous allele for each DNA sequence in the genome. As a result, they are genetically indistinguishable. [290]. However, as it has been shown in the past, inbred mouse strains including C57BL/6J, commonly used in the production of transgenic mice, involve issues with breeding including small litters and are considered poor first-time moms, and will often cannibalize their first litter [291]. Mice are also more likely to cannibalise their abnormal, defected, or diseased infants, which makes it particularly challenging for treatment of mouse models of recessive genetic disorders. The aim of this study was to create a congenic mouse strain that carries the *Asl^Neo* allele in a CD1 background [20]. This CD1 congenic strain has several advantages: production of bigger litters and easier breeding, dams caring well after their pups [292] and white skin and hair, allowing easier intravenous injections.

3.2 Experimental Design

A mutation or pathogenic cassette can be transferred from one background strain to another through backcrossing [293]. Five generations of backcrossing produce a line ~96% derived from the recipient genome i.e., defined as congenic strain meaning that there is <5% difference of genetic background (**Figure 17**). This experiment was designed to assess whether CD1 ASL-deficient mice are able to recapitulate the phenotype of ASA patients as accurately as C57BL/6J ASL-deficient mice do. This congenic mouse strain was generated by

backcrossing of heterozygous C57BL/6J ASL-deficient mice with CD1 wild-type mice for 5 generations. The CD1 $Asl^{Neo/Neo}$ mice were then monitored for 2 months for assessing survival, growth, and urea cycle biomarkers (**Figure 18**).
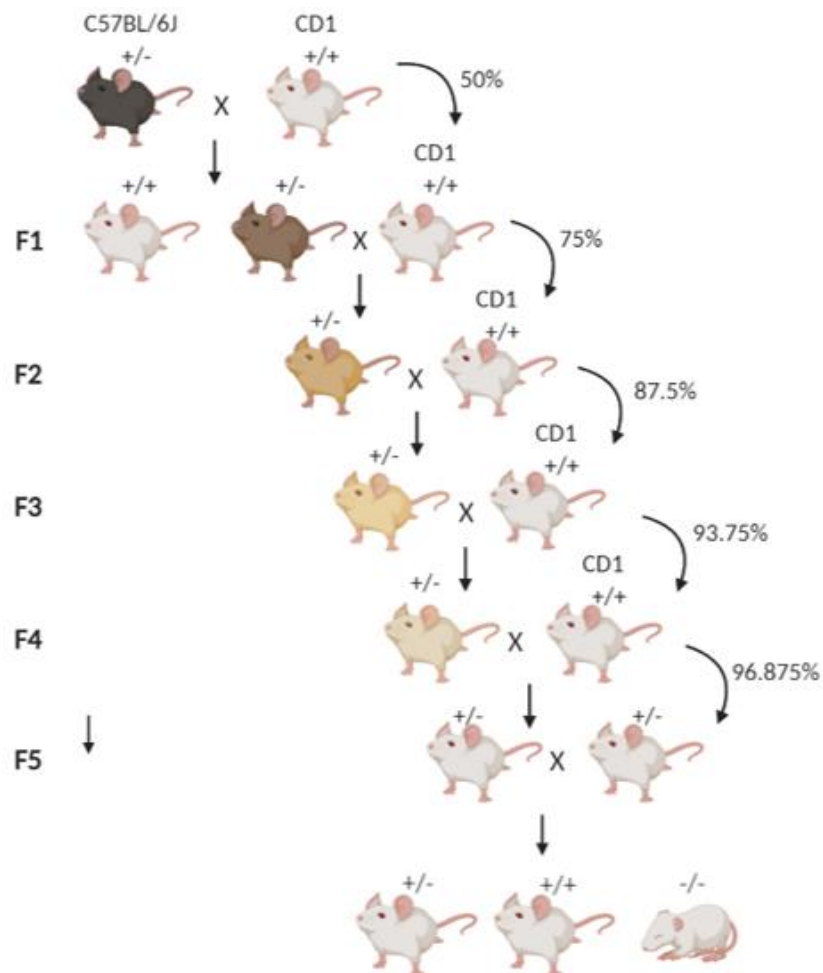
Figure 17. Schematic of the breeding scheme performed to backcross $Asl^{Neo/Neo}$ mice in C57BL/6J for into CD1 mice. Curved arrows represent the percentage of the recipient genome from one generation to the next. F5: generation 5.
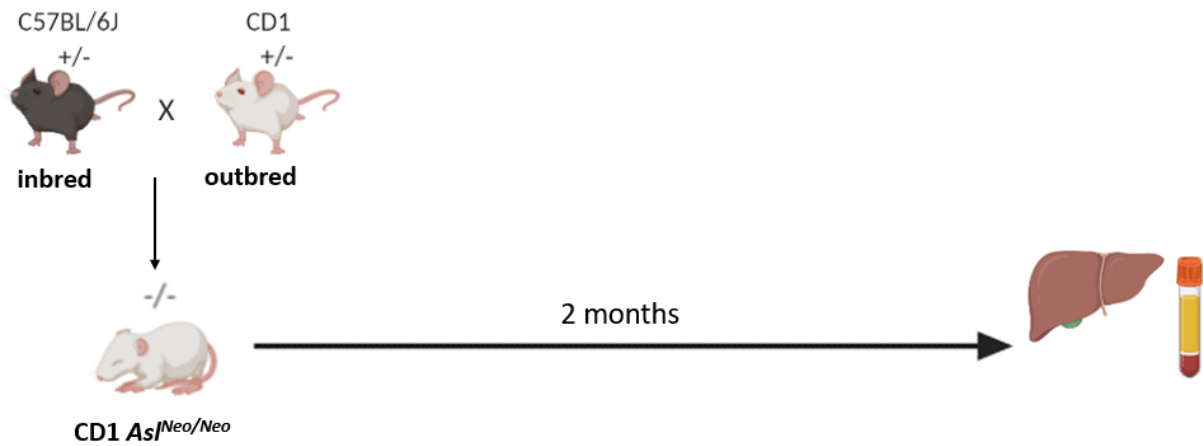
Figure 18. Schematic representation of the natural history study experimental design.

3.3 Macroscopic phenotype of CD1 *Asl*^{Neo/Neo} mice

3.3.1 Survival

There was a significant decrease in survival between CD1 *Asl*^{Neo/Neo} and wild-type mice (p=0.007) over the period of 2 months. However, there was also a high variability and a large interval of the observed age of death in CD1 *Asl*^{Neo/Neo} mice. Two of the eleven CD1 *Asl*^{Neo/Neo} mice presented with extremely severe phenotype and died within the second week of life from multi-organ failure, although, three mice, survived past the first month and two of them were sacrificed at 2 months after birth due to experiment end, not reaching humane endpoint (**Figure 19A**). Both male and female CD1 *Asl*^{Neo/Neo} mice showed large variability in survival. In this experiment, two out of six CD1 *Asl*^{Neo/Neo} males showed an extremely mild phenotype and survive until the end of the experiment, where they were sacrificed for sample analysis (**Figure 19B**). One of the four female CD1 *Asl*^{Neo/Neo} mice also revealed a very mild phenotype as it was sacrificed on day 57 due to critical weight loss, unlike the rest of the female mice in this group that were sacrificed within the first 3 weeks of life due to severe phenotype. (**Figure 19C**).
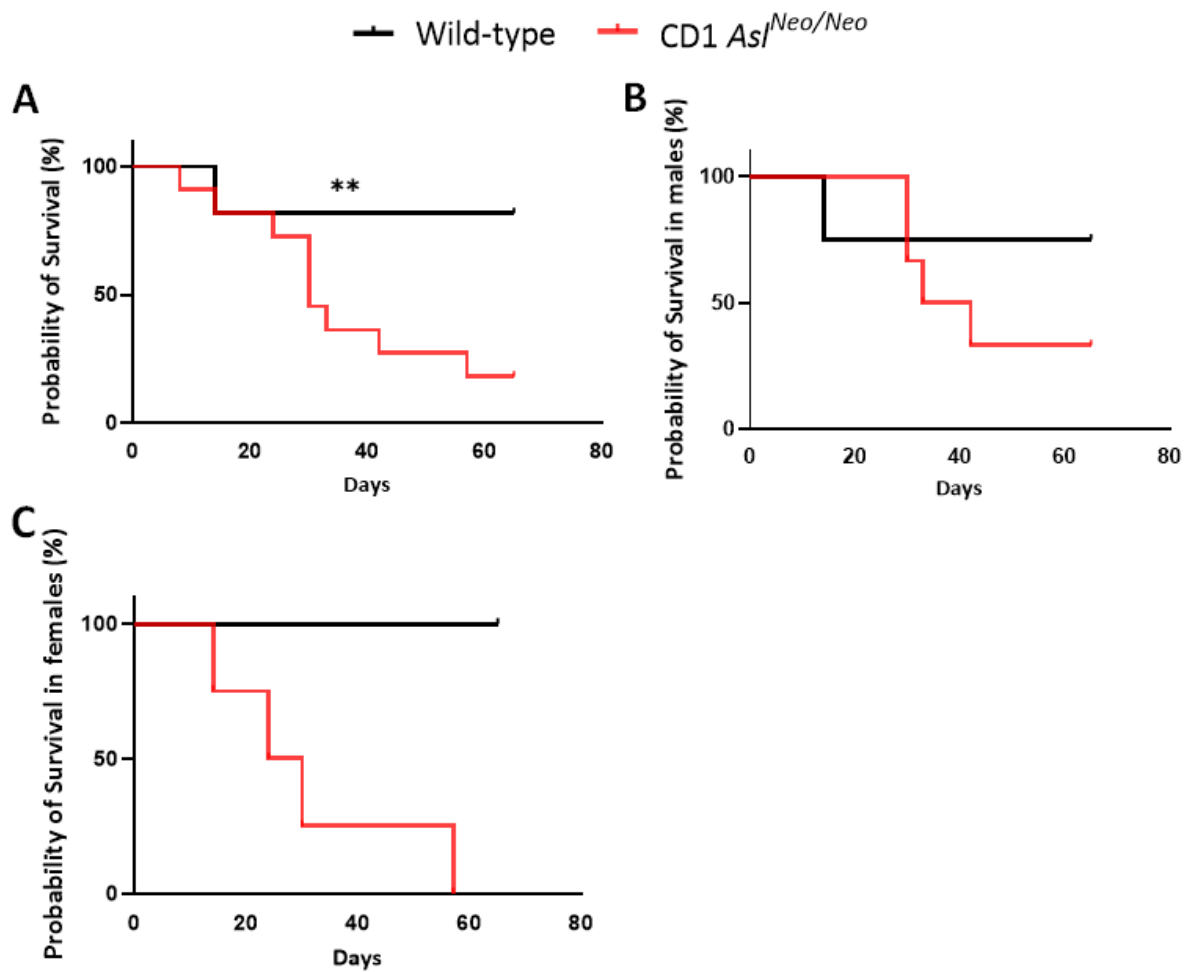
Figure 19. Survival curve of CD1 *Asl*^{Neo/Neo} mice. (A) Kaplan-Meyer survival curve of wild-type (n=11) and CD1 *Asl*^{Neo/Neo} (n=11) mice; **(B)** survival curve of male wild-type (n=8) and CD1 *Asl*^{Neo/Neo} (n=7) mice; **(C)** survival curve of female wild-type (n=3) and CD1 *Asl*^{Neo/Neo} (n=4) mice over 2 months. Log-rank ns: ** *p*<0.01.

3.3.2 Growth

Daily weight measurements showed a growth restriction between CD1 $Asl^{Neo/Neo}$ and wild-type control littermates, just reaching significance (p=0.05) (**Figure 20A**). Both male and female CD1 $Asl^{Neo/Neo}$ mice showed overall lower weight compared to the wild-type littermates for male (p=0.01) and female (p=0.05) CD1 $Asl^{Neo/Neo}$ animals. (**Figure 20B,C**).
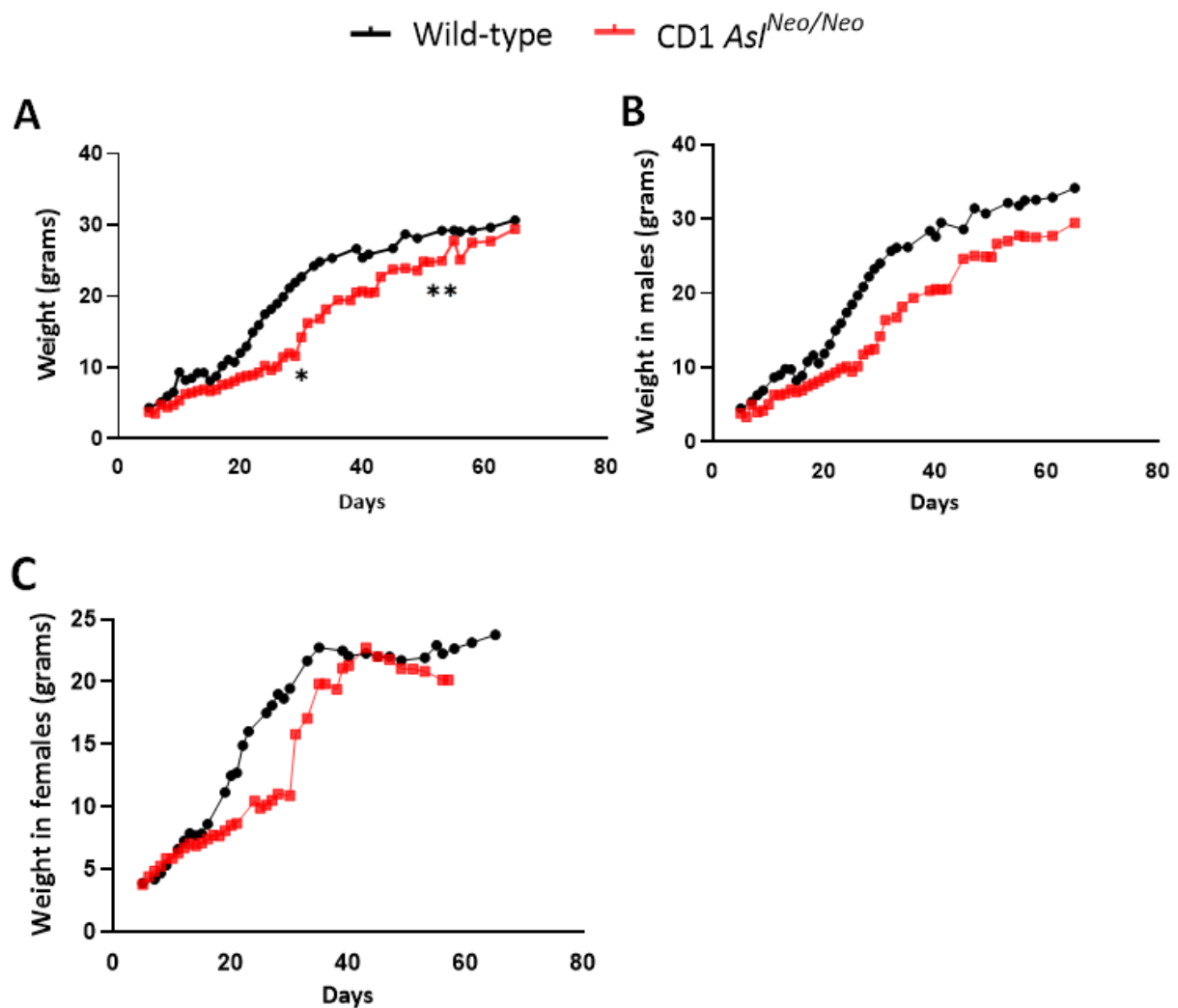
Figure 20. Growth curve of CD1 $Asl^{Neo/Neo}$ mice. (A) Mean growth of wild-type mice (n=11) and CD1 $Asl^{Neo/Neo}$ (n=11) over 2 months. * 50% and ** 18% of CD1 $Asl^{Neo/Neo}$ mice survived at day 30 and day 57, respectively. **(B)** Mean growth of male wild-type mice (n=8) and CD1 $Asl^{Neo/Neo}$ (n=7) over 2 months. **(C)** Mean growth of female wild-type mice (n=3) and CD1 $Asl^{Neo/Neo}$ (n=4) over 2 months. Horizontal lines display the mean ± standard deviation. Unpaired 2-tailed Student's t-test; * p<0.05.

Similar to C57BL/6J *Asl^{Neo/Neo}* mice, gross examination revealed that CD1 *Asl^{Neo/Neo}* congenic mice present abnormal fur pattern with brittle hair during the first week of life (**Figure 21A**). Several CD1 *Asl^{Neo/Neo}* mice however, appeared with more uniform fur pattern, and increased weight and size, particularly the ones that survived past day 30 of life (**Figures 21B**). This is contradicting with growth and fur pattern of C57BL/6J *Asl^{Neo/Neo}* mouse model where the phenotype shows a weight decline and brittle hair appearance from the second week of life.
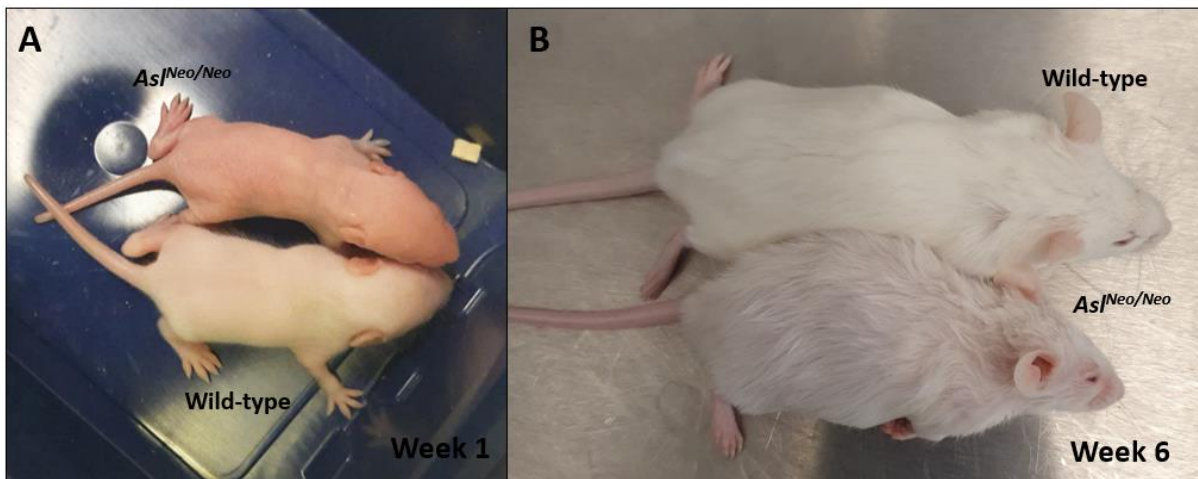
Figure 21. Representative pictures of the CD1 *Asl^{Neo/Neo}* mice macroscopic phenotype. (A) Image of wild-type and CD1 *Asl^{Neo/Neo}* mice at week 1 after birth. **(B)** Image of wild-type and CD1 *Asl^{Neo/Neo}* mice at week 6 after birth.

3.3.3 Liver Phenotype

ASL-deficient C57BL/6J mice present with impaired growth and significantly lower body weight in comparison to wild-type animals. In this experiment, the liver weight of CD1 *Asl^{Neo/Neo}* mice at harvest was significantly increased compared to wild-type littermates ($p<0.006$). Variability was also observed with half (n=3) of the animals measured showing values similar to wild-type levels (**Figure 22**).
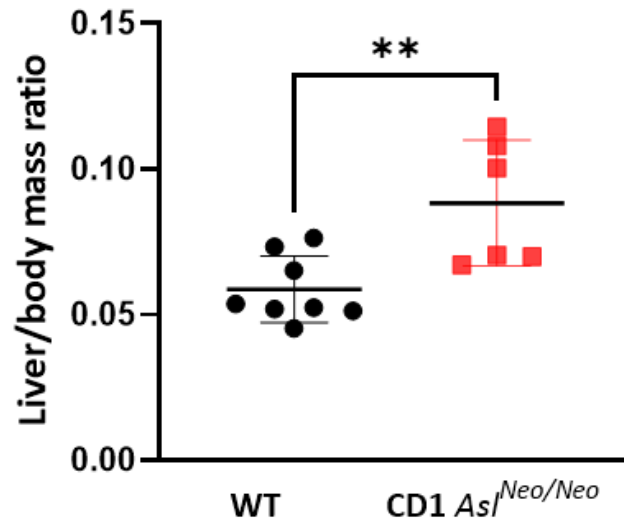
Figure 22. Hepatomegaly. Liver/body mass ratio in wild-type (n=8) and CD1 *Asl^{Neo/Neo}* mice (n=6) at culling. Horizontal lines display the mean ± standard deviation. Unpaired 2-tailed Student's t-test; ** *p*<0.01. WT: wild-type.

3.3.4 Urea cycle biomarkers

Biomarkers from plasma and dried blood spots were used to assess defective ureagenesis in CD1 *Asl^{Neo/Neo}* compared to wild-type mice (**Figure 23**). ASL deficiency causes high ASA, high citrulline, low arginine as well as increased glutamine + glutamate levels used as a buffer pathway to delay hyperammonaemia. CD1 *Asl^{Neo/Neo}* showed significantly increased plasma ammonia levels (*p*=0.005) compared to wild-type littermates (**Figure 23A**) at culling. Argininosuccinic acid levels in dried blood spots at culling showed a significant increase (*p*=0.02) in CD1 *Asl^{Neo/Neo}* mutants compared to wild-type littermates (**Figure 23B**). Compared to wild-type, arginine levels were significantly reduced in CD1 *Asl^{Neo/Neo}* (*p*=0.001) (**Figure 23C**). Citrulline levels were significantly increased in CD1 *Asl^{Neo/Neo}* compared to controls (*p*<0.0001) (**Figure 23D**) as well as glutamine and glutamate levels (*p*<0.0001) (**Figure 23E**).
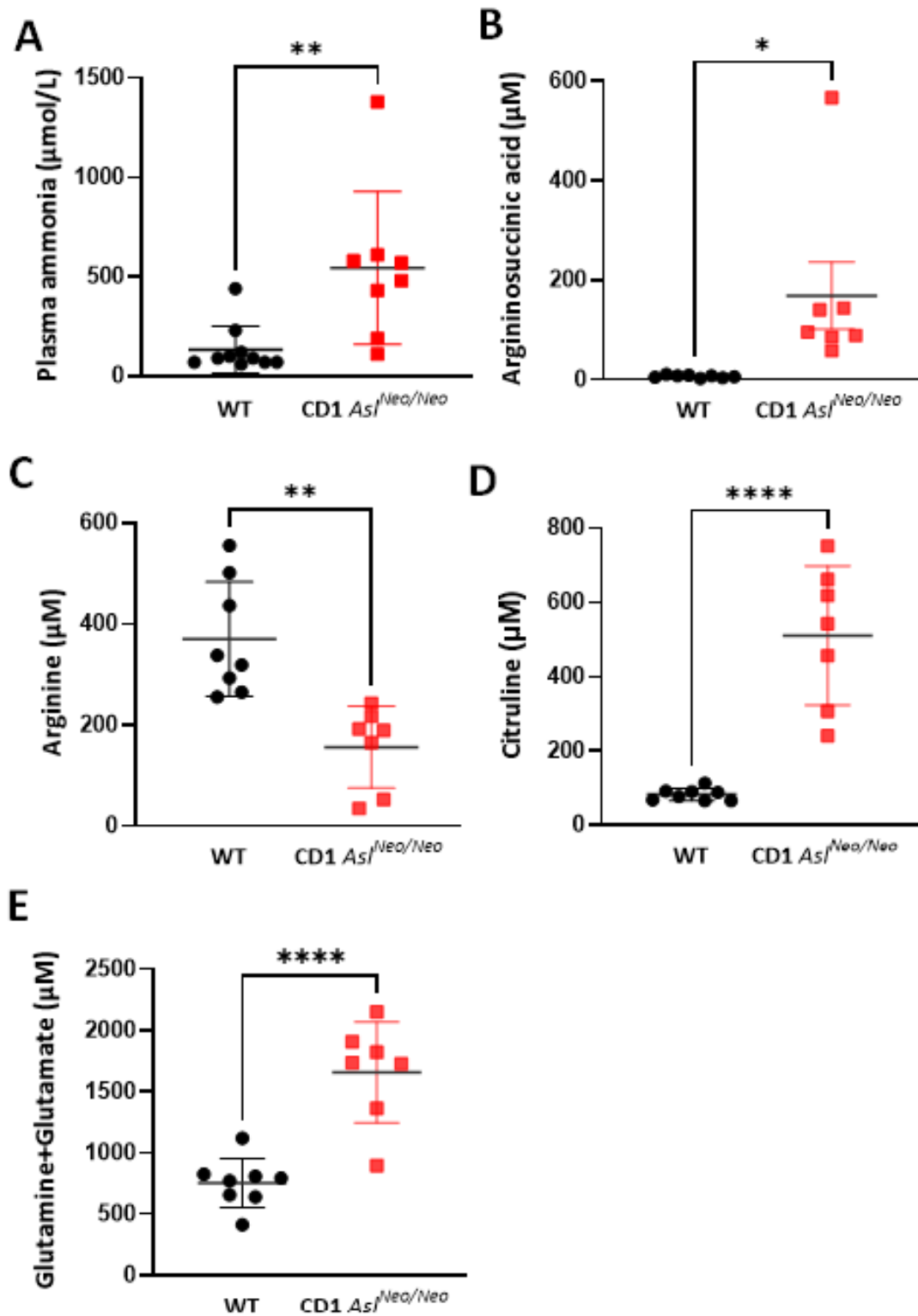
Figure 23. Urea cycle biomarkers. All the biomarkers were measured in wild-type (n=8-10) and CD1 *Asl^Neo/Neo* mice (n=7-8) at time of culling. **(A)** Plasma ammonia levels; **(B)** argininosuccinic acid levels from dried blood spots; **(C)** arginine levels from dried blood spots; **(D)** citrulline levels from dried blood spots; **(E)** orotate levels from dried urine spots. Horizontal lines display the mean ± standard deviation. Unpaired 2-tailed Student's t-test; * $p<0.05$, ** $p<0.01$, **** $p<0.0001$. WT: wild-type.

ASL activity in the liver of CD1 *Asl^Neo/Neo* mice was significantly lower compared to wild-type levels (*p*=0.002) (**Figure 24**).
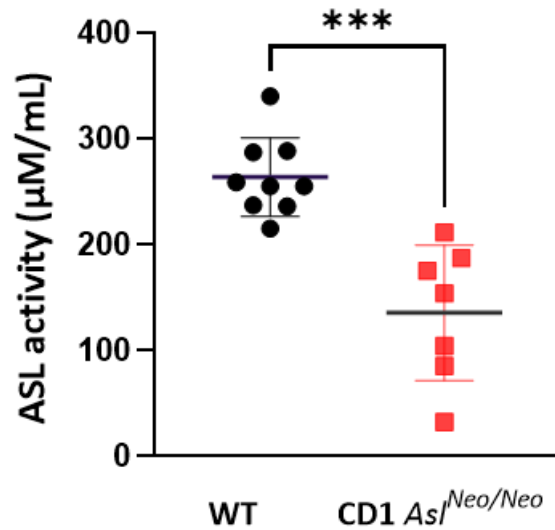
Figure 24. Liver ASL activity in whole liver. All the values were measured in wild-type (n=9) and CD1 *Asl^Neo/Neo* mice (n=7). Horizontal lines display the mean ± standard deviation. Unpaired 2-tailed Student's t-test; *** *p*<0.001. WT: wild-type.

3.4 Discussion

To facilitate *in vivo* testing of this lentiviral vector, we tried to modify the strain background of the *Asl^(Neo/Neo)* mouse model. C57BL/6J is an inbred mouse strain presented with less genetic heterogeneity, however breeding is more difficult. Outbred mouse strains, such as CD1 mice have several major advantages, including that they have big litters and that they are excellent breeders [292]. Congenic CD1 *Asl^(Neo/Neo)* mice recapitulated the phenotypical differences compared to wild-type mice observed in C57BL/6J *Asl^(Neo/Neo)* mice with increased plasma ammonia, argininosuccinic acid, citrulline, glutamine + glutamate levels, low arginine levels as well as low liver ASL activity. However, they presented with high variability. The variability of the phenotypical characteristics between CD1 *Asl^(Neo/Neo)* mice is possibly a result of CD1 being an outbred strain that is defined by high genetic heterogeneity which could have a role in epigenetic regulation of ASL in comparison with C57BL/6J which is an inbred strain and is genetically identical [294]. Results in **Section 3.3** demonstrated significantly reduced weight and survival of CD1 *Asl^(Neo/Neo)* mice compared to wild-type animals, which is also a characteristic of C57BL/6J ASL mutants. However, in this study, two out of eleven CD1 mutants survived until the end of the experiment presenting a milder phenotype with similar weight and fur pattern to the wild-type littermates. In accordance to previous publication describing the C57BL/6J *Asl^(Neo/Neo)* mouse model, results from CD1 *Asl^(Neo/Neo)* mice in this study revealed overall similar plasma ammonia levels between strains, however an over 2-fold higher ASL residual activity in the liver of CD1 compared to C57BL/6J *Asl^(Neo/Neo)* mice [20]. These results explain why CD1 *Asl^(Neo/Neo)* mice present with overall milder phenotype and significantly longer survival and weight. As a result, they are not the best animal model to test proof-of-concept of novel therapies.

3.5 Conclusion

In this study I created a congenic mouse strain that carries the homozygous Asl^{Neo} allele in the CD1 background. Results from this study have confirmed that even though CD1 $Asl^{Neo/Neo}$ mice present with a phenotype similar to C57BL/6J $Asl^{Neo/Neo}$ mouse model, they also show high variability, which complicates the assessment of efficacy of new therapies. Based on these findings, CD1 $Asl^{Neo/Neo}$ mice were not used in future gene therapy experiment.

4. *IN VIVO* LENTIVIRAL GENE THERAPY FOR THE TREATMENT OF NEONATAL *ASL*^{Neo/Neo} MICE

4.1 Introduction

ASA is a rare inherited metabolic disorder with a prevalence of 1/70.000 live births which is caused by the deficient function of the ASL enzyme, that leads to impaired ureagenesis and increased ammonia levels [31]. Patients present neonatal hyperammonaemic coma or life-threatening hyperammonaemic decompensation later in life. Epilepsy and neurocognitive deficit are also observed. A reliable gene delivery system is required to transfer the *hASL* gene to the liver for treating ASA. Previous *in vivo* studies using AAV vector have shown a highly efficient gene transfer to hepatocytes [83]. However, its efficacy remained limited in neonatal pups as AAV vectors integrate very marginally into the host genomic DNA [83].

Lentiviral transgene delivery has previously established sustained expression as a result of its ability to integrate into the host cell DNA [295]. As mentioned in **Section 1.3**, the hypomorphic *Asl*^{Neo/Neo} mouse model recapitulates the human phenotype of ASL deficiency with multi-organ dysfunction and NO deficiency [20]. The aim of this experiment was to assess the efficacy of lentiviral vector with *hASL* as a therapeutic gene injected in neonatal *Asl*^{Neo/Neo} mice. For this research, the lentiviral vector backbone employed was the pCCL SIN vector. Zufferey et al. created the CCL vector, which comprises roughly 10% of the unaltered HIV-1 genome [296]. The U3 promoter region's viral enhancers and TATA box have been removed from the 3'LTR in this backbone. This renders the promoter ineffective in the integrated provirus because the U3 region of the 3'LTR is duplicated into the 5'LTR during integration. Several vital elements were included in this lentiviral vector backbone such as *rev* response element (RRE) [297]. RRE enhances the vector's transduction efficiency and allows the efficient production of the therapeutic protein by exporting the unspliced or partially spliced viral mRNAs from the nucleus to the cytoplasm in the presence of *rev* [297, 298]. Central

Polypurine Tract/Central Termination Sequence (cPPT/CTS) are also crucial elements of the lentiviral vector backbone as they enhance transduction efficiency, and the ability of the virus to introduce its genetic material into the host cell. The cPPT sequence helps generate a DNA 'flap' structure during reverse transcription, facilitating the nuclear import of the viral DNA. The CTS works alongside the cPPT to promote the efficient transduction of non-dividing cells [299]. In addition to the CCL backbone, the synthetic liver-specific promoter 1 (LP1) was also chosen to maximise the liver expression of the vector. The LP1 promoter consists of the liver-specific *hAAT* promoter in combination with the Apolipoprotein E (ApoE) -HCR that is used to promote a restrict transcription of lentiviral vector to hepatocytes. LP1 promoter has previously shown the strongest signal in the liver when compared to elongation factor-1α (EF1α), phosphoglycerate kinase (PGK), and human ubiquitin C (UbiC) promoter 1 month following intravenous injection [300, 301]. WPRE was also included in the transgene backbone for increasing transgene expression in the target organ [242, 302]. This is extremely critical for liver inherited metabolic diseases such as ASA, where most patients show a severe phenotype in infancy/early childhood, when the liver is still rapidly growing.

4.2 Experimental design

This experiment was designed to assess whether a single neonatal injection of CCL.LP1.*hASL* vector is able to improve the severe phenotype of *Asl*[Neo/Neo] mice. The second-generation lentiviral vector system was used for vector production. For this study, three groups of animals were monitored: wild-type, treated *Asl*[Neo/Neo] and untreated *Asl*[Neo/Neo] mice. Treated *Asl*[Neo/Neo] pups received a single neonatal intravenous injection at P0-P3 (**Figure 25**) at the medium dose of 9.5e9TU/Kg, while untreated *Asl*[Neo/Neo] mice were uninjected and used as negative controls. One of the main focuses in this study was to treat the hypomorphic mice as early as possible in order to target the neonatal liver prior to its rapid growth that takes place during the first 4 weeks of life. This enables the maximum transduction of hepatocytes due to the ability of lentiviral vector to integrate. During liver growth, a significant percentage

of the transduced hepatic cells will expand, leading to a higher number of hepatocytes expressing hASL compared to adult-treated mice [303]. Following the neonatal injection with lentiviral vector, all groups were monitored daily for 6 weeks. No supportive treatment was given to any of the groups involved in this experiment.
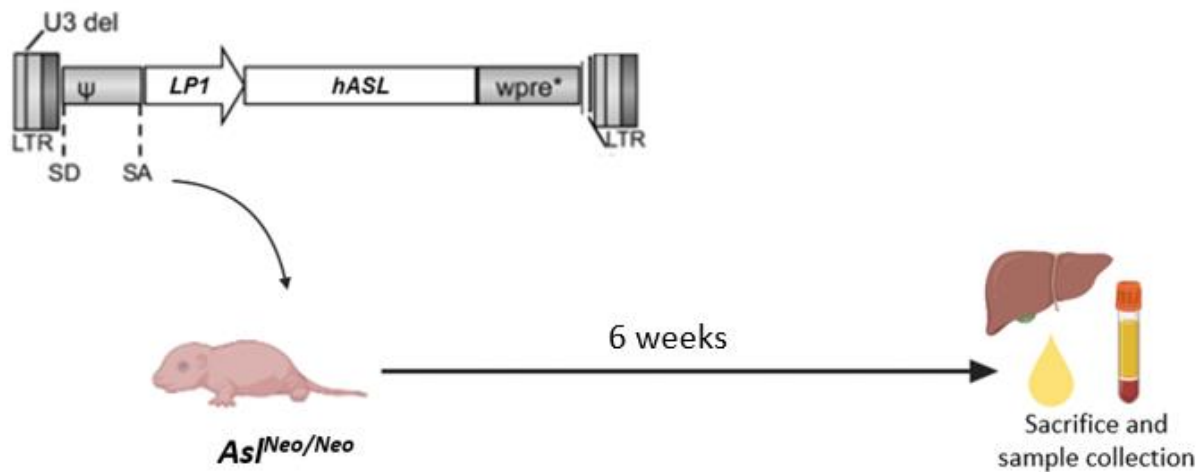
Figure 25. Schematic representation of the gene therapy with CCL.LP1.*hASL* vector experimental design. hASL: human argininosuccinate lyase; LP1: liver specific 1 promoter; LTR: long terminal repeats; SA: *tat*/*rev* splice acceptor; SD: splice donor; U3: unique 3' region; WPRE: woodchuck hepatitis virus post-transcriptional regulatory element.

4.3 Effect of gene therapy with CCL.LP1.*hASL* vector on macroscopic phenotype

4.3.1 Survival

A trend towards improvement of survival was shown in lentiviral vector treated $Asl^{Neo/Neo}$ animals in comparison to the untreated ones although without statistical significance (p=0.93) (**Figure 26A**). Both male and female untreated mice showed poor survival as they needed to be sacrificed within the third and fourth week of life, respectively. In this experiment, three out of four treated animals were males, with one of them surviving until the end of the experiment. One female was sacrificed within the fourth week following treatment due to the severe phenotype. (**Figure 26B,C**). Out of the four $Asl^{Neo/Neo}$ mice that received the CCL.LP1.*hASL* vector, only one $Asl^{Neo/Neo}$ treated mouse presented with significantly longer survival period and it was sacrificed at 6 weeks of age due to termination of experiment for proceeding with sample analysis. The rest of the $Asl^{Neo/Neo}$ treated mice died within the third and fourth week of life, similarly to untreated $Asl^{Neo/Neo}$ mice due to the severity of the phenotype (**Figure 26**).
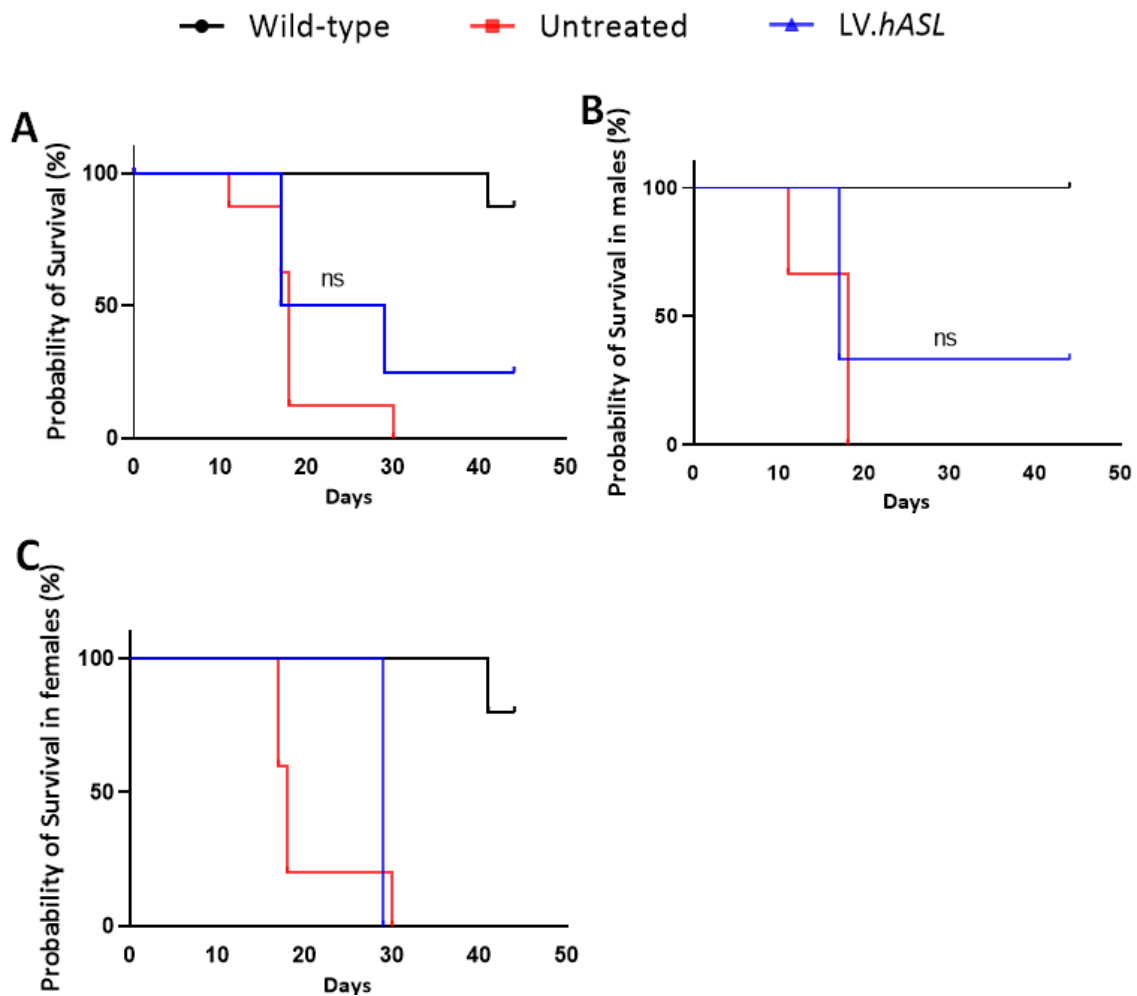
Figure 26. Survival curve gene therapy-injected *Asl^Neo/Neo* mice. (A) Kaplan-Meyer survival curve of wild-type (n=8); untreated *Asl^Neo/Neo* (n=4) and treated *Asl^Neo/Neo* (n=4) mice; **(B)** survival curve of male wild-type (n=3), untreated *Asl^Neo/Neo* (n=3) and treated *Asl^Neo/Neo* (n=3) mice; **(C)** survival curve of female wild-type (n=5), untreated *Asl^Neo/Neo* (n=5) and treated *Asl^Neo/Neo* (n=1) mice over 6 weeks. Log-rank ns: not significant.

4.3.2 Growth

Daily weight measurements did not show any sustained growth correction in treated versus untreated *Asl^Neo/Neo* mice (*p*= 0.5) (**Figure 27A**). No benefit could be seen when an analysis per gender was performed (**Figure 27B, C**)
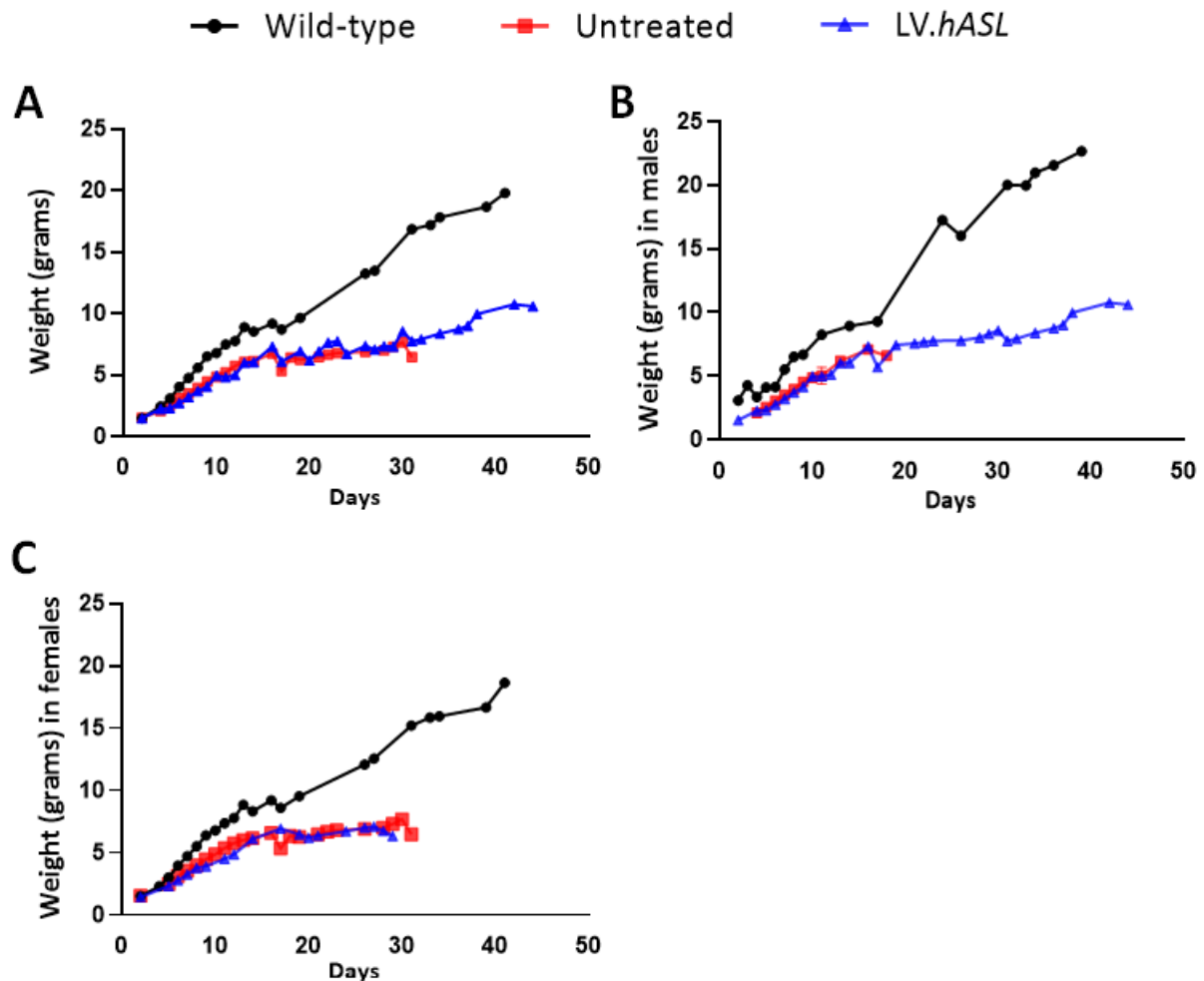
Figure 27. Growth of gene therapy-injected *Asl^Neo/Neo* mice compared to wild-type and untreated *Asl^Neo/Neo* mice. (A) Mean growth of wild-type (n=8), untreated *Asl^Neo/Neo* (n=8) and treated *Asl^Neo/Neo* (n=4) mice; **(B)** mean growth of male wild-type (n=3), untreated *Asl^Neo/Neo* (n=3) and treated *Asl^Neo/Neo* (n=3) mice; **(C)** mean growth of female wild-type (n=5), untreated *Asl^Neo/Neo* (n=5) and treated *Asl^Neo/Neo* (n=1) mice over 6 weeks. Horizontal lines display the mean ± standard deviation.

Brittle fur is a distinct characteristic of the *Asl^{Neo/Neo}* mouse model. Daily observation and monitoring of all mice revealed an improvement in the phenotype of one treated *Asl^{Neo/Neo}* mouse compared to the untreated littermates from the second week following lentiviral treatment. This treated *Asl^{Neo/Neo}* mouse showed fur improvement with a more uniform fur pattern with the hair shaft becoming straighter and more regular (**Figure 28A-B**). Fur pattern improvements were accompanied by a whole-body growth which was maintained until the end of the experiment. Despite the phenotypical improvements of one treated *Asl^{Neo/Neo}* mouse, the rest of the treated *Asl^{Neo/Neo}* littermates did not show any correction of the fur pattern and size which was maintained low until they were sacrificed within 4 weeks after birth (**Figure 28C-D**).
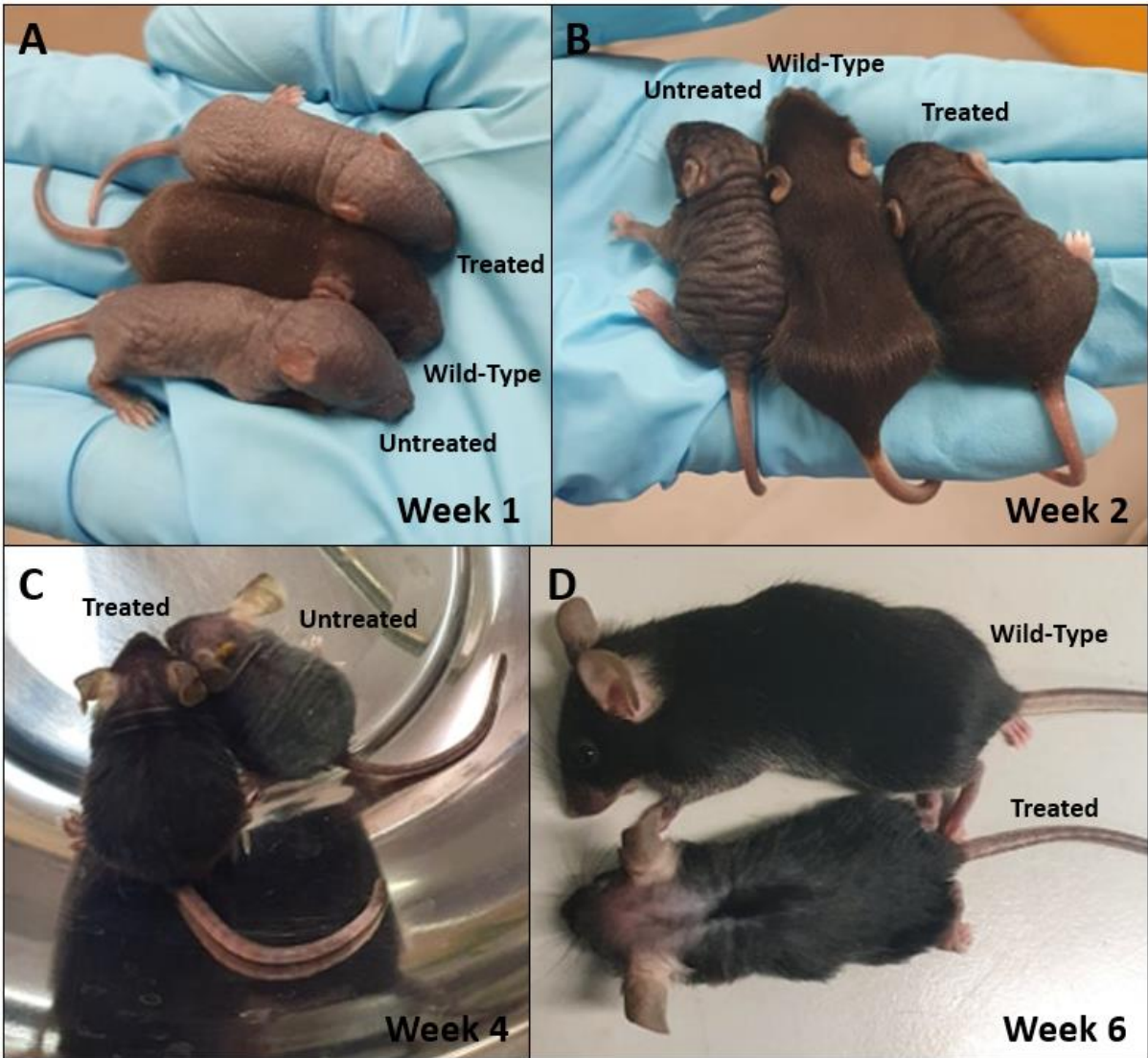
Figure 28. Macroscopic aspect of CCL.LP1.*hASL* vector-injected *Asl^{Neo/Neo}* mouse compared to wild-type and untreated *Asl^{Neo/Neo}* mice. (A-B) Images of wild-type, untreated and treated *Asl^{Neo/Neo}* mice; **(C)** image of treated and untreated *Asl^{Neo/Neo}* mice; **(D)** image of wild-type and treated *Asl^{Neo/Neo}* mouse.

4.4 Effect of lentiviral gene therapy on ureagenesis

4.4.1 Urea cycle biomarkers

Due to loss of *ASL* function and compared to the wild-type mice, *Asl^Neo/Neo^* untreated mutants present with increased ammonia, argininosuccinic acid and citrulline levels, as well as reduced arginine levels. At harvest, *Asl^Neo/Neo^* treated mice showed similar plasma ammonia levels compared to the untreated animals (p=0.9) and significantly increased (p=0.008) compared to wild-type littermates (**Figure 29A**). The *Asl^Neo/Neo^* treated mouse with some degree of improvement noted on survival, weight and fur was the one presenting the lowest ammonia levels in this cohort (**Figure 26A, 27A, 28D, 29A**). Argininosuccinic acid levels measured in dried blood spots at harvest in treated *Asl^Neo/Neo^* mice did not show any difference (p=0.8) with untreated *Asl^Neo/Neo^* mice and remained significantly increased compared to wild-type group (p<0.0001) (**Figure 29B**). Comparable results were identified in the rest of amino acids measured from dried blood spots in treated compared to untreated *Asl^Neo/Neo^* animals, including arginine (p=0.9) (**Figure 29C**) and citrulline (p=0.9) levels at harvest (**Figures 29D**).
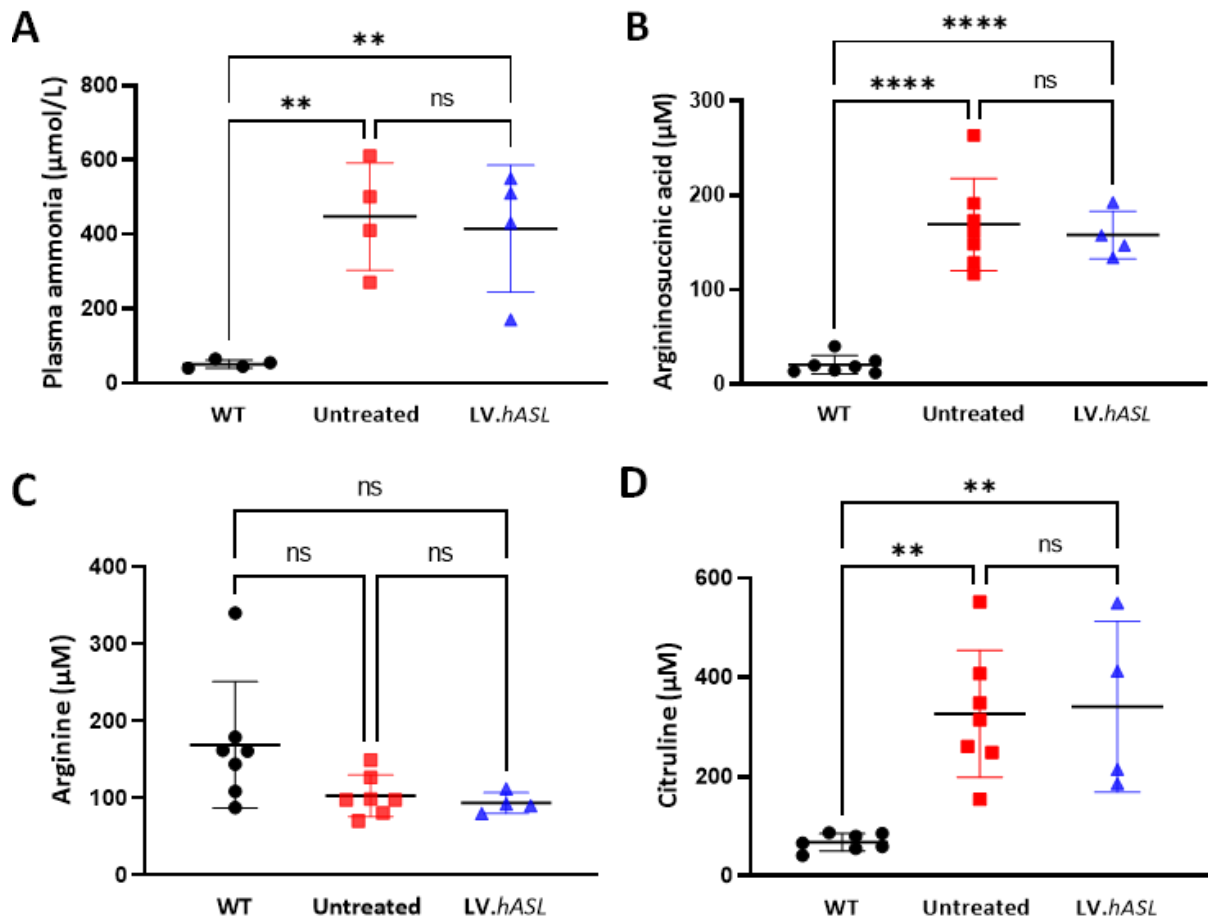
Figure 29. Urea cycle biomarkers. All the biomarkers were measured in wild-type (n=4-7), untreated *Asl^{Neo/Neo}* (n=4-7) and treated *Asl^{Neo/Neo}* mice (n=4) at time of culling. **(A)** Plasma ammonia levels; **(B)** argininosuccinic acid levels from dried blood spots; **(C)** arginine levels from dried blood spots; **(D)** citrulline levels from dried blood spots at 6 weeks following treatment. Horizontal lines display the mean ± standard deviation. One-way ANOVA with Tukey's multiple comparisons test; ns: not significant, ** $p<0.01$, **** $p<0.0001$.

4.4.2 ASL liver enzymatic activity and liver transduction

ASL activity in liver of the treated *Asl^{Neo/Neo}* animals, did not show any significant difference ($p=0.9$) compared to untreated controls and was significantly reduced ($p=0.006$) in comparison to the wild-type littermates (**Figure 30A**) at harvest.

VCN in the liver of lentiviral vector treated *Asl^{Neo/Neo}* mice was significantly increased compared to untreated controls ($p=0.01$) with value of 0.5 vector copies per cell.

Furthermore, results from the *Asl^Neo/Neo* treated mouse that showed the highest VCN with value of 0.7, correlated with the lower ammonia levels, the fur pattern improvement, and better weight gain (**Figures 28D, 29A, 30B**).

The liver immunostaining levels of ASL indicated that ASL expression was significantly lower in both treated and untreated *Asl^Neo/Neo* animals when compared to their wild-type littermates ($p<0.0001$). ASL expression in livers of the untreated group was 0.08% of the wild-type expression. An increasing trend was shown in treated *Asl^Neo/Neo* mice compared to untreated controls; however, it did not present statistical significance (*p*=0.7) with ASL expression of 4% of the wild-type expression in the liver. One treated *Asl^Neo/Neo* mouse had an increased ASL expression in the liver compared to the rest of the mice from its group, with 13% of the wild-type expression. This result is associated with the significantly lower ammonia levels, the highest liver VCN, and the partial correction of fur pattern and weight gain in that treated *Asl^Neo/Neo* mouse (**Figures 28D, 29A, 30B, 30C**). Observation of immunostaining results revealed more scattered and sparse expression in the treated *Asl^Neo/Neo* mice with no predominant expression in periportal or pericentral hepatocytes (**Figure 31**).
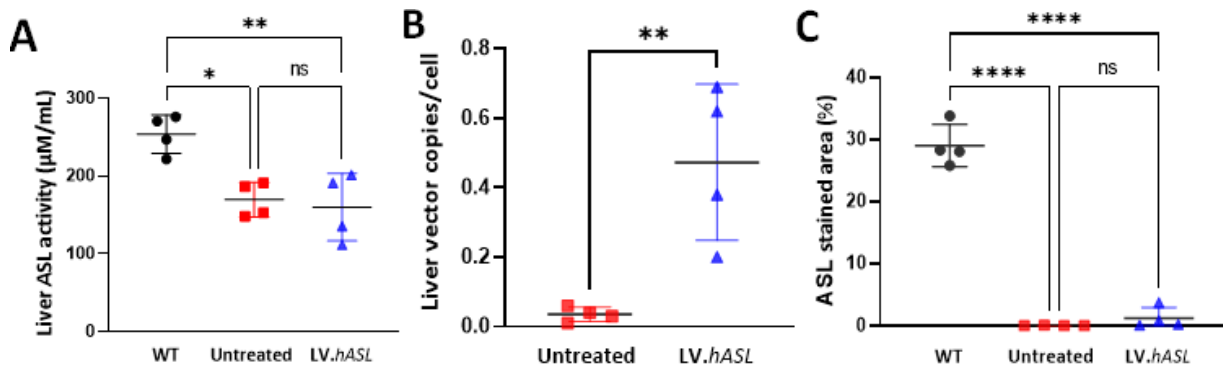
Figure 30. Liver ASL activity, liver transduction, and liver VCN. All the values were measured in wild-type (n=4), untreated *Asl^Neo/Neo* (n=4) and treated *Asl^Neo/Neo* mice (n=4). **(A)** ASL activity in whole liver; **(B)** VCN per cell in whole liver; **(C)** percentage of area in the liver expressing *ASL* at 6 weeks following treatment. Horizontal lines display the mean ± standard deviation. One-way ANOVA with Tukey's multiple comparisons test; ns: not significant, * *p*<0.05, ** *p*<0.01, **** *p*<0.0001.
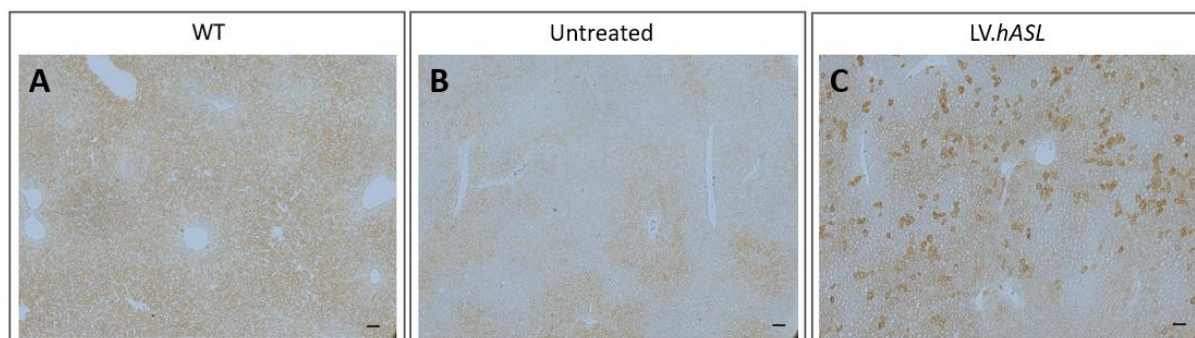
Figure 31. hASL immunostaining in liver sections. (A) wild-type, **(B)** untreated *Asl^(Neo/Neo)* and, **(C)** treated *Asl^(Neo/Neo)* mice. Scale bar: 100µm; n=4 animals per group. WT: wild-type.

4.5 Discussion

The main parameters for a reliable gene delivery system, which can reverse the clinical phenotype of the disease, include vector design, route and dose of delivery and host parameters [304]. Sustained expression of lentiviral vector *in vivo* has previously been observed in several studies [305-307]. In this lentiviral mediated gene therapy study, one out of four treated *Asl^(Neo/Neo)* mice displayed a partial correction of the urea cycle through various parameters including, survival, growth, fur pattern and plasma ammonia levels [308]. However, other biomarkers, such as amino acids of the urea cycle from dried blood spots as well as ASL activity levels in the liver did not show a significant improvement. Disease-specific markers are dependent on residual enzymatic activity [309]. A recent *in vivo* study focusing on the treatment of hemophilia B, showed highly reduced pre-existing anti-FIX antibodies and eradicated FIX inhibitors in hemophilia B mice. This study reported significant rise of FIX expression reaching 50% of normal levels, following a single injection of lentiviral vectors expressing hFIX with hepatocyte-specific Enhanced Transthyretin (ET) promoter, at the high dose of 0.75–1e9TU/mouse [310]. More recently, the same group focusing on the treatment of hemophilia A *in vivo* using lentiviral vector injected both neonatal and adult mice using a high lentiviral vector dose of 2.5e10TU/Kg and 8e10TU/Kg, respectively [241]. It is likely that a higher vector titer is required to enable higher residual ASL activity to improve ureagenesis and phenotype in *Asl^(Neo/Neo)* mice. An alternate explanation could be that due to the

persistence of severe multi-organ disease, not all extra-hepatic tissues were corrected, which prevented the improvement of the overall phenotype. VCN in the liver of the treated $Asl^{Neo/Neo}$ mice was proven significantly higher, compared to untreated controls, however, it might be that the total liver VCN does not reflect the percentage of transduced hepatocytes expressed in liver sections. This is likely a result of biodistribution of lentiviral vector between different liver cell subpopulations. It has been previously shown that below a threshold dose of 4.5e7TU/mouse, high amount of lentiviral vector DNA is uptaken by liver non parenchymal (nPCs) cell populations and especially from liver macrophages and spleen that provide a major clearance mechanism for blood-born particles, such as viral vectors [144]. Therefore, inhibition of liver phagocytic cells by overexpression of CD47 from lentiviral vectors has shown fourfold higher lentiviral VCN in targeted hepatocytes [144]. Previous studies on improving transduction using adenoviral vectors suggested that injection of clodronate-encapsulated liposomes prior to vector administration can also deplete liver and splenic macrophages leading to significantly increased vector transduction. However, clodronate liposomes have not been used in combination with lentiviral vectors yet [311, 312].

In future experiments, a higher lentiviral vector dose is needed for the effective treatment of $Asl^{Neo/Neo}$ mice [144]. Thus, more hepatocytes will be transduced with the lentiviral vector resulting in a corrected ASA phenotype in $Asl^{Neo/Neo}$ mice. A codon-optimized *hASL* vector will be used, to maximise the expression of the hASL in the liver. An assessment of the VCN in spleen would help to understand the amount of vector sequestrated in other organs.

4.6 Conclusion

This experimental work with *in vivo* lentiviral gene therapy did not correct the mouse model of argininosuccinic aciduria. Administration of a medium dose of lentiviral vector has shown suboptimal improvement of the *Asl^{Neo/Neo}* mouse. Efficacy remains limited to enable clinical translation. Next steps of this work to enhance the correction of the mouse phenotype will include a refinement of the vector design using codon-optimisation of the transgene, generation of a higher vector titre, and development of strategies to minimise transduction of alternative liver cells other than hepatocytes. These different options will maximise the possibilities of developing a candidate lentiviral vector for patients' benefits.

5. ENHANCEMENT OF EXPRESSION *IN VITRO* WITH CODON-OPTIMISED LENTIVIRAL VECTOR

5.1 Introduction

Synonymous codons that encode identical amino acids were previously described as redundant. Similarly, mutations in synonymous codons that have no effect on protein sequences were deemed silent. Nonetheless, current discoveries have demonstrated that codon usage performs several functions involving the regulation of gene expression as well as the antigen structure via both translation-dependent and -independent pathways. The occurrence rate of codons in the genome is associated with the corresponding transfer RNA (tRNA) in the species. Concentration of tRNA regulates the amount of available amino acids for protein translation extension, that consecutively effects the capacity of protein synthesis [313, 314]. As a result, protein expression is closely linked to a phenomenon known as codon usage bias, which involves the preferential utilization of specific synonymous codons. There is now compelling evidence that codon usage plays a critical role in determining protein expression levels [315-318], and codon usage bias has a crucial function in enhancing translation efficiency. Studies have demonstrated that infrequent codons have a detrimental impact on the translation rate, leading to ribosome stalling on mRNA in the course of translation. This phenomenon, particularly in eukaryotes, can trigger the premature ending of translation, which is facilitated by termination factors [319].

As mentioned in **Chapter 2**, gene therapy using CCL.LP1.*hASL* vector in neonatal *Asl*[Neo/Neo] mice showed suboptimal improvement of the *Asl*[Neo/Neo] mouse phenotype, however, efficacy remains limited to enable clinical translation. For that reason, the aim of this experiment was to produce and assess whether a codon-optimized *hASL* plasmid and lentiviral vector (CCL.LP1.*co-hASL*) could increase ASL efficacy *in vitro.*

5.1.2 *In vitro* Assessment of lentiviral vector with *co-hASL.*

GeneArt software influences the codon usage that influences the kinetics of translation, and the GC sequence repeats to ensure RNA stability within the cell. These parameters are taken into consideration by a specific bioinformatic algorithm to generate a coding DNA sequence for the hASL to increase the ASL protein expression by synonymous substitution (**Supplementary Figure 1**) [313]. Codon optimised hASL sequence presented with a higher quality codon (**Supplementary Figure 2A,B**). In addition, optimization of the GC content for the generation of co-hASL sequence was performed, which is known to exert an influence on local chromatin structure (**Supplementary Figure 2C,D**) [320]. In-cell western was used as an efficacy endpoint. We measured the kinetic response of ASL protein expression following first plasmid, then lentiviral vector encoding *co-hASL.* Experiments were performed in a human cell line derived from hepatocellular carcinoma, Huh7 cells, at high and low multiplicity of infections (MOIs).

Results from measuring the protein expression of co-hASL and with ASL plasmids at 8, 24, 48, 72 hours, and at 7 days after transfection, revealed a significant increase of hASL expression starting from 24 hours post transfection that was sustained for up to 7 days post transfection (**Figure 32**).
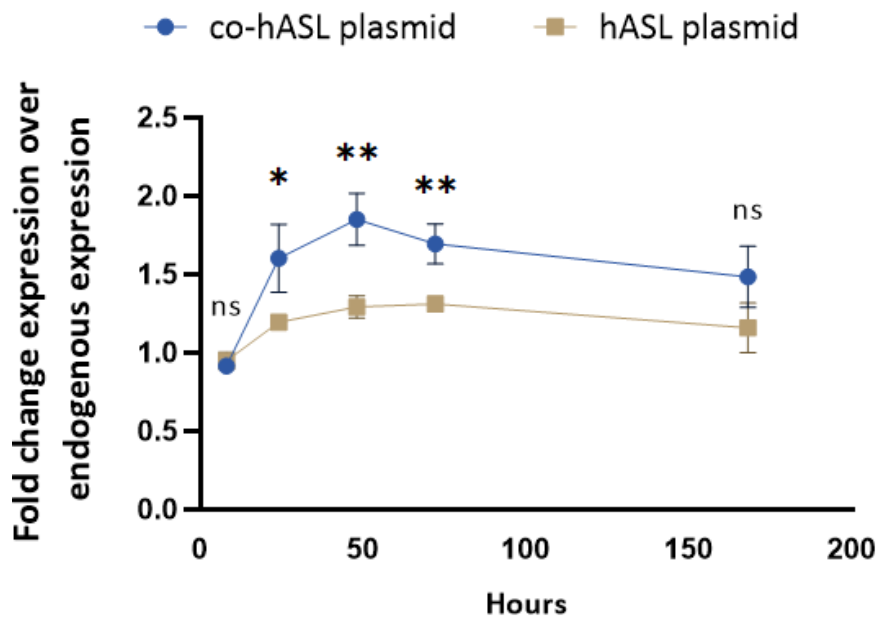
Figure 32. Expression of codon and non-codon-optimised hASL plasmid. Results were measured at 8h, 24h, 48h, 72h, and 7 days post transfection of Huh7 cells and a single dose of 100ng/well (n=3 wells per plasmid/time point). Fisher exact t test ns: not significant, (*) $p<0.05$, (**) $p<0.01$ Graph represents mean $\pm$ standard deviation for each group. Co-hASL: codon-optimised human argininosuccinate lyase.

Both CCL.LP1.*hASL* and CCL.LP1.*co-hASL* vectors were manufactured. *Co-hASL* lentiviral vector expression was compared to wild-type *-hASL* vector in Huh7 cells, at different MOIs ranging between high dose of MOI 70 and low dose of MOI 1, for each vector. The vectors were incubated for 72 hours after transduction before measurement of protein expression. Results revealed a significant increase ($p=0.025$) of the antigen expression following transduction with CCL.LP1.*co-hASL* compared to CCL.LP1.*hASL* vector by 2-fold in high dose (MOI 70). A dose response was further observed from MOI 70 to MOI 10 in *co-hASL* vector expression (**Figure 33A**).

A kinetic response of *hASL* protein expression was then performed using in-cell western in transduced with CCL.LP1.*hASL* and CCL.LP1.*co-hASL* vectors Huh7 cells. Results revealed an initial increase of ASL expression at 48 hours post transduction before the antigen expression plateaued for both vectors. There was a significant increase of protein expression of *co-hASL* compared to non-*co-hASL* lentiviral vector at higher doses of MOI 70 ($p=0.006$), which was maintained for up to 7 days post transduction ($p=0.03$). The lowest protein expression levels were shown from CCL.LP1.*hASL* vector at the lower dose of MOI 20 (**Figure 33B**).
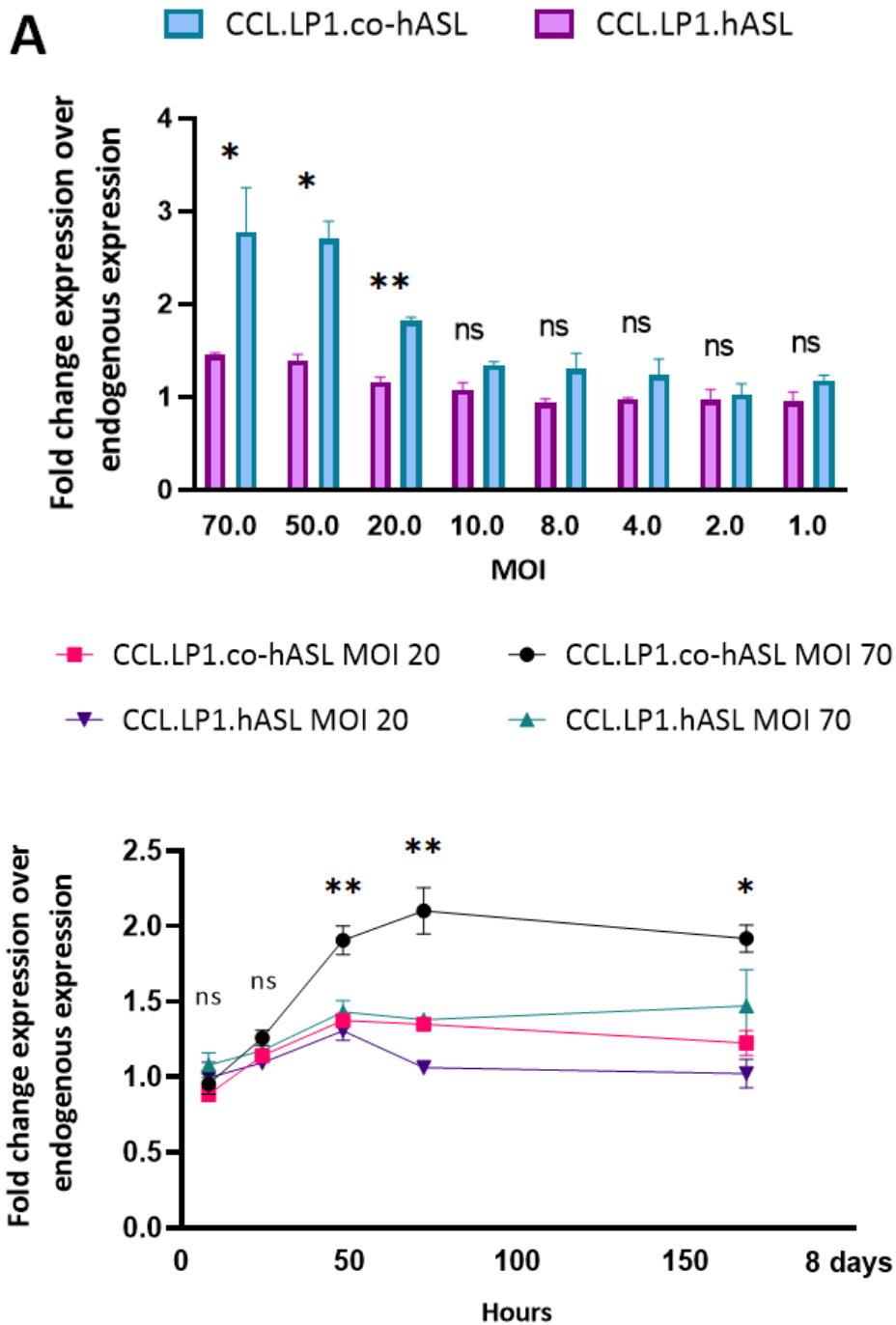
Figure 33. hASL expression in Huh7 cells after transduction with CCL.LP1.*hASL* versus CCL.LP1.*co-hASL* vectors. (A) *ASL* expression in Huh7 cells after transduction with *co-hASL* versus *hASL* lentiviral vectors at a range of MOIs from MOI 70 to MOI 1. In-cell western was performed in duplicates. **(B)** Expression of both codon and non-codon-optimised plasmids were measured with In-cell western at 8, 24, 48, and 72 hours, and at 7 days post transduction of Huh7 cells at high (MOI 70) and low (MOI 20) dose. In-cell western was performed in triplicates. Fisher exact t test; ns: not significant, * $p<0.05$, ** $p<0.01$. Graph represents mean ± standard deviation for each group. MOI: multiplicity of infection.

5.2 Discussion

The process of codon optimization has been employed to enhance the transgene's expression in various gene therapy applications [294, 321-323]. Subsequently, we have produced a *co-hASL* lentiviral vector that increases the expression of ASL protein in the liver, presenting a significant 2-fold higher expression in hepatic cells *in vitro*, compared to the non-*co-hASL* vector as described in **Section 3.3.2**. Previous *in vitro* study showed a 7- to 30-fold increase in the expression of FVIII in HEK293T cells following transfection with *co-hFVIII* lentiviral vector [322]. This strategy can positively improve the treatment of metabolic disorders such as ASA in infancy by improving the efficacy of lentiviral vector gene therapy and increasing the expression of the transgene, leading to a quicker and better correction of the phenotype [20]. In future *in vivo* experiments, co-*hASL* lentiviral vector will be used, to maximise the expression of the hASL in the liver of the neonatally treated *Asl*$^{Neo/Neo}$ mice.

5.3 Conclusion

This experimental work has confirmed that codon optimization of *hASL* transgene in CCL.LP1.*co-hASL* vector is able to significantly increase the antigen expression *in vitro*. Gene therapy in neonatal *Asl*$^{Neo/Neo}$ mice using CCL.LP1.*hASL* vector showed suboptimal improvement in the mouse model's phenotype. Efficacy remains limited to enable clinical translation. In future gene therapy experiments for ASA mouse, CCL.LP1.*co-hASL* vector will be used instead to maximise the expression of *hASL* in the liver and potentially improve the correction of the disease *in vivo*.

6. *IN VIVO* LENTIVIRAL GENE THERAPY FOR THE TREATMENT OF NEONATAL *Asl^{Neo/Neo}* MICE USING CODON-OPTIMISED TRANSGENE

6.1 Introduction

The hypomorphic *Asl^{Neo/Neo}* mouse model recapitulates the human phenotype of ASL deficiency with hyperammonaemia, multi-organ dysfunction and NO deficiency [20]. Previous findings have shown that an intravenous single dose of 9.5e9TU/Kg of CCL.LP1.*hASL* vector in neonatal *Asl^{Neo/Neo}* mice was unable to correct the disease phenotype.

Codon-optimization of the CCL.LP1.*hASL* plasmid leads to significantly increased expression of ASL *in vitro* following transduction of CCL.LP1.*co-hASL* vector in Huh7 cells. Additionally, below the threshold dose of 3e10TU/Kg, a large number of lentiviral vectors is uptaken by liver macrophages, leading to reduced transduction of hepatocytes [144]. Therefore, we performed an optimised liver-directed gene therapy approach for the treatment of neonatal *Asl^{Neo/Neo}* mice with intravenous administration of a more than 4 times higher dose (4e10TU/Kg) CCL.LP1.*co-hASL* vector. Third generation lentiviral vector technology was used to further promote safety [324]. The efficacy of this gene therapy was assessed in neonatal *Asl^{Neo/Neo}* mice to determine the correction of the phenotype *in vivo*.

6.2 Experimental design

This experiment was designed to assess whether a single systemic neonatal injection of CCL.LP1.*co-hASL* vector can correct the phenotype of *Asl^(Neo/Neo)* mice over 3 months following vector injection. For this study, three groups of animals were monitored: wild-type, untreated *Asl^(Neo/Neo)* and treated *Asl^(Neo/Neo)* mice that received CCL.LP1.*GFP and* CCL.LP1.*co-hASL* vector at 4e10TU/Kg, respectively. *Asl^(Neo/Neo)* pups were genotyped at birth and received a single neonatal intravenous injection of the vectors at P0-P3 (**Figure 34**) in the superficial temporal vein. As previously mentioned, neonatal injections enable to transduce a maximum number of hepatocytes before extensive liver growth during the first 5 weeks of animal's life [303], which will then expand during liver growth. Following the neonatal injection with lentiviral vector, all groups were monitored daily for 3 months. Weights were recorded and mice that were losing between 10% and 15% of their weight, were sacrificed, and samples were collected. No supportive treatment was given to any of the groups involved in this experiment.
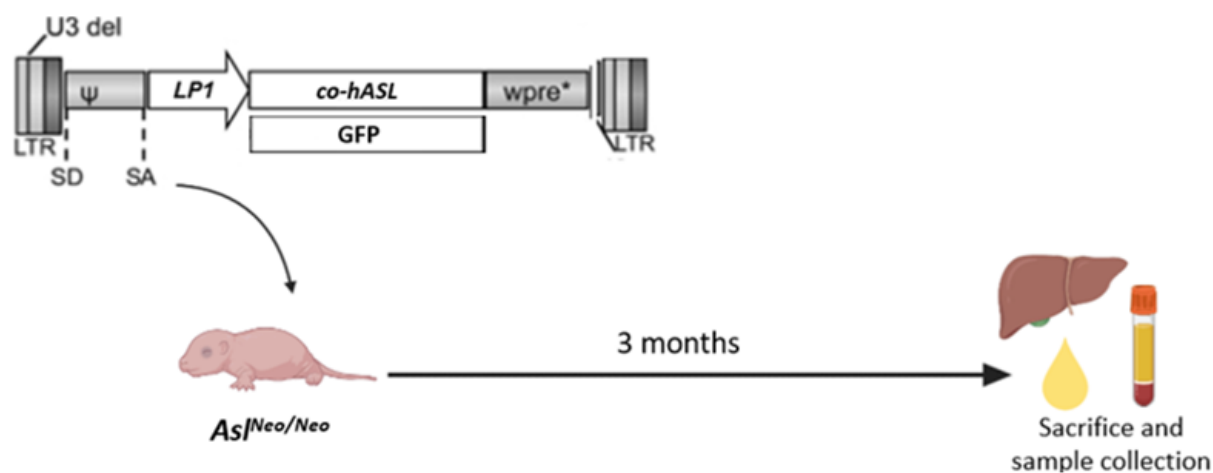
Figure 34. Schematic representation of the experimental design of systemic neonatal injection of lentiviral gene therapy with CCL.LP1.*co-hASL* vector in *Asl^(Neo/Neo)* mice. *co-hASL*: codon-optimised human argininosuccinate lyase; LP1: liver specific 1 promoter; LTR: long terminal repeats; SA: *tat/rev* splice acceptor; SD: splice donor; U3: unique 3' region; WPRE: woodchuck hepatitis virus post-transcriptional regulatory element.

6.3 Effect of gene therapy with CCL.LP1.*co-hASL* vector on macroscopic phenotype

6.3.1 Survival

Survival was completely normalised in the *hASL* treated *Asl$^{Neo/Neo}$* group compared to the *GFP* group for 12 weeks (*p*<0.0001) (**Figure 35**). These results demonstrate a clinical correction where mice receiving lower dose of non-codon-optimised CCL.LP1.*hASL* vector had died by 5 weeks following neonatal administration.
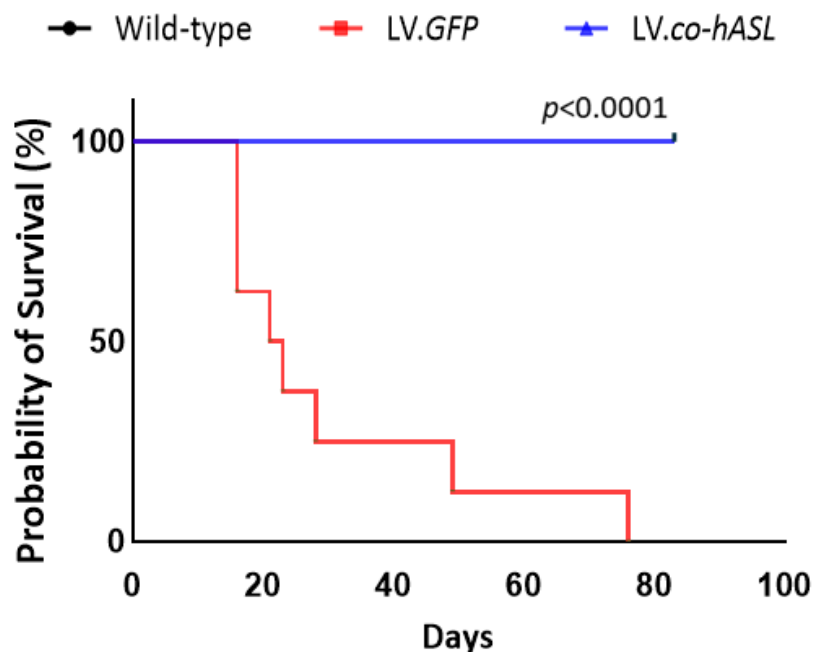
Figure 35. Survival curve of the gene therapy-treated *Asl$^{Neo/Neo}$* mice. Kaplan-Meyer survival curve of wild-type (n=8), *GFP* (n=8) and *hASL* treated *Asl$^{Neo/Neo}$* mice (n=8). Log-rank (Mantel-Cox) test (*p*<0.0001).

6.3.2 Growth

Daily weight measurements showed a complete and long-lasting correction of the weight in *hASL* treated *Asl*$^{Neo/Neo}$ mice compared to *GFP* treated littermates. Normalization of the weight was maintained until weaning, with a significant decrease between day 20 until 45, then coming back to normal in *hASL* treated *Asl*$^{Neo/Neo}$ mice. In contrast, the *GFP* controls appeared with significantly reduced weight from the third week post administration of CCL.LP1.*GFP* vector, which presented with rapid decrease towards the end of their life (**Figure 36A**). Both male and female *hASL* treated *Asl*$^{Neo/Neo}$ mice showed weight normalization from day 50 and 40 respectively (**Figure 36B,C**), when the vast majority (75%) of *GFP Asl*$^{Neo/Neo}$ mice died within the first 2-3 weeks of life due to the severe phenotype (**Figure 36C**).
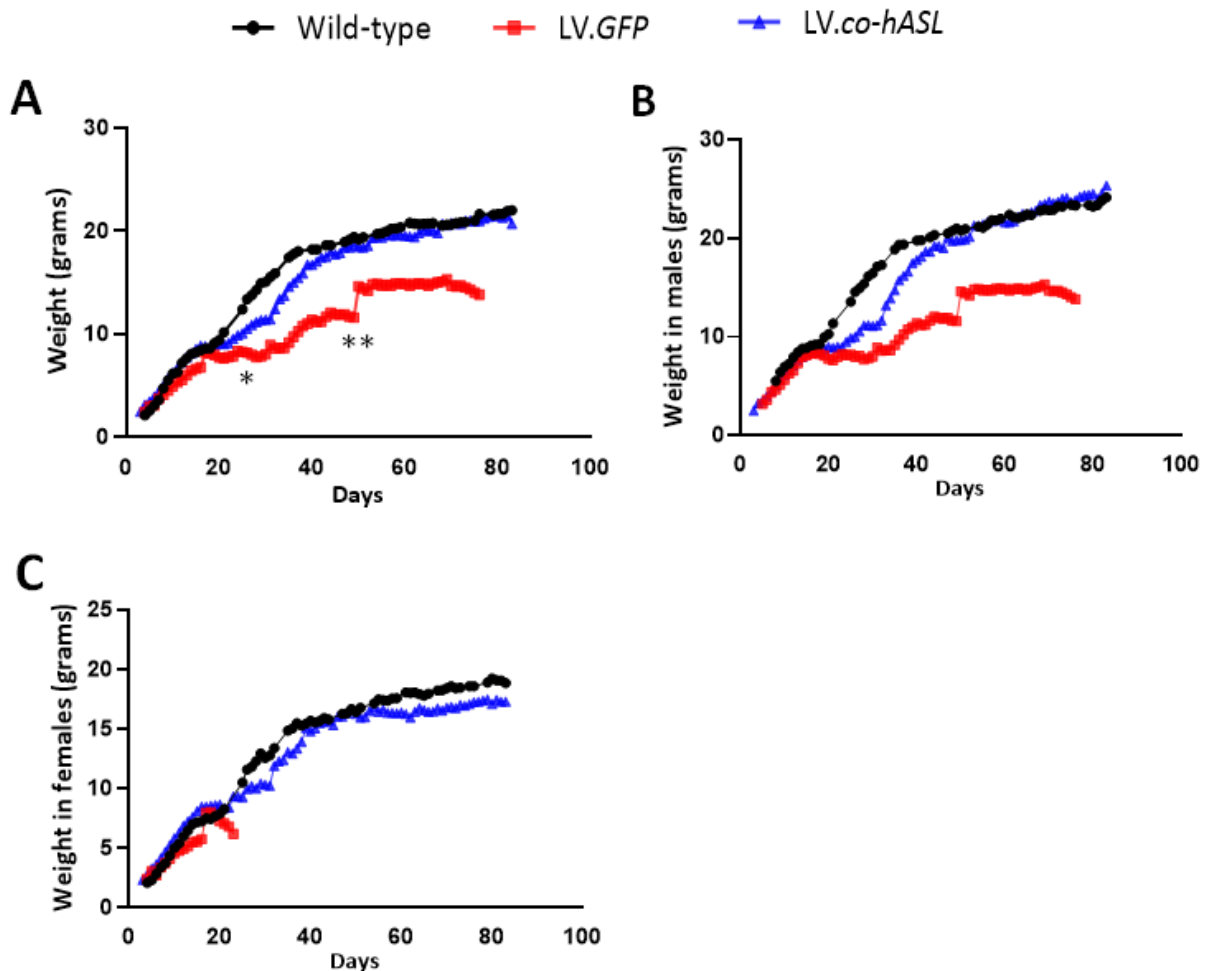
Figure 36. Growth of gene therapy-injected Asl^{Neo/Neo} mice compared to wild-type and untreated Asl^{Neo/Neo} mice. (A) Mean growth of wild-type (n=8), *GFP* (n=8), and *hASL* treated *Asl^{Neo/Neo}* mice (n=8) over 3 months. * 25% and ** 12,5% of *GFP Asl^{Neo/Neo}* mice survived at day 28 and day 50, respectively. **(B)** Mean growth of male wild-type (n=4), *GFP* (n=3) and *hASL* treated *Asl^{Neo/Neo}* mice (n=5) over 3 months. **(C)** Mean growth of wild-type (n=4), *GFP* (n=5) and *hASL* treated *Asl^{Neo/Neo}* mice (n=3) over 3 months. Horizontal lines display the mean ± standard deviation.

Gross examination revealed an improvement in growth from the third week post lentiviral injection for *ASL* treated *Asl^{Neo/Neo}* mice compared to *GFP* treated group (**Figure 37A-B**). In addition, *hASL Asl^{Neo/Neo}* mice showed growth normalization from the fourth week after injection which was followed by a weight normalization from the fifth week and was maintained until the end of the experiment (**Figure 37C**). This growth correction was also associated with the complete correction of the fur pattern, especially from the fifth week of life for the treated animals as they looked very similar to their wild-type littermates. This correction of the fur was maintained until the end of the experiment (**Figure 37D-F**).
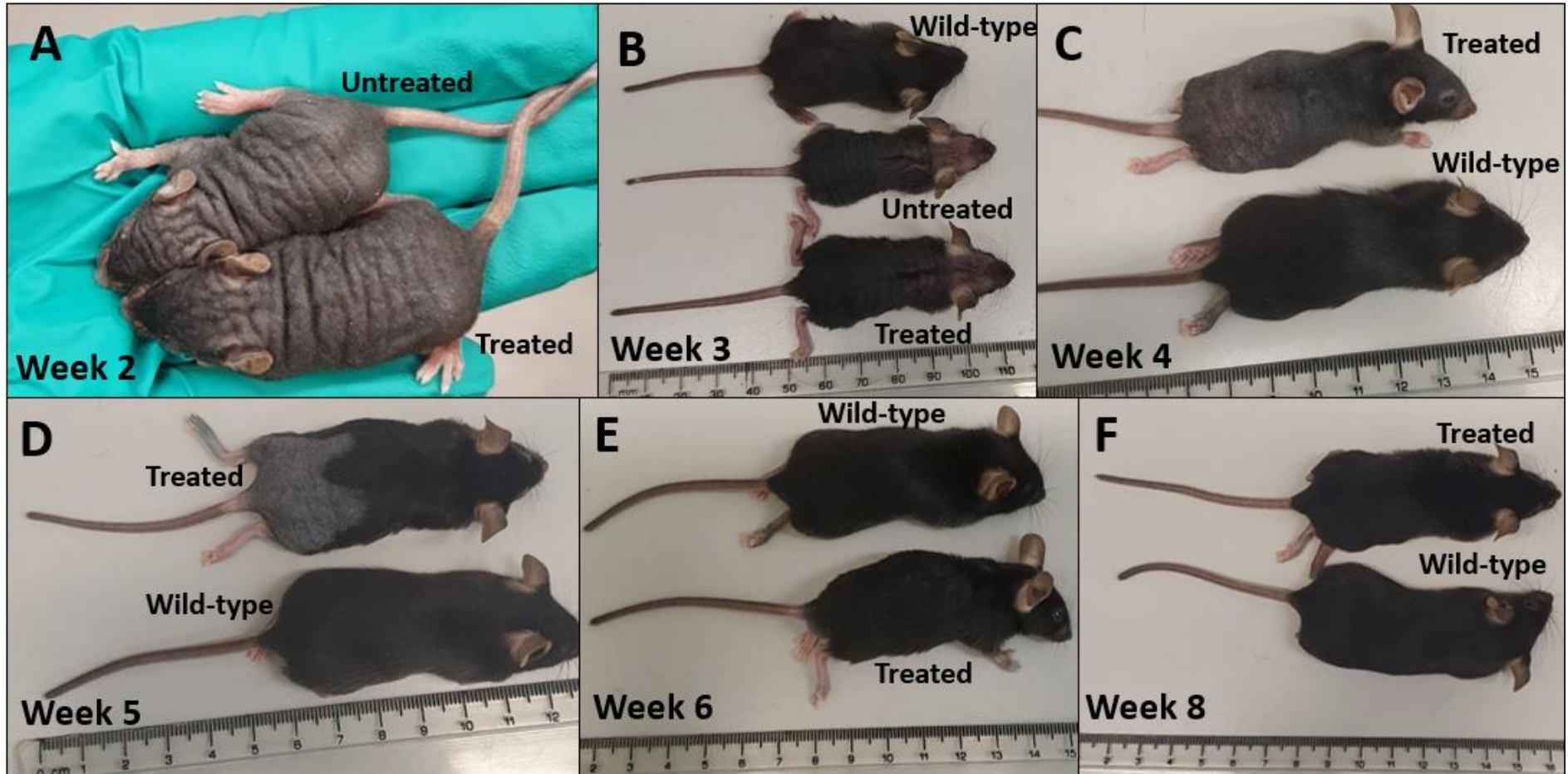
Figure 37. Macroscopic aspect of CCL.LP1.*co-hASL* vector-injected *Asl^{Neo/Neo}* compared to wild-type and CCL.LP1.*GFP* vector-injected *Asl^{Neo/Neo}* mice. (A) Image of *GFP* and *hASL* treated *Asl^{Neo/Neo}* mice. **(B)** Image of wild-type, *GFP*, and *hASL* treated *Asl^{Neo/Neo}* mice. **(C-F)** Images of wild-type and *hASL* treated *Asl^{Neo/Neo}* mice.

6.4 Effect of lentiviral gene therapy on ureagenesis

6.4.1 Liver phenotype

$Asl^{Neo/Neo}$ mice show hepatomegaly caused by glycogen storage deposit [31]. As expected, liver weight of *GFP* treated $Asl^{Neo/Neo}$ mice at harvest was increased as shown by a significant increase of the liver/body weight ratio ($p<0.0001$). In *hASL* treated $Asl^{Neo/Neo}$ mice, hepatomegaly at harvest was significantly improved ($p=0.0009$) compared to *GFP* treated group (**Figure 38**), but not to wild-type levels.
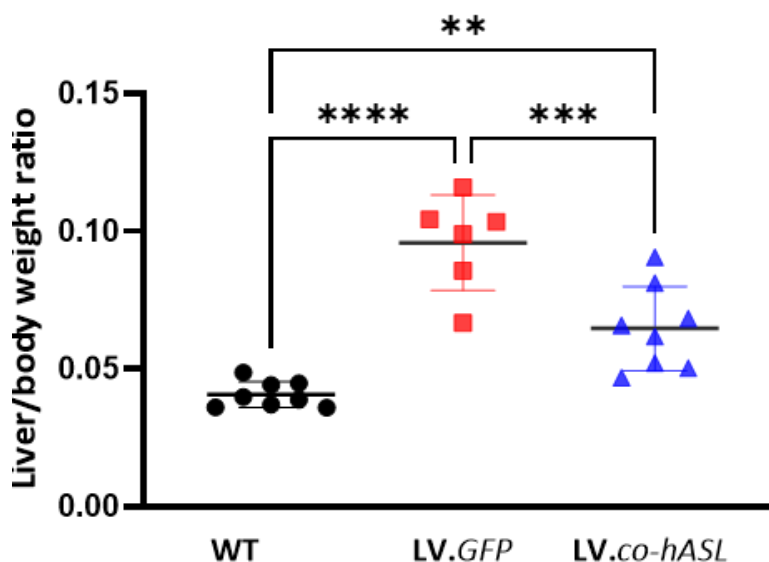
Figure 38. Hepatomegaly is improved in *hASL* versus *GFP* treated $Asl^{Neo/Neo}$ animals. Liver/body mass ratio in wild-type (n=8), *GFP* (n=6), and *hASL* treated $Asl^{Neo/Neo}$ mice (n=8) at harvest. WT: wild-type. Horizontal lines display the mean ± standard deviation. One-way ANOVA with Tukey's multiple comparisons test; ** $p<0.01$, *** $p<0.001$, **** $p<0.0001$.

Electron microscopy of liver tissue from wild-type (**Figure 39A,B**) and gene therapy treated $Asl^{Neo/Neo}$ mice (**Figure 39C,D**) was performed at the time of culling. Results in livers from *hASL* treated $Asl^{Neo/Neo}$ mice were similar to wild-type livers with no difference of the content of glycogen, lipid droplets, or clusters of cytoplasmic vesicles previously described [325]. These

are characteristics of the chronic liver disease observed in *Asl^Neo/Neo* mice [326]. The above observations were kindly verified by Dr Glenn Anderson, electron microscopist at Great Ormond Street Hospital, London.
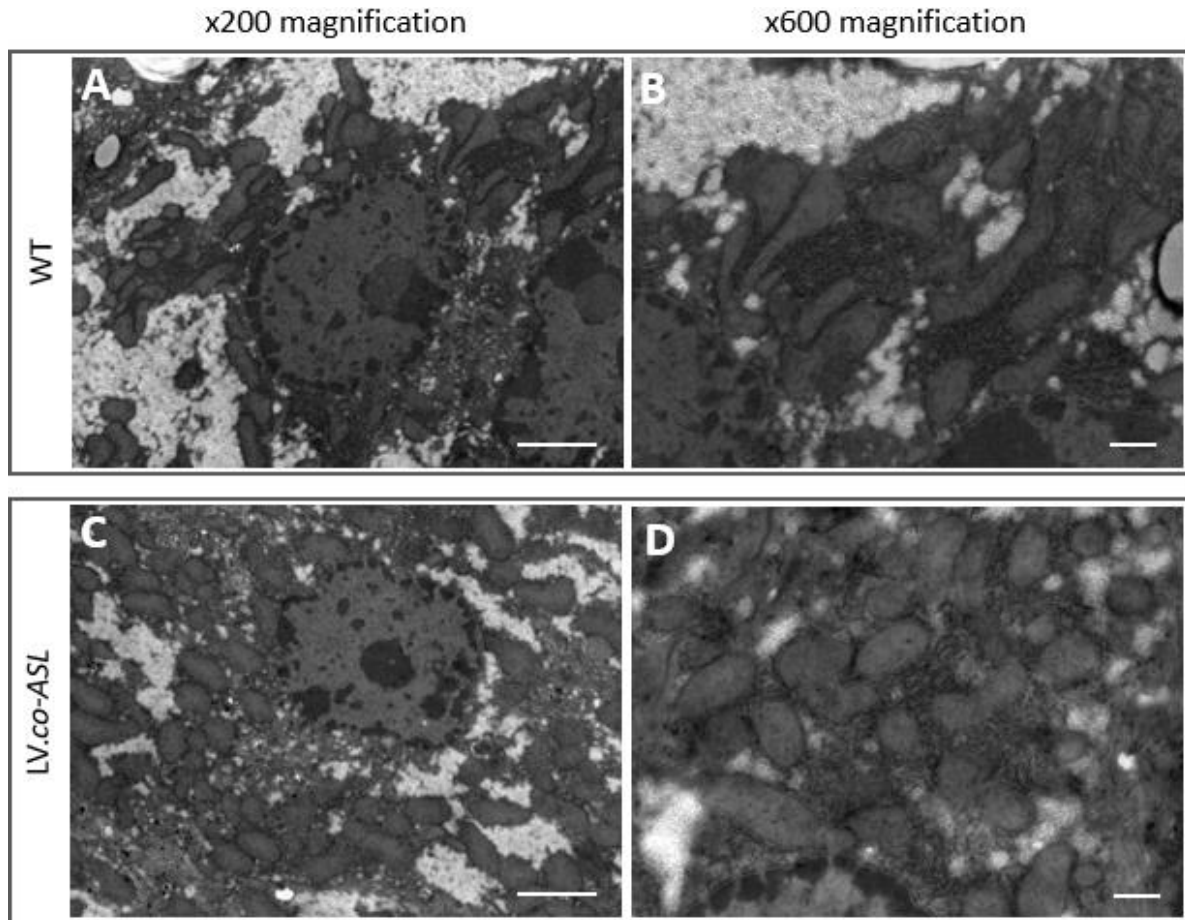
Figure 39. No significant difference of hepatocyte morphology and content assessed by electron microscopy of liver samples from treated *Asl^Neo/Neo* and wild-type mice. Liver samples from **(A)** wild-type x200 magnification; **(B)** wild-type x600 magnification (n=4), **(C)** *hASL* treated *Asl^Neo/Neo* x200 magnification; **(D)** *hASL* treated *Asl^Neo/Neo* x600 magnification (n=3) mice. Scale bars are 2μm for x200 magnification and 500nm for x600 magnification, respectively. WT: wild-type.

6.4.2 Urea cycle biomarkers

Several urea cycle-related biomarkers were assessed at harvest. Ammonia was assessed both in whole blood in real time immediately following harvest and in plasma in a single batch experiment for all samples. At the time of sacrifice, plasma ammonia levels were normalised in the *hASL* treated group compared to wild-type littermates and significantly decreased compared to *GFP Asl^{Neo/Neo}* group (**Figure 40A**). Whole blood ammonia levels presented significantly reduced ($p<0.0001$) in the *hASL* treated group compared to *GFP Asl^{Neo/Neo}* mice, with 4 out of 8 gene therapy treated *Asl^{Neo/Neo}* mice having ammonia levels similar of those of wild-type animals (**Figure… 40B**). Argininosuccinic acid levels from dried blood spots were also normalised in the *hASL* treated animals compared to wild-type littermates, and significantly reduced compared to *GFP Asl^{Neo/Neo}* mice ($p<0.0001$) at 3 months following lentiviral injection (**Figure 40C**). Levels of arginine in dried blood spots of the *hASL* treated *Asl^{Neo/Neo}* group showed an increasing trend compared to *GFP* controls; however, they did not show significant difference (**Figure 40D**). At harvest, citrulline levels in dried blood spots were normalised to wild-type levels ($p=0.6$) in *hASL* treated *Asl^{Neo/Neo}* mice compared to *GFP* controls ($p=0.009$) (**Figure 40E**). No significant difference in orotate levels was observed at harvest between *hASL* treated *Asl^{Neo/Neo}* and wild-type mice, while orotate levels in the *GFP Asl^{Neo/Neo}* group were significantly increased ($p=0.03$) with high variability between values (**Figure 40F**).

126
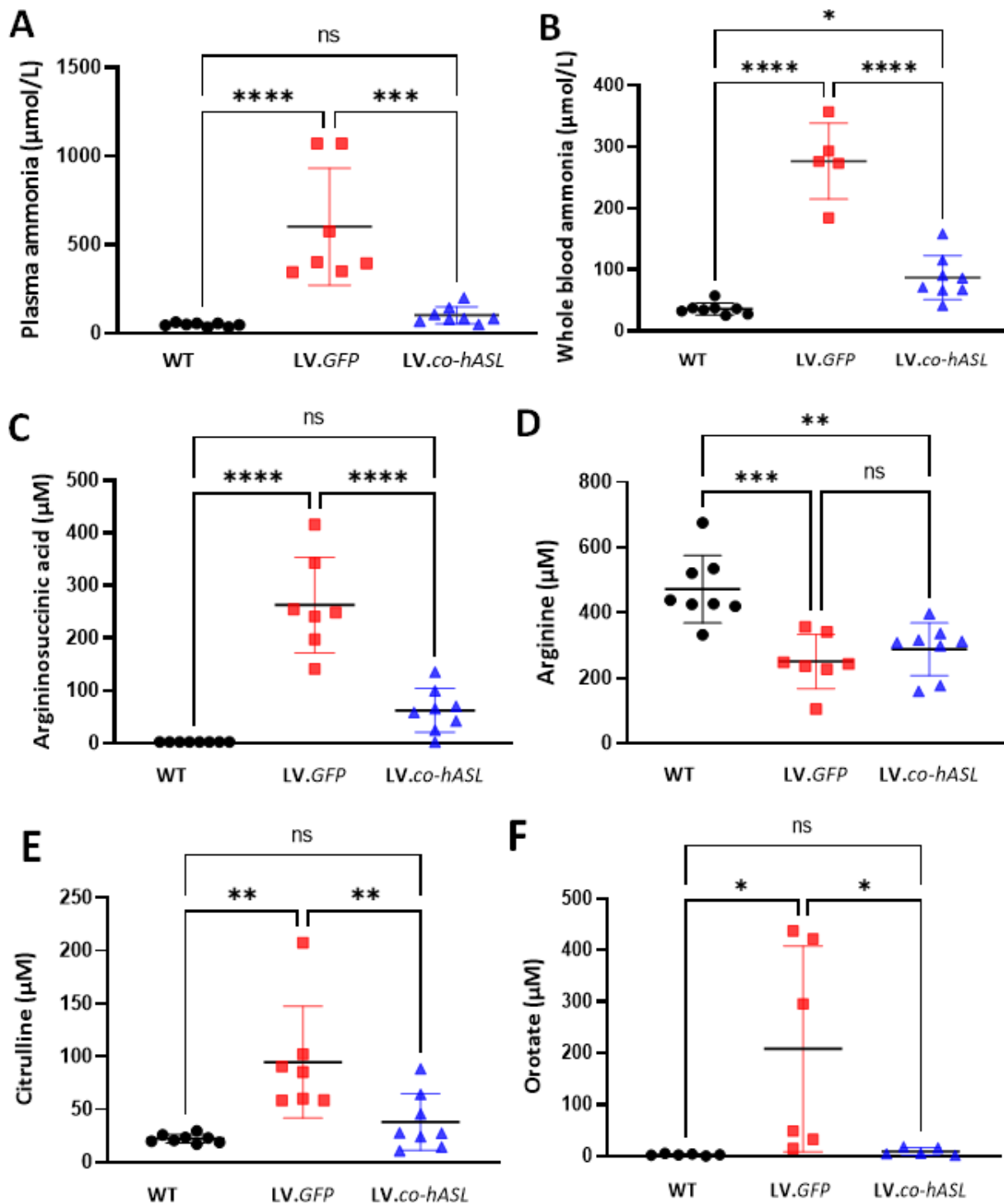
Figure 40. Urea cycle biomarkers. All the biomarkers were measured in wild-type (n=6-8), *GFP* (n=5-8) and *hASL* treated *Asl^{Neo/Neo}* mice (n=5-8) at 3 months of age. **(A)** Plasma ammonia levels; **(B)** whole blood ammonia levels; **(C)** argininosuccinic acid levels from dried blood spots; **(D)** arginine levels from dried blood spots; **(E)** citrulline levels from dried blood spots; **(F)** orotate levels from dried urine spots. Horizontal lines display the mean ± standard deviation. One-way ANOVA with Tukey's multiple comparisons test; ns: not significant, * $p<0.05$, ** $p<0.01$, *** $p<0.001$, **** $p<0.0001$.

Levels of plasma alanine aminotransferase were measured at the time of sacrifice, and they did not show significant difference between wild-type, *hASL* or *GFP* treated *Asl*^{Neo/Neo} groups. However, alanine aminotransferase levels in *hASL* treated *Asl*^{Neo/Neo} mice revealed a decreasing trend, similar to the wild-type mice ($p=0.9$), compared to *GFP* controls ($p=0.25$), further indicating the improvement of the chronic liver disease with reduced hepatomegaly and glycogen storage, highlighting the safety and absence of liver damage following lentiviral injection (**Figure 41**).
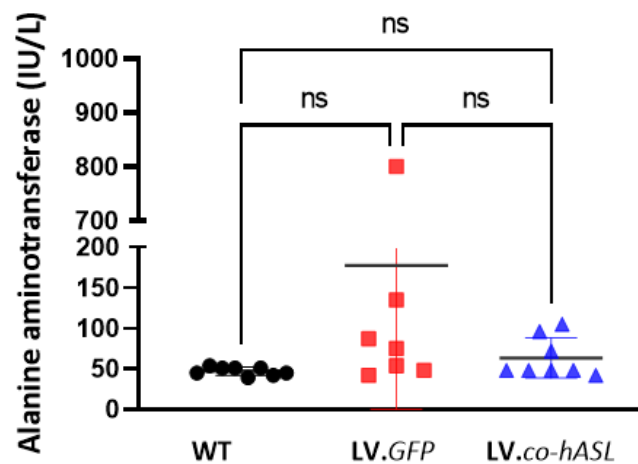
Figure 41. Alanine aminotransferase activity. Plasma alanine aminotransferase levels were measured in wild-type (n=8), *GFP* (n=7), and *hASL* treated *Asl*^{Neo/Neo} mice (n=8) at 3 months of age. Horizontal lines display the mean ± standard deviation. One-way ANOVA with Tukey's multiple comparisons test; ns: not significant.

6.4.3 ASL liver enzymatic activity and transduction

Residual ASL activity in untreated *GFP* *Asl*^{Neo/Neo} mice was significantly lower compared to wild-type levels ($p<0.0001$). This increased significantly ($p=0.003$) in *hASL* treated *Asl*^{Neo/Neo} mice at harvest (**Figure 42A**) although still lower than physiological levels ($p=0.0005$).

VCN in the liver showed similar values of VCN between *hASL* and *GFP* treated *Asl*^{Neo/Neo} mice with 1.13 and 1.3 vector copies per cell respectively, confirming that both groups received the same dose of lentiviral vector (**Figure 42B**). Previous studies have described high uptake of lentiviral vectors by liver and splenic macrophages leading to a lower lentiviral vector

transduction efficacy in hepatocytes [144]. Similar results were shown in this experiment as VCN in spleen was similar in both lentiviral-injected groups with values of 1.3 and 1.4 for *hASL* and *GFP* treated *Asl^Neo/Neo* groups respectively (**Figure 42C**). These values are similar to VCN in liver of injected mice supporting evidence of high vector uptake by the spleen.

ASL immunostaining in liver was assessed. The automated quantification of liver immunostaining against ASL showed the presence of the antigen's expression in the liver that was 0.23% of the wild-type expression in *GFP Asl^Neo/Neo* mice and 22.4% in the *hASL* treated *Asl^Neo/Neo* mice at the time of culling (**Figure 42D**). Observation of immunostaining results revealed more scattered and sparse expression in the treated *Asl^Neo/Neo* mice with no predominant liver zonation and preferential expression in periportal or pericentral hepatocytes (**Figure 43**).
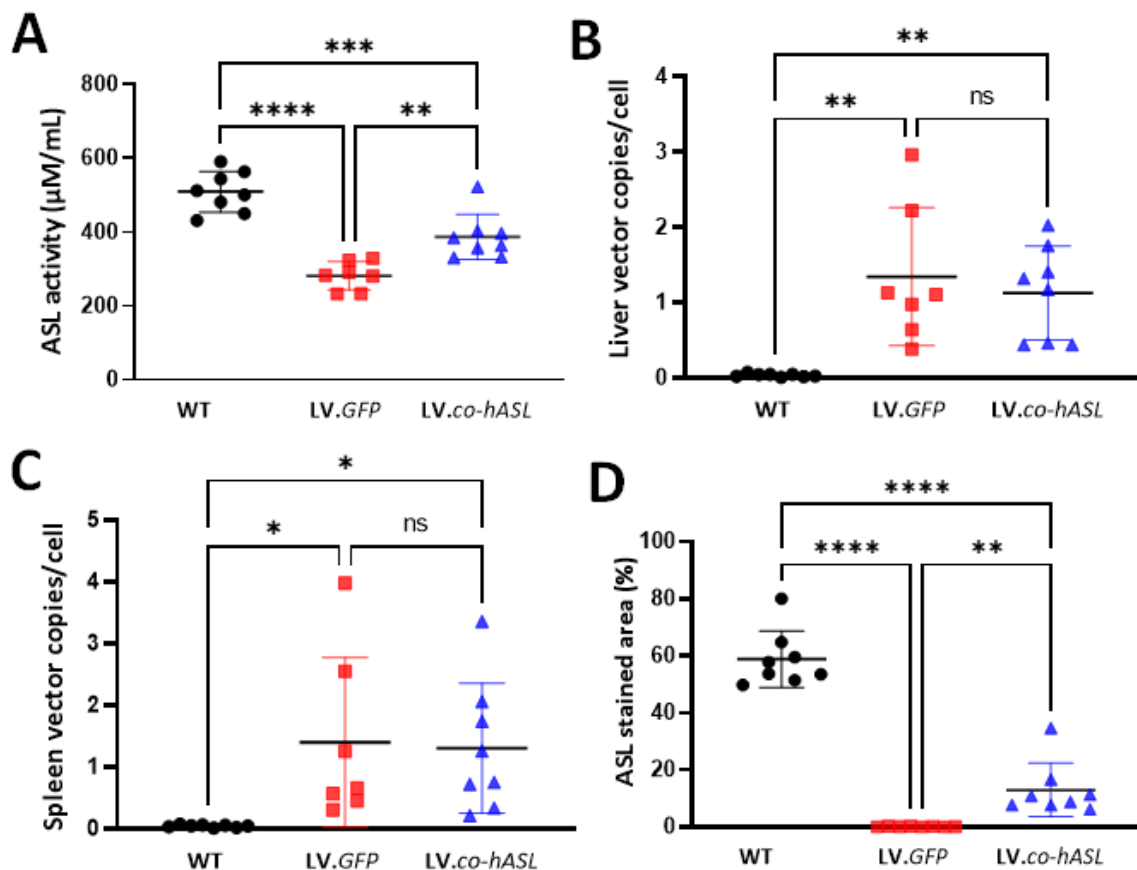
Figure 42. Liver and spleen expression. All the values were measured in wild-type (n=8), *GFP* (n=7-8), and *hASL* treated *Asl^Neo/Neo* mice (n=8) at 3 months of age. **(A)** ASL activity in whole liver; **(B)** vector genome copies per cell in whole liver; **(C)** *ASL* vector genome copies per cell in spleen; **(D)** percentage of area in the liver expressing. Horizontal lines display the mean ± standard deviation. One-way ANOVA with Tukey's multiple comparisons test; ns: not significant, * $p<0.05$, ** $p<0.01$, *** $p<0.001$, **** $p<0.0001$.
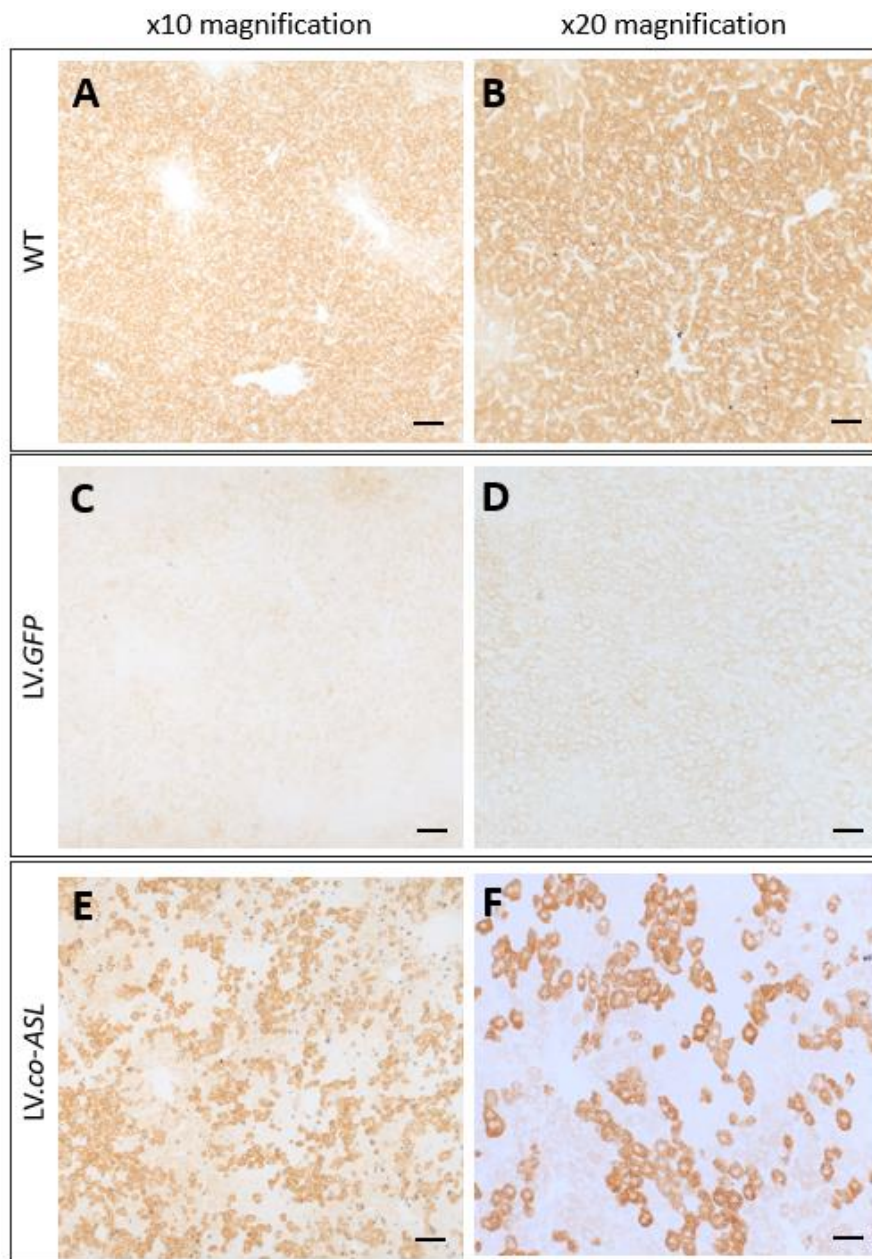
Figure 43. Representative images of ASL immunostaining in liver. (A,B) wild-type mice x10 and x20 magnification; **(C,D)** *GFP* treated *Asl^{Neo/Neo}* mice x10 and x20 magnification; **(E,F)** *hASL* treated *Asl^{Neo/Neo}* mice x10 and x20 magnification. Scale bars are 100μm for x10 magnification and 50μm for x20 magnification, respectively; n=8 animals per group.

6.5 Effect of liver-targeting lentiviral gene therapy on redox imbalance

6.5.1 *In vivo* evidence of redox imbalance in *Asl^Neo/Neo^* mice

ASL participates in the citrulline-NO cycle, which generates NO by directing extracellular arginine to NOS. *Asl^Neo/Neo^* mice experience a significant burden of chronic liver disorders, including increased serum transaminase levels, hepatomegaly, fibrosis, steatosis, hepatocellular injury, and glycogen accumulation [47]. The exact mechanisms that cause liver disease remain uncertain, but several factors have been proposed, including elevated levels of ammonia in the blood, low levels of arginine, toxicity from argininosuccinate, reduced levels of nitric oxide, and increased oxidative stress. To assess whether liver directed lentiviral gene therapy corrects redox imbalance in *Asl^Neo/Neo^* mice, we employed a non-invasive diagnostic method using the radiotracer (S)-4-(3-18F-fluoropropyl)-L-glutamate ([18F]FSPG) and positron emission tomography (PET) to evaluate the degree of liver disease in ASA mice. [18F]FSPG is a glutamate analog and its retention in tissues reflects the activity of the membrane transporter xCT, a glutamate-cystine antiporter [327, 328]. The synthesis of the master anti-oxidant glutathione, as a physiological response to oxidative stress requires an increased flux of the precursor metabolite cysteine, via intracellular uptake of cystine at the expense of glutamate [329, 330]. It has recently been shown that NO deficiency contributes to the reduced biosynthesis of glutathione in the liver of *Asl^Neo/Neo^* mice via downregulation of the rate-limiting enzyme glutamate cysteine ligase [94].

To evaluate changes in the antioxidant glutathione biosynthesis pathway, PET imaging was performed after intravenous administration of [18F]FSPG in 2-week-old *Asl^Neo/Neo^* mice and wild-type mice to visualize the retention of the radiotracer over time. [18F]FSPG retention in the liver of *Asl^Neo/Neo^* mice was significantly higher ($p=0.002$) than of wild-type littermates post [18F]FSPG injection (**Figure 44A,B**). Unexpectedly, high [18F]FSPG retention was also present in the skin of *Asl^Neo/Neo^* mice ($p=0.002$), which was not the case in wild-type group (**Figure 44C,D**). [18F]FSPG is therefore a useful non-invasive biomarker regarding the redox imbalance in both liver and skin of *Asl^Neo/Neo^* mice (**Figure 44E**), mediated via upregulation of the xCT antiporter.
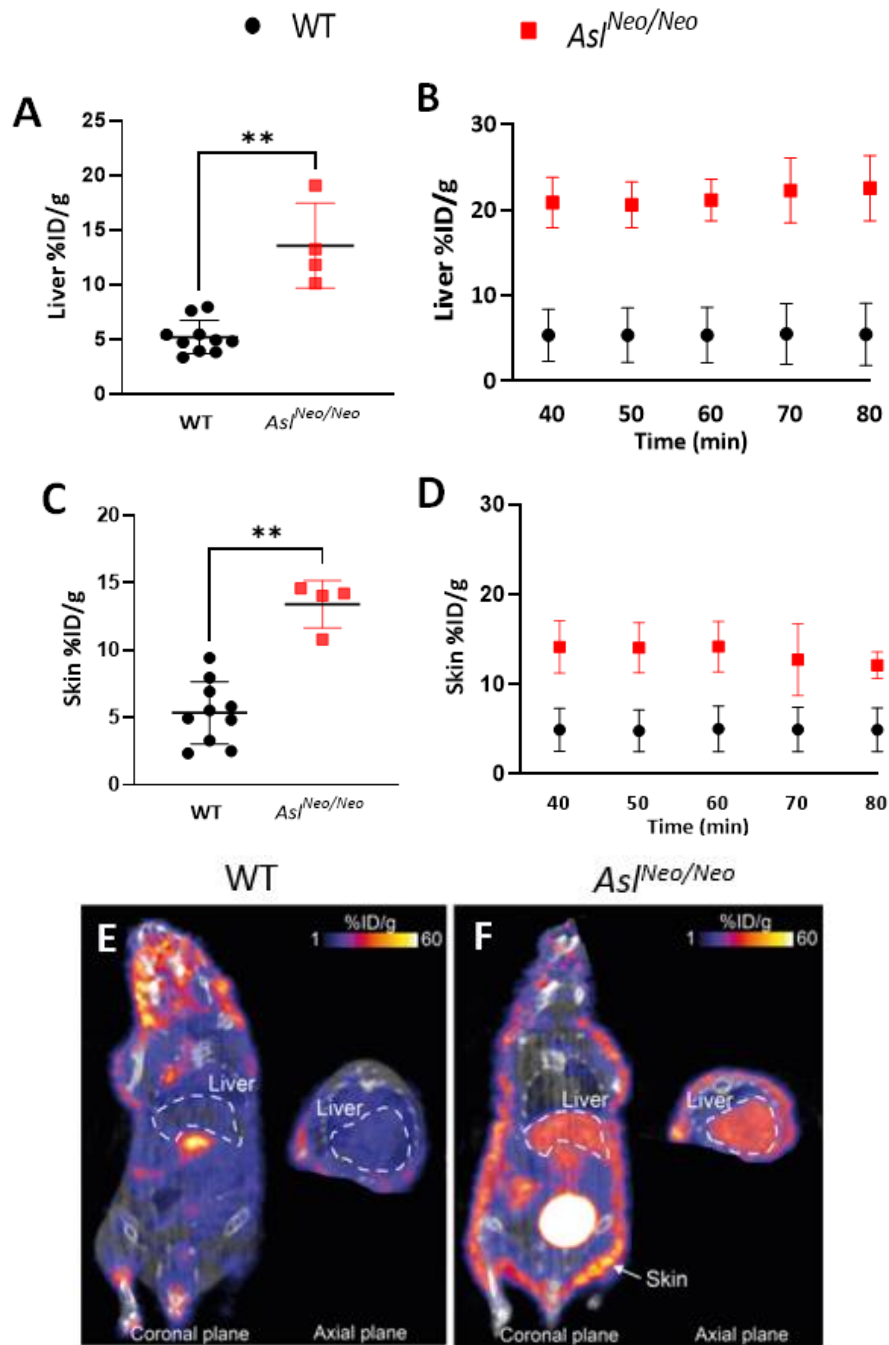
Figure 44. *In vivo* functional validation of impaired NO production. All the values were measured in wild-type (n=10) and *Asl*^{Neo/Neo} mice (n=4). **(A)** Quantified [^{18}F]FSPG retention in the liver at 60 minutes post injection; **(B)** between 40- and 80-minutes post injection. **(C)** Quantified [^{18}F]FSPG retention in the skin at 60 minutes post injection; **(D)** between 40- and 80-minutes post injection. Horizontal lines display the mean ± standard deviation. Mann-Whitney test; ** $p<0.01$. **(E-F)** Representative PET/CT images of [^{18}F]FSPG distribution (%ID/g), in the coronal and axial plane, of 2-week-old wild-type and *Asl*^{Neo/Neo} mice. ID/g: injected dose per gram of tissue; min: minutes.

6.5.2 Gene therapy with lentiviral vector normalizes the redox imbalance in *Asl*^{*Neo/Neo*} mouse

To explore the possible utility of [^{18}F]FSPG PET as a non-invasive indicator for evaluating the effectiveness of lentiviral therapy, [^{18}F]FSPG was administered intravenously to 2-weeks-old *GFP* treated *Asl*$^{Neo/Neo}$ mice, and sequentially at 2- and 6- weeks-old wild-type littermates and *hASL* treated *Asl*$^{Neo/Neo}$ mice (**Figure 45**). Two *Asl*$^{Neo/Neo}$ mice were treated as neonates with *hASL* lentiviral vector, however one of these animals was sacrificed at 2.5 weeks of age due to significant phenotypical decline. The mouse survived presented with a milder phenotype that recapitulated the phenotype in ASA patients, and it was administered intravenously with [^{18}F]FSPG at 6 weeks for analysis.
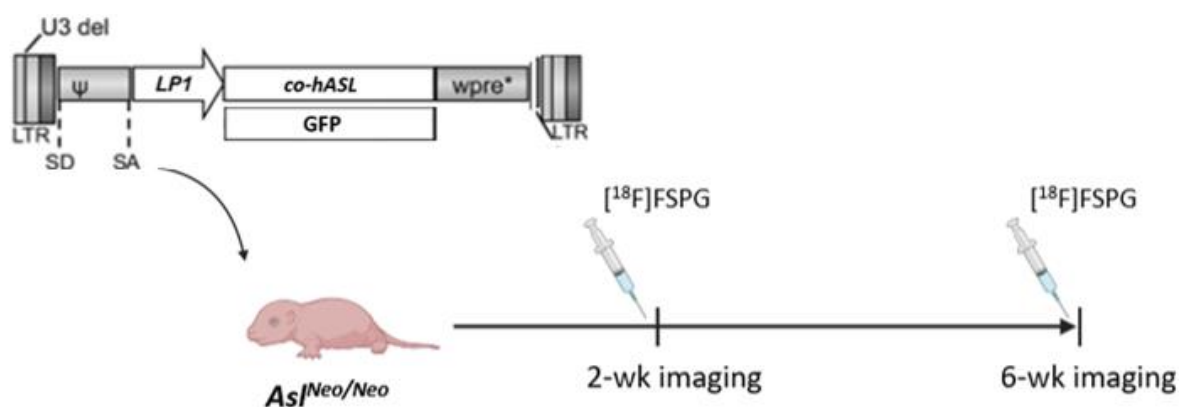
Figure 45. Schematic representation of the experimental plan for [^{18}F]FSPG retention following neonatal injection with lentiviral vector. [^{18}F]FSPG: (S)-4-(3-18F-fluoropropyl)-ʟ-glutamate; *co-hASL*: codon-optimised human argininosuccinate lyase; LP1: liver specific 1 promoter; LTR: long terminal repeats; SA: *tat/rev* splice acceptor; SD: splice donor; U3: unique 3' region; wk: weeks; WPRE: woodchuck hepatitis virus post-transcriptional regulatory element.

[18F]FSPG retention was significantly reduced in the liver of 2-weeks-old, *hASL* compared to *GFP* treated *Asl*Neo/Neo group (p=0.01) and was maintained until the sixth week of the experiment for the surviving mouse (p=0.03) (**Figure 46A, B**). Similarly, skin [18F]FSPG retention presented with normalized levels in *hASL* treated *Asl*Neo/Neo animal presenting similar levels to the wild-type littermates at 2 and 6 weeks post gene therapy lentiviral injection (p=1) (**Figure 46C, D**). In line with these results, gene therapy using lentiviral vector was able to normalise the redox imbalance in both liver and skin from the second week post *hASL* treatment of *Asl*Neo/Neo mouse, which is determined from the normalisation of the cystine/glutamate antiporter system xC- (**Figure 46E,F**).
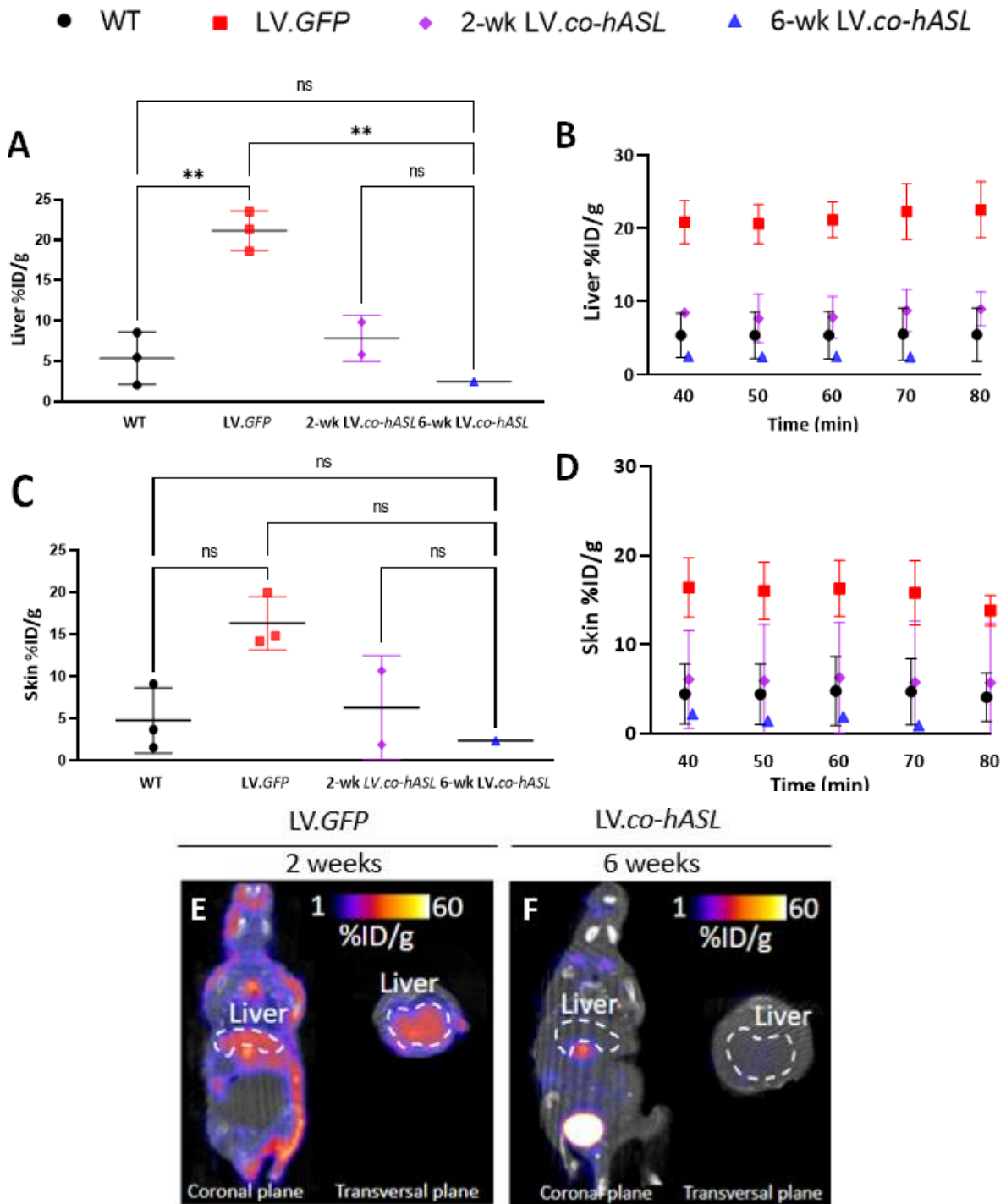
Figure 46. Lentiviral gene therapy corrects the impaired NO production in *Asl^Neo/Neo* mice. All the values were measured in 6-weeks-old wild-type (n=3), 2-weeks-old *GFP* (n=3), and 2- and 6-weeks-old *hASL* treated *Asl^Neo/Neo* mice (n=1-2). **(A)** Quantified [^{18}F]FSPG retention in liver at 60 minutes post injection **(B)** between 40- and 80-minutes post injection. **(C)** Quantified [^{18}F]FSPG retention in skin at 60 minutes post injection **(D)** between 40- and 80-minutes post injection. Horizontal lines display the mean ± standard deviation. One-way ANOVA with Tukey's multiple comparisons test; ns: not significant, ** $p < 0.01$. **(E,F)** Representative PET/CT images of [^{18}F]FSPG distribution (%ID/g), in the coronal and axial plane. ID/g: injected dose per gram of tissue; min: minutes; wk: weeks.

6.6 Safety profile of lentiviral vector *in vivo*

Lentiviral vectors are derived from retroviruses. Gamma retroviruses were the first gene therapy vector to show long-term transgene expression due to their ability to integrate into the host-cell genome [297]. However, the initial clinical success was rapidly followed by genotoxicity, with major adverse events such as secondary leukemia or done marrow dysplasia observed in SCID-X1 trial [145]. This is a result of insertional mutagenesis which occurs following integration in specific loci in or near oncogenes, through trans-activation of oncogenes by promoters and enhancers from the inserted transgene cassette, leading to clonal expansion of transduced cells and in some cases to tumorigenicity. It has previously been reported that lentiviruses, however, can transduce cells and exhibit reduced insertional mutagenesis, presenting a significantly safer profile [231].

To better assess safety of lentiviral gene therapy, we performed a long-term blinded *in vivo* study with CD1 mice, which received intravenous neonatal injection of either CCL.LP1.*co-hASL* vector or PBS as negative control. Animals received a single neonatal intravenous injection of CCL.LP1.*co-hASL* vector at the dose of 4e10TU/Kg, or PBS at the same volume, respectively. Animals were regularly monitored. Nine months following neonatal injection, mice were sacrificed, and tissue samples were collected for analysis (**Figure 47**). A CD1 background was chosen due to the simpler breeding associated with this strain and easier access to big litters to inject large cohorts of animals in a short period of time.
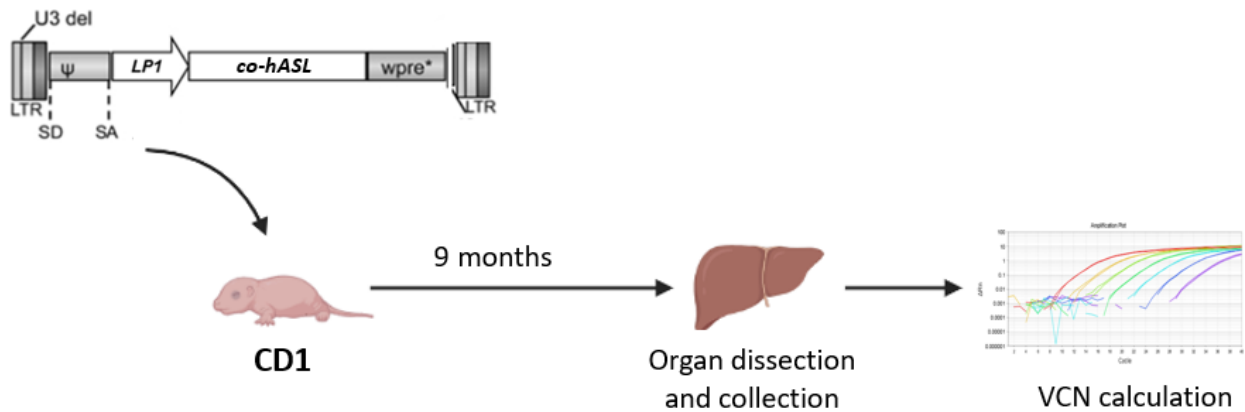
Figure 47. Schematic representation of the experimental plan for assessing safety of lentiviral vector
in vivo. *co-hASL:* codon-optimised human argininosuccinate lyase; LP1: liver specific 1 promoter; LTR: long terminal repeats; SA: tat/rev splice acceptor; SD: splice donor; U3: unique 3' region; VCN: number of vector copies per cell; WPRE: woodchuck hepatitis virus post-transcriptional regulatory element.

No significant difference of survival was shown between lentiviral- and PBS-injected mice (p=0.4). Three lentiviral-injected and two PBS control mice were found dead within the first 2 months following injection without any obvious explanation. The 3 lentiviral-injected animals with early death did not show evidence of tumour during dissection and pathological analysis. In addition, 4 out of 5 mice that died within the first 2 months post-injection, were from the same litter. Therefore, a death non-related to lentiviral vector was deemed more likely, especially in the context of death in PBS-treated animals. One more lentiviral-injected mouse needed to be culled at 6 months post injection due to severe wounds caused by fighting with littermates and judged again independent from the lentiviral vector injection (**Figure 48**).

Weekly weight did not differ between lentiviral or PBS-injected mice, with no difference according to sex, for the whole duration of the experiment (**Figure 49A-C**). Liver to body weight ratio was measured at harvest and was similar between both groups with no sex-related difference (p=0.4) (**Figure 50A-C**).
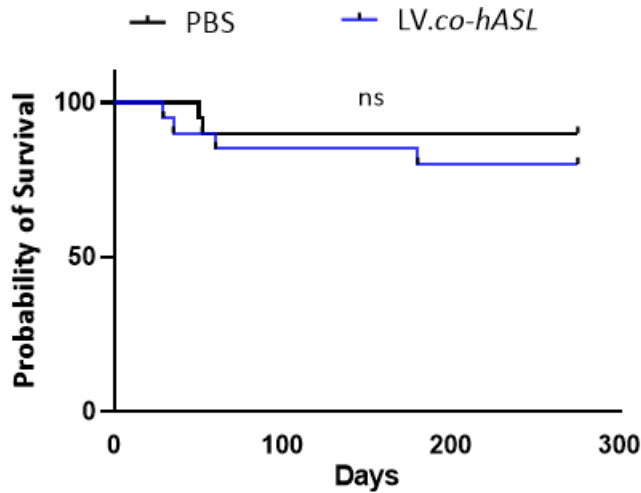
Figure 48. Survival curve for lentiviral-injected CD1 mice. Kaplan-Meyer survival curve of PBS-injected control (n=20) and lentiviral-injected (n=20) mice. PBS: phosphate buffer solution. Log-rank (Mantel-Cox) test; ns: not significant.
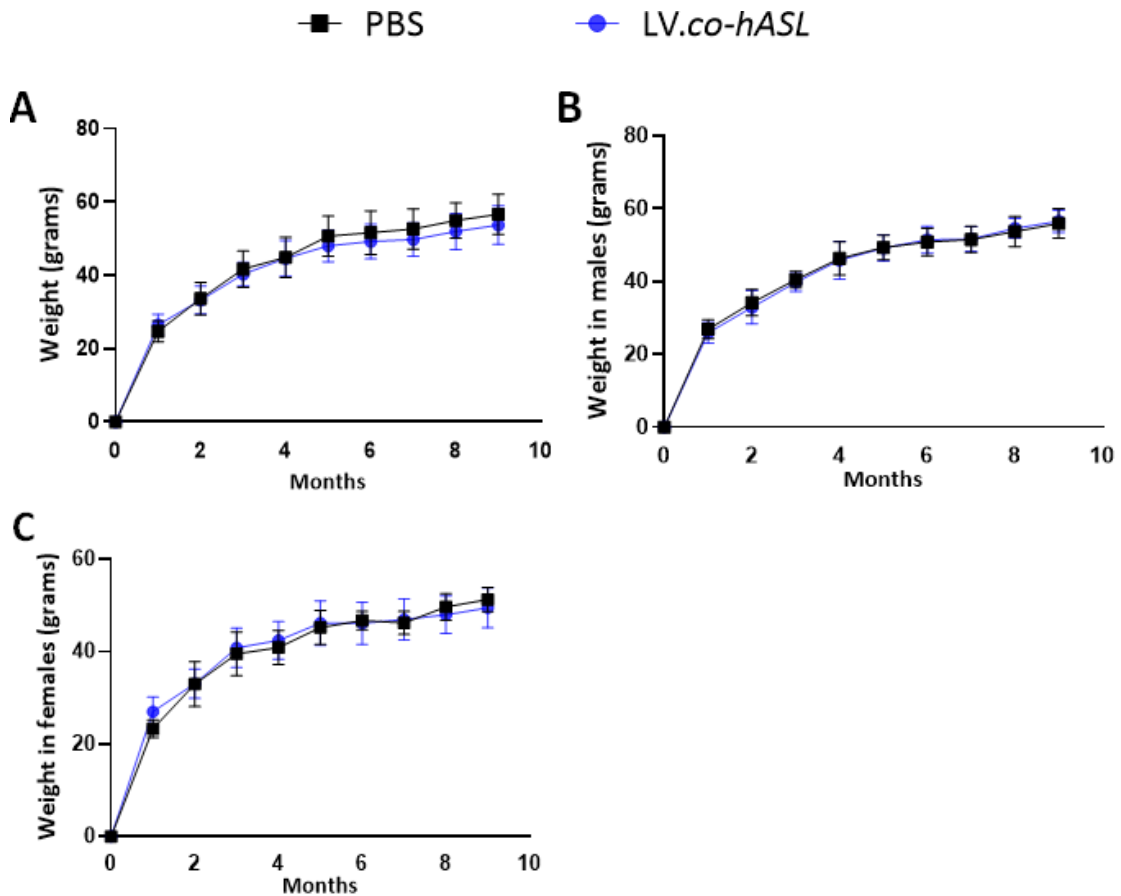
Figure 49. Growth of lentivirus-injected compared to PBS-injected control CD1 mice. (A) Mean growth of PBS- (n=20) and lentivirus-treated control mice (n=20) over 9 months. **(B)** Mean of male PBS- (n=10) and lentivirus-treated (n=8) mice. **(C)** Mean growth of female PBS- (n=10) and lentivirus-treated (n=12) mice. Horizontal lines display the mean ± standard deviation. PBS: phosphate buffer solution.

138
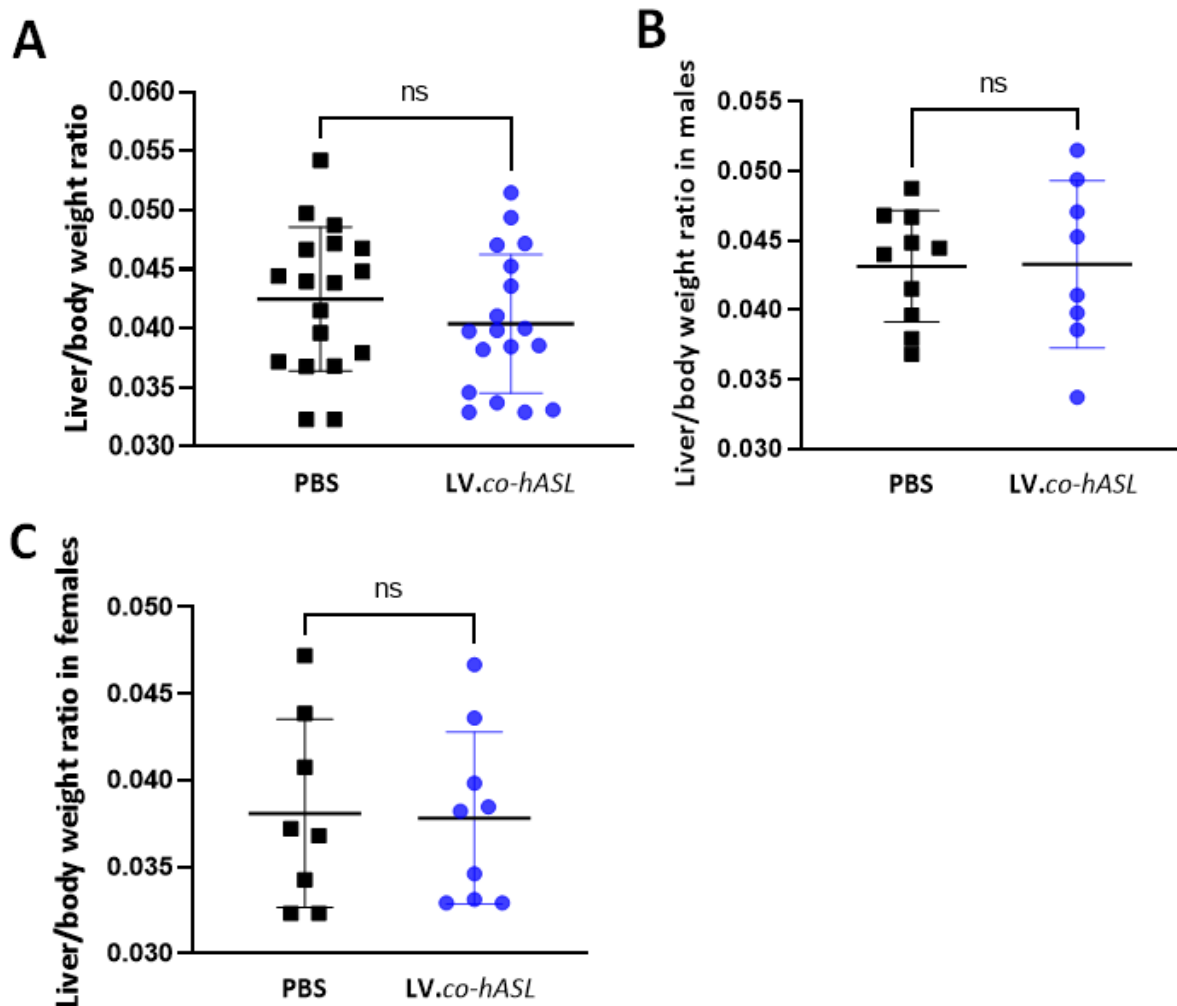
Figure 50. Hepatomegaly. (A) Liver/body mass ratio in PBS-(n=18) and lentiviral-injected CD1 mice (n=18) at 9 months of age. **(B)** Liver/body mass ratio in male PBS- (n=10) and lentiviral-injected CD1 mice (n=8) at 9 months of age. **(C)** Liver/body mass ratio in female PBS- (n=8) and lentiviral-injected CD1 mice (n=9) at time of culling. Horizontal lines display the mean ± standard deviation. Mann-Whitney test; ns: not significant. PBS: phosphate buffer solution.

After necroscopy, the lentiviral-mediated transgene DNA was measured in liver, spleen, heart, and other major organs of the lentiviral-injected mice (**Figure 51**). We found between 0.2 and 2 vector copies per cell in the liver (**Figure 51A**), accounting for almost 70% of all the retrieved lentiviral DNA in the rest of the organs measured. Additional organs showing some lentiviral vector expression included heart, lungs, bone marrow, kidney, and spleen with values of 0.06, 0.08, 0.03, 0.02 and 0.02, respectively. This shows that the lentiviral vector exhibits specific liver targeting in mice, with an over 5-log difference in VCN measured in the liver and the highest VCN measured in the other organs (**Figure 51B**). In addition, no expression was

observed in reproductive organs against a risk of germinal transmission of genetically modified cells. Pathology analysis and dissection of the liver, spleen, and major organs was performed at time of culling, and no lesions or signs of tumours were observed.
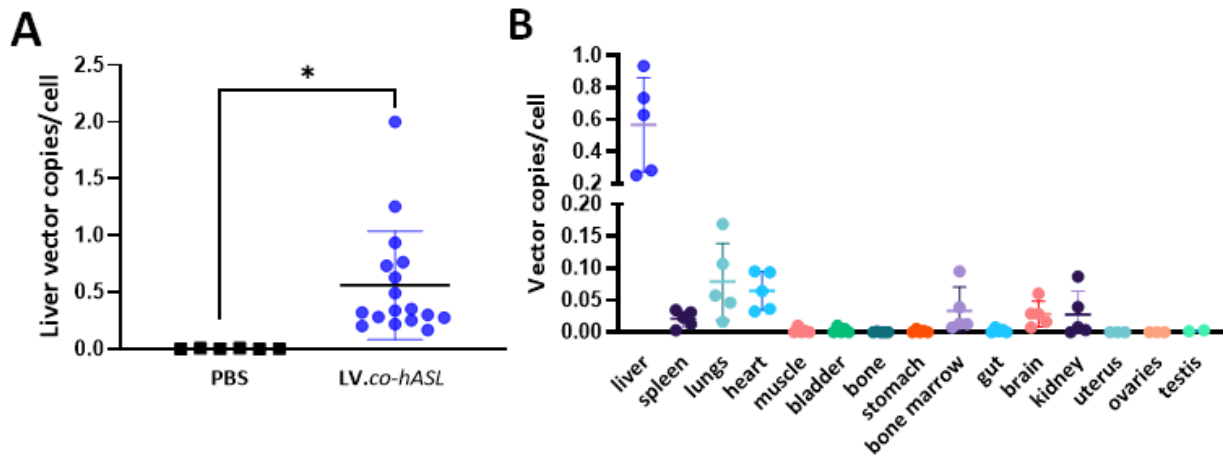
Figure 51. Lentivirus transduction biodistribution. (A) Single values of lentiviral vector copies per cell in the livers of PBS- (n=6) and lentiviral-injected (n=17) CD1 mice at 9 months of age. **(B)** Single values of lentiviral vector copies per cell in the indicated organs in lentiviral-injected mice (n=5). Horizontal lines display the mean ± standard deviation. Mann-Whitney test; * $p<0.05$. PBS: phosphate buffer solution.

6.7 Discussion

6.7.1 Correction of ureagenesis

All *hASL* treated *Asl*[Neo/Neo] mice displayed normalisation of phenotype involving survival, weight, fur pattern, as well as urea cycle related biomarkers including plasma ammonia levels, argininosuccinic acid, citrulline and orotate levels [308]. This finding is in line with earlier research, which has shown sustained correction after a solitary *in vivo* administration of lentiviral vector in animal models of inherited metabolic disorders of the liver such as hereditary tyrosinemia type 1 [331], hemophilia A [241], and hemophilia B [144] where vectors used contained the same VSV-G lentiviral capsid, a liver specific promoter and the dose administered was ranging between 2 – 8e10TU/Kg with no adverse events and no signs of insertional mutagenesis for any of the animals tested. The chronic liver disease in the *Asl*[Neo/Neo] mouse presents with hepatomegaly, elevated alanine aminotransferase and glycogen storage [59]. In this study, there was a significant correction of hepatomegaly in *hASL* treated *Asl*[Neo/Neo] mice and no evidence of glycogen storage in excess following lentiviral injection. This outcome is likely a result of the correction of the complex pathophysiological liver disease by restoration of ASL expression in hepatocytes.

Arginine levels from dried blood spots did not show significant improvement in *hASL* treated *Asl*[Neo/Neo] mice. The kidney is responsible for the endogenous production of arginine, which involves the presence of ASS and ASL enzymes. In ASA, the synthesis of arginine is hindered, causing arginine to become an essential amino acid. Even after a liver transplant, the renal production of arginine remains deficient, leading to the same outcome [28]. Hypoargininaemia in ASL- and ASS-deficient mice causes a fur phenotype, as arginine comprises around 10% of hair composition [18]. The treated group showed an improvement in plasma alanine aminotransferase levels, indicating that the correction of ammonia levels had a direct effect on the liver's pathophysiology.

These results have shown experimental evidence that a single neonatal intravenous injection of lentiviral vector in the high dose of 4e10TU/Kg was able to successfully transduce sufficient

number of hepatocytes for the correction of ureagenesis and liver pathophysiology in the *hASL* treated *Asl^{Neo/Neo}* mice. This is likely a result of different distribution of lentiviral vector DNA observed within the different liver cell subpopulations. It has been previously shown that below a threshold dose of 4.5x10E7vg/mouse, high amount of lentiviral vector DNA is uptaken by liver phagocytic cells [144]. Periportal hepatocytes demonstrate the predominant metabolic zonation of the liver, indicating the prevailing physiological activity of the urea cycle [332]. However, in this experiment, the pattern of hepatocyte transduction does not show a preferential pattern of transduction in pericentral or periportal hepatocytes. On the contrary, it shows a more uniform biodistribution.

The *Asl^{Neo/Neo}* mouse model exhibits hypomorphic characteristics, with a significant residual activity of argininosuccinate lyase [20]. Thus, the level of increase needed to achieve the threshold for controlling ammonia levels is lower in this hypomorphic mouse model compared to a knockout model. In this study, there was a 30% increase of ASL activity in the livers of the *hASL* treated *Asl^{Neo/Neo}* mice. This significant increase of liver ASL activity was sufficient for the normalization of argininosuccinic acid levels from dried blood spots. As it has been previously discovered, normalising amino acids requires more ASL liver activity in this mouse model than normalising ammonia [83]. Previous study for ASA treatment using AAV vector *in vivo* succeeded partial correction of plasma argininosuccinic acid levels of adult treated *Asl^{Neo/Neo}* mice [83] while more recent *in vivo* study in neonatal *Asl^{Neo/Neo}* mouse model was also able to normalise levels of argininosuccinic acid in dried blood spots at 48 hours post *hASL* mRNA therapy however, this is a treatment that requires weekly administration as it does not integrate [94].

Results in this study also demonstrate experimental evidence that the LP1 promoter, when delivered intravenously in neonatal mice through the superficial temporal vein, is successful in targeting the liver area and presenting long-term expression as shown in **Section 6.6** of this work. These results are consistent with other studies, where lentiviral vectors with LP1 promoter showed the strongest signal in the liver when compared to EF1α, PGK, and UbiC promoter 1 month following intravenous injection [300, 301].

Results revealed similar vector copies per cell in the liver of *hASL* and *GFP* treated *Asl^{Neo/Neo}* mice, respectively. These VCN are in line with findings from previous *in vivo* studies using

lentiviral vector, which showed safe and efficient liver transduction [144]. Unsurprisingly, the organ principally affected by off-target effect was the spleen. These results are comparable with vector copy values in spleen in previously published *in vivo* studies using lentiviral vectors, due to the high uptake of the vector upon intravenous injection from the splenic macrophages [144, 241, 331]. This high uptake by spleen and liver macrophages decreases the amount of vector available for hepatocyte transduction leading to a reduced efficacy *in vivo*. This finding led to exploring novel gene therapy approaches aiming at detargeting or depleting macrophages, in order to increase liver transduction hence efficacy while minimizing injected dose i.e., improving safety. Recent studies were successful in significantly reducing lentiviral transduction of liver macrophages using a phagocytosis-shielded (CD47hi) lentiviral vector technology *in vivo*, by inhibiting lentiviral vector uptake by liver macrophages and spleen [144]. Our group has recently combined clodronate liposome's technology used to deplete microphages in liver and spleen following systemic injection with lentiviral vector *in vivo*, significantly reducing uptake of the vector by the spleen leading to enhanced lentiviral transduction in liver [333]. Such approaches could potentially be beneficial for further improving the correction of the *Asl^Neo/Neo* phenotype whilst using a lower lentiviral vector dose.

6.7.2 Correction redox imbalance in *Asl^Neo/Neo* mice

ASA is well-known to exhibit pathophysiological mechanisms associated with oxidative stress. High levels of oxidative stress either systemically [47], affecting neuronal [83] or endothelial [84] cells have been reported, which could be due to either reduced arginine levels or NOS uncoupling [83] or caused by direct toxicity from argininosuccinic acid and derived conjugates such as guanidinosuccinate [45, 334, 335]. However, it has recently been confirmed that the *Asl^Neo/Neo* mouse only shows moderate evidence of oxidative stress in the liver despite evidence of systemic and liver NO deficiency. NO-induced upregulation of glutamate cysteine ligase in human hepatocytes has further been determined providing a mechanistic connection between hepatic NO deficiency and glutathione depletion [94]. Liver showing an upregulation of the xCT transporter, indicates a potential feedback mechanism aimed at mitigating the

effects of glutathione depletion. In this study we observed similar upregulation of intracellular cystine uptake via the xCT antiporter in $Asl^{Neo/Neo}$ livers. The mechanism of enhancing glutathione biosynthesis and promoting cell survival used by cancer cells through increasing the intracellular cysteine pool has been observed in monogenic liver diseases as well [336-338]. Significantly increased xCT levels in $Asl^{Neo/Neo}$ livers indicate similar plasticity. An additional surprising finding from [^{18}]FSPG-PET is the retention of the radiotracer in the skin of the $Asl^{Neo/Neo}$ mice. This probably indicates the presence of skin inflammation seen in some patients and the fur malformations and inflamed skin observed in the $Asl^{Neo/Neo}$ mice, underscoring the multi-organ nature of ASA pathophysiology [70, 339]. However, the detailed pathophysiology is not known.

The utilization of [^{18}F]FSPG-PET imaging in this study demonstrates the promising ability of non-invasive diagnostic tools to sensitively assess liver disease and investigate its underlying mechanisms in ASA animal models *in vivo*. Considering the outcomes, we opted to employ this technology for evaluating the treatment response. We were then able to monitor the intracellular cystine uptake via the xCT antiporter in *hASL* treated $Asl^{Neo/Neo}$ mice. Both liver and skin [^{18}F]FSPG retention in neonatally *hASL* treated animals were completely normalized at 2 weeks post injection compared to *GFP* controls. This indicates the correction of liver disease. Normalization of [^{18}F]FSPG retention in the skin can potentially be a result of correction of cystine uptake and subsequently, glutathione levels in the liver having downstream effects on glutathione levels in the skin [340]. Consistent with a recent study utilizing *hASL* mRNA therapy in $Asl^{Neo/Neo}$ mouse model, which improved liver function but not skin abnormalities, we observed a similar pattern in [^{18}F]FSPG retention in neonatally-treated animals [94]. In a similar manner, that study showed a correction of [^{18}F]FSPG retention as well as glutathione dysfunction at 2 weeks of age [94]. However, *hASL* mRNA gene therapy typically results in transient gene expression, making re-injection of *hASL* mRNA therapy necessary to maintain the therapeutic effect [94, 341]. In contrast, lentiviral vectors can result in long-term expression following a single systemic administration.

6.7.3 Safety profile of lentiviral vector *in vivo*

For maintaining the therapeutic transgene in dividing cells, the integration of lentiviral vector in the genome of target cells is crucial. However, this raises concerns about the possibility of induced insertional mutagenesis. Despite this, accumulating evidence suggests that lentiviral vector has low genotoxicity. This entails different constructs, different transgenes, and long term follow up for up to 8 years [342, 343]. Additionally, previous studies have reported no evidence of genotoxicity after liver-targeting lentiviral gene therapy *in vivo* in different animal models i.e., mouse, pig, and non-human primate [144, 240, 331]. Safety data from ongoing lentiviral *ex vivo* gene therapy clinical trials provide some reassurance about the safety profile of the vectors. Early preclinical safety data generated in this work show no evidence of genotoxicity, especially in liver, and a satisfactory biodistribution profile targeting almost exclusively the liver with limited off-target organ transduction. Previous studies have confirmed that animal presenting tumors have significantly reduced weight compared to healthy mice [344, 345]. In this study, three lentiviral-injected and two control mice died within the first 2 months of life. However, this is not related to the injection as no evidence of insertional mutagenesis was shown at pathology analysis. Furthermore, four out of five mice that died within the first 2 months post injection, were derived from the same litter including the two PBS-injected mice, indicating a possible litter-related underlying issues.

Liver VCN calculation revealed 0.6 vector copied per cell in lentiviral injected mice at 9 months post neonatal injection. This is in line with previous *in vivo* studies using lentiviral vector, that reported similar vector copy values in the liver of animals injected with similar dose, several months following administration, and presenting no sign of insertional oncogenesis [144, 241]. Our experimental results regarding the liver VCN show an overall 2-log lower value at 9 months collection compared to 3-month liver collection in the gene therapy experiment as shown in **Section 6.4.3**. Despite the disparity in mean values observed between the gene therapy treated *Asl^{Neo/Neo}* mice and the CD1 mice in this safety study, where the overall VCN was 1.2 and 0.6, respectively, both cohorts exhibited considerable variability in terms of the VCN range, spanning from 0.2 to 2 copies per cell in the liver of both groups. This may be a result of technical difficulties in neonatal injection from different operators. No difference in

liver transduction has been reported previously between different mouse strains. The VCN results of five animals that were injected with lentiviral vectors demonstrated that VSV-G-pseudotyped lentiviral vectors exhibit a selective gene transfer to the liver, as shown by the higher gene transfer in the liver compared to other major organs such as the spleen. This observation is noteworthy given that VSV-G is known for its wide tropism. The preferential targeting of the liver by VSV-G positive vectors may be attributed to the ability of hepatocytes to uptake such vectors through low-density lipoprotein (LDL) receptors [346].

This study represents a significant advancement in gene therapy for ASA, as it demonstrates proof-of-concept for correcting the phenotype in the $Asl^{Neo/Neo}$ mouse model *in vivo* using lentiviral vector technology. In comparison, previous studies have evaluated other gene therapy approaches for ASA, each one presenting with its own strengths and limitations. For example, AAV gene therapy achieved complete survival in adult, but with very limited correction of the phenotype in neonatally treated $Asl^{Neo/Neo}$ mice [83]. This makes it an unsuitable sustained strategy for paediatric correction of the disease. Another gene therapy approach, using *hASL* mRNA encapsulated in lipid nanoparticles and delivered systemically, has shown promising results in neonatal $Asl^{Neo/Neo}$ mice following weekly systemic administration of 1 mg/kg *hASL* mRNA with complete normalization of ureagenesis and the liver disease phenotype. In young-adult $Asl^{Neo/Neo}$ mice, only partial correction was observed with improved weight but not reaching the wild-type weight, likely due to the late start of the therapy [94]. While this approach offers the potential for long-lasting correction of the phenotype, it would require life-long re-administration of the treatment.

This study demonstrated impressive results using lentiviral vector gene therapy, which effectively restored the macroscopic phenotype, biomarkers, *in vivo* ureagenesis, liver ASL expression and activity to normal levels without safety concern over a prolonged period of time in a large cohort of animals. While more research is needed to evaluate its long-term efficacy and safety before clinical translation, these results provide a strong foundation for further clinical development of this integrating approach.

6.8 Conclusion

Lentiviral vector including the codon-optimised *hASL* transgene under the transcriptional activity of the LP1 promoter and delivered intravenously in neonatal *Asl^(Neo/Neo)* mice, has shown proof-of-concept enabling long-term correction of the *Asl^(Neo/Neo)* mouse phenotype.

This vector did not display any signs of long-term insertional mutagenesis, which suggests, in line with other preclinical safety studies from other groups, low genotoxicity of lentiviral vector *in vivo*. The biodistribution showed a successful liver-targeting with minimal off-target effect, supporting additional safety. This work suggests *in vivo* liver-targeting lentiviral-mediated gene therapy is a safe and efficient therapy for patients affected by argininosuccinic aciduria, in particularly neonates with the highest unmet needs.

7. MACROPHAGE INHIBITOR CLODRONATE ENHANCES LIVER TRANSDUCTION OF LENTIVIRAL BUT NOT AAV VECTORS *IN VIVO*

7.1 Introduction

Over the last two decades, gene therapy has transformed the therapeutic landscape of monogenic diseases demonstrating maturity with numerous clinical successes [347-349]. At present, AAV vectors are considered the preferred vector for liver targeting, as they primarily distribute an episomal transgene that is not maintained during cellular division [350-352]. However, to sustain clinical efficacy in paediatric liver, there is a need to establish further optimised vector administration methods to minimise concerns associated with viral vector-mediated gene therapies such as new integration strategies including lentiviral vectors. Viral vector associated risks include, severe innate and adaptive immune responses for adenoviral [353, 354] and AAV [355-358] vectors, off- target tropism, as well as safety issues such as risk of genotoxicity for viral vectors integrating in the host genome [217, 359]. Anti-AAV immune response currently prevents AAV re-injections in humans. Despite well-recognised for many years, these adverse events have not been overcome by neither vector engineering nor immunosuppressive technologies and are still a prominent concern of the field. Reducing the dose of lentiviral or AAV gene therapy while maintaining the transduction efficacy in the target organ could minimise or prevent several viral vector-mediated adverse events, which prevalence is partly related to the injected dose. As an alternative approach, integrative lentiviral vectors are presently under development to allow for extended expression of transgenes, particularly during liver development in children [360-362]. Studies conducted prior to clinical trials have indicated that liver-targeting lentiviral gene therapy has limited effectiveness *in vivo*, primarily because of excessive uptake by macrophages in the splenic

marginal zone, which are critical for the removal of pathogens present in the bloodstream [144, 241, 363, 364].

Liposomes are artificial spheres, which contain concentric phospholipid bilayers [365]. Phospholipid bilayers are separated by hydrophilic compartments, where hydrophilic molecules are located and encapsulated. Clodronate (dichloroethylene-bisphosphonate or Cl2MBP) is a hydrophilic molecule that can be entrapped between phospholipid bilayers. Free clodronate has a short half-life as it is rapidly cleared from the circulation by the kidney. However, the clodronate encapsulated in a liposome is preferentially uptaken by macrophages [366]. Phospholipid bilayers are degraded by lysosomal phospholipases, whereas clodronate is not enzymatically degraded and stays in the macrophages (**Figure 52**). Clodronate is metabolised intracellularly to β,γ-Dichloromethylene ATP, which is cytotoxic to macrophages, disrupting cellular energy metabolism. Hence, clodronate accumulation leads to apoptosis [367].
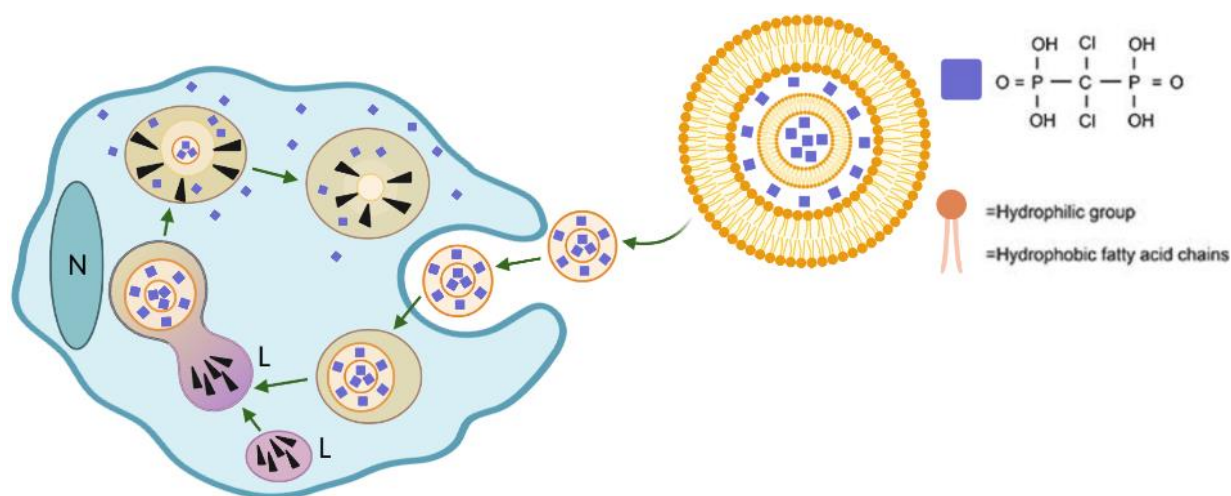
Figure 52. Schematic representation of clodronate liposome and its mechanism of action after macrophage uptake. The liposome is made of concentric phospholipid bilayers, divided by aqueous compartments. The bilayers include a hydrophilic and hydrophobic group. The clodronate molecules (purple squares) are dissolved in aqueous compartments and encapsulated within the liposome. Clodronate liposomes are uptaken by macrophages via endocytosis. Late endosomes then fuse with lysosomes (L). Lysosomal phospholipases (arrowheads) digest the liposome. Clodronate will then accumulate and generate a dose-dependent toxicity ultimately triggering apoptosis. N: nucleus.

Clodronate is a molecule from the family of bisphosphonates, routinely prescribed in clinical settings to prevent bone resorption in cancer [368-370]. Clodronate is generally well tolerated, with few adverse events, including transient hypocalcaemia, gastrointestinal disturbance, transient increase in serum creatinine and parathyroid hormone levels [368]. In the literature, most studies about clodronate liposomes achieved a transient depletion of 90% macrophages in both red pulp of the spleen and Kupffer cells in the liver at 24 hours after intravenous injection [366, 371].

It has previously been determined that administration of adenovirus and AAV vectors results in the activation of the innate immune system leading to the elimination of transduced cells [372-379]. The liver's resident macrophages, in addition to marginal zone macrophages, function as the initial immune response against pathogens present in the bloodstream, and therefore, are accountable for the majority of absorbed vector particles [144, 363, 364, 380-383]. Previous studies using adenoviral and AAV vectors have suggested that pre-administration of clodronate liposomes prior to the administration of viral vectors depletes macrophages and allows higher vector transduction *in vivo* [311, 384, 385]. Temporary elimination of macrophages via intravenous infusion of clodronate liposomes has led to better transfer of adenoviral DNA to the liver, accompanied by increased expression of transgenes and delayed clearance of vector DNA [385]. In contrast to the positive results seen with adenoviral vectors, administering clodronate before AAV vector injection *in vivo* produced a considerable reduction in transgene expression within the liver, as well as only moderate transduction of the spleen's white pulp [386].

We hypothesised that gene therapy mediated by lentiviral vector will also benefit from transient macrophage depletion to increase vector availability for hepatocytes following a pre-treatment using clodronate liposomes. In addition, we wanted to further delineate the transduction efficacy with AAV vector following clodronate liposomes exposure *in vivo* with different age groups and doses from the literature [386]. In this study, we assessed liver transduction after intraperitoneal injections of clodronate liposomes prior to systemic administration of lentiviral or AAV vectors, in neonatal and young-adult wild-type mice.

The purpose of these experiments in neonatal mice was to assess any improvement of transduction in neonatal liver and potentially use clodronate liposomes with gene therapy vector for the rescue of neonatal *Asl^{Neo/Neo}* mice. Improvement of liver transduction following

clodronate injections was further investigated in young-adult wild-type mice to assess any improvement of transduction in 2.5-weeks-old liver and potentially use clodronate liposomes with gene therapy vector for a rescue gene therapy approach in young-adult $Asl^{Neo/Neo}$ mice. $Asl^{Neo/Neo}$ mice present with a highly severe phenotype that leads to death within the first 3-4 weeks of life due to multi-organ disfunction [20]. Tail vein systemic administration of lentiviral vector is challenging before 8-10 days of age due to the reduced size and severe phenotype of $Asl^{Neo/Neo}$ mice. By increasing the liver transduction of lentiviral vector with clodronate pre-administration, it could lead to a faster correction of the disease, which is vital for $Asl^{Neo/Neo}$ mice with rapid disease progression.

7.2 Lentiviral liver transduction using clodronate liposomes in CD1 mice

7.2.1 Experimental design

This experiment was designed to assess liver transduction following systemic administration of clodronate liposomes prior to intravenous lentiviral injection, in neonatal and young-adult wild-type mice. For this study, CD1 mice received repeated intraperitoneal injections of clodronate or PBS liposomes at 30 and 6 hours before intravenous injection with the CCL.LP1.*GFP* vector at the dose of 4e10TU/Kg. This vector backbone was the same as in the gene therapy studies in **Chapters 4 & 6**, containing LP1 promoter, and WPRE for targeting hepatocytes and increasing transgene expression respectively. *GFP* was used as a reporter gene for quantification and expression of GFP antigen. This high dose was chosen based on its increased liver transduction efficacy in $Asl^{Neo/Neo}$ mice following *in vivo* gene therapy. By using the same dose, we would be able to assess clodronate liposome's efficacy and compare it to previous experiments and potentially use it as a reference for future gene therapy studies. One month following the injection of lentiviral vector, mice were harvested, and livers

were collected for analysis (**Figure 53**). A 4-week interval was deemed sufficient for lentiviral vector to mediate a stable transduction of hepatocytes. The readouts were VCN and liver immunostaining.
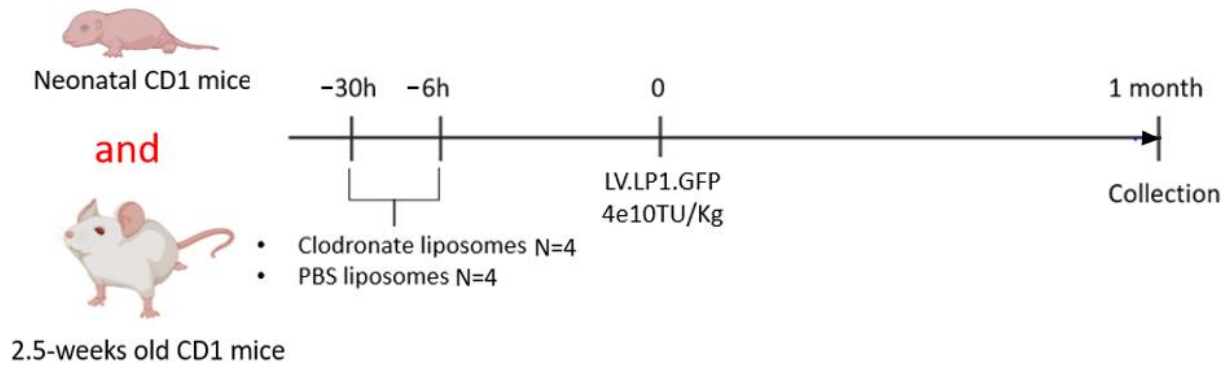
Figure 53. Schematic representation of the experimental design testing lentiviral transduction following pre-treatment with clodronate liposomes in CD1 mice. GFP: green fluorescent protein; h: hours; Kg: kilograms; LP1: liver specific 1 promoter; LV: lentivirus; PBS: Phosphate Buffer Solution; TU: transduced units.

7.2.2 Lentiviral transduction in neonatally-injected CD1 mice

Liver VCN showed a not-significant 2-fold increase of liver transduction in the clodronate- versus PBS-treated animals with values of 0.33 and 0.15 vector copies per cell respectively (**Figure 54A**). Similarly, liver immunostaining shown a 12-fold increase in clodronate- versus PBS-treated animals with 15% and 1.2% of GFP expression respectively (**Figure 54B**). The pattern of hepatocyte transduction revealed a homogeneous and scattered expression in all injected mice with no predominant expression in periportal or perivenous hepatocytes (**Figure 54C**).

Figure 54. Lentiviral transduction in livers of neonatally-injected CD1 mice. (A) Lentiviral vector genome copies per cell; **(B)** GFP immunostaining. Horizontal lines display the mean ± standard deviation. One-way ANOVA with Tukey's multiple comparisons test. **(C-E)** GFP immunostaining in liver sections. Scale bars are 100µm for x10 magnification. All the values were measured in untreated (n=3), PBS liposome injected- (n=4) and clodronate liposome injected-mice (n=4). Clod: clodronate liposomes; LV: lentivirus; PBS: Phosphate Buffer Solution.

7.2.3 Lentiviral liver transduction in young-adult CD1 mice

Liver VCN in young-adult injected CD1 mice that received PBS and clodronate liposomes prior to intravenous lentiviral vector administration, revealed 0.1 and 0.8 values respectively (**Figure 55A**). These results showed a 7-fold increase of the liver VCN in the animals, which had received clodronate compared to controls. In addition, a significant increase (p=0.002) of liver transduction was observed following immunostaining of young-adult-injected CD1 mice livers that received clodronate compared to PBS liposomes, with 28% and 12% GFP expression respectively (**Figure 55B**). Overall, these findings demonstrated similar transduction

percentages between 2.5-weeks-old and the neonatally-injected groups, that received clodronate liposomes with lentiviral vector as described in **Section 7.2.2**. Findings of immunostaining results in young-adult mice were similar to neonatally-injected CD1 mice, also exposing more scattered and sparse expression with no predominant expression in periportal or pericentral hepatocytes (**Figure 55C**).
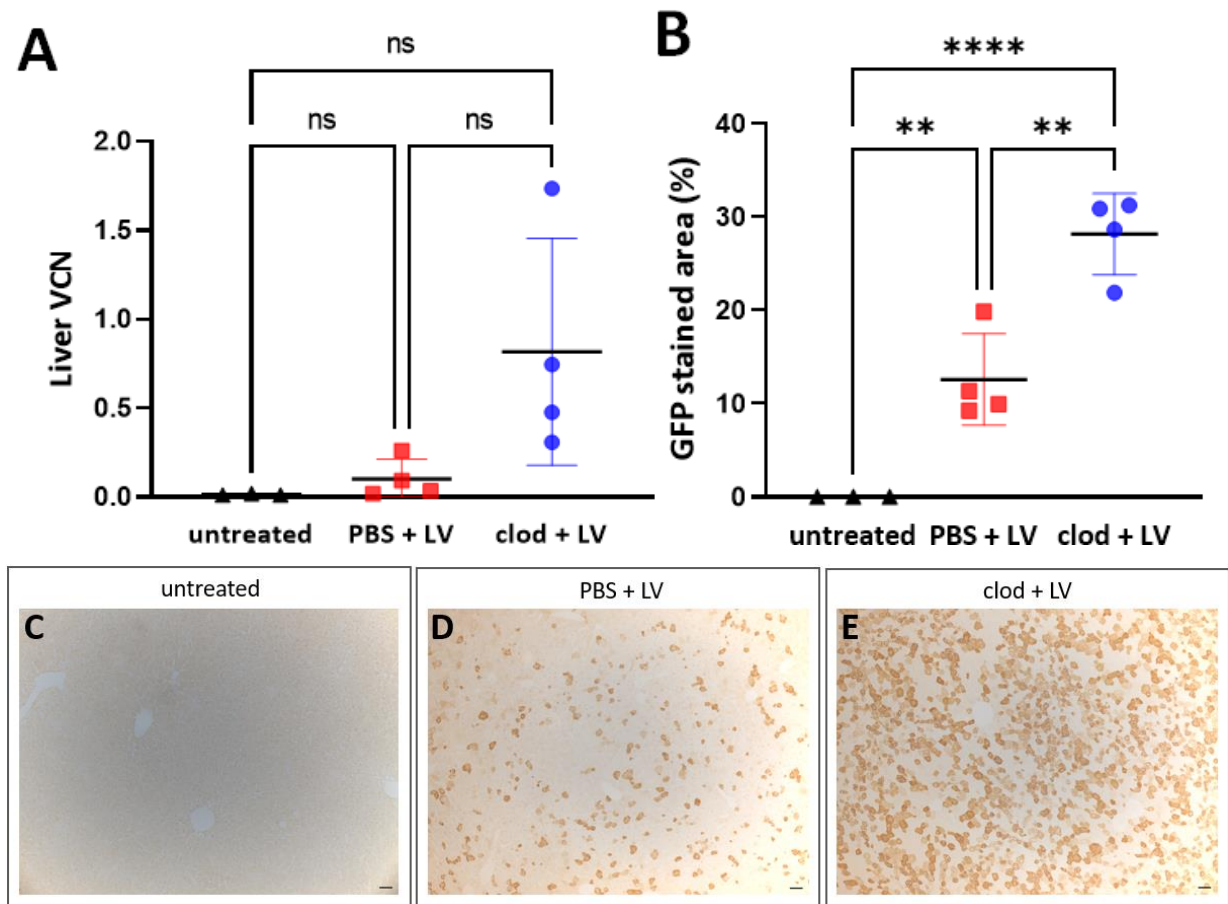
Figure 55. Lentiviral transduction in young-adult CD1 mice. (A) Lentiviral vector genome copies per cell in whole liver; **(B)** percentage of area in the liver expressing. Horizontal lines display the mean ± standard deviation. One-way ANOVA with Tukey's multiple comparisons test; **(C-E)** GFP immunostaining in liver sections. Scale bars are 100µm for x10 magnification. All the values were measured in untreated (n=4), PBS liposome injected (n=4) and clodronate liposome injected mice (n=4). ns: not significant, ** $p<0.01$, **** $p<0.0001$. Clod: clodronate liposomes; LV: lentivirus; PBS: Phosphate Buffer Solution.

7.3 Lentiviral liver transduction using clodronate liposomes in C57BL/6J mice

7.3.1 Translating clodronate liposome efficacy to improve liver transduction from CD1 to C57BL/6J mice

As described in **Section 7.2**, injection of clodronate liposomes prior to systemic administration of lentiviral vector presented a significantly better outcome in improving the liver transduction in both neonatal pups and young-adult CD1 mice compared to PBS controls. CD1 mice were used initially due to easier breeding with large litters, which can accommodate several experimental groups sparing time and cost [387, 388]. Then, we decided to confirm these results in the C57BL/6J strain, the background of *Asl^Neo/Neo* mice. CD1 are outbred mice that have more genetic diversity, are more robust, and produce larger litter sizes than inbred mice like C57BL/6J mice, an inbred strain mice which has less genetic variability, which is easier for the interpretation of experimental work [389-391].

7.3.2 Experimental design

This experimental design was identical to the one used for CD1 animals. We assessed liver transduction after repeated systemic injections of clodronate liposomes prior to intravenous lentiviral injection, in neonatal and young-adult wild-type mice. C57BL/6J mice received injections of clodronate or PBS liposomes at 30 and 6 hours before injection with CCL.LP1.GFP vector at 4e10TU/Kg. One month following the lentiviral injection, mice were harvested, and liver and spleen were collected for analysis (**Figure 56**).
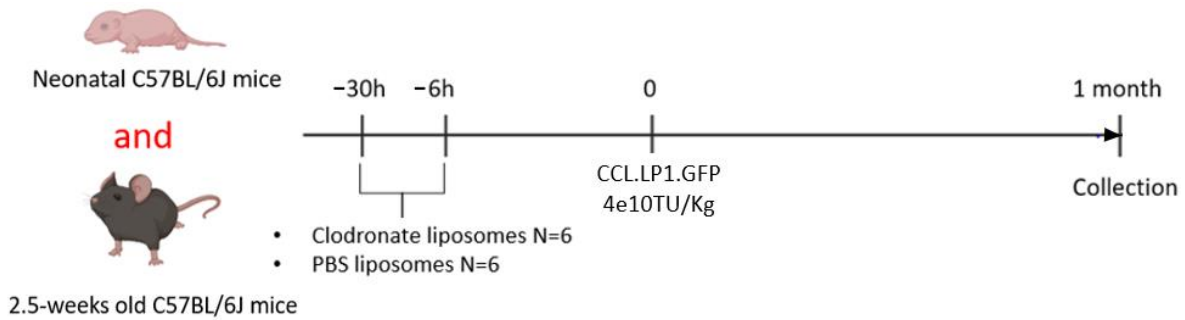
Figure 56. Schematic representation of lentiviral biodistribution with clodronate liposomes experimental design. GFP: green fluorescent protein; h: hours; Kg: kilograms; LP1: liver specific 1 promoter; LV: lentiviral vector; PBS: Phosphate Buffer Solution; TU: transduced units.

7.3.3 Lentiviral transduction in neonatally-injected C57BL/6J mice

VCN in the liver of mice that received PBS and clodronate liposomes prior to lentiviral injection, showed values of 0.3 and 0.4 vector copies per cell respectively (**Figure 57A**). These results, similar to the results in CD1 animals in **Section 7.2.2**, determined an increasing trend of the liver transduction in the animals that received clodronate compared to PBS controls. For this study, we measured the VCN in the spleen in order to determine whether injection with clodronate liposomes will affect and potentially reduce the vector uptake by the spleen due to splenic macrophage depletion. Spleen VCN revealed a decreasing trend of spleen transduction following injections with clodronate liposomes compared to controls, with values of 0.07 and 0.14 vector copies per cell respectively (**Figure 57B**). Furthermore, quantification of liver immunostaining against GFP demonstrated over 2-fold increase of liver transduction in the clodronate group compared to PBS controls with 24% and 9% liver expression respectively at the time of culling (**Figure 57C**). Immunostaining results revealed a scattered and sparse expression in all injected mice with no predominant expression in periportal or pericentral hepatocytes (**Figure 57D**).
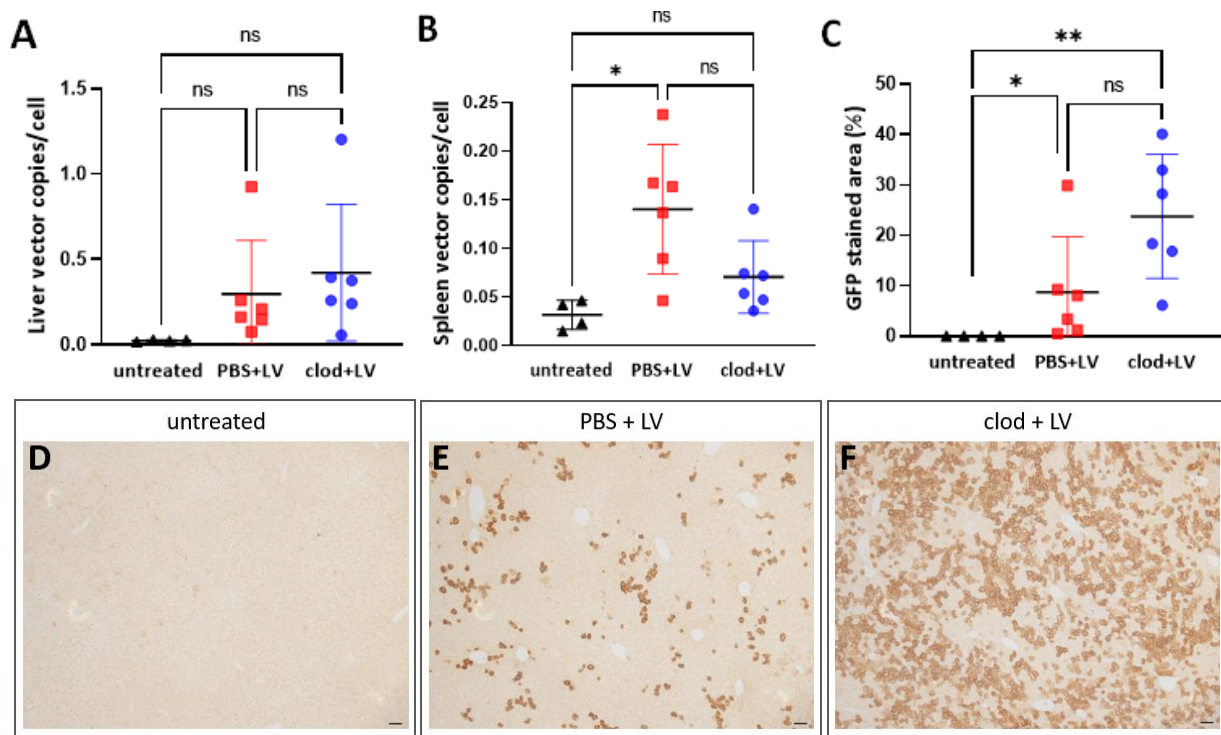
Figure 57. Lentiviral transduction in neonatally-injected C57BL/6J mice. (A) Lentiviral vector genome copies per cell in whole liver; **(B)** vector genome copies per cell in whole spleen; **(C)** percentage of area in the liver expressing GFP. Horizontal lines display the mean ± standard deviation. One-way ANOVA with Tukey's multiple comparisons test. **(D-F)** GFP immunostaining in liver sections. Scale bars are 100µm for x10 magnification. All the values were measured in untreated (n=4), PBS liposome injected-(n=6) and clodronate liposome injected-mice (n=6). ns: not significant, * $p<0.05$, ** $p<0.01$. Clod: clodronate liposomes; LV: lentivirus; PBS: Phosphate Buffer Solution.

7.3.4 Lentiviral transduction in young-adult C57BL/6J mice

Liver VCN of young-adult injected C57BL/6J mice that received PBS and clodronate liposomes prior to lentiviral vector administration, revealed values of 0.2 and 0.6 respectively (**Figure 58A**). Similar to the study with neonatal mice, these results also showed a significant 2-fold increase ($p=0.008$) of liver VCN in the clodronate group compared to PBS controls. In addition, spleen VCN revealed a significant 3-fold decrease ($p=0.0002$) of spleen transduction in the clodronate group compared to PBS controls, with values of 0.1 and 0.33 respectively (**Figure 58B**). These results correlate with an over 4-fold significant increase ($p=0.006$) of liver transduction showed from GFP immunostaining in young-adult C57BL/6J liver sections

treated with clodronate compared to PBS liposomes, with 21% and 5% liver expression respectively (**Figure 58C**). These findings demonstrated similar transduction percentages of the 2.5-week-old mice and the neonatal pups. Liver immunostaining showed similar results to neonatally-injected C57BL/6J mice, with scattered and sparse liver expression in all injected mice with no predominant expression in periportal or pericentral hepatocytes (**Figure 58D**).
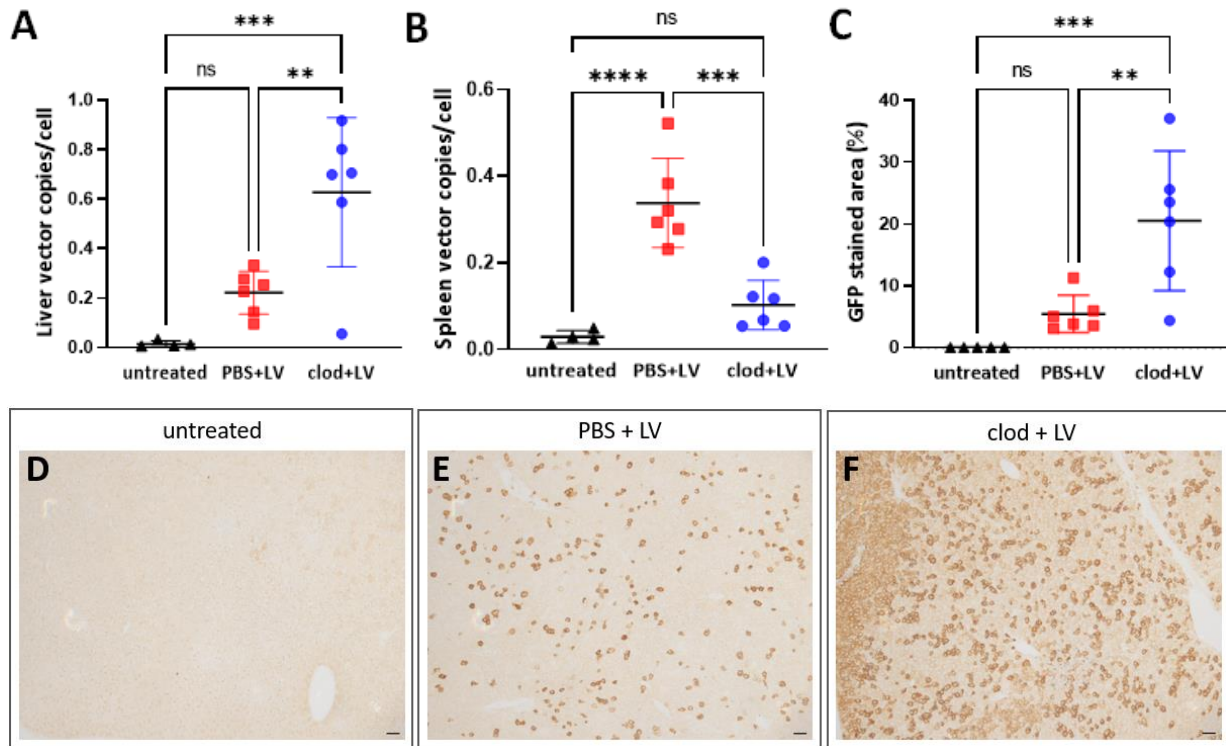
Figure 58. Lentiviral transduction in young-adult C57BL/6J mice. (A) Lentiviral vector genome copies per cell in whole liver; **(B)** vector genome copies per cell in whole spleen; **(C)** percentage of area in the liver expressing. Horizontal lines display the mean ± standard deviation. One-way ANOVA with Tukey's multiple comparisons test. All the values were measured in untreated (n=4), PBS liposome injected- (n=6) and clodronate liposome injected-mice (n=6). **(D-F)** GFP immunostaining in liver sections. Scale bars are 100μm for x10 magnification. ns: not significant, * $p<0.05$, ** $p<0.01$, *** $p<0.001$, **** $p<0.0001$. Clod: clodronate liposomes; LV: lentivirus; PBS: Phosphate Buffer Solution.

7.4 AAV liver transduction using clodronate liposomes in CD1 mice

7.4.1 Experimental design

My results showed increased liver transduction with lentiviral vectors with prior systemic injection of clodronate liposomes. AAV vectors are currently the leading viral vector for liver targeting in clinical settings. We wanted to test whether AAV vectors would benefit as well of an enhanced liver transduction with a transient macrophage depletion with clodronate liposome prior to AAV injection. A previous study had shown that pre-treatment with clodronate prior to AAV injections had significantly reduced transgene expression in the liver [386]. However, animals were 8-week-old animals, and the AAV vector dose was particularly high at $5x10^{13}$ Vg/Kg.

For this experiment, we used the same design as used for lentiviral vectors. Neonatal and young-adult CD1 mice received repeated intraperitoneal injections of clodronate or PBS liposomes at 30 and 6 hours before they received intravenous injection of AAV serotype 8, AAV8.LP1.*GFP* vector at the medium dose of $1x10^{13}$Vg/Kg. The AAV vector construct, similarly to the lentiviral vector previously used, contained the LP1 promoter and WPRE sequences. Similarly, to lentiviral vector experiments, mice were harvested one month after AAV injection, and liver and spleen were collected (**Figure 59).**
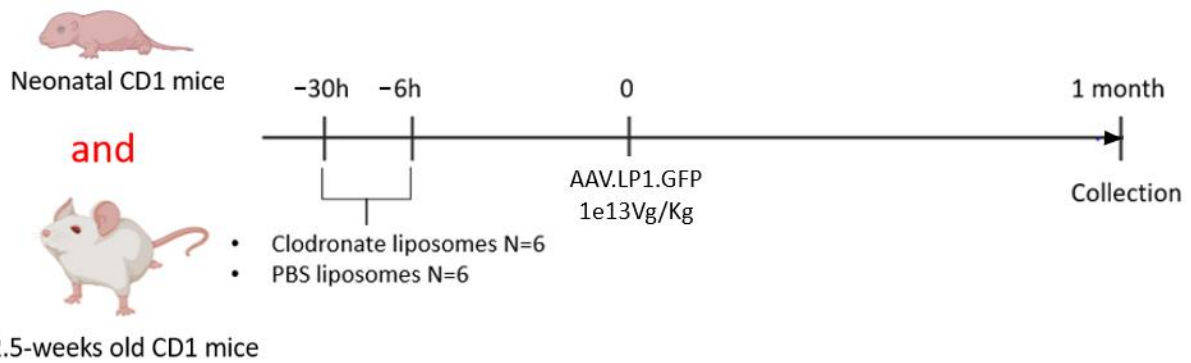
Figure 59. Schematic representation of the experimental design testing AAV transduction following pre-treatment with clodronate liposomes in CD1 mice. AAV: adeno-associated virus; GFP: green fluorescent protein; h: hours; Kg: kilograms; LP1: liver specific 1 promoter; PBS: Phosphate Buffer Solution; TU: transduced units; Vg: vector genomes.

7.4.2 AAV transduction in neonatally-injected CD1 mice

Liver VCN of the neonatally-injected CD1 mice that received PBS and clodronate liposomes prior to injection with AAV vector, showed values of 0.16 and 0.036 vector copies per cell respectively (**Figure 60A**). These results are not significantly different (p=0.9) between the two groups indicating an absence of better hepatic transduction in the clodronate group compared to PBS controls. Similarly, liver immunostaining and its quantification also demonstrated no significant difference (p=0.9) between clodronate and PBS groups with 0.7% and 0.63% of liver GFP expression respectively (**Figure 60B**). Overall, these data represented an extremely low hepatocyte transduction rate, which is likely the result of the AAV-mediated transduction with an episomal transgene and its low integration. This is a well-described feature of murine neonatal AAV injection which shows a rapid decrease of the episomes, which are not transmitted to daughter cells during cell division, in parallel with the liver growth. AAV-mediated liver transduction following neonatal intravenous injection also revealed scattered and sparse expression in all injected mice with no predominant expression in periportal or pericentral hepatocytes (**Figure 60C**).
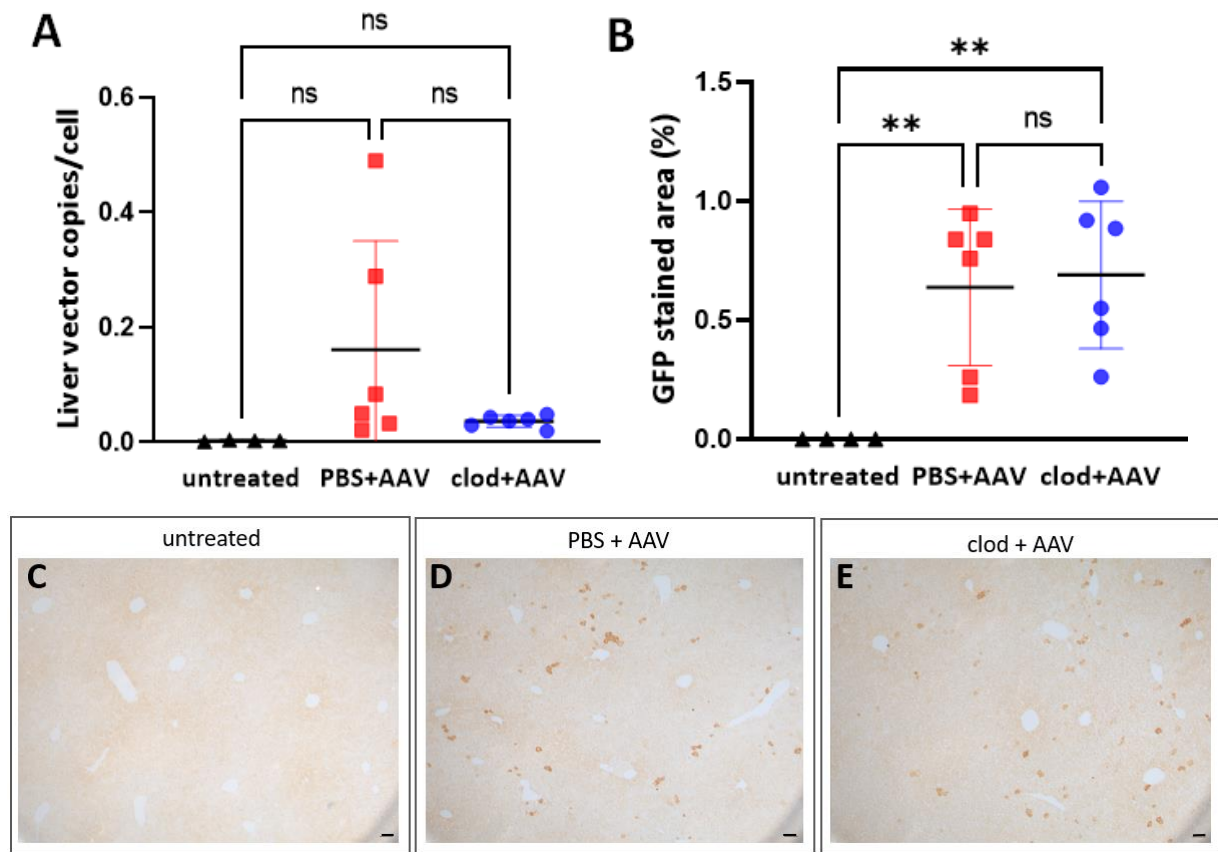
Figure 60. AAV transduction in neonatally-injected CD1 mice. All the values were measured in untreated (n=4), PBS liposome injected- (n=6) and clodronate liposome injected-mice (n=6). **(A)** AAV vector genome copies per cell in whole liver; **(B)** percentage of area in the liver expressing. Horizontal lines display the mean ± standard deviation. One-way ANOVA with Tukey's multiple comparisons test. **(C-E)** GFP immunostaining in liver sections. Scale bars are 100µm for x10 magnification. All the values were measured in untreated (n=4), PBS liposome injected- (n=6) and clodronate liposome injected-mice (n=6). ns: not significant, ** *p*<0.01. AAV: adeno-associated virus; Clod: clodronate liposomes; PBS: Phosphate Buffer Solution.

7.4.3 AAV transduction in young-adult CD1 mice

Liver VCN in young-adult CD1 mice that received PBS or clodronate liposomes, revealed similar values of vector copies per cell with values of 0.74 and 0.45 respectively at 1 month following the administration (**Figure 61A**). Suggested results were comparable (*p*=0.3) between both groups, indicating an absence of benefit of transient macrophage inhibition for AAV transduction. Similarly, quantification of GFP liver immunostaining demonstrated no

significant difference (*p*=0.3) in liver transduction in clodronate and PBS groups in young-adult CD1 mice, with 0.8% and 0.5% of GFP expression in liver respectively at the time of culling (**Figure 61B**). In addition, transduction of AAV vector following 2.5-week-old intravenous injection revealed no predominant expression in periportal or pericentral hepatocytes in all injected mice (**Figure 61C**).
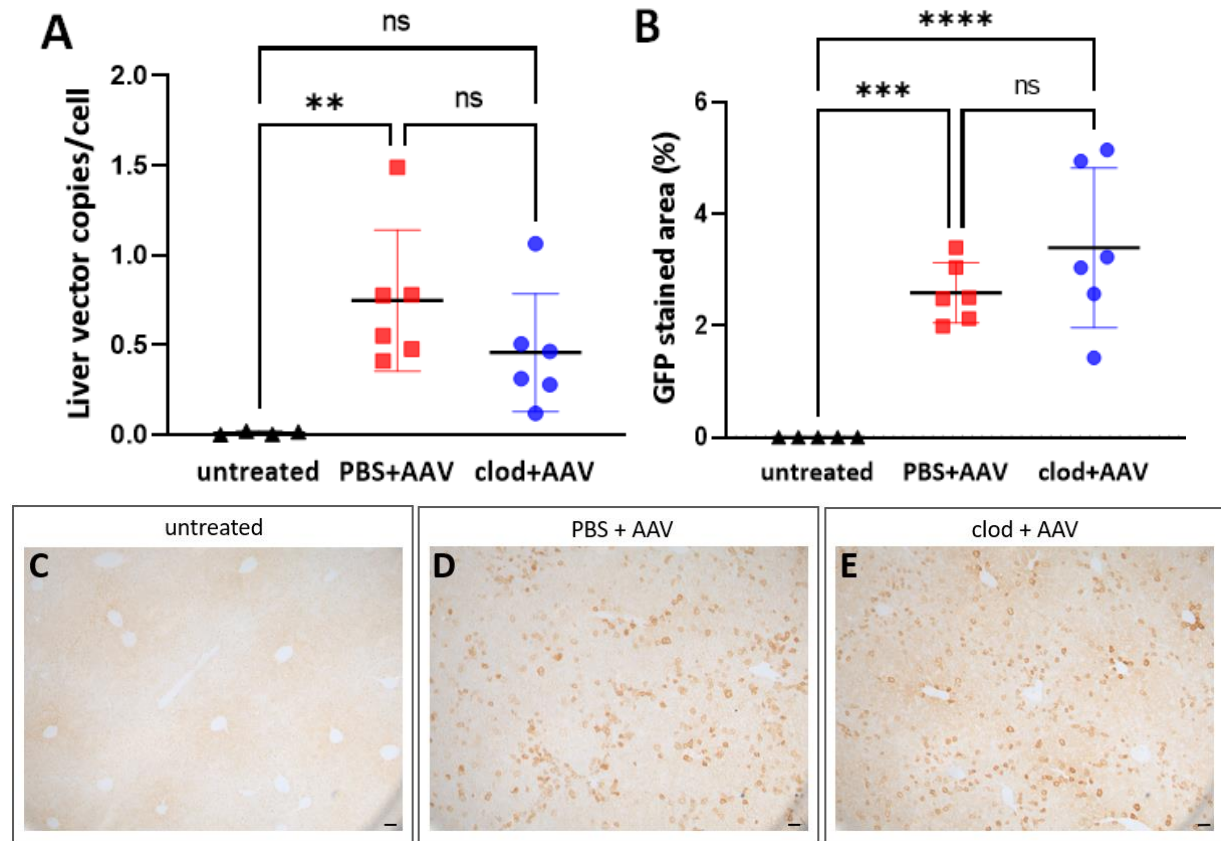
Figure 61. AAV transduction in young-adult CD1 mice. (A) AAV vector genome copies per cell in whole liver; **(B)** percentage of area in the liver expressing. Horizontal lines display the mean ± standard deviation. One-way ANOVA with Tukey's multiple comparisons test. **(C-D)** GFP immunostaining in liver sections. Scale bars are 100μm for x10 magnification. All the values were measured in untreated (n=4), PBS liposome injected- (n=6) and clodronate liposome injected-mice (n=6). ns: not significant, ** *p*<0.01, *** *p*<0.001, **** *p*<0.0001. AAV: adeno-associated virus; Clod: clodronate liposomes; PBS: Phosphate Buffer Solution.

7.5 Discussion

7.5.1 Enhanced lentiviral-mediated liver transduction in neonatal and young-adult CD1 mice after systemic clodronate exposure

When faced with viral infections, the innate immune system is activated via the complement system, and phagocytes found in the bloodstream and tissues. VSV-G-pseudotyped lentiviral vectors have a demonstrated sensitivity to inactivation by the complement system in human serum [155, 282], probably due to the existence of cross-reacting not neutralizing but complement-fixing anti-VSV-G antibodies in humans.

Following intravenous injection, it has been previously discussed that lentiviral vectors will transduce hepatocytes after they have initially transduced the liver sinusoids, that are lined by Kupffer cells, the largest part of the resident liver macrophages, and spleen [392, 393]. Apart from their capacity to eliminate viral particles, Kupffer cells can also be transduced by VSV-G-pseudotyped lentiviral vector [394]. For that reason, it is suggested that depleting liver and splenic macrophages can increase the transduction efficacy of lentiviral vectors in the liver as target organ. Here, the hypothesis was that the depletion of macrophages via repeated intraperitoneal injections of liposome-encapsulated clodronate could enhance liver transduction if administered prior to systemic lentiviral vector injection, as it has been proven with adenoviral vector [312]. That study assessed the impact of temporary and specific elimination of liver macrophages through the administration of clodronate liposomes on the transduction of adenoviral vectors *in vivo*. In macrophage-depleted C57BL/6J mice, enhanced and stabilized hAAT levels were detected after intravenous administration of adenoviral vectors expressing hAAT. Findings revealed selective depletion of Kupffer cells effectively inhibited the production of anti-AAT antibodies, leading to prolonged expression of the transgene. Consequently, transient and targeted depletion of hepatic and splenic macrophages simultaneously markedly enhanced hepatic transgene expression and in a mitigation of the humoral immune response against the transgenic protein as was shown in 8-week old treated mice [312].

Similarly to what has been observed with enhanced adenoviral-mediated liver transduction following macrophage depletion, our hypothesis was that pre-treatment with clodronate could increase lentiviral-mediated liver transgene expression in both neonatal and young-adult CD1 mice.

Liver VCN of both neonatally and young-adult-injected CD1 mice was increased in the animals that received injections of clodronate liposomes prior to lentiviral vector administration compared to PBS controls. These results are in line with clodronate-induced depletion of both macrophages and dendritic cells in liver and spleen [395-397]. The absence of liver and splenic macrophages allows to spare large amount of lentiviral vector, which will be left available for hepatocyte transduction instead, as hepatocytes make up to 80% of liver mass [398].

An unexpected finding in this experiment was the higher liver transduction in the clodronate group in young-adult mice compared to neonatal pups, which was observed in CD1 and partly in C57BL/6J groups. These results are contradicting previous publications supporting that neonatal injection of lentiviral vector leads to higher transduction of the liver due to higher hepatocyte uptake of lentiviral vector due to a lower number of active liver macrophages [399, 400]. However, more recent findings showed the contrary as lentiviral-mediated FIX transduction in 2-week-old mice showed 3-fold higher FIX expression compared to mice treated as neonates. Further evaluation of clonal proliferation of lentiviral-transduced and untransduced hepatocytes during animal growth showed that only a fraction of hepatocytes in neonatal pups generated a cluster expansion, while others were remaining quiescent [401]. These results explain the higher liver transduction in young-adult animals treated with lentiviral vector compared to neonates. The phenotypic and antigenic characterisation of these hepatocyte progenitors expanding preferentially in the neonatal mouse liver remain unpublished. Whether this finding can be extrapolated to the neonatal human liver remains an open question.

7.5.2 Increased lentiviral-mediated liver transduction after clodronate exposure is conserved between inbred and outbred mouse strains

CD1 mice are outbred and C57BL6/J mice are inbred, which affect different immune response patterns of the 2 strains due to mutations and polymorphisms of inbred strains including C57BL6/J mice [402]. We aimed to examine whether the benefit of pre-exposure with clodronate on lentiviral-mediated liver transduction could be extrapolated to the same background strain as the hypomorphic $Asl^{Neo/Neo}$ mouse model.

In agreement with my findings in CD1 mice, systemic pre-treatment with clodronate liposomes also enhanced lentiviral vector transduction in the liver for both neonatally- and 2.5-week-old injected C57BL6/J mice. In addition, at both ages, the vector copies per cell decreased in the spleen in the clodronate compared to the control group. This significant increase in liver transduction was mirroring the significant reduction of vector presence in the spleen at 1 month following lentiviral vector administration in the young-adult animals. The high uptake of lentiviral vector by macrophages has previously been reported in liver and spleen, as over 70% of lentiviral DNA integrated in non-parenchymal cells in 8-weeks-old-injected C57BL/6J mice. It has further been discovered that almost 50% of the liver-directed vector is uptaken by the spleen in non-human primates [144]. The fact that VSV-G-pseudotyped lentiviral vectors display a preference for gene transfer to the spleen, despite their systemic administration and known VSV-G pantropism, is hypothesized to be attributed to the abundant blood supply to such an efficient filtering organ[346].

Similarly to my findings in CD1 mice, this experiment also revealed a more significant increase in liver transduction in the 2.5-week-old mice compared to neonatal pups. It is suggested that an increased number of macrophages in liver and spleen at a later age would lead to a higher benefit of any intervention to deplete macrophages [399, 400].

In summary, systemic administration of clodronate liposomes revealed a significant improved transduction in both strains confirming that a transient macrophage depletion could enhance lentiviral-mediated liver transduction for both inbred and outbred strains.

7.5.3 Clodronate liposomes do not enhance AAV-mediated liver transduction

Currently, AAV vectors are considered the preferred vector for liver-specific targeting since they primarily carry an episomal transgene that is susceptible to loss during cell division. In contradistinction to the enhancements in transgene expression noticed with adenoviral and lentiviral vectors, repeated injection of clodronate liposomes and AAV vector in both neonatal and 2.5-week-old CD1 mice did not show any significant difference in liver transduction efficacy compared to PBS controls at 1 month following AAV administration. These results are in line with a recent study using clodronate liposomes with AAV vectors in 8-weeks-old C57BL6/J mice, confirming the absence of enhanced transduction by clodronate liposome injections [386]. This study even described a significant detrimental effect on AAV-mediated liver transduction following intravenous injection of clodronate compared to controls. However, this detrimental effect was not observed in this experiment performed with younger animals at time of AAV injections.

These differences of liver transduction following clodronate administration between lentiviral, but not AAV vectors are likely caused by the different features of capsids for each vector, and the activation of effector cells involved in the innate immune response.

It has previously been reported that AAV vectors induce a relatively mild although detectable innate immune response however to a lesser extent than adenovirus and lentiviral vectors do [403-406]. The natural immune response to AAV vectors primarily involves the activation of TLRs, which trigger the production of proinflammatory cytokines and chemokines in the transduced tissue. This anti-viral signalling is typically of low intensity and transient [407, 408]. These compounds subsequently stimulate the activation and induction of immune cells, which initiate and expand anti-transgene and/or anti-capsid adaptive immune cells, primarily CD8+ T cells, *in vivo* [409-411]. It is thought that AAV vectors are not triggering or to a low extent innate immune response mediated by liver macrophages [412].

As it was earlier discovered, adenovirus and lentiviral vectors trigger the activation of the innate immune system by inducing inflammatory reactions shortly after the administration of the vector [374, 413-416]. VSV-G-pseudotyped lentiviral vectors are also sensitive to inactivation by human serum as a result of the presence of cross-reacting not neutralizing

however complement-fixing anti-VSV-G antibodies [155, 417]. Lentiviral-binding antibodies as well as complement structures can opsonize lentiviral vector particles for phagocytosis by liver and splenic macrophages and professional antigen presenting cells [278-280]. Due to immune response and the complement activation upon systemic administration, high amount of lentiviral vector transduces liver and splenic macrophages instead of hepatocytes.

Adenoviral vectors activate a strong innate immune response through both TLR–dependent and independent pathways resulting in upregulation of type I Interferon and inflammatory cytokines [418-420]. In addition, the spleen plays a key-role in triggering the production of several cytokines and chemokines following systemic administration of adenoviral vector [418]. Adenoviruses have also found to significant interact and activate the complement via antibodies in individuals having pre-existing immunity [421].

Overall, increased expression of AAV vector in the liver is observed in the young-adult-injected group compared to neonates in both liposome-treated groups. This is explained by the dilution of the AAV transgene caused by liver growth as only 1% of AAV vectors integrate into the cell genome [350, 351]. The mouse liver doubles in size at 2, 7, 15, 24, and 45 days of life and there is a 70% reduction of liver AAV transduction at 1 and 2 weeks post neonatal administration [303]. Based on this finding, a 2.5-week-old mouse liver will lose much less transgene due to large mass increase until the second week of life prior to AAV injection, compared to the neonatal mice, which will have already had a 3 doubling of the original neonatal liver size at 2 weeks.

7.6 Conclusion

Successful proof-of-concept of systemic administration of clodronate liposomes *in vivo* prior to lentiviral vector injections was observed both in neonatal and young-adult CD1 and C57BL/6J mice. AAV-treated neonatal and young-adult CD1 mice did not exhibit any benefit of liver transduction with prior administration of clodronate injection. These findings highlight the difference of innate immune response between the 2 vectors. Further experiments are warranted to better understand the difference of efficacy observed at different age and how this could be extrapolated for clinical translation. These findings are critical to support clinical translational of liver-targeting lentiviral gene therapy programmes and minimise vector dose for a better safety.

8. SUMMARY AND FUTURE WORK

ASA, resulting from a deficiency in ASL, is the second most prevalent urea cycle defect. This hereditary metabolic disorder has been a subject of study for almost half a century. A high incidence of neurological symptoms is reported in ASA despite the relatively infrequent occurrence of hyperammonaemic crises, creating a paradox. A range of plausible pathophysiological explanations has been proposed, many of which have been explored and demonstrated through research utilizing an ASL-deficient mouse model, specifically the *Asl*$^{Neo/Neo}$ mouse.

8.1. CD1 *Asl*$^{Neo/Neo}$ mice do not recapitulate ASA disease in human, presenting milder phenotype with increased residual ASL activity

As described in **Section 1.3**, the *Asl*$^{Neo/Neo}$ mouse model effectively mimics the human phenotype, showcasing symptoms including hyperammonaemia, severe multi-organ dysfunction, and systemic NO deficiency. Unfortunately, 75% of these mice do not survive beyond 3 weeks of age. Even with the residual 16% of wild-type ASL activity present in the liver and brain, this model is currently being utilized for gene therapy research. In this study we aimed to generate a safe gene therapy technology for the life-long treatment of these ASA hypomorphic mice with C57BL/6J background.

Before implementing gene therapy on this severe mouse model, we aimed to establish a congenic mouse strain carrying the *Asl*^{Neo} allele, which could be easily bred, thereby facilitating gene therapy experiments. CD1 *Asl*$^{Neo/Neo}$ congenic mice were generated by backcrossing of heterozygous C57BL/6J ASL-deficient mice with CD1 wild-type mice for 5 generations. Despite easier breeding, CD1 *Asl*$^{Neo/Neo}$ mice displayed a generally milder phenotype, with elevated residual ASL activity and improved survival compared to C57BL/6J *Asl*$^{Neo/Neo}$ mice. Given these results CD1 *Asl*$^{Neo/Neo}$ mice were not used further for gene therapy studies as they failed to fully mimic the human ASA disease phenotype (**Chapter 3**).

8.2. Proof-of-concept of *in vivo* lentiviral vector-mediated gene therapy in ASA

A lentiviral vector construct was designed and appropriately optimised using codon-optimization technology, to transduce the liver and show high levels of transgene expression containing the human *ASL* gene. Systemic neonatal administration of high dose of the gene therapy lentiviral vector was able to completely correct the phenotype of the C57BL/6J *Asl^Neo/Neo* mouse model, normalise the urea cycle amino acids as well as significantly increase the ASL expression and activity in the liver at 3 months post treatment (**Sections 6.3 & 6.4**). Further correction of the redox imbalance in liver and skin was shown at 6 weeks post neonatal lentiviral injection further confirming the importance of beneficial effects are mediated by correction of ureagenesis in C57BL/6J *Asl^Neo/Neo* mice (**Section 6.5**). Finally, we tested the risk of lentiviral-mediated genotoxicity, and organ biodistribution, by performing a long-term blinded *in vivo* study with large number of wild-type animals, which received systemic neonatal injection of codon-optimised *hASL* lentiviral vector. Pathology analysis and dissection of the liver, spleen, and major organs showed no lesions, cysts, or any signs of tumours confirming lentiviral vector's safety profile (**Section 6.6**). Overall, those preliminary studies demonstrated proof-of-concept of *in vivo* lentiviral gene therapy for ASA and its safety profile.

The advancement of this project relies on a deeper understanding and assessment of the safety of our lentiviral vector construct, which will involve integration site analysis of DNA samples derived from the animals involved in long-term *in vivo* exposure to the vector (**Section 6.6**). This will facilitate the evaluation of potential risks associated with insertional mutagenesis in a sizable population of animals. To extend our safety analysis, we will explore the implications of transducing human hepatocytes with the CCL.LP1.*co-hASL*, contributing to our comprehension of safety post-transduction in human cells.

Building on the foundations of our preliminary studies and demonstration of efficient liver targeting, we anticipate the applicability of this vector backbone to treat additional urea cycle disorders, such as ASS deficiency. These prospective investigations are predicated on the

results from these gene therapy preliminary studies, which include successful design and optimization of a lentiviral vector construct, using codon-optimization technology for enhanced transgene expression and elevated liver transduction levels.

8.3. Macrophage inhibitor clodronate enhances liver transduction of lentiviral but not AAV vectors *in vivo*

Liver-targeted gene therapy has demonstrated clinical effectiveness in addressing genetic disorders over the past two decades. While AAV vectors are currently the vector of choice for liver targeting, anti-AAV immune responses limit their re-injection in humans. As an alternative, integrative lentiviral vectors are being designed to enable sustained transgene expression, particularly during liver development in paediatrics. Nonetheless, preclinical investigations have revealed reduced effectiveness of lentiviral gene therapy *in vivo* as a result of significant uptake by macrophages in liver and spleen.

To address this, the efficacy of lentiviral and AAV injections following systemic administration of clodronate, a bisphosphonate known to achieve 80-90% transient macrophage depletion in the liver and spleen, was assessed in neonatal and young-adult wild-type mice. Results showed a significant increase in liver transduction with lentiviral vectors but no difference with AAV vectors after clodronate liposome administration. This suggests that the capsid of each vector reacts differently with the innate immune response, leading to differences in liver transduction (**Chapter 7**).

Expanding upon the observed increase in liver transduction following the administration of macrophage inhibitors in combination with a lentiviral vector, prospective studies could investigate the use of clodronate pre-treatment alongside different gene therapy vectors, such as mRNA LNP. This would aim to assess whether such an approach can also enhance hepatocyte uptake of the vector, thereby reducing the necessary dosage and potentially enhancing the safety profile. Furthermore, future research might explore the application of clodronate liposomes in conjunction with the CCL.LP1.*co-hASL* vector in *Asl^{Neo/Neo}* mice, to

determine whether pre-emptive macrophage depletion could expedite disease correction with treatment with lentiviral vector.

8.4 Overall conclusion

This study has highlighted the necessity of exploring alternative treatments for individuals with ASA, as the current therapeutic recommendations are insufficient in preventing the development of a severe neurological condition. A suggested treatment strategy involving lentiviral vector-based gene therapy has demonstrated the concept of safe, long-lasting ureagenesis correction after a single systemic administration of the gene therapy construct. A transduction optimization technology has further been determined which allows the safer lentiviral gene therapy approach by raising the possibility of using a lowed lentiviral vector dose. The findings of this study create a path towards clinical implementation and, more generally, offer a promising outlook for individuals with inherited metabolic diseases.

9. REFERENCES

1.   Dasarathy, S., et al., *Ammonia toxicity: from head to toe?* Metab Brain Dis, 2017. **32**(2): p. 529-538.

2.   Walker, V., *Ammonia metabolism and hyperammonemic disorders.* Adv Clin Chem, 2014. **67**: p. 73-150.

3.   Weiner, I.D. and J.W. Verlander, *Renal ammonia metabolism and transport.* Compr Physiol, 2013. **3**(1): p. 201-20.

4.   Wu, G. and S.M. Morris, Jr., *Arginine metabolism: nitric oxide and beyond.* Biochemical Journal, 1998. **336**(1): p. 1-17.

5.   Ah Mew, N., et al., *Urea Cycle Disorders Overview*, in *GeneReviews(®)*, M.P. Adam, et al., Editors. 1993, University of Washington, Seattle

6.   Brusilow, S. and A. Horwich, *The metabolic and molecular bases of inherited disease.* Scriver, CR.; Beaudet, AL.; Sly, WS, 2001: p. 1909-1963.

7.   Gropman, A., M. Summar, and J. Leonard, *Neurological implications of urea cycle disorders.* Journal of inherited metabolic disease, 2007. **30**(6): p. 865-879.

8.   Trevisson, E., et al., *Argininosuccinate lyase deficiency: mutational spectrum in Italian patients and identification of a novel ASL pseudogene.* Human mutation, 2007. **28**(7): p. 694-702.

9.   Anderson, P.M. and A. Meister, *Evidence for an activated form of carbon dioxide in the reaction catalyzed by Escherichia coli carbamyl phosphate synthetase.* Biochemistry, 1965. **4**(12): p. 2803-9.

10.   Camacho, J.A., et al., *Hyperornithinaemia-hyperammonaemia-homocitrullinuria syndrome is caused by mutations in a gene encoding a mitochondrial ornithine transporter.* Nature genetics, 1999. **22**(2): p. 151-158.

11.   INDIVERI, C., et al., *The purified and reconstituted ornithine/citrulline carrier from rat liver mitochondria catalyses a second transport mode: ornithine+/H+ exchange.* Biochemical Journal, 1999. **341**(3): p. 705-711.

12.   Gropman, A.L. and M.L. Batshaw, *Cognitive outcome in urea cycle disorders.* Mol Genet Metab, 2004. **81 Suppl 1**: p. S58-62.

13. Summar, M.L., et al., *The incidence of urea cycle disorders.* Molecular Genetics and Metabolism, 2013. **110**(1): p. 179-180.

14. Machado, M.C. and F. Pinheiro da Silva, *Hyperammonemia due to urea cycle disorders: a potentially fatal condition in the intensive care setting.* J Intensive Care, 2014. **2**(1): p. 22.

15. Matsumoto, S., et al., *Urea cycle disorders—update.* Journal of Human Genetics, 2019. **64**(9): p. 833-847.

16. Wolf, N.I., T. Bast, and R. Surtees, *Epilepsy in inborn errors of metabolism.* Epileptic Disord, 2005. **7**(2): p. 67-81.

17. Häberle, J., et al., *Suggested guidelines for the diagnosis and management of urea cycle disorders.* Orphanet journal of rare diseases, 2012. **7**(1): p. 32.

18. Nagamani, S.C., A. Erez, and B. Lee, *Argininosuccinate lyase deficiency.* Genet Med, 2012. **14**(5): p. 501-7.

19. Ratner, S., *Enzymes of arginine and urea synthesis.* Adv Enzymol Relat Areas Mol Biol, 1973. **39**: p. 1-90.

20. Erez, A., et al., *Requirement of argininosuccinate lyase for systemic nitric oxide production.* Nat Med, 2011. **17**(12): p. 1619-26.

21. Baruteau, J., et al., *Expanding the phenotype in argininosuccinic aciduria: need for new therapies.* J Inherit Metab Dis, 2017. **40**(3): p. 357-368.

22. Turner, M.A., et al., *Human argininosuccinate lyase: a structural basis for intragenic complementation.* Proc Natl Acad Sci U S A, 1997. **94**(17): p. 9063-8.

23. Balmer, C., et al., *Mutations and polymorphisms in the human argininosuccinate lyase (ASL) gene.* Hum Mutat, 2014. **35**(1): p. 27-35.

24. Sampaleanu, L.M., B. Yu, and P.L. Howell, *Mutational analysis of duck delta 2 crystallin and the structure of an inactive mutant with bound substrate provide insight into the enzymatic mechanism of argininosuccinate lyase.* J Biol Chem, 2002. **277**(6): p. 4166-75.

25. O'Brien, W.E., et al., *Cloning and sequence analysis of cDNA for human argininosuccinate lyase.* Proc Natl Acad Sci U S A, 1986. **83**(19): p. 7211-5.

26. Crosas, E., et al., *The yeast ζ-crystallin/NADPH:quinone oxidoreductase (Zta1p) is under nutritional control by the target of rapamycin pathway and is involved in the*

regulation of argininosuccinate lyase mRNA half-life. Febs j, 2015. **282**(10): p. 1953-64.

27.   Xia, J., N. Yamaji, and J.F. Ma, *An appropriate concentration of arginine is required for normal root growth in rice.* Plant Signal Behav, 2014. **9**(3): p. e28717.

28.   Rabier, D., et al., *Arginine remains an essential amino acid after liver transplantation in urea cycle enzyme deficiencies.* J Inherit Metab Dis, 1991. **14**(3): p. 277-80.

29.   Kurz, S. and D.G. Harrison, *Insulin and the arginine paradox.* J Clin Invest, 1997. **99**(3): p. 369-70.

30.   Li, C., et al., *Interaction of the endothelial nitric oxide synthase with the CAT-1 arginine transporter enhances NO release by a mechanism not involving arginine transport.* Biochem J, 2005. **386**(Pt 3): p. 567-74.

31.   Baruteau, J., et al., *Argininosuccinic aciduria: Recent pathophysiological insights and therapeutic prospects.* J Inherit Metab Dis, 2019. **42**(6): p. 1147-1161.

32.   Braissant, O., *Ammonia toxicity to the brain: effects on creatine metabolism and transport and protective roles of creatine.* Mol Genet Metab, 2010. **100 Suppl 1**: p. S53-8.

33.   Guertin, S.R., M.W. Levinsohn, and B.B. Dahms, *Small-droplet steatosis and intracranial hypertension in argininosuccinic lyase deficiency.* J Pediatr, 1983. **102**(5): p. 736-40.

34.   Bergeron, M., et al., *Effect of ammonia on brain serotonin metabolism in relation to function in the portacaval shunted rat.* J Neurochem, 1990. **55**(1): p. 222-9.

35.   Monfort, P., M.D. Muñoz, and V. Felipo, *Molecular mechanisms of the alterations in NMDA receptor-dependent long-term potentiation in hyperammonemia.* Metab Brain Dis, 2005. **20**(4): p. 265-74.

36.   Rangroo Thrane, V., et al., *Ammonia triggers neuronal disinhibition and seizures by impairing astrocyte potassium buffering.* Nat Med, 2013. **19**(12): p. 1643-8.

37.   Morris, S.M., Jr., *Arginine metabolism: boundaries of our knowledge.* J Nutr, 2007. **137**(6 Suppl 2): p. 1602s-1609s.

38.   Morris, S.M., Jr., *Arginases and arginine deficiency syndromes.* Curr Opin Clin Nutr Metab Care, 2012. **15**(1): p. 64-70.

39.   Gladwin, M.T. and J. Tejero, *Nitrite-NO bailout for a NOS complex too big to fail.* Nat Med, 2011. **17**(12): p. 1556-7.

40.   Yi, J., et al., *L-arginine and Alzheimer's disease.* International journal of clinical and experimental pathology, 2009. **2**(3): p. 211-238.

41.   Morris, S.M., Jr., *Enzymes of Arginine Metabolism.* The Journal of Nutrition, 2004. **134**(10): p. 2743S-2747S.

42.   Natesan, V., R. Mani, and R. Arumugam, *Clinical aspects of urea cycle dysfunction and altered brain energy metabolism on modulation of glutamate receptors and transporters in acute and chronic hyperammonemia.* Biomed Pharmacother, 2016. **81**: p. 192-202.

43.   Boenzi, S., et al., *Creatine metabolism in urea cycle defects.* J Inherit Metab Dis, 2012. **35**(4): p. 647-53.

44.   Arias, A., J. Garcia-Villoria, and A. Ribes, *Guanidinoacetate and creatine/creatinine levels in controls and patients with urea cycle defects.* Mol Genet Metab, 2004. **82**(3): p. 220-3.

45.   Nagamani, S.C., et al., *A randomized controlled trial to evaluate the effects of high-dose versus low-dose of arginine therapy on hepatic function tests in argininosuccinic aciduria.* Mol Genet Metab, 2012. **107**(3): p. 315-21.

46.   Bigot, A., et al., *Liver involvement in urea cycle disorders: a review of the literature.* J Inherit Metab Dis, 2017. **40**(6): p. 757-769.

47.   Nagamani, S.C., et al., *Nitric-oxide supplementation for treatment of long-term complications in argininosuccinic aciduria.* Am J Hum Genet, 2012. **90**(5): p. 836-46.

48.   Lin, M.I., et al., *Phosphorylation of threonine 497 in endothelial nitric-oxide synthase coordinates the coupling of L-arginine metabolism to efficient nitric oxide production.* J Biol Chem, 2003. **278**(45): p. 44719-26.

49.   Pignitter, M., et al., *Inefficient spin trapping of superoxide in the presence of nitric-oxide: implications for studies on nitric-oxide synthase uncoupling.* Free Radic Biol Med, 2006. **41**(3): p. 455-63.

50.   Nakamura, T. and S.A. Lipton, *'SNO'-Storms Compromise Protein Activity and Mitochondrial Metabolism in Neurodegenerative Disorders.* Trends Endocrinol Metab, 2017. **28**(12): p. 879-892.

51.   Gegg, M.E., et al., *Differential effect of nitric oxide on glutathione metabolism and mitochondrial function in astrocytes and neurones: implications for neuroprotection/neurodegeneration?* J Neurochem, 2003. **86**(1): p. 228-37.

52. Nassogne, M.C., et al., *Urea cycle defects: management and outcome.* J Inherit Metab Dis, 2005. **28**(3): p. 407-14.

53. Kleijer, W.J., et al., *Clinical, enzymatic, and molecular genetic characterization of a biochemical variant type of argininosuccinic aciduria: prenatal and postnatal diagnosis in five unrelated families.* J Inherit Metab Dis, 2002. **25**(5): p. 399-410.

54. Parsons, H.G., et al., *Argininosuccinic aciduria: long-term treatment with arginine.* J Inherit Metab Dis, 1987. **10**(2): p. 152-61.

55. Mori, T., et al., *Progressive liver fibrosis in late-onset argininosuccinate lyase deficiency.* Pediatr Dev Pathol, 2002. **5**(6): p. 597-601.

56. Odent, S., et al., *[Argininosuccinic aciduria. A new case revealed by psychiatric disorders].* J Genet Hum, 1989. **37**(1): p. 39-42.

57. Marble, M., et al., *Living related liver transplant in a patient with argininosuccinic aciduria and cirrhosis: metabolic follow-up.* J Pediatr Gastroenterol Nutr, 2008. **46**(4): p. 453-6.

58. Mercimek-Mahmutoglu, S., et al., *Long-term outcome of patients with argininosuccinate lyase deficiency diagnosed by newborn screening in Austria.* Mol Genet Metab, 2010. **100**(1): p. 24-8.

59. Yaplito-Lee, J., C.W. Chow, and A. Boneh, *Histopathological findings in livers of patients with urea cycle disorders.* Mol Genet Metab, 2013. **108**(3): p. 161-5.

60. Zimmermann, A., C. Bachmann, and R. Baumgartner, *Severe liver fibrosis in argininosuccinic aciduria.* Arch Pathol Lab Med, 1986. **110**(2): p. 136-40.

61. Miles, L., J.E. Heubi, and K.E. Bove, *Hepatocyte glycogen accumulation in patients undergoing dietary management of urea cycle defects mimics storage disease.* J Pediatr Gastroenterol Nutr, 2005. **40**(4): p. 471-6.

62. Ficicioglu, C., R. Mandell, and V.E. Shih, *Argininosuccinate lyase deficiency: longterm outcome of 13 patients detected by newborn screening.* Mol Genet Metab, 2009. **98**(3): p. 273-7.

63. Lågas, P.A. and A. Ruokonen, *Late onset argininosuccinic aciduria in a paranoid retardate.* Biol Psychiatry, 1991. **30**(12): p. 1229-32.

64. Gerrits, G.P., et al., *Argininosuccinic aciduria: clinical and biochemical findings in three children with the late onset form, with special emphasis on cerebrospinal fluid findings of amino acids and pyrimidines.* Neuropediatrics, 1993. **24**(1): p. 15-8.

65. Grioni, D., et al., *Epilepsy and argininosuccinic aciduria.* Neuropediatrics, 2011. **42**(3): p. 97-103.

66. Wiwattanadittakul, N., et al., *The utility of EEG monitoring in neonates with hyperammonemia due to inborn errors of metabolism.* Mol Genet Metab, 2018. **125**(3): p. 235-240.

67. Sijens, P.E., et al., *Cerebral 1H MR spectroscopy showing elevation of brain guanidinoacetate in argininosuccinate lyase deficiency.* Mol Genet Metab, 2006. **88**(1): p. 100-2.

68. Kölker, S., et al., *The phenotypic spectrum of organic acidurias and urea cycle disorders. Part 1: the initial presentation.* J Inherit Metab Dis, 2015. **38**(6): p. 1041-57.

69. Coulter, D.L., T.F. Beals, and R.J. Allen, *Neurotrichosis: hair-shaft abnormalities associated with neurological diseases.* Dev Med Child Neurol, 1982. **24**(5): p. 634-44.

70. Hambraeus, L., et al., *Argininosuccinic aciduria. Report of three cases and the effect of high and reduced protein intake on the clinical state.* Acta Paediatr Scand, 1974. **63**(4): p. 525-36.

71. Schutgens, R.B.H., et al., *Mild variant of argininosuccinic aciduria.* Journal of Inherited Metabolic Disease, 1979. **2**(1): p. 13-14.

72. Widhalm, K., et al., *Long-term follow-up of 12 patients with the late-onset variant of argininosuccinic acid lyase deficiency: no impairment of intellectual and psychomotor development during therapy.* Pediatrics, 1992. **89**(6 Pt 2): p. 1182-4.

73. Rüegger, C.M., et al., *Cross-sectional observational study of 208 patients with non-classical urea cycle disorders.* J Inherit Metab Dis, 2014. **37**(1): p. 21-30.

74. Summar, M.L., et al., *Diagnosis, symptoms, frequency and mortality of 260 patients with urea cycle disorders from a 21-year, multicentre study of acute hyperammonaemic episodes.* Acta Paediatr, 2008. **97**(10): p. 1420-5.

75. Kido, J., et al., *Long-term outcome and intervention of urea cycle disorders in Japan.* J Inherit Metab Dis, 2012. **35**(5): p. 777-85.

76. Maestri, N.E., K.D. McGowan, and S.W. Brusilow, *Plasma glutamine concentration: a guide in the management of urea cycle disorders.* J Pediatr, 1992. **121**(2): p. 259-61.

77. Kleijer, W.J., et al., *Prenatal diagnosis of citrullinemia and argininosuccinic aciduria: evidence for a transmission ratio distortion in citrullinemia.* Prenat Diagn, 2006. **26**(3): p. 242-7.

78. Adam, S., et al., *Dietary management of urea cycle disorders: European practice.* Mol Genet Metab, 2013. **110**(4): p. 439-45.

79. Scaglia, F., *New insights in nutritional management and amino acid supplementation in urea cycle disorders.* Mol Genet Metab, 2010. **100 Suppl 1**(Suppl 1): p. S72-6.

80. Foschi, F.G., et al., *Urea cycle disorders: a case report of a successful treatment with liver transplant and a literature review.* World journal of gastroenterology, 2015. **21**(13): p. 4063-4068.

81. Uçar, S.K., et al., *One Year Experience of Pheburane(®) (Sodium Phenylbutyrate) Treatment in a Patient with Argininosuccinate Lyase Deficiency.* JIMD reports, 2015. **19**: p. 31-33.

82. Nagamani, S.C.S., B. Lee, and A. Erez, *Optimizing therapy for argininosuccinic aciduria.* Molecular genetics and metabolism, 2012. **107**(1-2): p. 10-14.

83. Baruteau, J., et al., *Argininosuccinic aciduria fosters neuronal nitrosative stress reversed by Asl gene transfer.* Nat Commun, 2018. **9**(1): p. 3505.

84. Kho, J., et al., *Argininosuccinate Lyase Deficiency Causes an Endothelial-Dependent Form of Hypertension.* Am J Hum Genet, 2018. **103**(2): p. 276-287.

85. Bryan, N.S. and J.L. Ivy, *Inorganic nitrite and nitrate: evidence to support consideration as dietary nutrients.* Nutr Res, 2015. **35**(8): p. 643-54.

86. Kapil, V., et al., *Clinical evidence demonstrating the utility of inorganic nitrate in cardiovascular health.* Nitric Oxide, 2014. **38**: p. 45-57.

87. Kapil, V., A.J. Webb, and A. Ahluwalia, *Inorganic nitrate and the cardiovascular system.* Heart, 2010. **96**(21): p. 1703-9.

88. Lundberg, J.O., E. Weitzberg, and M.T. Gladwin, *The nitrate-nitrite-nitric oxide pathway in physiology and therapeutics.* Nat Rev Drug Discov, 2008. **7**(2): p. 156-67.

89. Omar, S.A., et al., *Therapeutic effects of inorganic nitrate and nitrite in cardiovascular and metabolic diseases.* J Intern Med, 2016. **279**(4): p. 315-36.

90. Baylor College of, M., *Nitric Oxide Supplementation in Argininosuccinic Aciduria*. 2018.

91. Dunbar, C.E., et al., *Gene therapy comes of age.* Science, 2018. **359**(6372).

92. Ashley, S.N., et al., *Adeno-associated viral gene therapy corrects a mouse model of argininosuccinic aciduria.* Mol Genet Metab, 2018. **125**(3): p. 241-250.

93. Robberecht, E., et al., *Successful liver transplantation for argininosuccinate lyase deficiency (ASLD).* J Inherit Metab Dis, 2006. **29**(1): p. 184-5.

94.   Gurung, S., et al., *mRNA therapy restores ureagenesis and corrects glutathione metabolism in argininosuccinic aciduria.* bioRxiv, 2022: p. 2022.10.19.512931.

95.   AlTassan, R., et al., *A retrospective biochemical, molecular, and neurocognitive review of Saudi patients with argininosuccinic aciduria.* Eur J Med Genet, 2018. **61**(6): p. 307-311.

96.   Kido, J., et al., *Liver transplantation may prevent neurodevelopmental deterioration in high-risk patients with urea cycle disorders.* Pediatr Transplant, 2017. **21**(6).

97.   Newnham, T., et al., *Liver transplantation for argininosuccinic aciduria: clinical, biochemical, and metabolic outcome.* Liver Transpl, 2008. **14**(1): p. 41-5.

98.   Özçay, F., et al., *Report of 3 Patients With Urea Cycle Defects Treated With Related Living-Donor Liver Transplant.* Exp Clin Transplant, 2015. **13 Suppl 3**: p. 126-30.

99.   Szymańska, E., et al., *Polish Experience with Liver Transplantation and Post-Transplant Outcomes in Children with Urea Cycle Disorders.* Ann Transplant, 2017. **22**: p. 555-562.

100.   Waisbren, S.E., et al., *Biochemical markers and neuropsychological functioning in distal urea cycle disorders.* J Inherit Metab Dis, 2018. **41**(4): p. 657-667.

101.   Yankol, Y., et al., *Argininosuccinic Aciduria-A Rare Indication for Liver Transplant: Report of Two Cases.* Exp Clin Transplant, 2017. **15**(5): p. 581-584.

102.   Reid Sutton, V., et al., *A mouse model of argininosuccinic aciduria: biochemical characterization.* Mol Genet Metab, 2003. **78**(1): p. 11-6.

103.   Felici, M.D., et al., *Bcl-2 and Bax regulation of apoptosis in germ cells during prenatal oogenesis in the mouse embryo.* Cell Death Differ, 1999. **6**(9): p. 908-15.

104.   Zhou, H.M., et al., *Lineage-specific responses to reduced embryonic Pax3 expression levels.* Dev Biol, 2008. **315**(2): p. 369-82.

105.   Li, H., et al., *Applications of genome editing technology in the targeted therapy of human diseases: mechanisms, advances and prospects.* Signal Transduction and Targeted Therapy, 2020. **5**(1): p. 1.

106.   Prakash, V., M. Moore, and R.J. Yáñez-Muñoz, *Current Progress in Therapeutic Gene Editing for Monogenic Diseases.* Mol Ther, 2016. **24**(3): p. 465-74.

107.   Friedmann, T. and R. Roblin, *Gene therapy for human genetic disease?* Science, 1972. **175**(4025): p. 949-55.

108.   Tebas, P., et al., *Gene editing of CCR5 in autologous CD4 T cells of persons infected with HIV.* New England Journal of Medicine, 2014. **370**(10): p. 901-910.

109. Powell, S.K., R. Rivera-Soto, and S.J. Gray, *Viral expression cassette elements to enhance transgene target specificity and expression in gene therapy.* Discov Med, 2015. **19**(102): p. 49-57.

110. Jones, I.M. and Y. Morikawa, *The molecular basis of HIV capsid assembly.* Reviews in medical virology, 1998. **8**(2): p. 87-95.

111. Li, G., et al., *Extensive promoter-centered chromatin interactions provide a topological basis for transcription regulation.* Cell, 2012. **148**(1-2): p. 84-98.

112. Verma, I.M. and N. Somia, *Gene therapy -- promises, problems and prospects.* Nature, 1997. **389**(6648): p. 239-42.

113. Wolff, J.A. and V. Budker, *The mechanism of naked DNA uptake and expression.* Adv Genet, 2005. **54**: p. 3-20.

114. Kay, M.A., C.Y. He, and Z.Y. Chen, *A robust system for production of minicircle DNA vectors.* Nat Biotechnol, 2010. **28**(12): p. 1287-9.

115. Chira, S., et al., *Progresses towards safe and efficient gene therapy vectors.* Oncotarget, 2015. **6**(31): p. 30675-703.

116. Elsabahy, M., A. Nazarali, and M. Foldvari, *Non-viral nucleic acid delivery: key challenges and future directions.* Curr Drug Deliv, 2011. **8**(3): p. 235-44.

117. Ramamoorth, M. and A. Narvekar, *Non viral vectors in gene therapy- an overview.* J Clin Diagn Res, 2015. **9**(1): p. Ge01-6.

118. Bulcha, J.T., et al., *Viral vector platforms within the gene therapy landscape.* Signal Transduction and Targeted Therapy, 2021. **6**(1): p. 53.

119. Foecking, M.K. and H. Hofstetter, *Powerful and versatile enhancer-promoter unit for mammalian expression vectors.* Gene, 1986. **45**(1): p. 101-105.

120. Thomsen, D.R., et al., *Promoter-regulatory region of the major immediate early gene of human cytomegalovirus.* Proceedings of the National Academy of Sciences, 1984. **81**(3): p. 659-663.

121. Maguire, C.A., et al., *Gene therapy for the nervous system: challenges and new strategies.* Neurotherapeutics, 2014. **11**: p. 817-839.

122. Piguet, F., S. Alves, and N. Cartier, *Clinical gene therapy for neurodegenerative diseases: past, present, and future.* Human gene therapy, 2017. **28**(11): p. 988-1003.

123. Colgan, D.F. and J.L. Manley, *Mechanism and regulation of mRNA polyadenylation.* Genes & development, 1997. **11**(21): p. 2755-2766.

124. Sachs, A., *Poly (A) tail metabolism and function in eucaryotes.* J Biol Chem, 1993. **268**: p. 22955-22958.

125. Donello, J.E., J.E. Loeb, and T.J. Hope, *Woodchuck hepatitis virus contains a tripartite posttranscriptional regulatory element.* Journal of virology, 1998. **72**(6): p. 5085-5092.

126. Loeb, J.E., et al., *Enhanced expression of transgenes from adeno-associated virus vectors with the woodchuck hepatitis virus posttranscriptional regulatory element: implications for gene therapy.* Human gene therapy, 1999. **10**(14): p. 2295-2305.

127. Xu, Z.-L., et al., *Woodchuck hepatitis virus post-transcriptional regulation element enhances transgene expression from adenovirus vectors.* Biochimica Et Biophysica Acta (BBA)-General Subjects, 2003. **1621**(3): p. 266-271.

128. Popa, I., et al., *CRM1-dependent function of a cis-acting RNA export element.* Molecular and cellular biology, 2002. **22**(7): p. 2057-2067.

129. Glover, C.P., et al., *Adenoviral-mediated, high-level, cell-specific transgene expression: a SYN1-WPRE cassette mediates increased transgene expression with no loss of neuron specificity.* Molecular Therapy, 2002. **5**(5): p. 509-516.

130. Cavener, D.R. and S.C. Ray, *Eukaryotic start and stop translation sites.* Nucleic acids research, 1991. **19**(12): p. 3185-3192.

131. Kozak, M., *An analysis of 5'-noncoding sequences from 699 vertebrate messenger RNAs.* Nucleic acids research, 1987. **15**(20): p. 8125-8148.

132. Gessler, D.J., et al., *Redirecting N-acetylaspartate metabolism in the central nervous system normalizes myelination and rescues Canavan disease.* JCI insight, 2017. **2**(3).

133. Carter, M. and J. Shieh, *Chapter 10 - Molecular Cloning and Recombinant DNA Technology*, in *Guide to Research Techniques in Neuroscience (Second Edition)*, M. Carter and J. Shieh, Editors. 2015, Academic Press: San Diego. p. 219-237.

134. Xu, Z., et al., *Non-integrating lentiviral vectors based on the minimal S/MAR sequence retain transgene expression in dividing cells.* Science China Life Sciences, 2016. **59**: p. 1024-1033.

135. Ley, D., et al., *MAR elements and transposons for improved transgene integration and expression.* PLoS One, 2013. **8**(4): p. e62784.

136. Walters, M.C., et al., *The chicken β-globin 5' HS4 boundary element blocks enhancer-mediated suppression of silencing.* Molecular and cellular biology, 1999. **19**(5): p. 3714-3726.

137. Cozmescu, A.C., J. Counsell, and P. Gissen, *Gene therapies targeting the liver.* J Hepatol, 2021. **74**(1): p. 235-236.

138. Raper, S.E., et al., *Fatal systemic inflammatory response syndrome in a ornithine transcarbamylase deficient patient following adenoviral gene transfer.* Mol Genet Metab, 2003. **80**(1-2): p. 148-58.

139. Mingozzi, F. and K.A. High, *Immune responses to AAV vectors: overcoming barriers to successful gene therapy.* Blood, 2013. **122**(1): p. 23-36.

140. D'Avola, D., et al., *Phase I open label liver-directed gene therapy clinical trial for acute intermittent porphyria.* J Hepatol, 2016. **65**(4): p. 776-783.

141. Gnant, M.F., et al., *Regional versus systemic delivery of recombinant vaccinia virus as suicide gene therapy for murine liver metastases.* Ann Surg, 1999. **230**(3): p. 352-60; discussion 360-1.

142. Nathwani, A.C., et al., *Safe and efficient transduction of the liver after peripheral vein infusion of self-complementary AAV vector results in stable therapeutic expression of human FIX in nonhuman primates.* Blood, 2007. **109**(4): p. 1414-21.

143. Sarkar, R., et al., *Long-term efficacy of adeno-associated virus serotypes 8 and 9 in hemophilia a dogs and mice.* Hum Gene Ther, 2006. **17**(4): p. 427-39.

144. Milani, M., et al., *Phagocytosis-shielded lentiviral vectors improve liver gene therapy in nonhuman primates.* Science Translational Medicine, 2019. **11**(493): p. eaav7325.

145. Cavazzana, M., et al., *Gene Therapy for X-Linked Severe Combined Immunodeficiency: Where Do We Stand?* Hum Gene Ther, 2016. **27**(2): p. 108-16.

146. Cartier, N., et al., *Hematopoietic stem cell gene therapy with a lentiviral vector in X-linked adrenoleukodystrophy.* Science, 2009. **326**(5954): p. 818-23.

147. Biffi, A., et al., *Lentiviral hematopoietic stem cell gene therapy benefits metachromatic leukodystrophy.* Science, 2013. **341**(6148): p. 1233158.

148. Møller, A.P. and N. Saino, *Immune response and survival.* Oikos, 2004. **104**(2): p. 299-304.

149. Medzhitov, R., *Toll-like receptors and innate immunity.* Nature Reviews Immunology, 2001. **1**(2): p. 135-145.

150. Chuah, M.K., D. Collen, and T. VandenDriessche, *Clinical gene transfer studies for hemophilia A.* Semin Thromb Hemost, 2004. **30**(2): p. 249-56.

151.   DeLisi, C., M. Boyle, and T. Borsos, *Analysis of the colloid osmotic step of complement-mediated immune hemolysis.* Journal of immunology (Baltimore, Md.: 1950), 1980. **125**(5): p. 2055-2062.

152.   Martinez, R. and S. Carroll, *Sequential metabolic expressions of the lethal process in human serum-treated Escherichia coli: role of lysozyme.* Infection and immunity, 1980. **28**(3): p. 735-745.

153.   Murphy, K. and P. Travers, *Walport M, Janeway C.* Janeway's Immunobiology. New York: Garland Science, 2012.

154.   Hänsch, G.M., M. Seitz, and M. Betz, *Effect of the late complement components C5b-9 on human monocytes: release of prostanoids, oxygen radicals and of a factor inducing cell proliferation.* International Archives of Allergy and Immunology, 1987. **82**(3-4): p. 317-320.

155.   DePolo, N.J., et al., *VSV-G pseudotyped lentiviral vector particles produced in human cells are inactivated by human serum.* Mol Ther, 2000. **2**(3): p. 218-22.

156.   Milani, M., et al., *Genome editing for scalable production of alloantigen-free lentiviral vectors for in vivo gene therapy.* EMBO molecular medicine, 2017. **9**(11): p. 1558-1573.

157.   Nayak, S. and R.W. Herzog, *Progress and prospects: immune responses to viral vectors.* Gene Ther, 2010. **17**(3): p. 295-304.

158.   Herzog, R.W., *Complexity of immune responses to AAV transgene products - Example of factor IX.* Cell Immunol, 2019. **342**: p. 103658.

159.   Martino, A.T. and D.M. Markusic, *Immune response mechanisms against AAV vectors in animal models.* Molecular Therapy-Methods & Clinical Development, 2020. **17**: p. 198-208.

160.   Li, H., et al., *A preclinical animal model to assess the effect of pre-existing immunity on AAV-mediated gene transfer.* Molecular Therapy, 2009. **17**(7): p. 1215-1224.

161.   Shirley, J.L., et al., *Immune responses to viral gene therapy vectors.* Molecular Therapy, 2020. **28**(3): p. 709-722.

162.   Pack, D.W., et al., *Design and development of polymers for gene delivery.* Nature reviews Drug discovery, 2005. **4**(7): p. 581-593.

163.   Mintzer, M.A. and E.E. Simanek, *Nonviral vectors for gene delivery.* Chemical reviews, 2009. **109**(2): p. 259-302.

164. An, D., et al., *Systemic Messenger RNA Therapy as a Treatment for Methylmalonic Acidemia.* Cell Rep, 2017. **21**(12): p. 3548-3558.

165. Jiang, L., et al., *Dual mRNA therapy restores metabolic function in long-term studies in mice with propionic acidemia.* Nat Commun, 2020. **11**(1): p. 5339.

166. An, D., et al., *Long-term efficacy and safety of mRNA therapy in two murine models of methylmalonic acidemia.* EBioMedicine, 2019. **45**: p. 519-528.

167. Yu, H., et al., *Restoring ornithine transcarbamylase (OTC) activity in an OTC-deficient mouse model using LUNAR-OTC mRNA.* Clinical and Translational Discovery, 2022. **2**(2): p. e33.

168. Breyer, B., et al., *Adenoviral vector-mediated gene transfer for human gene therapy.* Curr Gene Ther, 2001. **1**(2): p. 149-62.

169. Crystal, R.G., *Adenovirus: the first effective in vivo gene delivery vector.* Hum Gene Ther, 2014. **25**(1): p. 3-11.

170. Seymour, L.W. and K.D. Fisher, *Adenovirus: teaching an old dog new tricks.* Hum Gene Ther, 2011. **22**(9): p. 1041-2.

171. Tang, J., et al., *Human CD8+ cytotoxic T cell responses to adenovirus capsid proteins.* Virology, 2006. **350**(2): p. 312-22.

172. Thaci, B., et al., *The challenge for gene therapy: innate immune response to adenoviruses.* Oncotarget, 2011. **2**(3): p. 113-21.

173. Jaffe, H.A., et al., *Adenovirus-mediated in vivo gene transfer and expression in normal rat liver.* Nat Genet, 1992. **1**(5): p. 372-8.

174. Griesenbach, U., et al., *Gene therapy progress and prospects: cystic fibrosis.* Gene Ther, 2002. **9**(20): p. 1344-50.

175. Batshaw, M.L., et al., *Recombinant adenovirus gene transfer in adults with partial ornithine transcarbamylase deficiency (OTCD).* Hum Gene Ther, 1999. **10**(14): p. 2419-37.

176. Bramson, J.L., et al., *Pre-existing immunity to adenovirus does not prevent tumor regression following intratumoral administration of a vector expressing IL-12 but inhibits virus dissemination.* Gene Ther, 1997. **4**(10): p. 1069-76.

177. Sibbald, B., *Death but one unintended consequence of gene-therapy trial.* Cmaj, 2001. **164**(11): p. 1612.

178. Wu, Z., A. Asokan, and R.J. Samulski, *Adeno-associated virus serotypes: vector toolkit for human gene therapy.* Mol Ther, 2006. **14**(3): p. 316-27.

179. Hastie, E. and R.J. Samulski, *Adeno-associated virus at 50: a golden anniversary of discovery, research, and gene therapy success--a personal perspective.* Hum Gene Ther, 2015. **26**(5): p. 257-65.

180. Gao, G., et al., *Clades of Adeno-associated viruses are widely disseminated in human tissues.* J Virol, 2004. **78**(12): p. 6381-8.

181. Gao, G.P., et al., *Novel adeno-associated viruses from rhesus monkeys as vectors for human gene therapy.* Proc Natl Acad Sci U S A, 2002. **99**(18): p. 11854-9.

182. Asokan, A., D.V. Schaffer, and R.J. Samulski, *The AAV vector toolkit: poised at the clinical crossroads.* Mol Ther, 2012. **20**(4): p. 699-708.

183. Halder, S., et al., *Structure of neurotropic adeno-associated virus AAVrh.8.* J Struct Biol, 2015. **192**(1): p. 21-36.

184. Balakrishnan, B. and G. R Jayandharan, *Basic biology of adeno-associated virus (AAV) vectors used in gene therapy.* Current gene therapy, 2014. **14**(2): p. 86-100.

185. Gao, G., L.H. Vandenberghe, and J.M. Wilson, *New recombinant serotypes of AAV vectors.* Current gene therapy, 2005. **5**(3): p. 285-297.

186. Hastie, E. and R.J. Samulski, *Recombinant adeno-associated virus vectors in the treatment of rare diseases.* Expert Opin Orphan Drugs, 2015. **3**(6): p. 675-689.

187. Junge, N., et al., *Adeno-associated virus vector-based gene therapy for monogenetic metabolic diseases of the liver.* J Pediatr Gastroenterol Nutr, 2015. **60**(4): p. 433-40.

188. Angelis, A., D. Tordrup, and P. Kanavos, *Socio-economic burden of rare diseases: A systematic review of cost of illness evidence.* Health Policy, 2015. **119**(7): p. 964-79.

189. Zabaleta, N., et al., *Gene therapy for liver diseases — progress and challenges.* Nature Reviews Gastroenterology & Hepatology, 2023.

190. Manno, C.S., et al., *Successful transduction of liver in hemophilia by AAV-Factor IX and limitations imposed by the host immune response.* Nat Med, 2006. **12**(3): p. 342-7.

191. Nathwani, A.C., et al., *Long-term safety and efficacy of factor IX gene therapy in hemophilia B.* N Engl J Med, 2014. **371**(21): p. 1994-2004.

192. Von Drygalski, A., et al., *Etranacogene dezaparvovec (AMT-061 phase 2b): normal/near normal FIX activity and bleed cessation in hemophilia B.* Blood advances, 2019. **3**(21): p. 3241-3247.

193.   Zabaleta, N., et al., *Gene therapy for liver diseases—progress and challenges.* Nature Reviews Gastroenterology & Hepatology, 2023: p. 1-18.

194.   Pasi, K.J., et al., *Multiyear follow-up of AAV5-hFVIII-SQ gene therapy for hemophilia A.* New England Journal of Medicine, 2020. **382**(1): p. 29-40.

195.   Pasi, K.J., et al., *Persistence of haemostatic response following gene therapy with valoctocogene roxaparvovec in severe haemophilia A.* Haemophilia, 2021. **27**(6): p. 947-956.

196.   Kassim, S.H., et al., *Gene therapy in a humanized mouse model of familial hypercholesterolemia leads to marked regression of atherosclerosis.* PloS one, 2010. **5**(10): p. e13424.

197.   Ronzitti, G., et al., *A translationally optimized AAV-UGT1A1 vector drives safe and long-lasting correction of Crigler-Najjar syndrome.* Molecular Therapy-Methods & Clinical Development, 2016. **3**: p. 16049.

198.   Wang, L., et al., *AAV gene therapy corrects OTC deficiency and prevents liver fibrosis in aged OTC-knock out heterozygous mice.* Molecular genetics and metabolism, 2017. **120**(4): p. 299-305.

199.   Kaiser, R.A., et al., *Use of an adeno-associated virus serotype Anc80 to provide durable cure of phenylketonuria in a mouse model.* Journal of Inherited Metabolic Disease, 2021. **44**(6): p. 1369-1381.

200.   Murillo, O., et al., *Liver expression of a MiniATP7B gene results in long-term restoration of copper homeostasis in a Wilson disease model in mice.* Hepatology, 2019. **70**(1): p. 108-126.

201.   Unzu, C., et al., *Sustained enzymatic correction by rAAV-mediated liver gene therapy protects against induced motor neuropathy in acute porphyria mice.* Molecular Therapy, 2011. **19**(2): p. 243-250.

202.   Weber, N.D., et al., *Gene therapy for progressive familial intrahepatic cholestasis type 3 in a clinically relevant mouse model.* Nature Communications, 2019. **10**(1): p. 5694.

203.   Lee, Y.M., et al., *Long-term safety and efficacy of AAV gene therapy in the canine model of glycogen storage disease type Ia.* Journal of Inherited Metabolic Disease, 2018. **41**: p. 977-984.

204. Ilyinskii, P.O., et al., *ImmTOR nanoparticles enhance AAV transgene expression after initial and repeat dosing in a mouse model of methylmalonic acidemia.* Molecular Therapy-Methods & Clinical Development, 2021. **22**: p. 279-292.

205. Nguyen, G.N., et al., *A long-term study of AAV gene therapy in dogs with hemophilia A identifies clonal expansions of transduced liver cells.* Nat Biotechnol, 2021. **39**(1): p. 47-55.

206. Vogt, V.M. and M.N. Simon, *Mass determination of rous sarcoma virus virions by scanning transmission electron microscopy.* J Virol, 1999. **73**(8): p. 7050-5.

207. Miller, D.G., M.A. Adam, and A.D. Miller, *Gene transfer by retrovirus vectors occurs only in cells that are actively replicating at the time of infection.* Mol Cell Biol, 1990. **10**(8): p. 4239-42.

208. Grossman, M., et al., *A pilot study of ex vivo gene therapy for homozygous familial hypercholesterolaemia.* Nat Med, 1995. **1**(11): p. 1148-54.

209. Grossman, M., et al., *Successful ex vivo gene therapy directed to liver in a patient with familial hypercholesterolaemia.* Nat Genet, 1994. **6**(4): p. 335-41.

210. Baruteau, J., et al., *Gene therapy for monogenic liver diseases: clinical successes, current challenges and future prospects.* Journal of inherited metabolic disease, 2017. **40**(4): p. 497-517.

211. Nguyen, T.H., et al., *Ex vivo liver-directed gene therapy for the treatment of metabolic diseases: advances in hepatocyte transplantation and retroviral vectors.* Curr Gene Ther, 2009. **9**(2): p. 136-49.

212. Gramignoli, R., et al., *Clinical hepatocyte transplantation: practical limits and possible solutions.* Eur Surg Res, 2015. **54**(3-4): p. 162-77.

213. Powell, J.S., et al., *Phase 1 trial of FVIII gene transfer for severe hemophilia A using a retroviral construct administered by peripheral intravenous infusion.* Blood, 2003. **102**(6): p. 2038-45.

214. Rosenberg, S.A., et al., *The development of gene therapy for the treatment of cancer.* Annals of surgery, 1993. **218**(4): p. 455.

215. Rosenberg, S.A., *Gene therapy for cancer.* Jama, 1992. **268**(17): p. 2416-2419.

216. Rosenberg, S.A., et al., *Gene transfer into humans—immunotherapy of patients with advanced melanoma, using tumor-infiltrating lymphocytes modified by retroviral gene transduction.* New England Journal of Medicine, 1990. **323**(9): p. 570-578.

217. Check, E., *A tragic setback.* Nature, 2002. **420**(6912): p. 116-8.

218. Hacein-Bey-Abina, S., et al., *LMO2-associated clonal T cell proliferation in two patients after gene therapy for SCID-X1.* science, 2003. **302**(5644): p. 415-419.

219. Weiss, R.A., *Retrovirus classification and cell interactions.* Journal of Antimicrobial Chemotherapy, 1996. **37**(suppl_B): p. 1-11.

220. Vigna, E. and L. Naldini, *Lentiviral vectors: excellent tools for experimental gene transfer and promising candidates for gene therapy.* J Gene Med, 2000. **2**(5): p. 308-16.

221. Kay, M.A., J.C. Glorioso, and L. Naldini, *Viral vectors for gene therapy: the art of turning infectious agents into vehicles of therapeutics.* Nat Med, 2001. **7**(1): p. 33-40.

222. Burns, J.C., et al., *Vesicular stomatitis virus G glycoprotein pseudotyped retroviral vectors: concentration to very high titer and efficient gene transfer into mammalian and nonmammalian cells.* Proceedings of the National Academy of Sciences, 1993. **90**(17): p. 8033-8037.

223. Hopkins, N., *High titers of retrovirus (vesicular stomatitis virus) pseudotypes, at last.* Proceedings of the National Academy of Sciences, 1993. **90**(19): p. 8759-8760.

224. Hislop, J.N., et al., *Rabies virus envelope glycoprotein targets lentiviral vectors to the axonal retrograde pathway in motor neurons.* J Biol Chem, 2014. **289**(23): p. 16148-63.

225. Beard, B.C., et al., *Comparison of HIV-derived lentiviral and MLV-based gammaretroviral vector integration sites in primate repopulating cells.* Molecular therapy, 2007. **15**(7): p. 1356-1365.

226. Wu, X., et al., *Transcription start regions in the human genome are favored targets for MLV integration.* Science, 2003. **300**(5626): p. 1749-1751.

227. Okimoto, T., T. Friedmann, and A. Miyanohara, *VSV-G envelope glycoprotein forms complexes with plasmid DNA and MLV retrovirus-like particles in cell-free conditions and enhances DNA transfection.* Mol Ther, 2001. **4**(3): p. 232-8.

228. Ting-De Ravin, S.S., et al., *Correction of canine X-linked severe combined immunodeficiency by in vivo retroviral gene therapy.* Blood, 2006. **107**(8): p. 3091-7.

229. Nafchi, N.A.M., *Optimisation of lentiviral vectors for gene therapy of spinal muscular atrophy*. 2017, Royal Holloway, University of London.

230. Miyoshi, H., et al., *Development of a self-inactivating lentivirus vector.* J Virol, 1998. **72**(10): p. 8150-7.

231. Zufferey, R., et al., *Self-inactivating lentivirus vector for safe and efficient in vivo gene delivery.* J Virol, 1998. **72**(12): p. 9873-80.

232. Breda, L., et al., *Therapeutic hemoglobin levels after gene transfer in β-thalassemia mice and in hematopoietic cells of β-thalassemia and sickle cells disease patients.* PLoS One, 2012. **7**(3): p. e32345.

233. Cesana, D., et al., *Uncovering and dissecting the genotoxicity of self-inactivating lentiviral vectors in vivo.* Mol Ther, 2014. **22**(4): p. 774-85.

234. Wang, G., et al., *Feline immunodeficiency virus vectors persistently transduce nondividing airway epithelia and correct the cystic fibrosis defect.* J Clin Invest, 1999. **104**(11): p. R55-62.

235. Anderson, W.F., *Prospects for human gene therapy.* Science, 1984. **226**(4673): p. 401-9.

236. Eichler, F., et al., *Hematopoietic Stem-Cell Gene Therapy for Cerebral Adrenoleukodystrophy.* New England Journal of Medicine, 2017. **377**(17): p. 1630-1638.

237. Hickey, R.D., et al., *Curative ex vivo liver-directed gene therapy in a pig model of hereditary tyrosinemia type 1.* Sci Transl Med, 2016. **8**(349): p. 349ra99.

238. Brown, B.D., et al., *Endogenous microRNA can be broadly exploited to regulate transgene expression according to tissue, lineage and differentiation state.* Nat Biotechnol, 2007. **25**(12): p. 1457-67.

239. Cantore, A., et al., *Hyperfunctional coagulation factor IX improves the efficacy of gene therapy in hemophilic mice.* Blood, The Journal of the American Society of Hematology, 2012. **120**(23): p. 4517-4520.

240. Cantore, A., et al., *Liver-directed lentiviral gene therapy in a dog model of hemophilia B.* Sci Transl Med, 2015. **7**(277): p. 277ra28.

241. Milani, M., et al., *Liver-directed lentiviral gene therapy corrects hemophilia A mice and achieves normal-range factor VIII activity in non-human primates.* Nat Commun, 2022. **13**(1): p. 2454.

242. Escors, D. and K. Breckpot, *Lentiviral vectors in gene therapy: their current status and future potential.* Archivum immunologiae et therapiae experimentalis, 2010. **58**(2): p. 107-119.

243. Ryu, W.-S., *Chapter 17 - Retroviruses*, in *Molecular Virology of Human Pathogenic Viruses*, W.-S. Ryu, Editor. 2017, Academic Press: Boston. p. 227-246.

244. Bucci, M., *HIV seals an envelope.* Nature Chemical Biology, 2019. **15**(3): p. 207-207.

245. Wang, H., et al., *Partially Open HIV-1 Envelope Structures Exhibit Conformational Changes Relevant for Coreceptor Binding and Fusion.* Cell Host & Microbe, 2018. **24**(4): p. 579-592.e4.

246. Marin, M., et al., *HIV-1 Fusion with CD4+ T cells Is Promoted by Proteins Involved in Endocytosis and Intracellular Membrane Trafficking.* Viruses, 2019. **11**(2).

247. Larsen, K.P., et al., *Architecture of an HIV-1 reverse transcriptase initiation complex.* Nature, 2018. **557**(7703): p. 118-122.

248. Milone, M.C. and U. O'Doherty, *Clinical use of lentiviral vectors.* Leukemia, 2018. **32**(7): p. 1529-1541.

249. Novikova, M., et al., *Multiple Roles of HIV-1 Capsid during the Virus Replication Cycle.* Virologica Sinica, 2019. **34**(2): p. 119-134.

250. Batisse, J., et al., *Structures and Functions of the HIV-1 Pre-Integration Complexes.* Biophysical Journal, 2019. **116**(3): p. 62a.

251. Borrenberghs, D., et al., *Dynamic Oligomerization of Integrase Orchestrates HIV Nuclear Entry.* Scientific Reports, 2016. **6**(1): p. 36485.

252. Rai, S.K., et al., *Host factors that promote retrotransposon integration are similar in distantly related eukaryotes.* PLoS Genet, 2017. **13**(12): p. e1006775.

253. Ryu, W.-S., *Part III. RNA Viruses*, in *Molecular Virology of Human Pathogenic Viruses*, W.-S. Ryu, Editor. 2017, Academic Press: Boston. p. 149-150.

254. Faust, T.B., et al., *The HIV-1 Tat protein recruits a ubiquitin ligase to reorganize the 7SK snRNP for transcriptional activation.* Elife, 2018. **7**.

255. Sertznig, H., et al., *Behind the scenes of HIV-1 replication: Alternative splicing as the dependency factor on the quiet.* Virology, 2018. **516**: p. 176-188.

256. Gama-Norton, L., et al., *Lentivirus production is influenced by SV40 large T-antigen and chromosomal integration of the vector in HEK293 cells.* Hum Gene Ther, 2011. **22**(10): p. 1269-79.

257. Merten, O.W., et al., *Large-scale manufacture and characterization of a lentiviral vector produced for clinical ex vivo gene therapy application.* Hum Gene Ther, 2011. **22**(3): p. 343-56.

258. Ausubel, L.J., et al., *Production of CGMP-Grade Lentiviral Vectors.* Bioprocess Int, 2012. **10**(2): p. 32-43.

259. Dropulic, B., et al., *Large-scale Purification of a Lentiviral Vector by Size Exclusion Chromatography or Mustang Q Ion Exchange Capsule.* BioProcessing Journal, 2003. **2**(5): p. 89-95.

260. Levine, B.L., et al., *Global Manufacturing of CAR T Cell Therapy.* Molecular therapy. Methods & clinical development, 2016. **4**: p. 92-101.

261. Merten, O.W., M. Hebben, and C. Bovolenta, *Production of lentiviral vectors.* Mol Ther Methods Clin Dev, 2016. **3**: p. 16017.

262. Kutner, R.H., X.Y. Zhang, and J. Reiser, *Production, concentration and titration of pseudotyped HIV-1-based lentiviral vectors.* Nat Protoc, 2009. **4**(4): p. 495-505.

263. Montini, E., et al., *The genotoxic potential of retroviral vectors is strongly modulated by vector design and integration site selection in a mouse model of HSC gene therapy.* The Journal of clinical investigation, 2009. **119**(4): p. 964-975.

264. Kool, J. and A. Berns, *High-throughput insertional mutagenesis screens in mice to identify oncogenic networks.* Nature Reviews Cancer, 2009. **9**(6): p. 389-399.

265. Ranzani, M., et al., *Lentiviral vector-based insertional mutagenesis identifies genes associated with liver cancer.* Nat Methods, 2013. **10**(2): p. 155-61.

266. Modlich, U., et al., *Cell-culture assays reveal the importance of retroviral vector design for insertional genotoxicity.* Blood, 2006. **108**(8): p. 2545-2553.

267. Zychlinski, D., et al., *Physiological promoters reduce the genotoxic risk of integrating gene vectors.* Molecular therapy, 2008. **16**(4): p. 718-725.

268. Montini, E., et al., *Hematopoietic stem cell gene transfer in a tumor-prone mouse model uncovers low genotoxicity of lentiviral vector integration.* Nature biotechnology, 2006. **24**(6): p. 687-696.

269. Berry, C., et al., *Selection of target sites for mobile DNA integration in the human genome.* PLoS computational biology, 2006. **2**(11): p. e157.

270. Wang, G.P., et al., *HIV integration site selection: analysis by massively parallel pyrosequencing reveals association with epigenetic modifications.* Genome research, 2007. **17**(8): p. 1186-1194.

271. Schroder, A., et al., *HIV-1 integration in the human genome favors active genes and local hotspots (2002) Cell, 110 (4)*. DOI 10.1016/S0092-8674 (02) 00864-4.

272. *<CTGTAC-06.09.22-06.10.22-Meeting-Briefing-Document-FDA-125755 (2).pdf>.*

273. Pfeifer, A., *Lentiviral transgenesis--a versatile tool for basic research and gene therapy.* Curr Gene Ther, 2006. **6**(4): p. 535-42.

274. Hampton, R.Y., et al., *Recognition and plasma clearance of endotoxin by scavenger receptors.* Nature, 1991. **352**(6333): p. 342-344.

275. Porter, D.L., et al., *Chimeric antigen receptor T cells persist and induce sustained remissions in relapsed refractory chronic lymphocytic leukemia.* Science translational medicine, 2015. **7**(303): p. 303ra139-303ra139.

276. Ricklin, D., et al., *Complement: a key system for immune surveillance and homeostasis.* Nat Immunol, 2010. **11**(9): p. 785-97.

277. Mastellos, D. and J.D. Lambris, *Complement: more than a 'guard' against invading pathogens?* Trends Immunol, 2002. **23**(10): p. 485-91.

278. Brown, B.D. and D. Lillicrap, *Dangerous liaisons: the role of "danger" signals in the immune response to gene therapy.* Blood, The Journal of the American Society of Hematology, 2002. **100**(4): p. 1133-1140.

279. Kawai, T. and S. Akira, *Innate immune recognition of viral infection.* Nature immunology, 2006. **7**(2): p. 131-137.

280. Akira, S., S. Uematsu, and O. Takeuchi, *Pathogen recognition and innate immunity.* Cell, 2006. **124**(4): p. 783-801.

281. Grommé, M. and J. Neefjes, *Antigen degradation or presentation by MHC class I molecules via classical and non-classical pathways.* Molecular immunology, 2002. **39**(3-4): p. 181-202.

282. Annoni, A., et al., *Modulation of immune responses in lentiviral vector-mediated gene transfer.* Cell Immunol, 2019. **342**: p. 103802.

283. Martínez-Molina, E., et al., *Large-Scale Production of Lentiviral Vectors: Current Perspectives and Challenges.* Pharmaceutics, 2020. **12**(11).

284.   Baekelandt, V., et al., *Optimized lentiviral vector production and purification procedure prevents immune response after transduction of mouse brain.* Gene Ther, 2003. **10**(23): p. 1933-40.

285.   Tanaka, M. and A. Miyajima, *Liver regeneration and fibrosis after inflammation.* Inflammation and Regeneration, 2016. **36**(1): p. 1-6.

286.   Jungermann, K., *Functional Heterogeneity of Periportal and Perivenous Hepatocytes.* Enzyme, 1986. **35**: p. 161-180.

287.   Nguyen, T.H., et al., *Highly efficient lentiviral vector-mediated transduction of nondividing, fully reimplantable primary hepatocytes.* Mol Ther, 2002. **6**(2): p. 199-209.

288.   Starinieri, F., et al. *Age of administration impacts the efficiency of lentiviral vector-mediated hepatocyte transduction in vivo and its distribution in the liver lobule*. in *HUMAN GENE THERAPY*. 2022. MARY ANN LIEBERT, INC 140 HUGUENOT STREET, 3RD FL, NEW ROCHELLE, NY 10801 USA.

289.   Edwards, R., et al., *Robust and Facile Automated Radiosynthesis of [(18)F]FSPG on the GE FASTlab.* Mol Imaging Biol, 2021. **23**(6): p. 854-864.

290.   Wright, S., *The genetics of vital characters of the guinea pig.* The genetics of vital characters of the guinea pig., 1960. **56**(Suppl. 1): p. 123-150.

291.   Weber, E.M., et al., *Influence of strain and parity on the risk of litter loss in laboratory mice.* Reprod Domest Anim, 2013. **48**(2): p. 292-6.

292.   Aldinger, K.A., et al., *Genetic variation and population substructure in outbred CD-1 mice: implications for genome-wide association studies.* PLoS One, 2009. **4**(3): p. e4729.

293.   Grove, E., S. Eckardt, and K.J. McLaughlin, *High-Speed Mouse Backcrossing Through the Female Germ Line.* PloS one, 2016. **11**(12): p. e0166822-e0166822.

294.   Whary, M.T., et al., *Biology and Diseases of Mice.* Laboratory Animal Medicine, 2015: p. 43-149.

295.   Naldini, L., *Gene therapy returns to centre stage.* Nature, 2015. **526**(7573): p. 351-360.

296.   Dull, T., et al., *A third-generation lentivirus vector with a conditional packaging system.* J Virol, 1998. **72**(11): p. 8463-71.

297.   Naldini, L., et al., *In vivo gene delivery and stable transduction of nondividing cells by a lentiviral vector.* Science, 1996. **272**(5259): p. 263-267.

298. Fernandes, J., B. Jayaraman, and A. Frankel, *The HIV-1 Rev response element: an RNA scaffold that directs the cooperative assembly of a homo-oligomeric ribonucleoprotein complex.* RNA biology, 2012. **9**(1): p. 6-11.

299. Hu, C., et al., *The HIV-1 central polypurine tract functions as a second line of defense against APOBEC3G/F.* J Virol, 2010. **84**(22): p. 11981-93.

300. Dalsgaard, T., et al., *Improved Lentiviral Gene Delivery to Mouse Liver by Hydrodynamic Vector Injection through Tail Vein.* Molecular therapy. Nucleic acids, 2018. **12**: p. 672-683.

301. Mikkelsen, J.G., et al., *Helper-Independent Sleeping Beauty transposon-transposase vectors for efficient nonviral gene delivery and persistent gene expression in vivo.* Mol Ther, 2003. **8**(4): p. 654-65.

302. Zufferey, R., et al., *Woodchuck hepatitis virus posttranscriptional regulatory element enhances expression of transgenes delivered by retroviral vectors.* J Virol, 1999. **73**(4): p. 2886-92.

303. Cunningham, S.C., et al., *Gene delivery to the juvenile mouse liver using AAV2/8 vectors.* Mol Ther, 2008. **16**(6): p. 1081-8.

304. Aravalli, R.N., J.D. Belcher, and C.J. Steer, *Liver-targeted gene therapy: Approaches and challenges.* Liver Transplantation, 2015. **21**(6): p. 718-737.

305. Follenzi, A., et al., *Efficient gene delivery and targeted expression to hepatocytes in vivo by improved lentiviral vectors.* Hum Gene Ther, 2002. **13**(2): p. 243-60.

306. Liechtenstein, T., N. Perez-Janices, and D. Escors, *Lentiviral vectors for cancer immunotherapy and clinical applications.* Cancers (Basel), 2013. **5**(3): p. 815-37.

307. Saida, H., et al., *One-year follow-up of transgene expression by integrase-defective lentiviral vectors and their therapeutic potential in spinocerebellar ataxia model mice.* Gene Therapy, 2014. **21**(9): p. 820-827.

308. Erez, A., *Argininosuccinic aciduria: from a monogenic to a complex disorder.* Genetics in Medicine, 2013. **15**(4): p. 251-257.

309. Cunningham, S.C., et al., *Induction and prevention of severe hyperammonemia in the spfash mouse model of ornithine transcarbamylase deficiency using shRNA and rAAV-mediated gene delivery.* Mol Ther, 2011. **19**(5): p. 854-9.

310. Annoni, A., et al., *Liver gene therapy by lentiviral vectors reverses anti-factor IX pre-existing immunity in haemophilic mice.* EMBO molecular medicine, 2013. **5**(11): p. 1684-1697.

311. Wang, S., et al., *Effect of clodronate on macrophage depletion and adenoviral-mediated transgene expression in salivary glands.* J Oral Pathol Med, 1999. **28**(4): p. 145-51.

312. Schiedner, G., et al., *Selective depletion or blockade of Kupffer cells leads to enhanced and prolonged hepatic transgene expression using high-capacity adenoviral vectors.* Mol Ther, 2003. **7**(1): p. 35-43.

313. Gustafsson, C., S. Govindarajan, and J. Minshull, *Codon bias and heterologous protein expression.* Trends Biotechnol, 2004. **22**(7): p. 346-53.

314. Karlin, S., et al., *Characterizations of highly expressed genes of four fast-growing bacteria.* J Bacteriol, 2001. **183**(17): p. 5025-40.

315. Yu, C.-H., et al., *Codon usage influences the local rate of translation elongation to regulate co-translational protein folding.* Molecular cell, 2015. **59**(5): p. 744-754.

316. Weinberg, D.E., et al., *Improved ribosome-footprint and mRNA measurements provide insights into dynamics and regulation of yeast translation.* Cell reports, 2016. **14**(7): p. 1787-1799.

317. Yang, Q., et al., *eRF1 mediates codon usage effects on mRNA translation efficiency through premature termination at rare codons.* Nucleic acids research, 2019. **47**(17): p. 9243-9258.

318. Hussmann, J.A., et al., *Understanding biases in ribosome profiling experiments reveals signatures of translation dynamics in yeast.* PLoS genetics, 2015. **11**(12): p. e1005732.

319. Ikemura, T., *Correlation between the abundance of Escherichia coli transfer RNAs and the occurrence of the respective codons in its protein genes: a proposal for a synonymous codon choice that is optimal for the E. coli translational system.* J Mol Biol, 1981. **151**(3): p. 389-409.

320. Plotkin, J.B. and G. Kudla, *Synonymous but not the same: the causes and consequences of codon bias.* Nature Reviews Genetics, 2011. **12**(1): p. 32-42.

321. Moreno-Carranza, B., et al., *Transgene optimization significantly improves SIN vector titers, gp91phox expression and reconstitution of superoxide production in X-CGD cells.* Gene Ther, 2009. **16**(1): p. 111-8.

322. Ward, N.J., et al., *Codon optimization of human factor VIII cDNAs leads to high-level expression.* Blood, 2011. **117**(3): p. 798-807.

323. Zhang, R., et al., *Optimized human factor IX expression cassettes for hepatic-directed gene therapy of hemophilia B.* Front Med, 2015. **9**(1): p. 90-9.

324. Schlimgen, R., et al., *Risks Associated With Lentiviral Vector Exposures and Prevention Strategies.* J Occup Environ Med, 2016. **58**(12): p. 1159-1166.

325. Soria, L.R., et al., *Beclin-1-mediated activation of autophagy improves proximal and distal urea cycle disorders.* EMBO Mol Med, 2021. **13**(2): p. e13158.

326. Bozzola, J.J., *Conventional specimen preparation techniques for transmission electron microscopy of cultured cells.* Methods Mol Biol, 2007. **369**: p. 1-18.

327. Kavanaugh, G., et al., *Utility of [18 F] FSPG PET to image hepatocellular carcinoma: first clinical evaluation in a US population.* Molecular imaging and biology, 2016. **18**: p. 924-934.

328. Baek, S., et al., *Exploratory Clinical Trial of (4S)-4-(3-[18F] fluoropropyl)-l-glutamate for Imaging xC− Transporter Using Positron Emission Tomography in Patients with Non–Small Cell Lung or Breast CancerPET Imaging of xC− Transporter in Lung and Breast Cancer.* Clinical cancer research, 2012. **18**(19): p. 5427-5437.

329. Lu, S.C., *Regulation of glutathione synthesis.* Molecular aspects of medicine, 2009. **30**(1-2): p. 42-59.

330. Vairetti, M., et al., *Changes in glutathione content in liver diseases: an update.* Antioxidants, 2021. **10**(3): p. 364.

331. Nicolas, C.T., et al., *In vivo lentiviral vector gene therapy to cure hereditary tyrosinemia type 1 and prevent development of precancerous and cancerous lesions.* Nature Communications, 2022. **13**(1): p. 5012.

332. Gebhardt, R. and M. Matz-Soja, *Liver zonation: Novel aspects of its regulation and its impact on homeostasis.* World J Gastroenterol, 2014. **20**(26): p. 8491-504.

333. Touramanidou, L., et al. *Macrophage inhibitor clodronate enhances liver transduction of lentiviral but not AAV vectors in vivo*. in *HUMAN GENE THERAPY*. 2022. MARY ANN LIEBERT, INC 140 HUGUENOT STREET, 3RD FL, NEW ROCHELLE, NY 10801 USA.

334. Seminotti, B., et al., *Free Radical Scavengers Prevent Argininosuccinic Acid-Induced Oxidative Stress in the Brain of Developing Rats: a New Adjuvant Therapy for Argininosuccinate Lyase Deficiency?* Mol Neurobiol, 2020. **57**(2): p. 1233-1244.

335. Aoyagi, K., et al., *Role of reactive oxygen and argininosuccinate in guanidinosuccinate synthesis in isolated rat hepatocytes.* Enzyme Protein, 1996. **49**(4): p. 205-11.

336. Liu, X., et al., *NADPH debt drives redox bankruptcy: SLC7A11/xCT-mediated cystine uptake as a double-edged sword in cellular redox regulation.* Genes Dis, 2021. **8**(6): p. 731-745.

337. Liu, J., X. Xia, and P. Huang, *xCT: a critical molecule that links cancer metabolism to redox signaling.* Molecular Therapy, 2020. **28**(11): p. 2358-2366.

338. Liu, X., et al., *NADPH debt drives redox bankruptcy: SLC7A11/xCT-mediated cystine uptake as a double-edged sword in cellular redox regulation.* Genes & diseases, 2021. **8**(6): p. 731-745.

339. Schutgens, R.B., et al., *Mild variant of argininosuccinic aciduria.* J Inherit Metab Dis, 1980. **2**(1): p. 13-4.

340. Ramos, O., et al., *Arsenic increased lipid peroxidation in rat tissues by a mechanism independent of glutathione levels.* Environmental Health Perspectives, 1995. **103**(suppl 1): p. 85-88.

341. Conway, A., et al., *Non-viral Delivery of Zinc Finger Nuclease mRNA Enables Highly Efficient In Vivo Genome Editing of Multiple Therapeutic Gene Targets.* Molecular Therapy, 2019. **27**(4): p. 866-877.

342. Tucci, F., et al., *Update on Clinical Ex Vivo Hematopoietic Stem Cell Gene Therapy for Inherited Monogenic Diseases.* Molecular Therapy, 2021. **29**(2): p. 489-504.

343. *Long-Term Follow-Up of a Phase I/II Study of ProSavin, a Lentiviral Vector Gene Therapy for Parkinson's Disease.* Human Gene Therapy Clinical Development, 2018. **29**(3): p. 148-155.

344. Xu, X., et al., *The effect of acupuncture on tumor growth and gut microbiota in mice inoculated with osteosarcoma cells.* Chin Med, 2020. **15**: p. 33.

345. Seilkop, S.K., *The effect of body weight on tumor incidence and carcinogenicity testing in B6C3F1 mice and F344 rats.* Fundam Appl Toxicol, 1995. **24**(2): p. 247-59.

346. Finkelshtein, D., et al., *LDL receptor and its family members serve as the cellular receptors for vesicular stomatitis virus.* Proceedings of the National Academy of Sciences, 2013. **110**(18): p. 7306-7311.

347. Darrow, J.J., *Luxturna: FDA documents reveal the value of a costly gene therapy.* Drug discovery today, 2019. **24**(4): p. 949-954.

348. Hoy, S.M., *Onasemnogene abeparvovec: first global approval.* Drugs, 2019. **79**(11): p. 1255-1262.

349. He, X., et al., *Evolving AAV-delivered therapeutics towards ultimate cures.* Journal of Molecular Medicine, 2021. **99**(5): p. 593-617.

350. Penaud-Budloo, M., et al., *Adeno-associated virus vector genomes persist as episomal chromatin in primate muscle.* J Virol, 2008. **82**(16): p. 7875-85.

351. Deyle, D.R. and D.W. Russell, *Adeno-associated virus vector integration.* Curr Opin Mol Ther, 2009. **11**(4): p. 442-7.

352. Dalwadi, D.A., et al., *AAV integration in human hepatocytes.* Mol Ther, 2021. **29**(10): p. 2898-2909.

353. Khare, R., et al., *Circulating Antibodies and Macrophages as Modulators of Adenovirus Pharmacology.* Journal of Virology, 2013. **87**(7): p. 3678-3686.

354. McEwan, W.A., et al., *Intracellular antibody-bound pathogens stimulate immune signaling via the Fc receptor TRIM21.* Nature Immunology, 2013. **14**(4): p. 327-336.

355. Calcedo, R., et al., *Worldwide Epidemiology of Neutralizing Antibodies to Adeno-Associated Viruses.* The Journal of Infectious Diseases, 2009. **199**(3): p. 381-390.

356. Wang, L., et al., *The Pleiotropic Effects of Natural AAV Infections on Liver-directed Gene Transfer in Macaques.* Molecular Therapy, 2010. **18**(1): p. 126-134.

357. Perocheau, D.P., et al., *Age-Related Seroprevalence of Antibodies Against AAV-LK03 in a UK Population Cohort.* Human Gene Therapy, 2018. **30**(1): p. 79-87.

358. Fitzpatrick, Z., et al., *Influence of Pre-existing Anti-capsid Neutralizing and Binding Antibodies on AAV Vector Transduction.* Molecular Therapy - Methods & Clinical Development, 2018. **9**: p. 119-129.

359. De Ravin, S.S., et al., *Lentiviral hematopoietic stem cell gene therapy for X-linked severe combined immunodeficiency.* Science Translational Medicine, 2016. **8**(335): p. 335ra57-335ra57.

360. Hackett, P.B., *Integrating DNA vectors for gene therapy.* Mol Ther, 2007. **15**(1): p. 10-2.

361. Schagen, F.H.E., et al., *Insertion vectors for gene therapy.* Gene Therapy, 2000. **7**(4): p. 271-272.

362. Buchschacher, G.L., Jr. and F. Wong-Staal, *Development of lentiviral vectors for gene therapy for human diseases.* Blood, 2000. **95**(8): p. 2499-2504.

363.   Noelia, A. and A. Castrillo, *Origin and specialization of splenic macrophages.* Cellular immunology, 2018. **330**: p. 151-158.

364.   Kashimura, M., *The human spleen as the center of the blood defense system.* International Journal of Hematology, 2020. **112**(2): p. 147-158.

365.   Akbarzadeh, A., et al., *Liposome: classification, preparation, and applications.* Nanoscale Res Lett, 2013. **8**(1): p. 102.

366.   van Rooijen, N. and E. van Kesteren-Hendrikx, *CLODRONATE LIPOSOMES: PERSPECTIVES IN RESEARCH AND THERAPEUTICS.* Journal of Liposome Research, 2002. **12**(1-2): p. 81-94.

367.   van Rooijen, N., A. Sanders, and T.K. van den Berg, *Apoptosis of macrophages induced by liposome-mediated intracellular delivery of clodronate and propamidine.* J Immunol Methods, 1996. **193**(1): p. 93-9.

368.   Hurst, M. and S. Noble, *Clodronate.* Drugs & Aging, 1999. **15**(2): p. 143-167.

369.   Green, J.R., *Antitumor effects of bisphosphonates.* Cancer, 2003. **97**(3 Suppl): p. 840-7.

370.   Santini, D., et al., *The antineoplastic role of bisphosphonates: from basic research to clinical evidence.* Ann Oncol, 2003. **14**(10): p. 1468-76.

371.   Van Rooijen, N. and A. Sanders, *Liposome mediated depletion of macrophages: mechanism of action, preparation of liposomes and applications.* J Immunol Methods, 1994. **174**(1-2): p. 83-93.

372.   Yang, Y., et al., *Cellular immunity to viral antigens limits E1-deleted adenoviruses for gene therapy.* Proceedings of the National Academy of Sciences, 1994. **91**(10): p. 4407-4411.

373.   Yang, Y., et al., *Immune responses to viral antigens versus transgene product in the elimination of recombinant adenovirus-infected hepatocytes in vivo.* Gene therapy, 1996. **3**(2): p. 137-144.

374.   Crystal, R.G., et al., *Administration of an adenovirus containing the human CFTR cDNA to the respiratory tract of individuals with cystic fibrosis.* Nature genetics, 1994. **8**(1): p. 42-51.

375.   Zhang, H.-G., et al., *Inhibition of tumor necrosis factor α decreases inflammation and prolongs adenovirus gene expression in lung and liver.* Human gene therapy, 1998. **9**(13): p. 1875-1884.

376. Raper, S.E., et al., *A pilot study of in vivo liver-directed gene transfer with an adenoviral vector in partial ornithine transcarbamylase deficiency.* Human gene therapy, 2002. **13**(1): p. 163-175.

377. Tuohy, G.P. and R. Megaw, *A systematic review and meta-analyses of interventional clinical trial studies for gene therapies for the inherited retinal degenerations (IRDs).* Biomolecules, 2021. **11**(5): p. 760.

378. Halbert, C.L., et al., *Capsid-expressing DNA in AAV vectors and its elimination by use of an oversize capsid gene for vector production.* Gene therapy, 2011. **18**(4): p. 411-417.

379. Russell, S., et al., *Efficacy and safety of voretigene neparvovec (AAV2-hRPE65v2) in patients with RPE65-mediated inherited retinal dystrophy: a randomised, controlled, open-label, phase 3 trial.* The Lancet, 2017. **390**(10097): p. 849-860.

380. Den Haan, J.M. and G. Kraal, *Innate immune functions of macrophage subpopulations in the spleen.* Journal of innate immunity, 2012. **4**(5-6): p. 437-445.

381. Di Paolo, N.C., et al., *Virus binding to a plasma membrane receptor triggers interleukin-1α-mediated proinflammatory macrophage response in vivo.* Immunity, 2009. **31**(1): p. 110-121.

382. Worgall, S., et al., *Innate immune mechanisms dominate elimination of adenoviral vectors following in vivo administration.* Human gene therapy, 1997. **8**(1): p. 37-44.

383. Alemany, R., K. Suzuki, and D.T. Curiel, *Blood clearance rates of adenovirus type 5 in mice.* Journal of General Virology, 2000. **81**(11): p. 2605-2609.

384. Alzuguren, P., et al., *Transient depletion of specific immune cell populations to improve adenovirus-mediated transgene expression in the liver.* Liver International, 2015. **35**(4): p. 1274-1289.

385. Wolff, G., et al., *Enhancement of in vivo adenovirus-mediated gene transfer and expression by prior depletion of tissue macrophages in the target organ.* Journal of virology, 1997. **71**(1): p. 624-629.

386. Yu, D.L., et al., *Macrophage Depletion via Clodronate Pretreatment Reduces Transgene Expression from AAV Vectors In Vivo.* Viruses, 2021. **13**(10).

387. Hsieh, L.S., et al., *Outbred CD1 mice are as suitable as inbred C57BL/6J mice in performing social tasks.* Neurosci Lett, 2017. **637**: p. 142-147.

388. Gad, S.C., *Diesel Fuel*, in *Encyclopedia of Toxicology (Third Edition)*, P. Wexler, Editor. 2014, Academic Press: Oxford. p. 115-118.

389. Silver, L., *Inbred Strain*, in *Brenner's Encyclopedia of Genetics (Second Edition)*, S. Maloy and K. Hughes, Editors. 2001, Academic Press: San Diego. p. 53.

390. Casellas, J., *Inbred mouse strains and genetic stability: a review.* Animal, 2011. **5**(1): p. 1-7.

391. Roderick, T.H., *Mouse*, in *Brenner's Encyclopedia of Genetics (Second Edition)*, S. Maloy and K. Hughes, Editors. 2013, Academic Press: San Diego. p. 482-485.

392. Follenzi, A., L. Santambrogio, and A. Annoni, *Immune responses to lentiviral vectors.* Curr Gene Ther, 2007. **7**(5): p. 306-15.

393. Blériot, C. and F. Ginhoux, *Understanding the heterogeneity of resident liver macrophages.* Frontiers in immunology, 2019. **10**: p. 2694.

394. van Til, N.P., et al., *Kupffer Cells and Not Liver Sinusoidal Endothelial Cells Prevent Lentiviral Transduction of Hepatocytes.* Molecular Therapy, 2005. **11**(1): p. 26-34.

395. Weisser, S.B., N. van Rooijen, and L.M. Sly, *Depletion and reconstitution of macrophages in mice.* JoVE (Journal of Visualized Experiments), 2012(66): p. e4105.

396. Watanabe, N., *Elimination of local macrophages in the intestine prevents chronic colitis in IL-10 deficient mice.* Dig Dis Sci, 2003.

397. Zhao, H., et al., *Isoliquiritigenin, a flavonoid from licorice, blocks M2 macrophage polarization in colitis-associated tumorigenesis through downregulating PGE2 and IL-6.* Toxicology and applied pharmacology, 2014. **279**(3): p. 311-321.

398. Hansel, M.C., et al., *The history and use of human hepatocytes for the treatment of liver diseases: the first 100 patients.* Curr Protoc Toxicol, 2014. **62**: p. 14.12.1-23.

399. Dixon, L.J., et al., *Kupffer cells in the liver.* Compr Physiol, 2013. **3**(2): p. 785-97.

400. Perdiguero, E.G. and F. Geissmann, *The development and maintenance of resident macrophages.* Nat Immunol, 2016. **17**(1): p. 2-8.

401. Milani, M., et al. *Investigating the Stability of Lentiviral Vector Targeted Liver Cells During Post-Natal Growth for In Vivo Gene Therapy Applications*. in *MOLECULAR THERAPY*. 2020. CELL PRESS 50 HAMPSHIRE ST, FLOOR 5, CAMBRIDGE, MA 02139 USA.

402. Simpson, E.M., et al., *Genetic variation among 129 substrains and its importance for targeted mutagenesis in mice.* Nature genetics, 1997. **16**(1): p. 19-27.

403. Büeler, H., *Adeno-associated viral vectors for gene transfer and gene therapy.* Biological chemistry, 1999. **380**(6): p. 613-622.

404. Kay, M.A., J.C. Glorioso, and L. Naldini, *Viral vectors for gene therapy: the art of turning infectious agents into vehicles of therapeutics.* Nature medicine, 2001. **7**(1): p. 33-40.

405. Carter, P. and R. Samulski, *Adeno-associated viral vectors as gene delivery vehicles.* International journal of molecular medicine, 2000. **6**(1): p. 17-44.

406. Zaiss, A.K., et al., *Differential activation of innate immune responses by adenovirus and adeno-associated virus vectors.* J Virol, 2002. **76**(9): p. 4580-90.

407. Zhu, J., X. Huang, and Y. Yang, *The TLR9-MyD88 pathway is critical for adaptive immune responses to adeno-associated virus gene therapy vectors in mice.* The Journal of clinical investigation, 2009. **119**(8): p. 2388-2398.

408. Zaiss, A.K., et al., *Complement is an essential component of the immune response to adeno-associated virus vectors.* Journal of virology, 2008. **82**(6): p. 2727-2740.

409. Ertl, H.C. and K.A. High, *Impact of AAV capsid-specific T-cell responses on design and outcome of clinical gene transfer trials with recombinant adeno-associated viral vectors: an evolving controversy.* Human gene therapy, 2017. **28**(4): p. 328-337.

410. Rogers, G.L., et al., *Innate immune responses to AAV vectors.* Frontiers in microbiology, 2011. **2**: p. 194.

411. Hösel, M., et al., *Toll-like receptor 2–mediated innate immune response in human nonparenchymal liver cells toward adeno-associated viral vectors.* Hepatology, 2012. **55**(1): p. 287-297.

412. Carestia, A., et al., *Modulation of the liver immune microenvironment by the adeno-associated virus serotype 8 gene therapy vector.* Mol Ther Methods Clin Dev, 2021. **20**: p. 95-108.

413. Benihoud, K., et al., *Efficient, repeated adenovirus-mediated gene transfer in mice lacking both tumor necrosis factor alpha and lymphotoxin α.* Journal of virology, 1998. **72**(12): p. 9514-9525.

414. Zhang, H.G., et al., *Inhibition of tumor necrosis factor alpha decreases inflammation and prolongs adenovirus gene expression in lung and liver.* Hum Gene Ther, 1998. **9**(13): p. 1875-84.

415. Muruve, D.A., et al., *Adenoviral gene therapy leads to rapid induction of multiple chemokines and acute neutrophil-dependent hepatic injury in vivo.* Human gene therapy, 1999. **10**(6): p. 965-976.

416.   Schnell, M.A., et al., *Activation of innate immunity in nonhuman primates following intraportal administration of adenoviral vectors.* Molecular Therapy, 2001. **3**(5): p. 708-722.

417.   Annoni, A., et al., *Liver gene therapy by lentiviral vectors reverses anti-factor IX pre-existing immunity in haemophilic mice.* EMBO Mol Med, 2013. **5**(11): p. 1684-97.

418.   Yamaguchi, T., et al., *Role of MyD88 and TLR9 in the innate immune response elicited by serotype 5 adenoviral vectors.* Human gene therapy, 2007. **18**(8): p. 753-762.

419.   Huang, X. and Y. Yang, *Innate immune recognition of viruses and viral vectors.* Human gene therapy, 2009. **20**(4): p. 293-301.

420.   Minari, J., S. Mochizuki, and K. Sakurai, *Enhanced cytokine secretion owing to multiple CpG side chains of DNA duplex.* Oligonucleotides, 2008. **18**(4): p. 337-344.

421.   Appledorn, D., et al., *Complex interactions with several arms of the complement system dictate innate and humoral immunity to adenoviral vectors.* Gene therapy, 2008. **15**(24): p. 1606-1617.

422.   Salmon, P. and D. Trono, *Production and titration of lentiviral vectors.* Current protocols in neuroscience, 2006. **37**(1): p. 4.21. 1-4.21. 24.

423.   Gombash Lampe, S.E., B.K. Kaspar, and K.D. Foust, *Intravenous injections in neonatal mice.* Journal of visualized experiments : JoVE, 2014(93): p. e52037-e52037.

10. APPENDICES

10.1 Lentiviral vector biodistribution study in *vivo*

10.1.1 Introduction

A reliable gene delivery system is required to transfer the *hASL* gene to the liver for treating ASA. Previous *in vitro* and *in vivo* studies using AAV vector have shown a highly efficient gene transfer to hepatocytes [83]. However, their expression has been time limited because AAV vectors integrate very marginally into the host genomic DNA [83]. Lentiviral transgene delivery has previously established effective long-term expression due to their ability to integrate into the host genome [295]. The LP1 promoter consists of the hAAT promoter combined with the ApoE-HCR and is used to promote a restrict transcription of lentiviral vector to hepatocytes.

10.1.2 Evaluation of LP1 promoter activity in liver by neonatal lentiviral vector delivery

Biodistribution was assessed using a CCL.LP1.*GFP/luc* vector. This vector was administered at the low dose of 2.8e8TU/Kg by neonatal intravenous injections to CD1 pups at P0. Luciferase activity as measured by live bioluminescence imaging, was followed for 41 days (at day 4, 8, 11, then weekly until culling) (**Figure 62**).
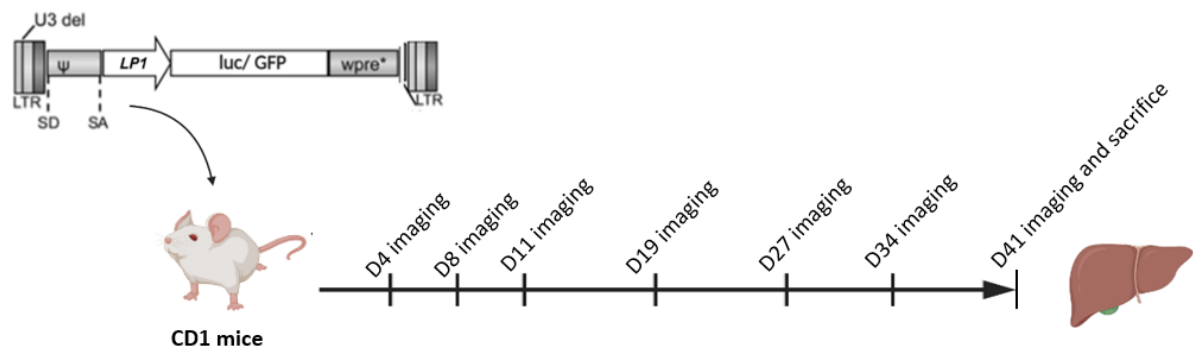
Figure 62. Schematic representation of LP1 promoter activity evaluation experimental design. GFP: green fluorescent protein; LP1: liver specific 1 promoter; LTR: long terminal repeats; luc: luciferase; SA: *tat/rev* splice acceptor; SD: splice donor; U3: unique 3' region; WPRE: woodchuck hepatitis virus post-transcriptional regulatory element.

Lentiviral vector showed early expression at day 4 (**Figure 63A**), high expression of luciferase between day 10 and day 20 post administration localised in the liver area (**Figure 63B, C**). After day 20, expression started to decrease until day 41 (**Figure 63D**) where the last measurement was taken (**Figure 63E, F**).
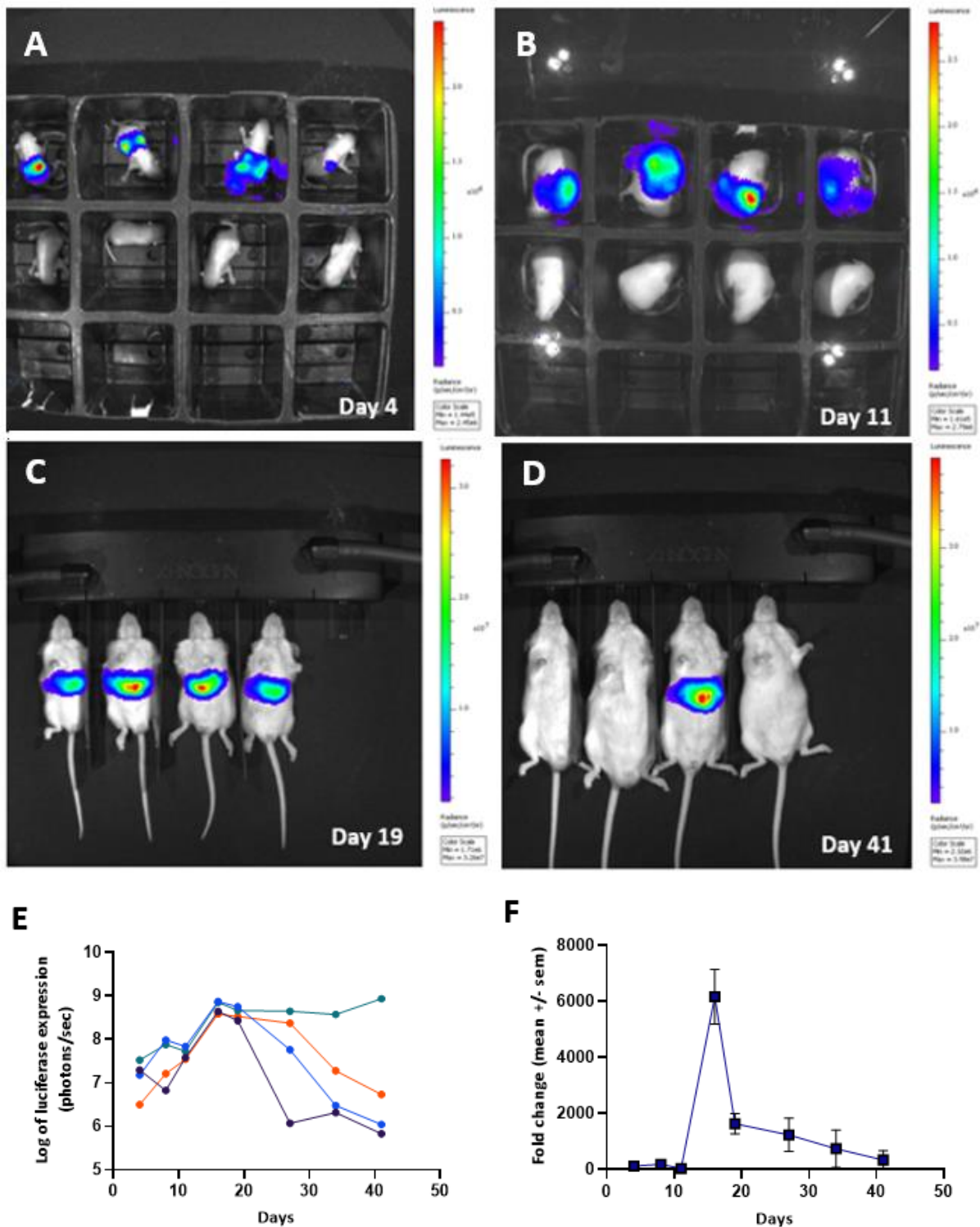
Figure 63. Biodistribution and short-term expression of liver specific lentiviral vector *in vivo*. Bioluminescence imaging of all mice show the location and expression level of the luciferase gene at **(A)** day 4, **(B)** day 11, **(C)** day 19, and **(D)** day 41. Coloured scale in each image represents radiance (photons/s/cm^2/steradian). **(E)** Radiance quantified within each ROI. **(F)** Results of ROI quantification of lentiviral treated animals normalised over the expression of controls. Graph represents mean $\pm$ SD for each group.

10.1.3 Long-term expression of lentiviral vectors *in vivo*

The CCL.LP1.*GFP* lentiviral vector was administered at a dose of 1e10TU/Kg to CD1 pups at day 3 by neonatal intravenous injection (**Figure 64**). Littermates were also used as non-injected controls. One year after injection, GFP expression was measured by live fluorescent imaging for 1 second of exposure under the fluorescent light.
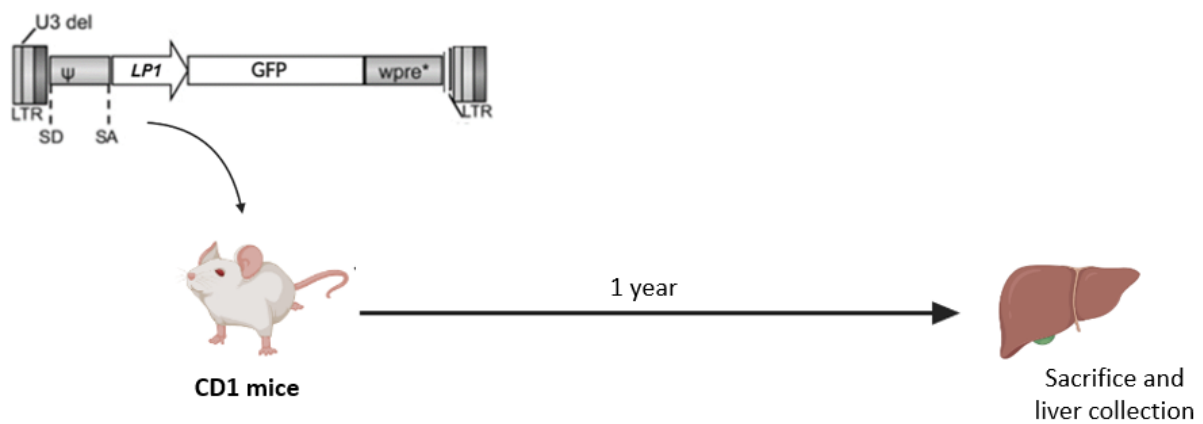
Figure 64. Schematic representation of long-term expression of lentiviral vectors experimental design. GFP: green fluorescent protein; LP1: liver specific 1 promoter; LTR: long terminal repeats; SA: *tat*/*rev* splice acceptor; SD: splice donor; U3: unique 3' region; WPRE: woodchuck hepatitis virus post-transcriptional regulatory element.

Results revealed that all CCL.LP1.*GFP* injected animals had significantly higher expression of GFP (*p*=0.032) one year post administration compared to control littermates (**Figure 65A-C**).
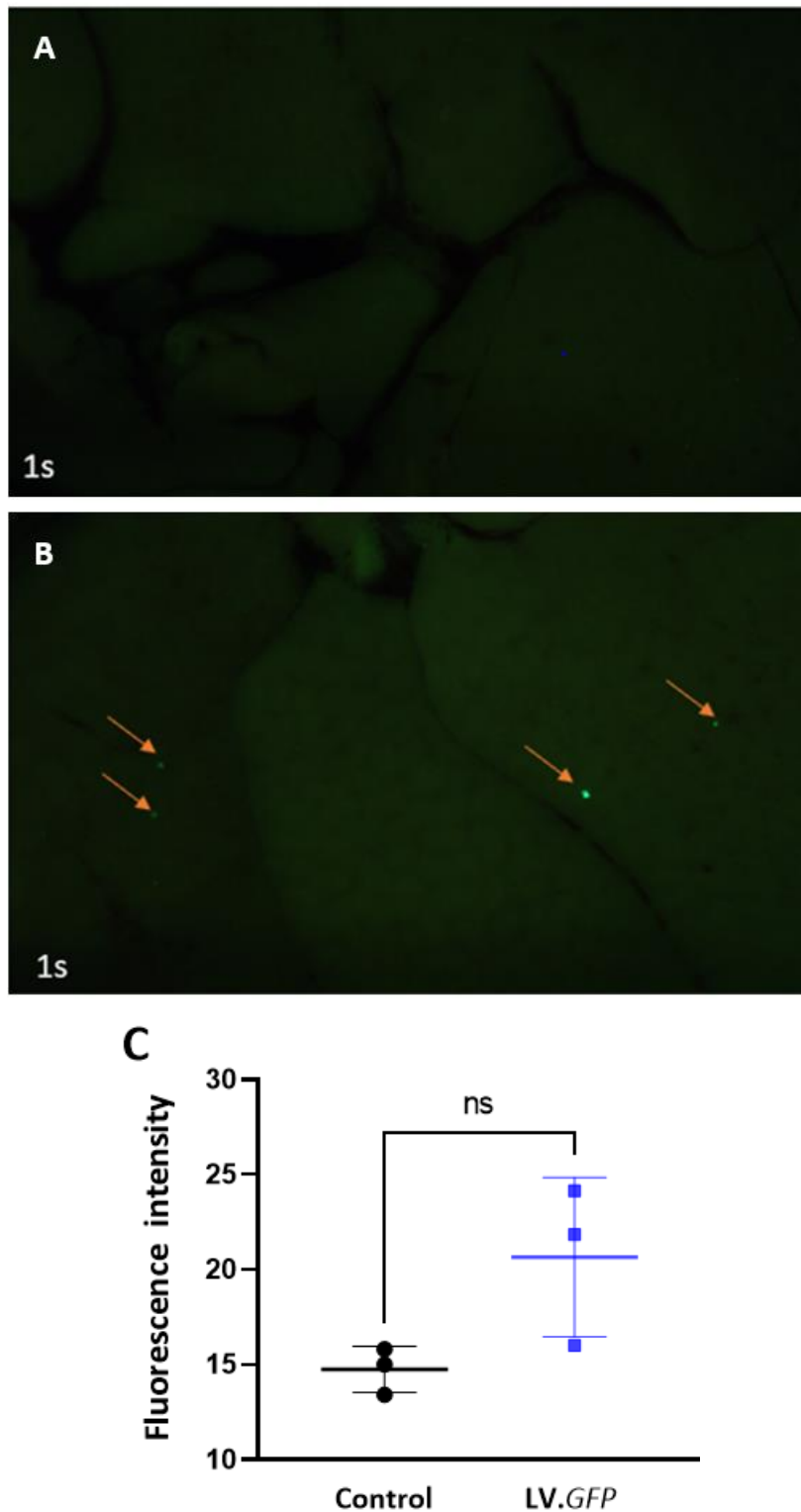
Figure 65. Quantification of GFP expression 1 year after neonatal injection with CCL.LP1.*GFP* vector in CD1 mice. (A) Representative image of the perfused whole liver from a control mouse. **(B)** Representative image of the perfused whole liver from a CCL.LP1.*GFP* vector injected mouse. **(C)** Quantification of fluorescence intensity in fresh livers of control and *GFP* treated mice. Control mice (n=3); *GFP* injected mice (n=4). Fisher exact t test * $p < 0.05$. Graph represents mean $\pm$ SD for each group. GFP: green fluorescent protein; 1s: 1 second.

Comparison of immunostaining in the liver section of control (**Figure 66A**) and lentiviral vector-injected CD1 littermates (**Figure 66B**) against GFP showed significantly increased staining (*p*=0.04) (**Figure 66C**).
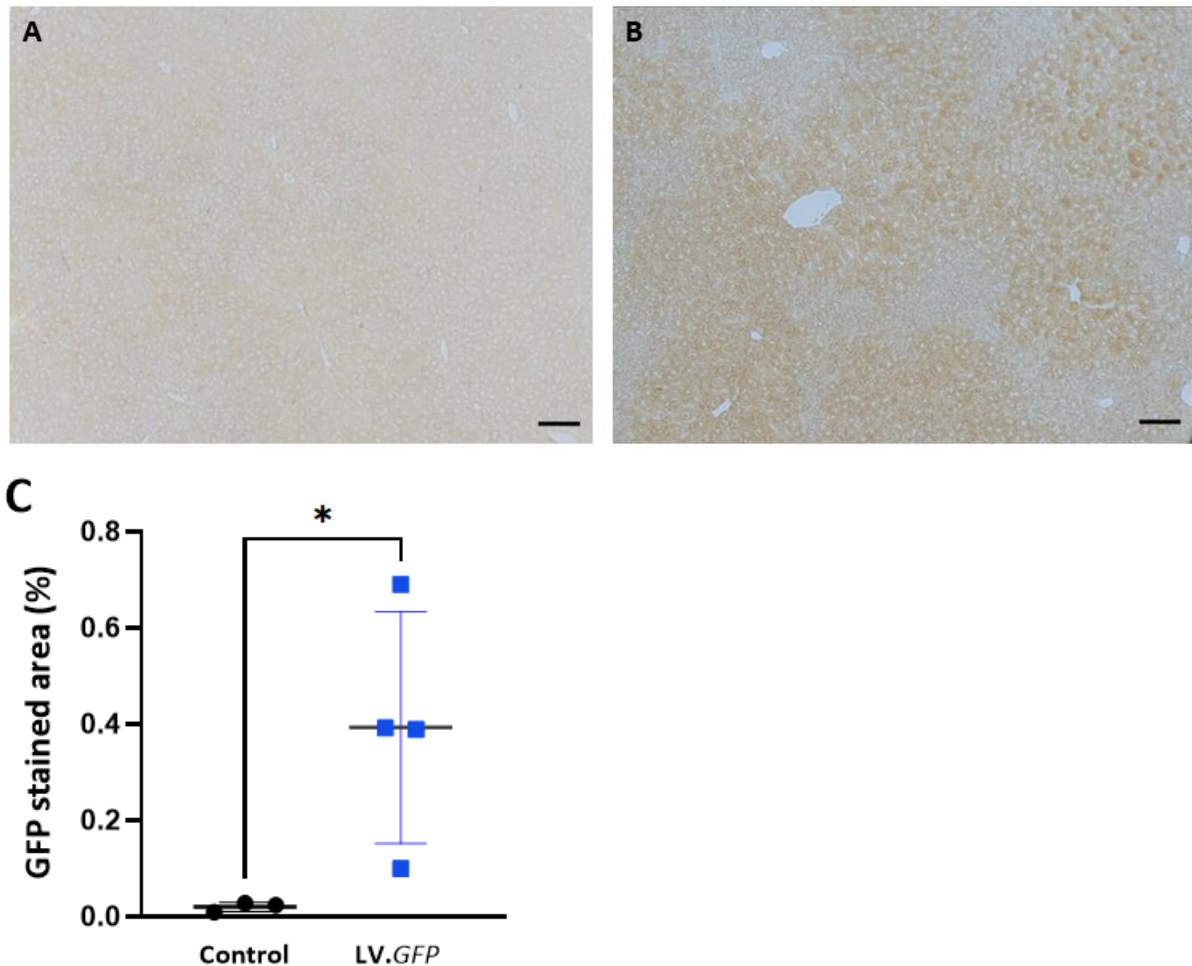
Figure 66. Immunostaining against GFP in CCL.LP1.*GFP* injected mice, and control littermates. Representative images of GFP immunostaining of liver sections from **(A)** control (n=3) and **(B)** CCL.LP1.*GFP* injected mice (n=4). **(C)** Percentage (%) of image area is identified in control and GFP mice. Scale bars of magnification: 100μm. Fisher exact t test * *p*< 0.05. Graph represents mean $\pm$ SD for each group. GFP: green fluorescent protein.

To certify the effectiveness of liver-directed lentiviral vector delivery, genomic DNA was extracted from the tissue samples from all livers and the vector genome copy number was measured, using a qPCR protocol, including amplification of the 5'LTR of the vector and normalization to *titin* which is a single-copy murine gene [422]. Analysis determined that there was a significant increase in VCN in livers of injected mice compared to the controls

(*p*=0.04) one year after CCL.LP1.*GFP* administration (**Figure 67**). These results correlated with the immunostaining results (**Figure 66C**) and confirmed the long-lasting expression of the vector and integration capacity *in vivo.*
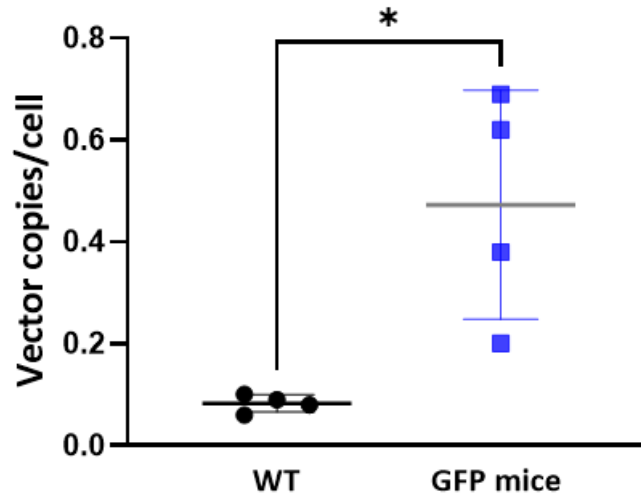
Figure 67. VCN presence in liver tissue 1 year post neonatal CCL.LP1.*GFP* vector administration. VCN in liver of control (n=4) and *GFP* animals (n=4). Fisher exact t test * *p*<0.05. Graph represents mean ± SD for each group. GFP: green fluorescent protein.

10.1.4 Discussion

The main parameters for a reliable gene delivery system, which can reverse the clinical phenotype of the disease, include the vector design, route and dose of delivery and host parameters [304]. Sustained expression of lentiviral vector *in vivo* has previously been observed in several studies [305-307]. This work shows experimental evidence that the LP1 promoter, when delivered intravenously in neonatal mice through the superficial temporal vein, was successful in targeting the liver area and presenting long-term expression as shown in **Sections 10.1.2 and 10.1.3**, with vectors encoding luciferase and GFP. These results are consistent with other studies, where lentiviral vectors with LP1 promoter showed the strongest signal in the liver when compared to EF1α, PGK, and UbiC promoter 1 month following intravenous injection [300, 301]. This is highly critical for liver inherited metabolic diseases such as ASA, whom most patients show a severe phenotype in infancy/early

childhood, when the liver is still rapidly growing. Increased vector genome copies per cell were correlated with higher GFP expression in the liver, however, variability of the vector's expression in liver tissue was also observed in **Section 10.1.3**. This could be partially a result of the technical challenges in the reproducibility of vector delivery through the superficial temporal vein, which is experimenter-dependent and highly demanding in $Asl^{Neo/Neo}$ mice as they have thinner skin [423].

11. Supplementary Material

```
              520         530         540         550         560         570         580         590
CCACTGGATTCTGAGCCACGCCGTGGCACTGACCCGAGACTCTGAGCGGCTGCTGGAGGTGCGGAAGCGGATCAATGTCCTGCCC
GGTGACCTAAGACTCGGTGCGGCACCGTGACTGGGCTCTGAGACTCGCCGACGACCTCCACGCCTTCGCCTAGTTACAGGACGGG
  H   W   I   L   S   H   A   V   A   L   I   K   D   S   E   K   L   L   E   V   R   K   R   I   N   V   L   P
            175             180             185             190             195

CCACTGGATTCTGAGCCACGCCGTGGCACTGACCCGAGACTCTGAGCGGCTGCTGGAGGTGCGGAAGCGGATCAATGTCCTGCCC
1 → CCACTGGATCCTGAGCCACGCCGTGGCACTGACAAGAGACTCTGAGAGACTGCTGGAAGTGCGGAAGCGGATCAACGTGCTGCCT


              600         610         620         630         640         650         660         670
CTGGGGAGTGGGGCCATTGCAGGCAATCCCCTGGGTGTGGACCGAGAGCTGCTCCGAGCAGAACTCAACTTTGGGGCCATCACTC
GACCCCTCACCCCGGTAACGTCCGTTAGGGGACCCACACCTGGCTCTCGACGAGGCTCGTCTTGAGTTGAAACCCCGGTAGTGAG
  L   G   S   G   A   I   A   G   N   P   L   G   V   D   R   E   L   L   R   A   E   L   N   F   G   A   I   T
    200             205             210             215             220             225

CTGGGGAGTGGGGCCATTGCAGGCAATCCCCTGGGTGTGGACCGAGAGCTGCTCCGAGCAGAACTCAACTTTGGGGCCATCACTC
1 → CTTGGATCTGGCGCTATCGCCGGAAATCCTCTGGGCGTTGACAGAGAGCTGCTGAGAGCCGAGCTGAACTTCGGCGCCATCACAC


              690         700         710         720         730         740         750         760
TCAACAGCATGGATGCCACTAGTGAGCGGGACTTTGTGGCCGAGTTCCTGTTCTGGGCTTCGCTGTGCATGACCCATCTCAGCAG
AGTTGTCGTACCTACGGTGATCACTCGCCCTGAAACACCGGCTCAAGGACAAGACCCGAAGCGACACGTACTGGGTAGAGTCGTC
  L   N   S   M   D   A   T   S   E   R   D   F   V   A   E   F   L   F   W   A   S   L   C   M   T   H   L   S   R
            230             235             240             245             250             255

TCAACAGCATGGATGCCACTAGTGAGCGGGACTTTGTGGCCGAGTTCCTGTTCTGGGCTTCGCTGTGCATGACCCATCTCAGCAG
1 → TGAATAGCATGGACGCCACCAGCGAGCGGGATTTCGTGGCCGAGTTTCTGTTTGGGCAGCCTGTGCATGACCCACCTGAGCAG


              770         780         790         800         810         820         830         840
GATGGCCGAGGACCTCATCCTCTACTGCACCAAGGAATTCAGCTTCGTGCAGCTCTCAGATGCCTACAGCACGGGAAGCAGCCTG
CTACCGGCTCCTGGAGTAGGAGATGACGTGGTTCCTTAAGTCGAAGCACGTCGAGAGTCTACGGATGTCGTGCCCTTCGTCGGAC
  M   A   E   D   L   I   L   Y   C   T   K   E   F   S   F   V   Q   L   S   D   A   Y   S   T   G   S   S   L
            260             265             270             275             280

GATGGCCGAGGACCTCATCCTCTACTGCACCAAGGAATTCAGCTTCGTGCAGCTCTCAGATGCCTACAGCACGGGAAGCAGCCTG
1 → AATGGCCGAGGACCTGATCCTGTACTGCACCAAAGAATTCAGCTTCGTGCAGCTGAGCGACGCCTACTCTACCGGAAGCTCTCTG


              860         870         880         890         900         910         920         930
ATGCCCCAGAAGAAAAACCCCGACAGTTTGGAGCTGATCCGGAGCAAGGCTGGGCGTGTGTTTGGGCGGTGTGCCGGGCTCCTGA
TACGGGGTCTTCTTTTTGGGGCTGTCAAACCTCGACTAGGCCTCGTTCCGACCCGCACACAAACCCGCCACACGGCCCGAGGACT
  M   P   Q   K   K   N   P   D   S   L   E   L   I   R   S   K   A   G   R   V   F   G   R   C   A   G   L   L
    285             290             295             300             305             310

ATGCCCCAGAAGAAAAACCCCGACAGTTTGGAGCTGATCCGGAGCAAGGCTGGGCGTGTGTTTGGGCGGTGTGCCGGGCTCCTGA
1 → ATGCCCCAGAAGAAGAACCCCGACAGCCTGGAACTGATCCGGTCTAAGGCCGGCAGAGTGTTCGGAAGATGTGCCGGACTGCTGA


              940         950         960         970         980         990         1000        1010
TGACCCTCAAGGGACTTCCCAGCACCTACAACAAAGACTTACAGGAGGACAAGGAAGCTGTGTTTGAAGTGTCAGACACTATGAG
ACTGGGAGTTCCCTGAAGGGTCGTGGATGTTGTTTCTGAATGTCCTCCTGTTCCTTCGACACAAACTTCACAGTCTGTGATACTC
  M   T   L   K   G   L   P   S   T   Y   N   K   D   L   Q   E   D   K   E   A   V   F   E   V   S   D   T   M   S
            315             320             325             330             335             340

TGACCCTCAAGGGACTTCCCAGCACCTACAACAAAGACTTACAGGAGGACAAGGAAGCTGTGTTTGAAGTGTCAGACACTATGAG
1 → TGACCCTGAAGGGCCTGCCTAGCACCTACAACAAGGACCTGCAAGAGGACAAAGAGGCCGTTTTCGAGGTTTCCGACACCATGTC
```

214

Supplementary Figure 1. Comparative analysis of codon optimization in hASL plasmid sequences. DNA sequence alignment between the wild-type hASL plasmid (top sequence, bold) and its codon-optimized variant, co-hASL (bottom sequence). The alignment visualized using SnapGene software, aids in the comprehensive analysis of nucleotide modifications implemented during the codon optimization process.
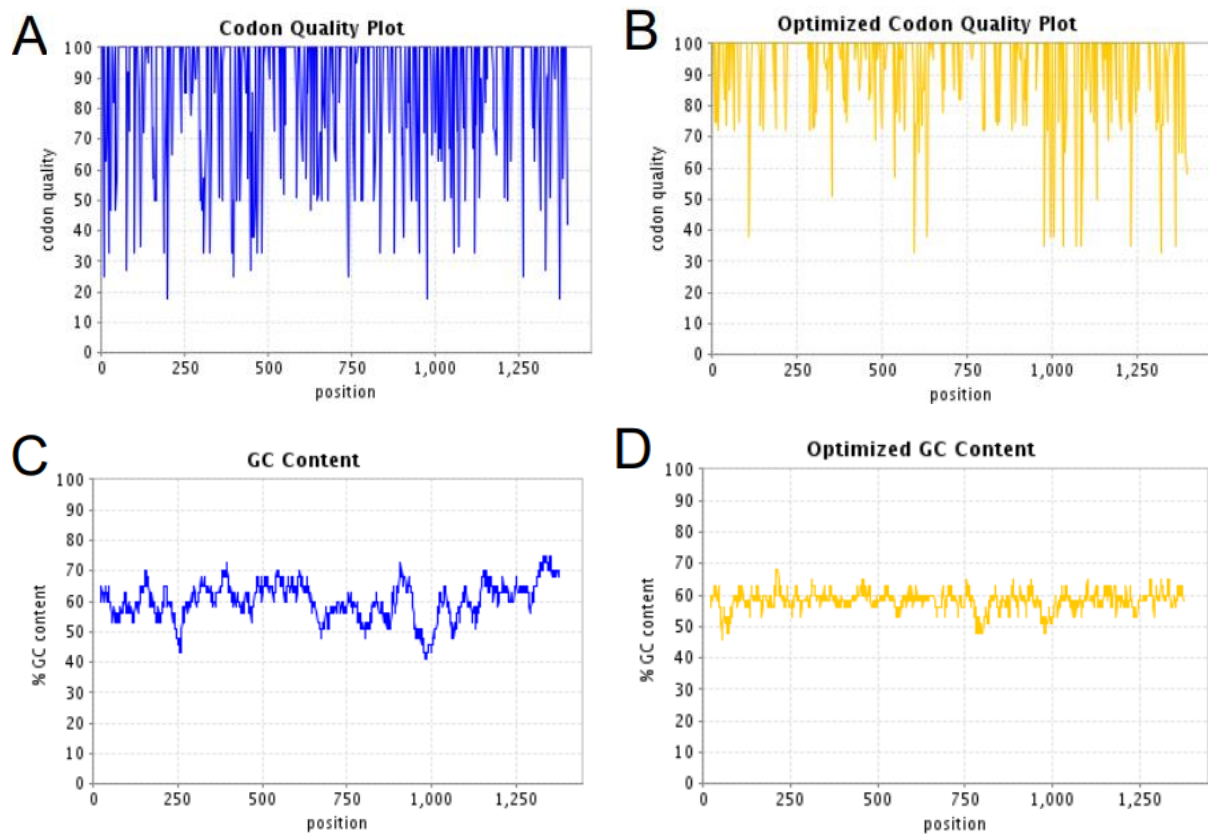
Supplementary Figure 2. Characteristics of codon optimized hASL plasmid using GenArt Software.
(A-B) The plots show the quality of the used codon at the indicated codon position. **(C-D)** The plots show the GC content in a 40 bp window centred at the indicated nucleotide position.